2017-05-09

Monitoring of Electroencephalographic and Multi-Rate Auditory Evoked Response Changes during Altered Levels of Consciousness

Alexander Castro-Llanos
University of Miami, alexcastro123@yahoo.com

UNIVERSITY OF MIAMI

MONITORING OF ELECTROENCEPHALOGRAPHIC AND MULTI-RATE AUDITORY EVOKED RESPONSE CHANGES DURING ALTERED LEVELS OF CONSCIOUSNESS

By

Alexander Castro-Llanos

A DISSERTATION

Submitted to the Faculty
of the University of Miami
in partial fulfillment of the requirements for
the degree of Doctor of Philosophy

Coral Gables, Florida
May 2017

UNIVERSITY OF MIAMI

A dissertation submitted in partial fulfillment of
the requirements for the degree of
Doctor of Philosophy

MONITORING OF ELECTROENCEPHALOGRAPHIC AND MULTI-RATE AUDITORY EVOKED RESPONSE CHANGES DURING ALTERED LEVELS OF CONSCIOUSNESS

Alexander Castro-Llanos

Approved:

_____
Jorge E. Bohórquez, Ph.D.
Associate Professor in Practice
Department of Biomedical Engineering

_____
Özcan Özdamar, Ph.D.
Professor and Chairman
Department of Biomedical Engineering
Secondary appointments in
Otolaryngology, Pediatrics, and
Neuroscience

_____
Suhrud M. Rajguru, Ph.D.
Assistant Professor
Department of Biomedical Engineering
Secondary Appointment in Otolaryngology

_____
Richard R. McNeer II, M.D., Ph.D.
Associate Professor of
Clinical Anesthesiology
Department of Anesthesiology,
Perioperative Medicine and
Pain Management

_____
Roman Dudaryk, M.D.
Assistant Professor of
Clinical Anesthesiology
Department of Anesthesiology,
Perioperative Medicine and
Pain Management

_____
Guillermo Prado, Ph.D.
Dean of the Graduate School

CASTRO - LLANOS, ALEXANDER (Ph.D., Biomedical Engineering)

Monitoring of Electroencephalographic and Multi-Rate Auditory Evoked Response Changes During Altered Levels of Consciousness (May 2017)

Abstract of a dissertation at the University of Miami.

Dissertation supervised by Professor Jorge E. Bohórquez
No. of pages in text. (234)

Background: There is a need to expand the research on intraoperative awareness to better understand the patient's neurologic responses and effectively predict and prevent unintended awareness. Previous studies in altered levels of consciousness in anesthesia and sleep have only focused on either electroencephalogram (EEG) or evoked potentials (EP) analysis. Additionally, EP studies only focused on either transient or steady-state response.

Purpose: To investigate the inherent patterns associated with altered levels of consciousness in both anesthesia and sleep models as extracted from the simultaneous acquisition of both multi-rate auditory EPs and EEG spectral descriptors.

Methods: Anesthesia recordings were acquired from five patients during elective surgery while sleep recordings were acquired from fourteen healthy volunteers. For anesthesia, a multi-rate stimulation paradigm composed of (a) 5 Hz isochronic (b) 20, 30, and 40 Hz short, low-jittered, and (c) silence regions were used. The sleep study stimulus consisted of (a) 5 Hz isochronic, (b) 30 Hz low-jittered, and (c) silence regions. In both anesthesia and sleep, the click stimulus was 200 μsec in duration, and it was delivered to

the right ear at 70 dB nHL and 60 dB nHL, respectively. Physiological data such as spontaneous respiration rate, expired agent concentration, bispectral index, heart rate, and core body temperature, were collected for all anesthesia patients. In anesthesia, EEG was continuously acquired from Fz-M2 channel, while in sleep it was acquired from Fz-A2 and Cz-A2 with additional channels for scoring. These EEG signals were analyzed using the full set of spectral descriptors. Trend analysis for EEG attributes and moving average for EP attributes were used for the anesthesia study while for the sleep study these attributes were investigated by contrasting between the sleep stages. Two independent investigators assigned the sleep stages to EEG segments with a manual computer-aided sleep scoring software, which was specifically developed for the sleep study. To extract both high-rate transient and steady-state responses the continuous loop averaging deconvolution (CLAD) method was used. The 5 Hz EPs responses were processed with broadband filtering, starting at 1Hz.

Findings and Conclusions: Spectral descriptors, extracted from EEG, showed that delta power ratio and median frequency showed significant separation between levels in both anesthesia and sleep. In the separation of anesthesia levels, the aforementioned features exhibited better performance than both spectral entropy (SE) and bispectral index (BIS). Channel Fz-A2 compared to Cz-A2 showed better discrimination between sleep stages. EPs elicited by low rate (5 Hz) stimulation, when acquired using low frequency preserving filters such as filters with broad frequency bands, showed greater sensitivity in separating anesthesia levels and in differentiating sleep stages. Future works should include an exhaustive study of delta power ratio and median frequency for EEG and low rate responses that consider low frequencies for EP.

DEDICATION

To my

father Humberto Luis Castro-Corzo

and

mother Danelia Castro-Llanos

because

I love you

and

to the heaven that smiles above me.

ACKNOWLEDGEMENTS

My deepest gratitude goes to the McKnight Doctoral Fellowship for funding my doctorate studies and research. Thank you, Dr. Lawrence Morehouse (President and CEO), for your guidance, mentorship, and support. You are a person of immense knowledge and deep understanding. I have learned a great deal from you by your example. To Jorge E. Bohórquez, Ph.D., my dissertation advisor and committee chair, it is a joy to have been your first doctoral graduate and successfully defended on your birthdate. An enduring memory of you is engraved especially annually on March 27. To Özcan Özdamar, Ph.D., (Professor and Chairman of the Department of Biomedical Engineering, Director of Neurosensory Engineering Laboratory) since my acceptance into the biomedical engineering department as an undergraduate you have been my advisor, thank you for your flexibility and rigor. To my committee members, I thank you each for being part of my dissertation and sharing your insights, honed from years of experience, and your humor. No one can ask for a better series of mentors and friends: Richard R. McNeer II, M.D., Ph.D., (Associate Professor of Clinical Anesthesiology in the Miller School of Medicine at the Department of Anesthesiology, Perioperative Medicine and Pain Management, University of Miami Jackson Memorial Hospital/Ryder Trauma Center), Roman Dudaryk, M.D., (Assistant Professor of Clinical Anesthesiology in the Miller School of Medicine at the Department of Anesthesiology, Perioperative Medicine and Pain Management, University of Miami Jackson Memorial Hospital/Ryder Trauma Center), and Suhrud M. Rajguru (Ph.D., Assistant Professor of Biomedical Engineering and Otolaryngology, University of Miami Ear Institute). To Raina Jeanmarie Moyer, (Research Associate, Department of Anesthesiology, Perioperative Medicine and

Pain Management, University of Miami Jackson Memorial Hospital/Ryder Trauma Center) I am your B.E.F.. You are one of the pillars of my success. To Oscar Luis Villalon your help gave me the confidence I needed, thank you. To Abhishek Prasad, Ph.D., (Director of Neural Interface Laboratory), thank you, for the incredible recognition as a post-doctoral researcher in your laboratory. Notably, the broad exposure to all aspects of research. To Justin C. Sanchez, Ph.D., (Office Director, Biological Technologies Office, DARPA), I always enjoyed talking with you about insights into investigative neuroscience and approaches to scientific thought. I esteem our friendship, thank you. To Khalid Alhussaini, Ph.D., It is an honor to have witnessed your success as scientist, poet, and father. To Ibrahim Kaya, your creative spark and intelligence will take you places. To David Toribio, thank you, "… and as always class, we use Dr. Toribio's 1st and 2nd law". To Doreen Yamamoto, thank you, for your insightful comments and most of all your reassurance. To Peter Tarjan, Ph.D., (Professor Emeritus of Biomedical Engineering), you are a fighter, I began the biomedical engineering graduate program, thanks to you. To Herman Cheung, Ph.D., (James L. Knight Professor) you are a great person thank you for your wisdom. To Edward A Dauer, M.D., thank you, I won't forget you. To Weiyong Gu, Ph.D., (Chair of the Department of Mechanical and Aerospace Engineering,) thanks for pointing out my typos we both know what I mean. To Loren Latta, Ph.D., P.E., (Director of Max Research Department Biedermann Institute for Biomechanics), thank you, for the opportunity to work with you in your laboratory, your humility is honorable, one I aspire to emulate. To Ramarathnam Narasimhan, Ph.D., "Dr. Ram", (Assistant Dean for Engineering Advising and Undergraduate) thank you, for navigating me through this rigorous doctoral program. To Fabrice Mann, Ph.D., (Chair of

Department of Biomedical Engineering) I always found repose in your humor during my tenacious doctoral journey, thank you. To Weizhou Zhou, Ph.D., (Professor of Biomedical Engineering) thank you primarily for believing in me; you have been an inspiration. To Nelson Salas, Ph.D., and Ray Montero, Ph.D., thank you both for your friendship. To Servando Muñoz, Ph.D., (Supramolecular Chemist) your intervention and mentorship shaped who I am. You always saw a scientist in me. To Jan Voda, M.D., Ph.D., thank you for teaching me about the neuroscience that is not found in textbooks. To Jacqueline Sagen, Ph.D., M.B.A., (Professor of Neurological Surgery, Miami Project to Cure Paralysis) thank you Jacky, for opening me to experience everything possible within neuroscience without restrictions when I conducted research in your laboratory. To Matthew J. Gounis, Ph.D., (Associate Professor, Department of Radiology, Director, New England Center for Stroke Research, Director of Scientific Affairs, AMRIC, UMass Medical School) thank you for seeing an engineer in me and your friendship. To Baruch Barry Lieber, Ph.D., (Professor, Department of Neurosurgery, Stony Brook Neuroscience Institute) thank you, I still remember your story about the shoemaker and apprentice, its one I carry with me since the day you told it to me. I am grateful to my sisters Helen Castro, E.M.S.T. and Maria del pilar Castro, M.B.A. for their assistance in my life. To my niece, Elizabeth and nephew, Anthony your both exceptionally sagacious scientists, I love you both very much. Umar Bukhari and Igal Zakhodin the greatest electrical engineers I call friends. Angie Del-Llano, Vivian Figueredo, and Christine Vignolio couldn't have done it without you! To Cris Cruz (Artist), thank you for empowering me. To Johnny Will Carter Jr., I believe in you, always have, always will because you are brilliant and life will recognize it. Alexander Castro-Llanos, B.M.E. Ph.D.

TABLE OF CONTENTS

LIST OF FIGURES

LIST OF TABLES

Chapter 1 BACKGROUND

1.1. Electroencephalogram

1.1.1 Neurological Basis for the Generation of Electroencephalogram

Neurons are the fundamental building block of the nervous system. Structured into vast networks, a network of neurons is able to perform complex computations required to complete functions of the nervous system. Neurons have three fundamental structures: the cell body, many dendrites, and a single axon (see Figure 1.1).

Axons from adjacent neurons bind to the dendrites (i.e., or cell bodies) of receiving neurons via junctions called synapses (see Figure 1.1). The cell body of a neuron is the centralized region where biosynthesis occurs. Dendrites are the branched projections of neurons that provide an enormous surface area for receiving input from other neurons. They function as the receptive-input region of a neuron.

An axon is a thread-like projection of a neuron that transmits electrical impulses called action potentials (APs) to the secretory-output region of the axon called the axon terminals (see Figure 1.1). Axons function as both the conductive and secretory-output region of neurons (Bear, Connors, & Paradiso, 2001). Synapses are unique junctions between the axon terminals of the transmitting neurons (i.e., presynaptic neurons) and the dendrites of the receiving neurons (i.e., postsynaptic neurons) (see Figure 1.1).

Also, synapses transmit graded potentials, which are electric potential differences that arise within the membrane of the neuron. Graded potentials are classified as either

excitatory or inhibitory postsynaptic potentials. Presynaptic neurons will transfer their graded potentials via synapses to dendrites (i.e., or cell bodies) of postsynaptic neurons. The dendrite branches of the postsynaptic neuron collectively integrate the graded potentials received from the network's presynaptic neurons resulting in a net membrane potential. Dendrites of target neurons transmit the net membrane potential to the cell body, i.e. soma, of postsynaptic neurons as a stimulus.

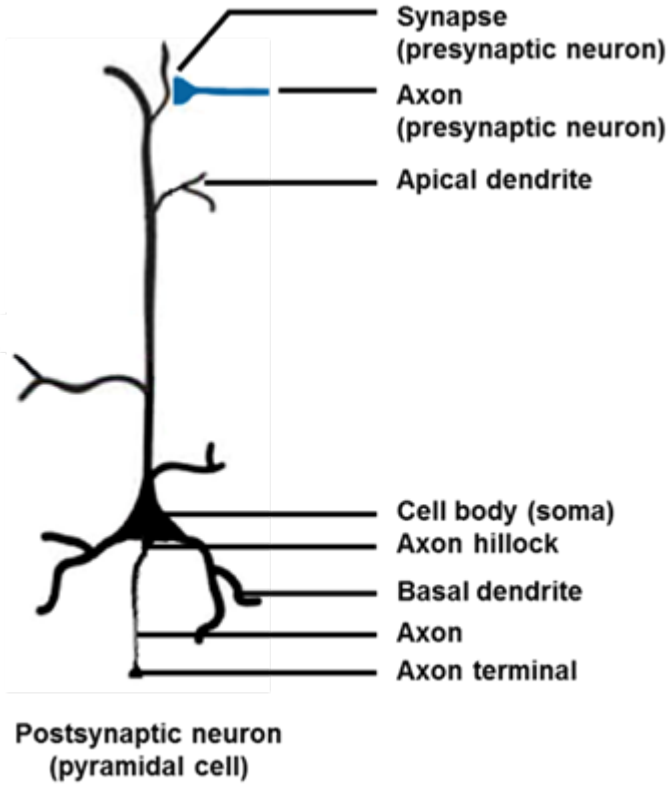

Figure 1.1 Structure of pyramidal neuron.

The axon hillock, which is the structure of the neuron that connects the cell body to a single axon, receives the net membrane potential. The axon hillock (see Figure 1.1) generates action potentials in response to the net membrane potential.

When the net membrane potential reaches or exceeds a specified membrane potential called threshold potential, it generates action potentials at a rate that correlates with the intensity of the stimulus. The greater the intensity of the net membrane potential the greater the rate of AP impulses transmitted down the axon by the axon hillock. Action potentials transmit away from the cell body to the terminal ends of the axon called axon terminals, i.e. synaptic terminals.

At the synaptic terminals, the series of APs impulses are translated from a coded electrical signal to a chemical signal. When an action potential reaches the axon terminal it causes synaptic vesicles to secrete chemical messengers, called neurotransmitters, into a space within the synapse called the synaptic cleft. Neurotransmitters bind "lock and key" to protein structures called receptors that are embedded in the membrane of the postsynaptic side of the synapse (Bear, Connors, & Paradiso, 2001; Marieb, 1991).

Neurotransmitters traverse the synaptic cleft from the presynaptic neuron to the postsynaptic neuron to bind to postsynaptic receptors. When neurotransmitters bind to the postsynaptic receptors of the postsynaptic neuron, it induces a graded potential in the membrane of the postsynaptic neuron's dendrite (i.e., or cell body). These graded potentials are at times commonly referred to as postsynaptic potentials (i.e., PSPs). The magnitude of a single postsynaptic potential is proportional to the number of postsynaptic receptors bound to neurotransmitters.

PSPs are graded according to the amount bound transmitters to receptors. If there are a greater number of excitatory neurotransmitters, then the graded potential generated at the dendrite will be excitatory postsynaptic potentials (i.e., EPSPs), which will make

the membrane potential more positive (i.e., depolarized). However, if there are a greater number of inhibitory neurotransmitters, then the graded potential generated at the dendrite will be inhibitory postsynaptic potentials (i.e., IPSPs), which will make the membrane potential more negative (i.e., hyperpolarized) (Bear, Connors, & Paradiso, 2001). Thus, neurons through the summation of the graded potentials that are integrated at the axon hillock either fire or inhibit an action potential.

The greater the resulting membrane potential that arrives at the axon hillock the greater the rate of action potentials delivered by the axon hillock to synaptic terminals. Synaptic terminals release neurotransmitters that bind to the receptors of on target neurons causing a graded potential. Networks of neurons are capable of performing complex computations because of the neuron have the ability to integrate and fire.

1.1.2 Genesis of Electroencephalogram

Electroencephalogram (i.e., EEG) is mainly considered the result of postsynaptic potentials and is not mainly considered the result of action potentials (Kandel, Schwartz, & Jessell, 2000; Mulert & Lemieux, 2010; Rampil, 1998). Action potentials provide a trivial contribution to the measured scalp surface electrical potentials of EEG.

Due to the asynchronous short-duration firing of action potentials and the random orientation of axon processes, action potentials cannot effectively sum to form the electrical potentials of EEG (Rampil, 1998). Instead of action potentials, EEG is the net result of local postsynaptic potentials that may be both excitatory and inhibitory and that may have durations of up to several tens of milliseconds (Rampil, 1998) (see Figure 1.2).

EEG is believed to originate from the cerebral cortex for reasons such as, the proximity of the cortex to the scalp, the large source-sink separations created by cortical pyramidal neurons, and the horizontal alignment of pyramidal neurons in cortical tissue

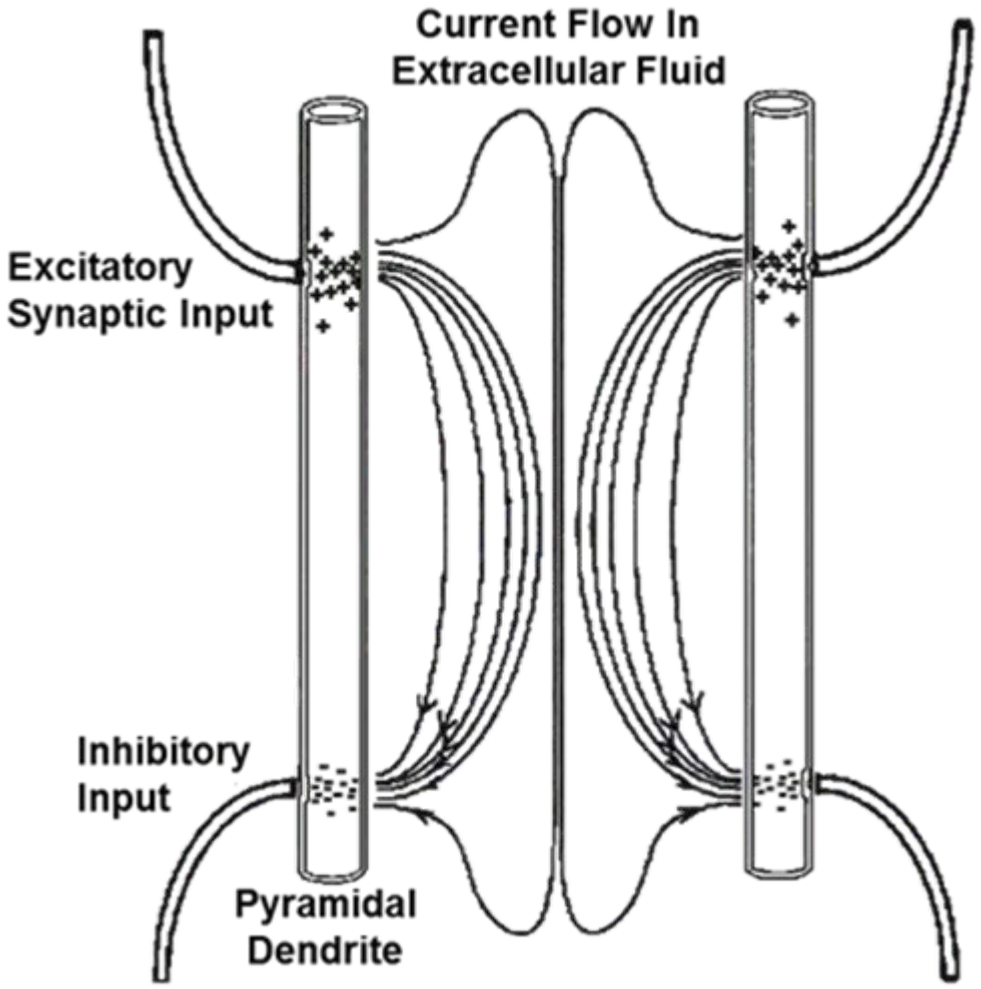

Figure 1.2 Parallel alignment of dendrites reason for summed postsynaptic potentials. The basis of EEG generation is the summing of postsynaptic potentials from cerebral neuron such as the pyramidal neuron. EEG is predominantly the net result of summing both excitatory and inhibitory local postsynaptic potentials, which have durations of up to several tens of milliseconds. Adapted from (Rampil, 1998)).

produce large dipole layers (Rampil, 1998) (see Figure 1.2). Pyramidal cells of the cortex's neural tissue are horizontally aligned and parallel to each other with all apical dendrites on one end and somata on the other and with their apical dendrites

perpendicular to the cortical surface (Kandel, Schwartz, & Jessell, 2000; Rampil, 1998) (see Figure 1.3). Dendrites are respectively divided into apical and basal depending on whether they are directed towards the surface of cortex or towards deeper brain sources (Bear, Connors, & Paradiso, 2001) (see Figure 1.1).

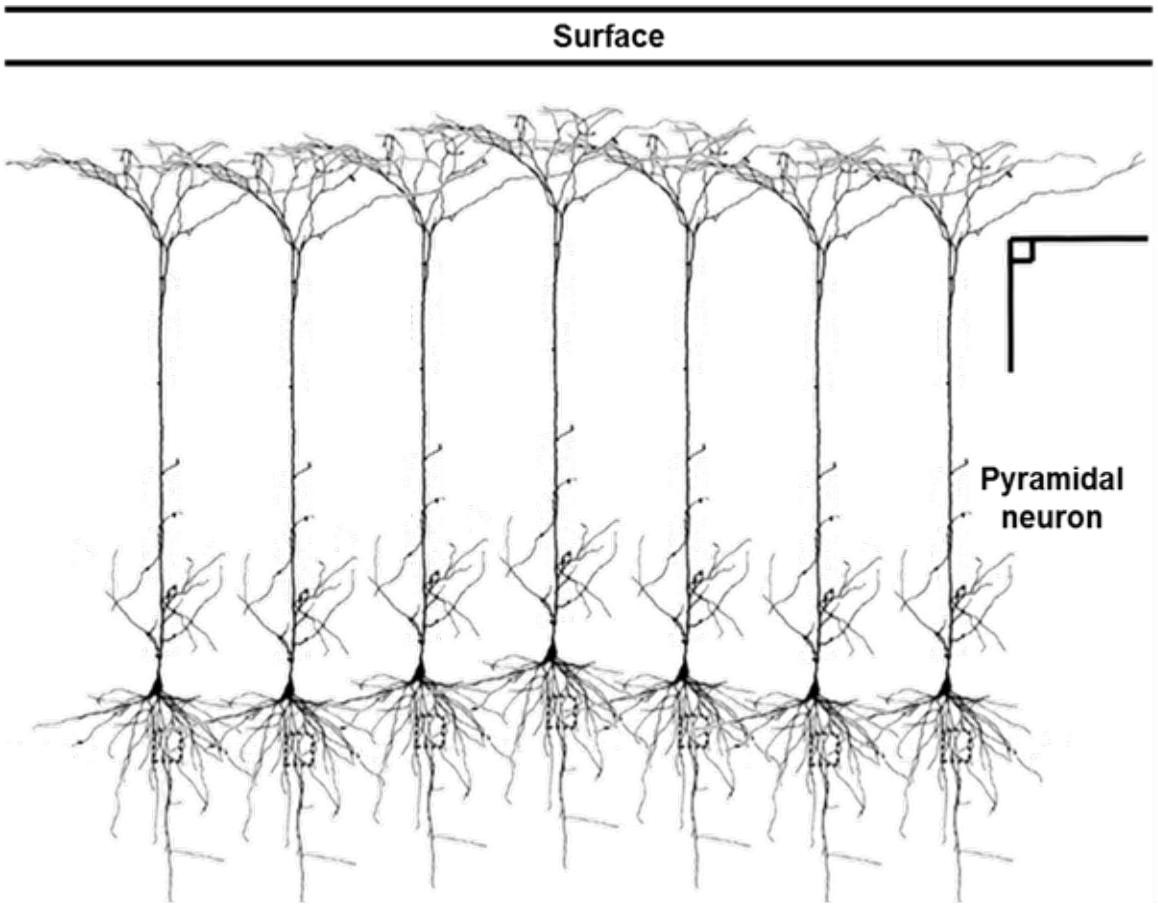

Figure 1.3 Pyramidal neurons are aligned in parallel. Pyramidal neurons are arranged parallel with respect to each other and are arranged perpendicular to surface with respect to the surface. The parallel arrangement of pyramidal neurons is important for the constructive summing of postsynaptic potentials.

Summed postsynaptic potentials from cortical pyramidal neuron cause differences of electrical potentials on the cortical pyramidal neuron (see Figure 1.4). These differences of electrical potentials create electrical dipoles between the cell body of a cortical pyramidal neuron and its apical dendrites. When most of the input at the

dendrites is inhibitory the neuron's electrical dipole will reverse (Rampil, 1998) (see Figure 1.4). The physical separations that exist between inhibitory and excitatory postsynaptic potentials on individual apical dendrite induces current loops that bridge

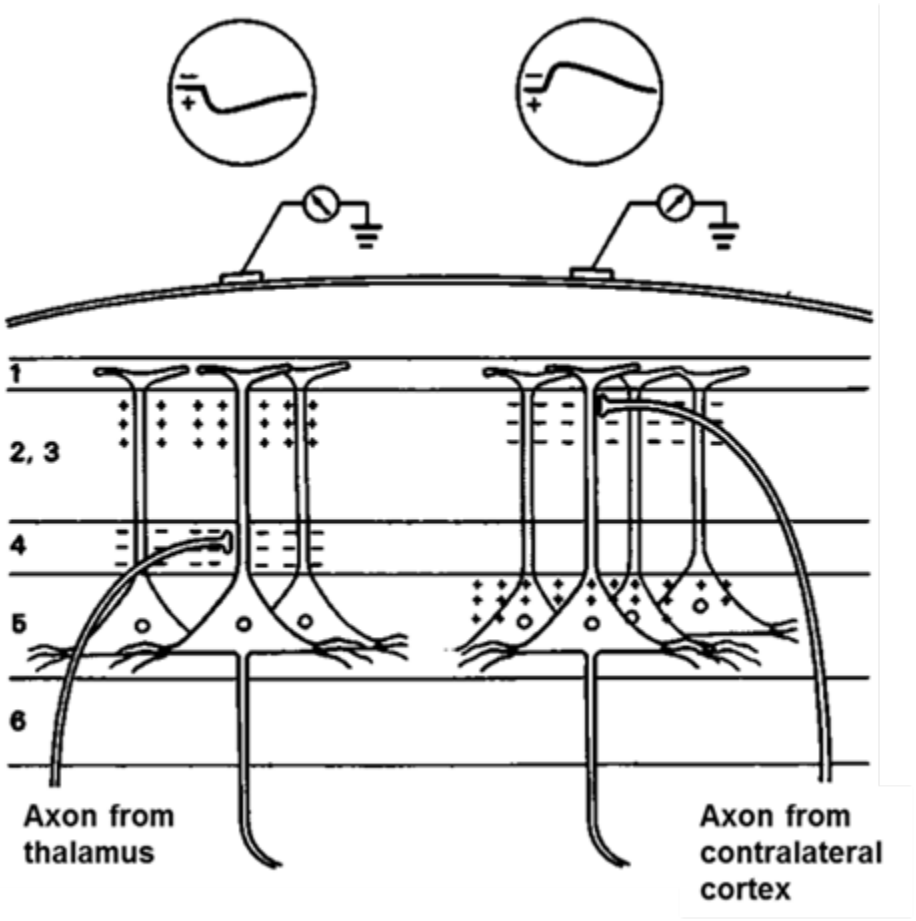

Figure 1.4 Changes in surface potentials is due to dipole orientation of neurons. Pyramidal neurons at two different dipole orientations correspond to the changes observed by the potentials measured at the surface. Differences in electric potentials are caused by summed postsynaptic potentials from cortical pyramidal neuron. The differences of electric potentials create electrical dipoles between the cell body of a cortical pyramidal neuron and its apical dendrites. If most of the input to the dendrites is inhibitory then the neuron's electrical dipole will reverse.

between the postsynaptic potentials (Rampil, 1998). The current loops of adjacent cortical pyramidal neurons additively combine in the extracellular fluid between the cells to form a larger regional current flow that can be measured by the voltage it creates on

the scalp (Kandel, Schwartz, & Jessell, 2000; Rampil, 1998) (see Figure 1.5). As the postsynaptic potential form and decay, the EEG scalp voltage changes over time.

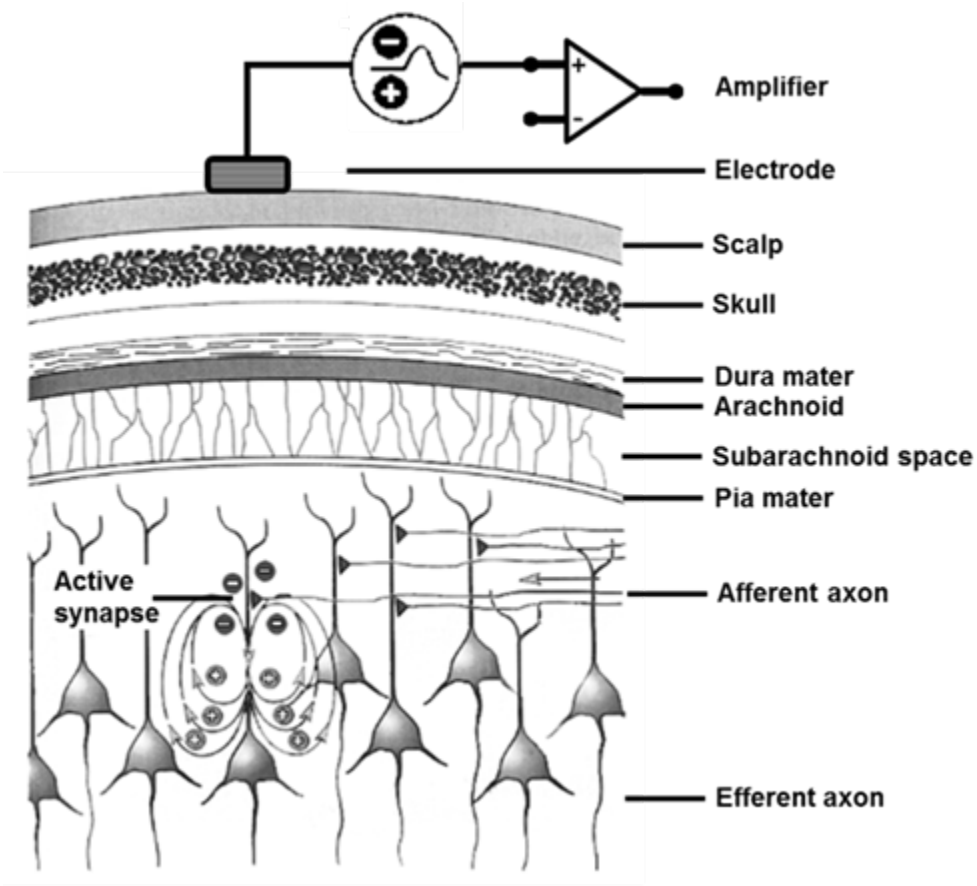

Figure 1.5 Current loops generated by pyramidal neurons are measured at the surface. Pyramidal neurons synchronously forming current loops surpass the attenuation cause by the surface and are measure at the surface. Current loops are induced between inhibitory and excitatory postsynaptic potentials in apical dendrite. When the neurons synchronously generate current loops, the current loops additively sum between the cells in the extracellular fluid, thereby forming larger regional current flow that can be measured by the voltage it induces on the surface of the scalp. The synchrony of activity of the neuron is important because the greater the degree of synchrony in the neuron activity, the greater the magnitude of the surface potential. The potential values measured at the surface must be amplified because the potential value is attenuated by the surface composition (e.g., skull, scalp, etc.). Adapted from (Bear, Connors, & Paradiso, 2001).

Therefore, the net postsynaptic potential contribution of pyramidal neurons measured at any given time is a function of the summation in space of the postsynaptic potential and of the degree of synchrony of pyramidal neuron activity (see Figure 1.5).

The degree of synchrony of pyramidal neurons determines the net magnitude and frequency of the EEG signal (Bear, Connors, & Paradiso, 2001).

1.1.3 Neural Correlates of EEG to States of Consciousness

Normally, the EEG signal has no obvious pattern referred to as spontaneous EEG (Tatum, Husain, Benbadis, & Kaplan, 2008). EEG patterns may be generated by mental and/or pathological states such as the ones created in sleep that synchronized activity in the cortical and thalamic neural structure thus inducing patterns such as waves, oscillations, spindles, spikes and bursts (Rampil, 1998).

EEG rhythms correlate with particular states of consciousness (Tatum, Husain, Benbadis, & Kaplan, 2008). These correlations are often referred to as neural correlates. EEG rhythms are classified according to frequency range: delta rhythms are less than 4 Hz, theta rhythms are within 4 to 7 Hz, alpha rhythms are within 8 to 13 Hz, beta rhythms are within 14 to 30 Hz, and gamma rhythms are within 30 to 70 Hz (Bear, Connors, & Paradiso, 2001) (see Figure 1.6).

Delta rhythms activity of EEG is normally seen during deep sleep (Bear, Connors, & Paradiso, 2001; Tatum, Husain, Benbadis, & Kaplan, 2008). In contrast, delta rhythms activity in awake-EEG indicates brain damage, and it has been observed after closed head trauma (Tatum, Husain, Benbadis, & Kaplan, 2008).

Theta rhythms activity of EEG has been observed during drowsiness and light sleep, during emotional stress in some adults (Kropotov, 2009). In addition, theta

rhythms activity has been observed on the waking state of mental diseases such as Alzheimer's disease and vascular dementia (Bear, Connors, & Paradiso, 2001).

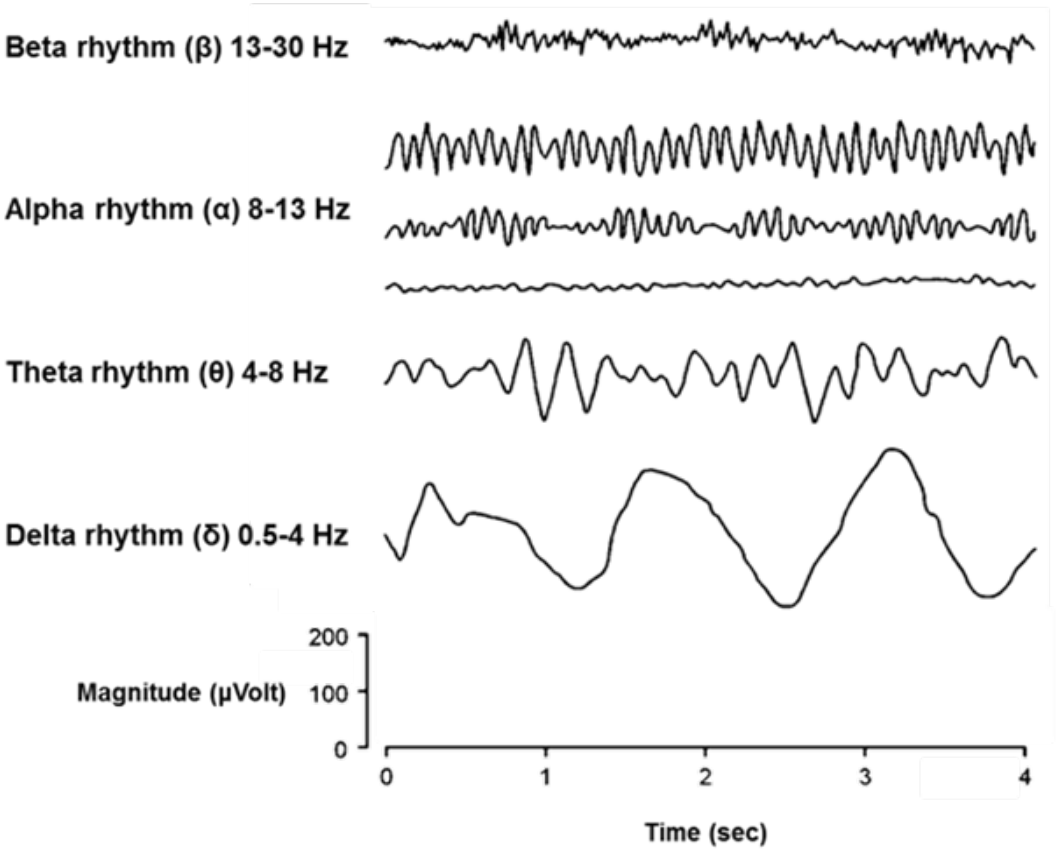

Figure 1.6 EEG rhythms are classified according to frequency range. Delta rhythms are less than 4 cycles per second. Theta rhythms are within 4 to 7 cycles per second. Alpha rhythms are within 8 to 13 cycles per second. Beta rhythms are within 14 to 30 cycles per second (Plonsey & Malmivuo, 1995).

Alpha rhythms activity of EEG occurs highest in the occipital region while a person is awake and relaxed but with eyes closed (Bear, Connors, & Paradiso, 2001). Alpha rhythms are enhanced by relaxation and by eye closure. Conversely, alpha rhythms are partially or completely blocked by mental activity and by eye opening (Kandel, Schwartz, & Jessell, 2000).

Beta rhythms activity of EEG is associated with active thinking, active attention, and excitement (Bear, Connors, & Paradiso, 2001; Kandel, Schwartz, & Jessell, 2000). GABAergic cortical inhibition is considered to have a role in the generation of beta oscillations. Beta rhythms activity has been shown to be increased by GABA-agonistic drugs such as benzodiazepines and barbiturates (Kropotov, 2009). However, the beta rhythms activity induces by GABA-agonistic drugs is believed to be a provoked cortical rhythm and not a normal one (Kropotov, 2009).

Gamma rhythms activity of EEG demonstrated that 40 Hz rhythm is associated to cortical arousal (Bear, Connors, & Paradiso, 2001; Tatum, Husain, Benbadis, & Kaplan, 2008). Moreover, Gamma rhythms activity of EEG is a good indication of event-related synchronization (i.e., ERS) of the brain (Bear, Connors, & Paradiso, 2001).

In view of the fact that electric currents must pass different layers including the scalp, skull, brain and many other thin layers in between to be observable on scalp thereby the signal attenuates and spreads spatially. The EEG signal is recorded from electrodes attached to human scalp according to the international 10/20 system. The EEG is a measure of the electrical potential difference between regions of the scalp with respects to a reference electrode. The reference electrode has a considerable effect on the observed signal and it is typically attached on mastoids or ear lobes (Tatum, Husain, Benbadis, & Kaplan, 2008). In the present day, EEG signals are acquired in digital form; in other words, EEG signals are acquired by taking discrete electrical potential measurements from the scalp. Acquiring EEG in digital form allows for digital signal processing techniques to be used to extract information from the EEG.

1.1.4 Spectral Descriptor Electroencephalogram

1.1.4.1 Power Spectral Density of Spectral Descriptors

Power spectral density (i.e., PSD) measures the power of a signal distributed over the frequency domain (Knight A., 2010). A PSD is defined as the Fourier transform of the autocorrelation function. This estimate, referred to as a periodogram, is equivalent to computing the squared magnitude of the Fourier transform of a signal normalized by the length of the signal. PSD estimation methods developed by Bartlett, Blackman and Tukey, and Welch are regularly employed for spectral estimation methods (Proakis & Manolakis, 1992).

The Welch method of PSD estimation is an extension of Bartlett, which simply divides the signal into smaller segments and averaged their periodograms. Also, the Welch method incorporates an idea promoted by Blackman and Tukey, which states that applying a window to each of the smaller segments smooths the spectrum estimate. In the Welch method, the signal is divided into overlapping or non-overlapping smaller segments and a window is applied to each segment prior to computing the squared magnitude Fourier transform, i.e., periodogram.

Welch's version of the periodogram, which incorporates overlapping of segments and windowing, is called a modified periodogram (see Appendix C, Welch, 1967). The averaging of the modified periodograms results in the Welch PSD estimate (Signal Processing Toolbox™ User's Guide, 2013). Windowing of each segment prior to calculating it squared magnitude reduces spectral leakage, which if not done would introduce spurious frequencies by the abrupt truncation of the rectangular window

(Welch, 1967; Kay, 1988; Signal Processing Toolbox™ User's Guide, 2013). Overlapping the segments reduces the variance of the PSD, but with a loss in frequency resolution and the addition of overlapping segment bias to the spectrum estimation (Welch, 1967). The type of window selected, length of the window, and the percent of overlap between successive windows are the parameters that affect the Welch estimation PSD.

In this study, the Welch estimation method is used to compute the PSD of the acquire EEG signal. In order to extract the most significant information of the PSD Fourier transform properties inherent in PSD are used. One of the properties of the discrete Fourier transform is redundancy, which states that the representation of the signal at positive frequencies is represented again at the negative frequencies (Proakis & Manolakis, 1992).

This property implies that only one side of the PSD is needed and the resulting PSD is referred to as a one-sided PSD. It should be noted that when only using one-sided PSD, the complex components of the PSD must be multiplied by a factor of two to compensate for the missing half of components and the purely real and imaginary components remain the same (Proakis & Manolakis, 1992). The purely real frequency component located at frequency zero is the non-oscillatory component of the PSD.

It is the mean of the signal often referred to as the direct current offset or direct current component (i.e., D.C.-component) of the signal. The D.C. component of an EEG signal reflects the constant voltage measured at the interface from electrode to scalp and its power is typically set to zero after acquisition. In contrast to the physical meaning of

the purely real component, the purely imaginary component of the PSD does not have any physical meaning. Its purpose is purely mathematical. The remaining complex frequency components, having both a real and imaginary component, are the oscillatory components of the PSD.

It is the variance of the signal at each frequency often referred to as the alternating current components (i.e., A.C.-component) of the signal. It is explicitly the oscillatory or A.C. components of the PSD which are of most significance because they represent the oscillatory activity of the EEG rhythms. In this study the oscillatory components of the EEG is computed to measure the power of the EEG rhythms and used to compute each spectral descriptor value.

1.1.4.2 Spectral Entropy

The father of information theory Claude E. Shannon described the fundamental laws of data compression and transmission in his 1948 publication titled "A Mathematical Theory of Communication". In this publication, Shannon describes a method to measure the rate of information produced by a process. Conventionally regarded as Shannon entropy, this entropy is an expression that measures the average information, i.e., expected value of information, contained in a random process (Cover & Thomas, 2006; Shannon, 1948).

In probabilistic terms, Shannon entropy is viewed as the measure of uncertainty that is associated to a random process. The term uncertainty refers to the notion of the greater the number of choices, the greater the uncertainty in the outcome a process will express (Shannon, 1948). In respect to data compression and transmission, a random

process is viewed as a process that cannot compress below the irreducibility and complexity it intrinsically possesses.

In this publication, Shannon derived a function to measure the irreducibility and complexity intrinsically possessed in a random process and to measure the minimum limit a data compression scheme can achieve (Cover & Thomas, 2006). A property of Shannon entropy is that it is additive for independent events, i.e., extensive, it is possible to add zero probability states without changing the Shannon entropy value. Shannon entropy does not depend on the actual values of the random variable, but only on the probabilities of the values occurring.

Spectral entropy (i.e., SE) is an extension of Shannon Entropy (see Equation 1.1). Spectral entropy measures the intrinsic irregularity, complexity, and uncertainty of the power spectrum computed from a signal (Cover & Thomas, 2006). The power spectrum of a discretely sampled signal is divided by the sum of the power spectrum. If the power spectrum is divided by the sum of the power spectrum, then the power spectrum is transformed into a probability mass function. The Shannon entropy is calculated from the probability mass function then it is normalized by dividing it by the maximum entropy value, such as $H\_max = 1/\log\_b(R)$ (Shannon, 1948). The resulting spectral entropy value is a scale-invariant measure graded from 0 to 1.

$$SE = -\frac{1}{\log_b(R)} \sum_{r=0}^{R-1} \left(\left(\frac{\widehat{P}(\omega_r)_{\text{A.C. Cmpt}}}{\sum_{r=0}^{R-1} \widehat{P}(\omega_r)_{\text{A.C. Cmpt}}} \right) \cdot \log_b \left(\frac{\widehat{P}(\omega_r)_{\text{A.C. Cmpt}}}{\sum_{r=0}^{R-1} \widehat{P}(\omega_r)_{\text{A.C. Cmpt}}} \right) \right) \quad (1.1)$$

Uniformly distributed probability mass function cause the spectral entropy expression to give a graded measure of 1. A Dirac distribution of the probability mass

function with zero variance causes the spectral entropy to give a graded measure of 0. Shown in Figure 1.7 is an array of different, normally distributed probability mass functions and spectral descriptor value it yields. From top to bottom the mean value of the distribution shifts from -3.5 to 3.5 and the variance of the distribution is a constant value. Shown in Figure 1.7, the spectral entropy values do not show a pronounced sensitivity to changes in mean of the normal distributions. From left to right the variance increases from a narrow distribution (i.e., Dirac distribution) to a wide distribution (i.e., uniform distribution) and the mean value of the distributions is a constant value.

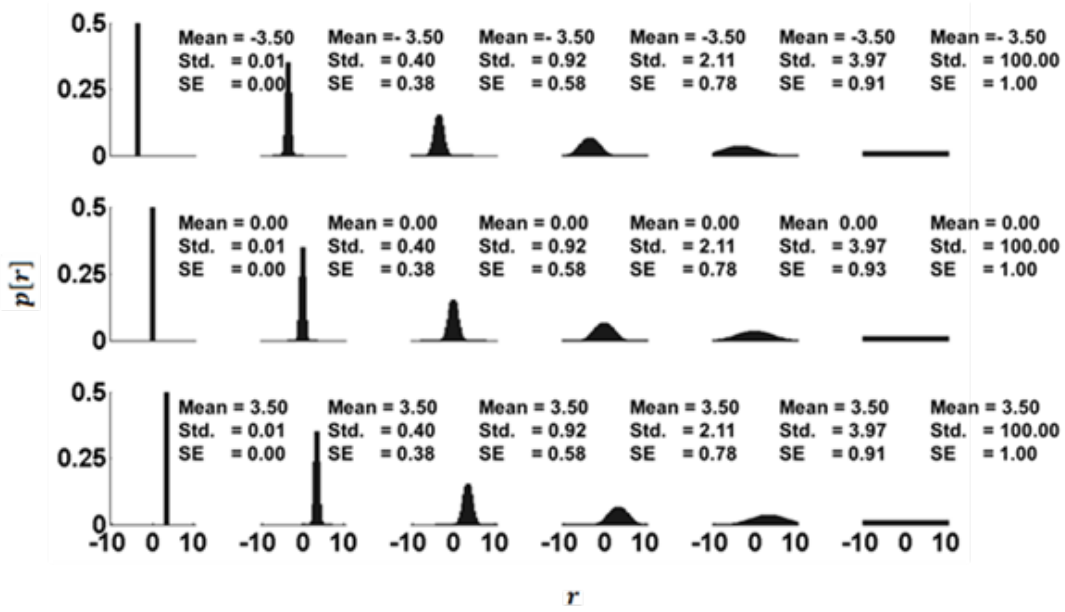

Figure 1.7 Spectral entropy for distributions varied by mean and variance. From top to bottom the mean value of the distribution shifts from -3.5 to 3.5 and the variance of the distribution is a constant value. From left to right the variance increases from a narrow distribution (i.e., Dirac distribution) to a wide distribution (i.e., uniform distribution) and the mean value of the distribution is a constant value. The spectral entropy values do not show a pronounced sensitivity to changes in mean value of the distribution and does show a pronounced sensitivity to changes in variance of the distribution.

Shown in Figure 1.7, the spectral entropy values do show sensitivity to changes in variance of the normal distribution. As shown in Figure 1.7, due to its sensitivity to the

spread of the probability mass function distribution, spectral entropy measures how different the probability mass function of a signal is from uniform distribution (i.e., white noise).

Stated differently it measures the flatness of the probability mass function distribution (Shannon, 1948). Spectral entropy does not account for the mean (i.e., central tendency) or the width of the variance of the probability mass function; it only accounts for the shape (i.e., sharpness or flatness) of the probability mass function. It grades the distinction the power spectrum has either from flat shape of the uniform distribution or the sharp shape of the Dirac distribution.

Spectral entropy grades the EEG power spectrum transition from a uniform distribution, i.e., horizontal-line shaped spectrum, to a Dirac distribution, i.e., a vertical-line shaped spectrum. Shown in Figure 1.8, (b), the power spectrum of spontaneous EEG for a subject in a resting wakefulness state resembles the broad and flat distribution similar to the uniform distribution.

Shown in Figure 1.8 (d), the power spectrum of spontaneous EEG for a subject in stage N3 sleep state the narrow and sharp distribution similar to the Dirac distribution. The EEG of the resting wakefulness subject, shown in Figure 1.8 (a) has greater complexity and irregularity in its EEG, which represent by the greater number of active frequency bins in its power spectrum, compared to the same subject under stage N3 sleep, shown in Figure 1.8 (c). Stage N3 sleep has less complexity and irregularity as reflected by reduction in frequency bins of EEG power spectrum. The low frequency high amplitude power spectrums of stage N3 sleep state.

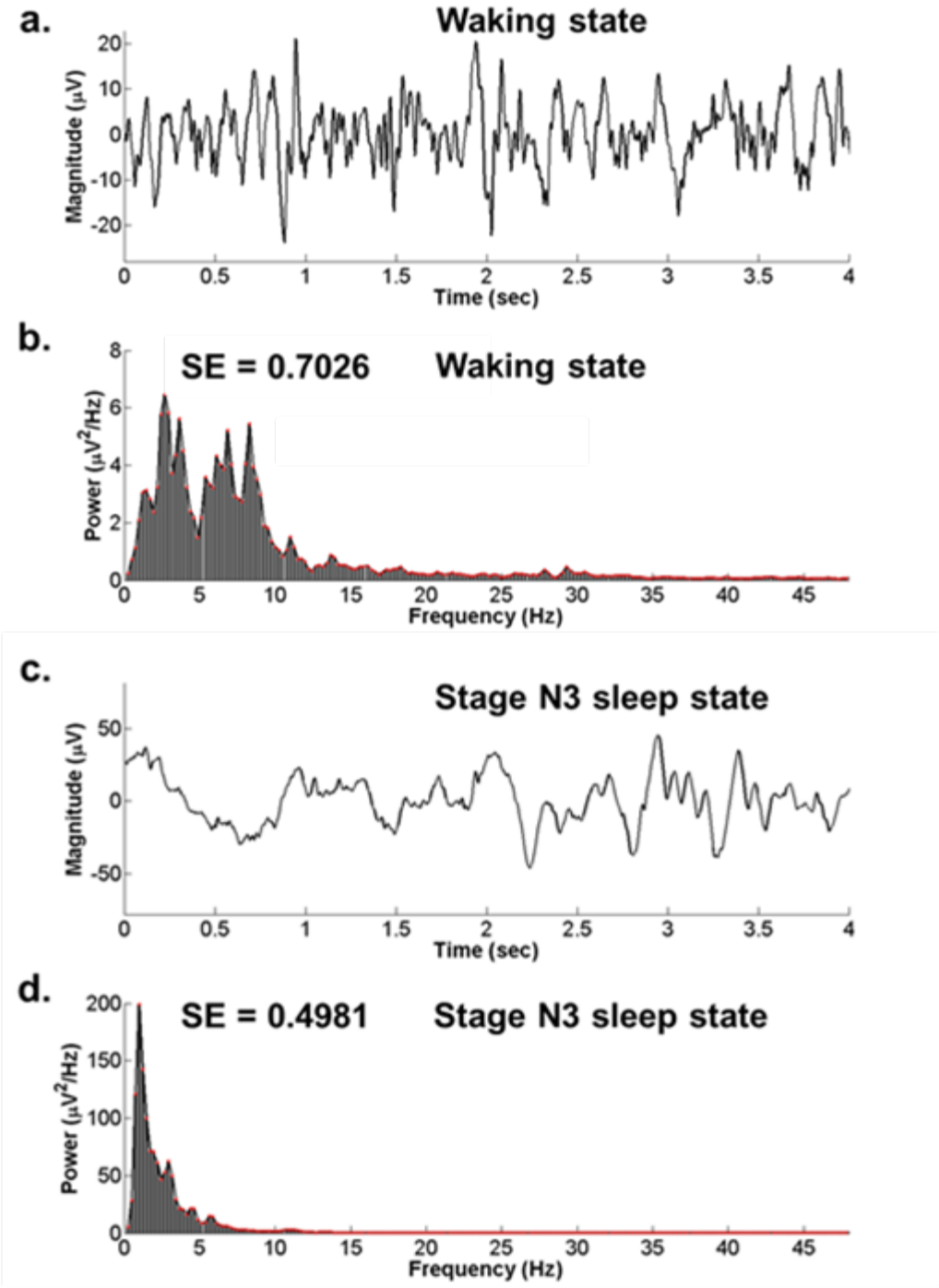

Figure 1.8 Spectral entropy for waking and stage N3 sleep stages. (a) Shows the EEG signal of a subject in waking state. (b) Shows the power spectrum of the signal in (a) and its spectral entropy value. (c) Shows the EEG signal of the same subject in stage N3 sleep state. (d) Shows the power spectrum of the signal in (c) and its spectral entropy value. The spectral entropy value is less for stage N3 sleep than for waking. Spectral entropy ranges from 0 (i.e., less complexity and irregularity of the EEG signal) to 1 (i.e., greater complexity and irregularity of the EEG signal).

EEG represents a greater synchronization of neuronal activity compared to the spontaneous EEG of the resting wakefulness state as shown by the increase of power in the delta band frequency (i.e., 1 to 4 Hz). The processes that created the higher frequency bins observed in spontaneous EEG are diminished by the regulatory sleep processes down-scaling the number of active neurons (Velluti, 2008).

Spectral entropy grades theses changes in the subject state reflected in the power spectrum with a score of SE = 0.7026 (see Figure 1.8 (b)) for resting wakefulness state and a score of SE = 0.4981 (see Figure 1.8 (d)) for stage N3 sleep state.

1.1.4.3 Spectral Edge Frequency

Spectral edge frequency (i.e., SEF) is a spectral descriptor that denotes the frequency value marking where 90 percent of the total power spectrum (see Equation 1.2). In the literature, different author measure the SEF either at 90 or 95 percent of the total power; however they do not indicate a physiological reason for the choice only that 95 percent of the total power provides a stricter limit than does 90 percent of the total power (see Equation 1.2).

The frequency component indicating 95 percent of the total power is analogous to the notion of using 95 percentile of the distribution in statistics. In statistics, the frequency component that indicates the 95th percentile boundary of the distribution reveals the number of active frequency components that are below it, that is, below the frequency component that indicates the 95th percentile boundary.

In this case, the SEF is the frequency that bisects the power distribution into 95% and 5% of the total power. The frequency component that indicates the 95th percentile of all frequencies of power contained in the signal is the spectral edge frequency (i.e., SEF).

$$SEF = \frac{1}{2\pi} arg\left(\hat{P}(\omega_r)_{A.C.\ Cmpt} = \frac{95}{100} \cdot \sum_{r=0}^{R-1} \hat{P}(\omega_r)_{A.C.\ Cmpt}\right) \quad (1.2)$$

This means that only 5% of all the frequencies under study are greater than SEF value and 95% of all frequencies under study are below SEF value.

Spectral entropy accounts for the sharpness or flatness of the distribution not its location (i.e., mean). SEF, in contrast, is sensitive to the mean and variance of the power spectrum distribution (see Figure 1.9). The SEF marks the outer edge of the power spectrum relative to its total power.

Shown in Figure 1.9 is the same array used in Figure 1.7 the spectral edge frequency value for each probability mass function is calculated. From top to bottom the mean value of probability mass function increases and the variance is held constant, and from left to right, the variance increases from a narrow distribution (i.e., Dirac distribution) to a wide distribution (i.e., uniform distribution) and the mean is held constant.

If the variance decreases and the mean increases of the probability mass function or visa-versa then SEF value will change relative to both of these values. Two different probability mass functions can give the same SEF value as shown in Figure 1.9 (row 3, col. 1 & row 2, col. 4). This is not observed in the spectral entropy values for the identical Figure 1.7 (row 3, col. 1 & row 2, col. 4).

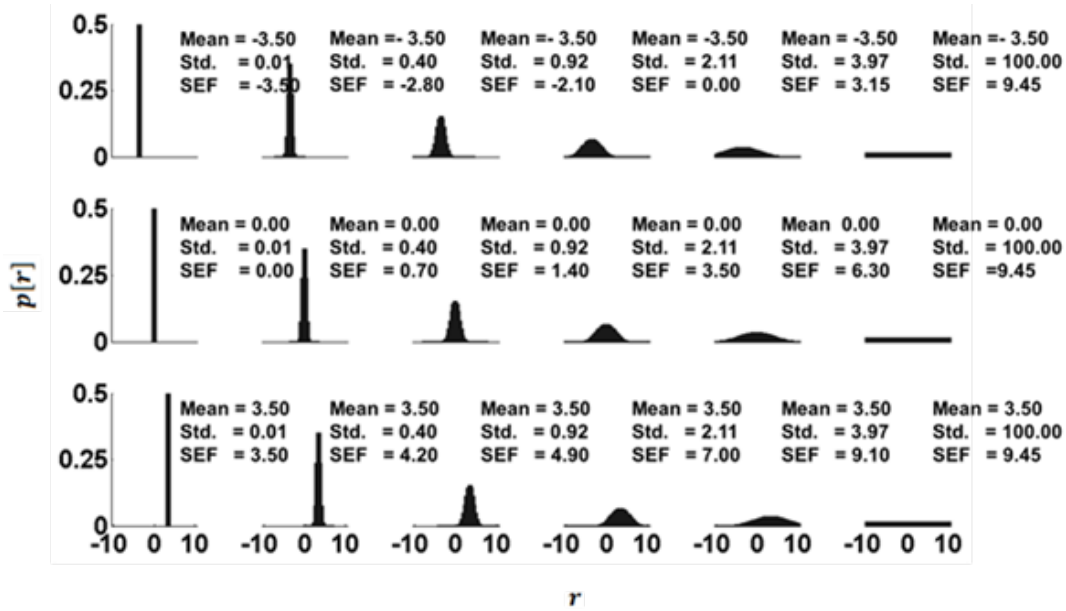

Figure 1.9 Spectral edge frequency for a distribution varied by mean and variance. From top to bottom the mean value of the distribution shifts from -3.5 to 3.5 and the variance of the distribution is a constant value. From left to right the variance increases from a narrow distribution (i.e., Dirac distribution) to a wide distribution (i.e., uniform distribution) and the mean value of the distribution is a constant value. The spectral edge frequency values show sensitivity to changes in mean and variance of the distribution.

EEG tends to transition from high-frequency, low-amplitude power spectrum (see Figure 1.10 (b)) to a low-frequency, high-amplitude power spectrum when it transition from resting wakefulness state to stage N3 sleep state (see Figure 1.10 (d)) and similarly in anesthesia EEG. The EEG's property of shifting its frequency towards lower frequency bands would reflect the shift of mean toward lower mean values. The processes that created the higher frequency bins observed in spontaneous EEG are diminished by the regulatory processes sleep down-scaling the number of active neurons (Velluti, 2008).

The SEF scores EEG of the resting wakefulness state of the subject SEF = 18.70 and the stage N3 sleep state as SEF = 4.90. The SEF reduced as both the central tendency and variance of the power spectrum decreased as the subject changed from

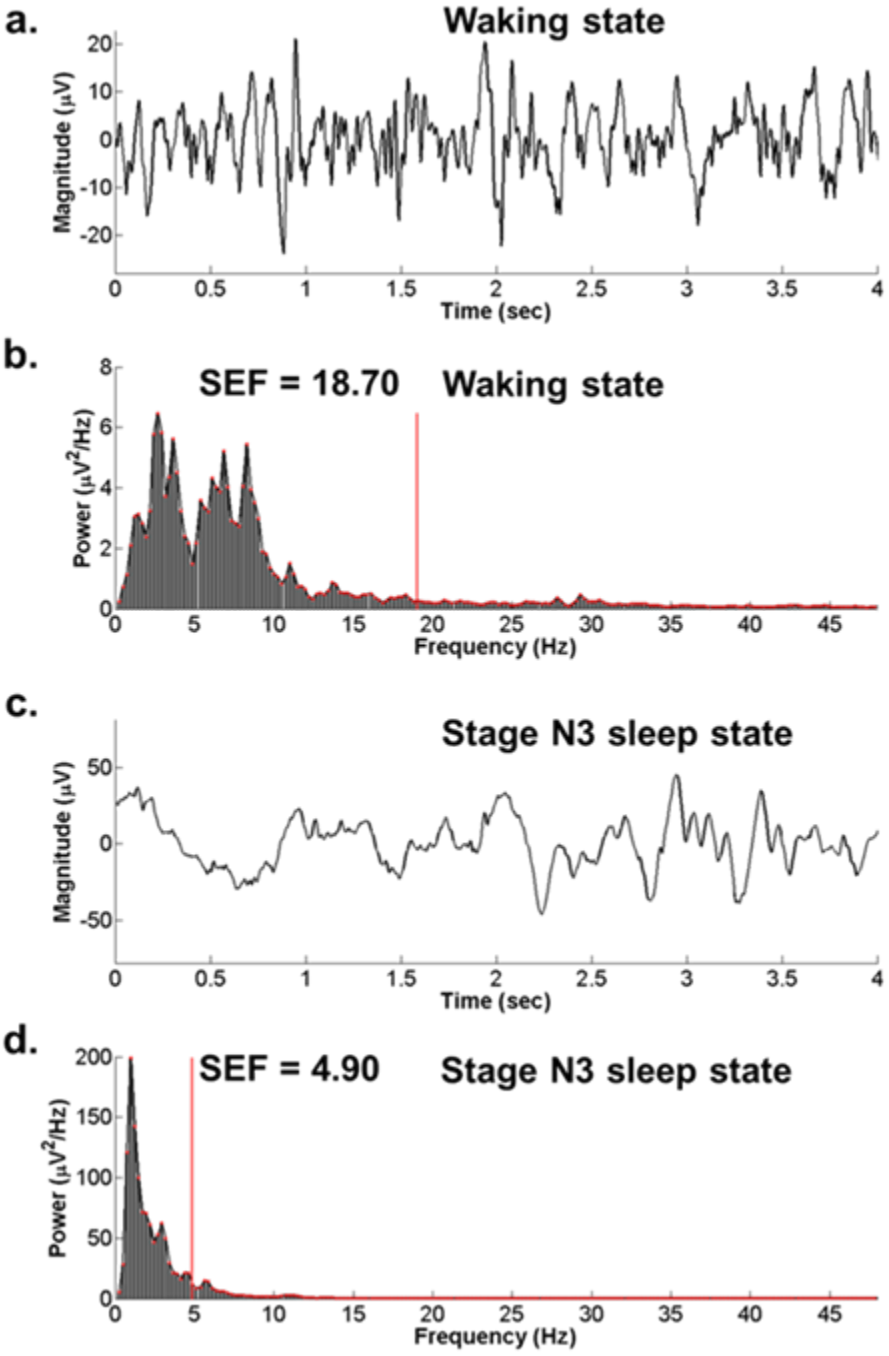

Figure 1.10 Spectral edge frequency Spectral entropy for waking and stage N3 sleep stages. (a) Shows the EEG signal of waking state. (b) Shows the power spectrum of the signal in row 1and the SEF value. (c) Shows the EEG signal of stage N3 sleep state. Row 4 shows the power spectrum of the signal in row 3 and the SEF value. The SEF value is less for sleep than for awake. The SEF marks the frequency indicating 95% of the total power contained in the power spectrum.

waking (see Figure 1.10 (b)) to sleep (see Figure 1.10 (d)). These changes in the EEG power spectrum distribution would most notably occur within each of the classical frequency band of the EEG.

1.1.4.4 Median Frequency

Median frequency (i.e., MF) is a spectral descriptor that denotes the frequency value marking where 50th percentile of the total power spectrum (see Equation 1.2). It is calculated similar to the SEF, but it is indicative of an important and different property of the power spectrums distribution than the SEF – the central tendency of the power spectrum. In statistics, the mean is the most common method used to measure the central tendency of a distribution. A beneficial property of measuring the central tendency using the median is that the median is not sensitive to small number of extreme values (i.e., outlier values). The mean as a measure of central tendency is sensitive to extreme values and in the event of an extreme value the measure central tendency would greatly deviate from its true central tendency. The MF bisected the distribution of the power spectrum into two equal portions.

$$MF = \frac{1}{2\pi} arg\left(\hat{P}(\omega_r)_{A.C.\ Cmpt} = \frac{50}{100} \cdot \sum_{r=0}^{R-1} \hat{P}(\omega_r)_{A.C.\ Cmpt}\right) \quad (1.3)$$

As the distribution of the probability mass function skews, the MF will move with the transitions of the distributions. Shown in Figure 1.11 is the same array used in Figure 1.7 and Figure 1.9 the median frequency value for each probability mass function is calculated. From top to bottom the mean value of probability mass function increases and the variance is held constant. From left to right the variance increases from a narrow distribution (i.e., Dirac distribution) to a wide distribution (i.e., uniform distribution) and

the mean is held constant. Shown Figure 1.11 the variance does not significantly change the MF values. The MF accurately measures the central tendency of the probability mass functions.

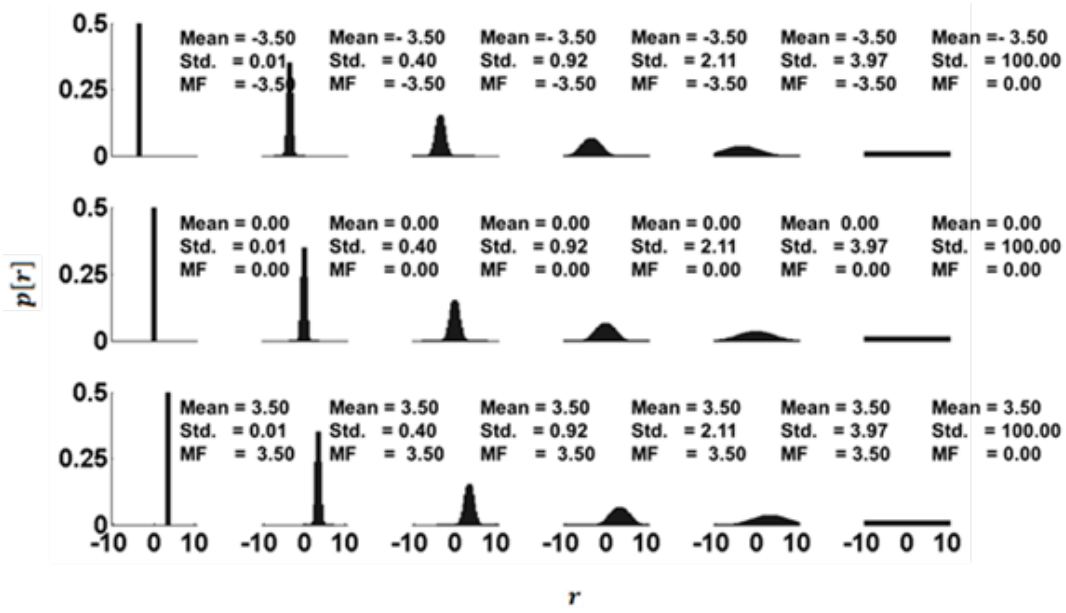

Figure 1.11 Median frequency for a distribution varied by mean and variance. From top to bottom the mean value of the distribution shifts from -3.5 to 3.5 and the variance of the distribution is a constant value. From left to right the variance increases from a narrow distribution (i.e., Dirac distribution) to a wide distribution (i.e., uniform distribution) and the mean value of the distribution is a constant value. The median frequency values show sensitivity to the changes in the mean and not to the changes in the variance of the of probability mass function.

As EEG transitions from high-frequency, low-amplitude power spectrum, e.g., waking state, (see Figure 1.12 (b) to a low-frequency, high-amplitude power spectrum, e.g., stage N3 sleep state, (see Figure 1.12 (d). The MF will move according to the shift in central tendency of the power spectrum.

MF is distinct in its sensitivity to changes in the power spectrum compared to SEF. The MF values are mostly sensitive to changes in the central tendency, while the SEF is sensitive to the composite of both the central tendency and the variance. MF is

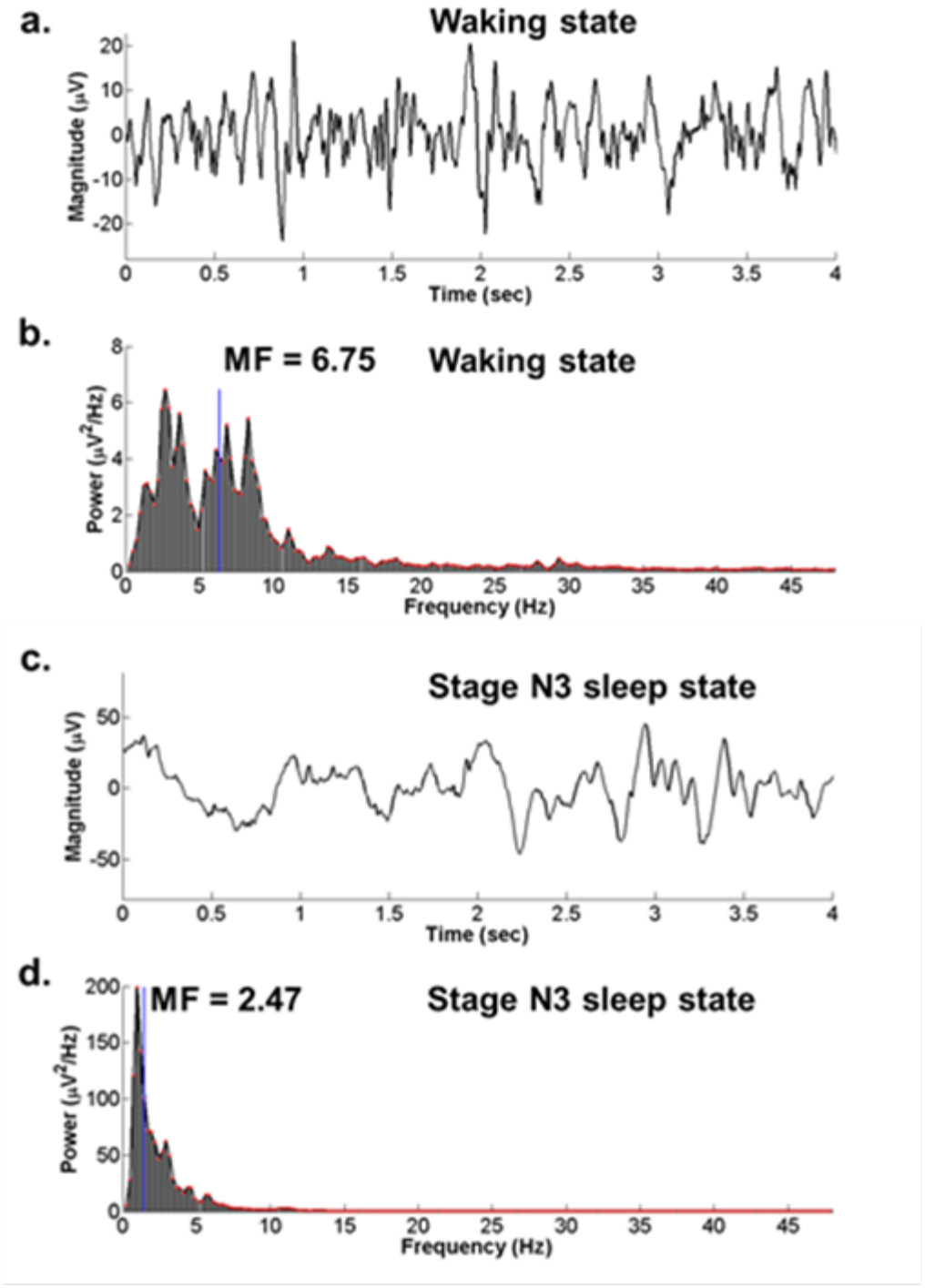

Figure 1.12 Median frequency for waking and stage N3 sleep stages. (a) Shows the EEG signal of waking state. (b) Shows the power spectrum of the signal in (a) and the MF value. (c) Shows an EEG signal of the stage N3 sleep state. (d) Shows the power spectrum of the signal in (c) and the MF value. The MF value is less for stage N3 sleep than waking. The MF indicates the central tendency of the power spectrum.

more resistant to changes in the power spectrum compared to the SEF as shown in Figure 1.2 (b) the MF for the waking state was MF = 6.75 and in the stage N3 sleep state was MF =2.47.

1.1.4.5 Power Ratio and Total Power

The power ratio (i.e., PR) is a power spectrum descriptor that is the ratio of power from each of the frequency band of the classical EEG rhythms divided by the total power within the power spectrum. It is a spectral descriptor that is exclusively calculated from EEG signal because it utilizes a core property of EEG - subject state is correlated to activity of specific frequency bands of EEG power spectrum.

PR is designated according to EEG rhythms such as: (a) Delta PR (δ-PR) is the power within the delta frequency band (1 to 4 Hz) divided by the total power of the spectrum (see Equation 1.4); (b) Theta PR (θ-PR) is the power within the theta frequency band (5 to 7 Hz) divided by the total power of the spectrum (see Equation 1.4); (c) Alpha PR (α-PR) is the power within the alpha frequency band (8 to 13 Hz) divided by the total power of the spectrum (see Equation 1.5); (d) Beta PR (β-PR) is the power within the beta frequency band (13 to 30 Hz) divided by the total power of the spectrum (see Equation 1.6); and (e) Gamma (γ-PR) is the power within the gamma frequency band (30 to 48 Hz) divided by the total power of the spectrum (see Equation 1.7).

In this study, gamma was set to 30 to 48 Hz because at increased depth of anesthesia and sleep a strong decline in power was observed beyond the 30 Hz. In light of the strong decline and to make our measured PR values comparable to previous research this range was used for gamma. In this study, the lower range of delta was set to

1 Hz because that is the lowest frequency setting of the acquisition instrument. The ratio of power within the EEG rhythms divided by the total power normalizes the of the power spectrum producing a probability density function of the power spectrum. It is multiplied by 100 to express its values in term of percentage, where 100 percent is the total power.

$$PR_{\delta} = 100 \cdot \frac{\hat{P}(\omega_r)_{A.C.\ Cmpt}\Big|_{\omega_r=2\pi\cdot 1Hz}^{\omega_r=2\pi\cdot 4Hz}}{\sum_{r=0}^{R-1}\hat{P}(\omega_r)_{A.C.\ Cmpt}}, \text{where } 1\ Hz < f_r \leq 4\ Hz \quad (1.4)$$

$$PR_{\alpha} = 100 \cdot \frac{\hat{P}(\omega_r)_{A.C.\ Cmpt}\Big|_{\omega_r=2\pi\cdot 8Hz}^{\omega_r=2\pi\cdot 13Hz}}{\sum_{r=0}^{R-1}\hat{P}(\omega_r)_{A.C.\ Cmpt}}, \text{where } 8\ Hz < f_r \leq 13\ Hz \quad (1.5)$$

$$PR_{\beta} = 100 \cdot \frac{\hat{P}(\omega_r)_{A.C.\ Cmpt}\Big|_{\omega_r=2\pi\cdot 13Hz}^{\omega_r=2\pi\cdot 30Hz}}{\sum_{r=0}^{R-1}\hat{P}(\omega_r)_{A.C.\ Cmpt}}, \text{where } 13\ Hz < f_r \leq 30\ Hz \quad (1.6)$$

$$PR_{\gamma} = 100 \cdot \frac{\hat{P}(\omega_r)_{A.C.\ Cmpt}\Big|_{\omega_r=2\pi\cdot 30Hz}^{\omega_r=2\pi\cdot 48Hz}}{\sum_{r=0}^{R-1}\hat{P}(\omega_r)_{A.C.\ Cmpt}}, \text{where } 30\ Hz < f_r \leq 48\ Hz \quad (1.7)$$

PR is only dependent on the power values within the EEG rhythms or on the total power of the power spectrum. As shown in Figure 3.13, the distribution of the probability density function of the EEG rhythms can be correlated to the state of the subject. The scale or range of power spectrum can undergo significant changes as the subject state changes.

The range of the power spectrum is within the range 0 to 8 μV2/Hz for the waking state (see Figure 1.13, (b)) and the range of the power spectrum is within the range 0 to 200 μV2/Hz for the stage N3 sleep state (see Figure 1.13, (d)). The power ratio does not account for the significant changes of the power range.

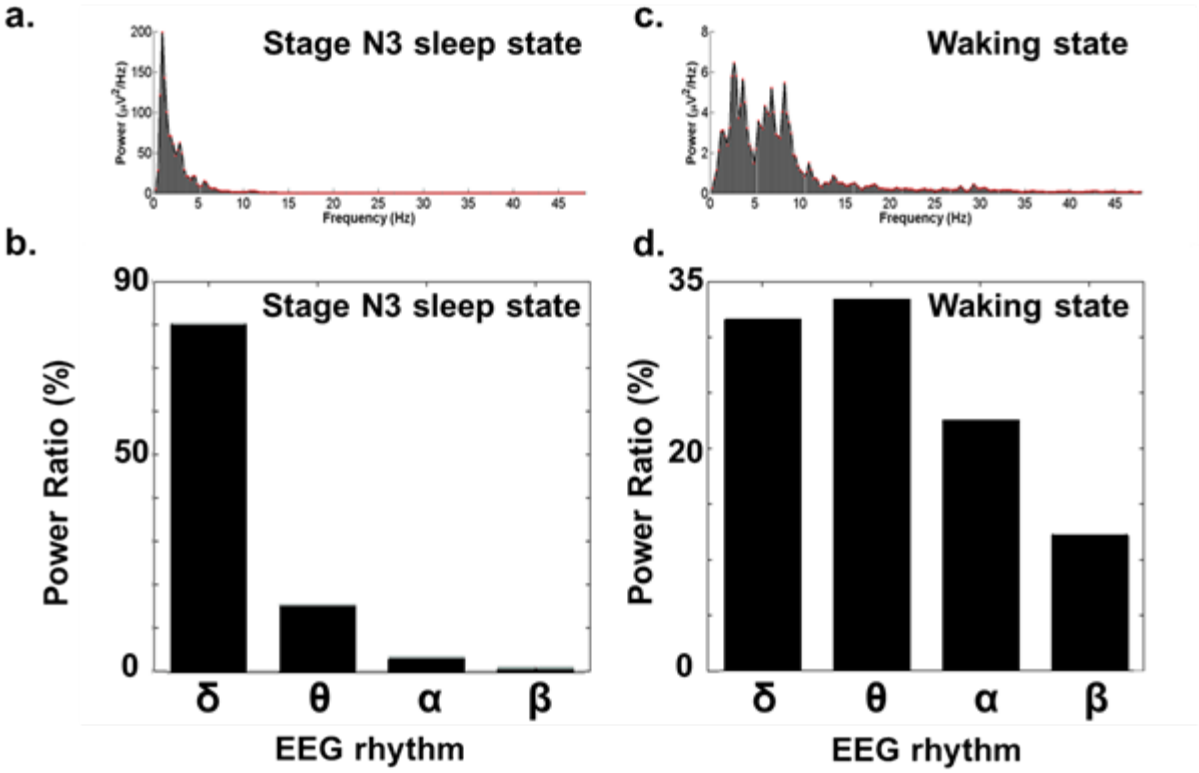

Figure 1.13 Power ratio for waking and stage N3 sleep stages. (a) Shows the power spectrum of the waking state. (b) Shows the PR in the waking state for each EEG rhythms, e.g., δ-delta, θ-theta, α-alpha, and β-beta. (c) Shows the power spectrum of stage N3 sleep state. (d) Shows the PR in the stage N3 sleep state for each EEG rhythms, e.g., δ-delta, θ-theta, α-alpha, and β-beta. The PR is expressed in percentage from 0 to 100%. Significant increase is observed in the lower frequency EEG rhythms and a significant decrease in the higher frequency EEG rhythms for the stage N3 sleep state compared to the waking state.

Total power (i.e., TP) is a spectral descriptor that indicated the total power contained in the power spectrum independent of the distribution of the power values (see Equation 1.8). It is a spectral descriptor that supplements the power ratio spectral descriptor and the previously mentioned descriptors. PR values are dependent on the total power used to calculate.

If the distribution of the power within the EEG rhythms changes proportionally with respect to the total power then the PR will not reflect this change. TP accounts for

the rise or decline of the strength of activity of the EEG's power spectrum. An increase in the EEG power spectrum is indicative a higher synchronization of neural activity (Bear, Connors, & Paradiso, 2001). TP represents the global activity of the observed EEG signal.

$$TP = \sum_{r=0}^{R-1} \hat{P}(\omega_r)_{A.C.\ Cmpt} \tag{1.8}$$

1.1.5 Effects of Anesthesia on Electroencephalogram

Anesthesia is defined as the reversible loss of consciousness, caused by a drug; from which arousal does not take place even after painful stimuli is applied (Duke, 2011; Miller, 2009; Mashour, 2010; Barach, Cullen, & Stoelting, 2006). General anesthetics are powerful nervous system suppressors (Orser, 2007).

Anesthetic drugs are empirically developed to produce anesthetic state properties commonly referred to as the four "A" (Sweeny, 2003) such as, Analgesia (i.e., absence of pain), Amnesia (i.e., loss of memory), Anesthesia (i.e., unconsciousness), and Akinesia (i.e., absence of motion) (Alkire, 2009).

Anesthetic drugs are broadly grouped into either intravenous or inhalation anesthetics drugs (Sweeny, 2003). Intravenous anesthetic drugs include the opiates such as fentanyl, remifentanil, sufentanil, alfetanil, morphine, hydromorphone, meperidino, methadone, and tramadol; the benzodiazepines such as midazolam, diazepom, and lorazepom, the barbituates such as propofol, thiopental, methohexical, etomidate, and ketamine (Alkire, 2009; Barach, Cullen, & Stoelting, 2006; Duke, 2011; Miller, 2009).

Intravenous anesthetic drugs are commonly used for rapid induction; however, continuous infusion of intravenous anesthetics may be used to sustain the maintenance stage of anesthesia (Sweeny, 2003). Another application of intravenous anesthetics is to provide sedation.

Inhalation anesthetics drugs include the nonhalogenated such as nitrous oxide and xenon; the halogenated such as isoflurane, desflurane, sevoflurane, and halothane (Alkire & Lukasz, 2004). An advantage of inhaled anesthetics is the concept of the minimum alveolar concentration (i.e., MAC) for assessing inhaled anesthetic potency (Sonner, et al., 2003; Alkire, 2009).

Calibrated vaporizers mix controlled doses of anesthetic agents with a carrier gas, such as oxygen. The vaporizer permits the anesthesiologist administering the inhaled agent to rapidly adjust the concentration of the inhaled agent by rotating the dial of the vaporizer device to a desire concentration according to the patient's requirement (Sweeny, 2003).

During surgery, the anesthetic end-point of general anesthesia is broadly divided into the induction phase of anesthesia, the maintenance phase, and the emergence phase (Duke, 2011; Sweeny, 2003). General anesthesia effects electroencephalogram towards an increase in high-amplitude, low-frequency activity as the state of general anesthesia deepens (Brown, Lydic, & Schiff, 2010). The EEG of a patient before induction will demonstrated alpha rhythm activity when eyes are closed and mixture of higher EEG rhythms.

A small dose of a hypnotic drug, e.g., propofol, a barbiturate, or etomidate will induce the patient into a sedative state. If the small dose of the hypnotic drug is increased slowly, the patient will be induced into a paradoxical excitation state – the agent is supposed to induce unconsciousness but instead induces paradoxical excitation (see Figure 1.14).

This state is characterized by the patient demonstrating incoherent speech, purposeless movements, and euphoria or dysphoria (Brown, Lydic, & Schiff, 2010), (Bevan , Veall, Macnab , Ries , & Marsland, 1997; Clark & Rosner, 1973; Gibbs, Gibbs, & Lennox, 1937; Kiersey, Bickford, & Faulconer, 1951; McCarthy, Brown, & Kopell , 2008; Rampil, 1998).

In the paradoxical excitation state, the EEG will demonstrate an increase in beta rhythm activity. Induction occurs, when a bolus dose of the hypnotic drug is given over a period of 10 to 15 seconds then the patient is induced into an unconsciousness state.

The maintenance period of general anesthesia is sustained by using a combination of intravenous anesthetics (i.e., hypnotic agents) and inhalation anesthetics (i.e., inhaled agents), opioids, muscle relaxants, sedatives, and cardiovascular drugs, together with ventilatory and thermoregulatory support (Posner, Saper , Schiff , & Plum, 2007; Gelb, Leslie, Stanski, & Shafer, 2009). The concentration of the anesthetic agents is adjusted in responds to the physiological indicators, which are monitored throughout the surgery (Gelb, Leslie, Stanski, & Shafer, 2009; Sweeny, 2003).

The maintenance period has four phases each with distinct EEG patterns (see Figure 1.14). Light state of general anesthesia (i.e., phase 1) has a decreased beta activity with increase alpha and delta activity (Feshchenko, Veselis, & Reinsel, 2004).

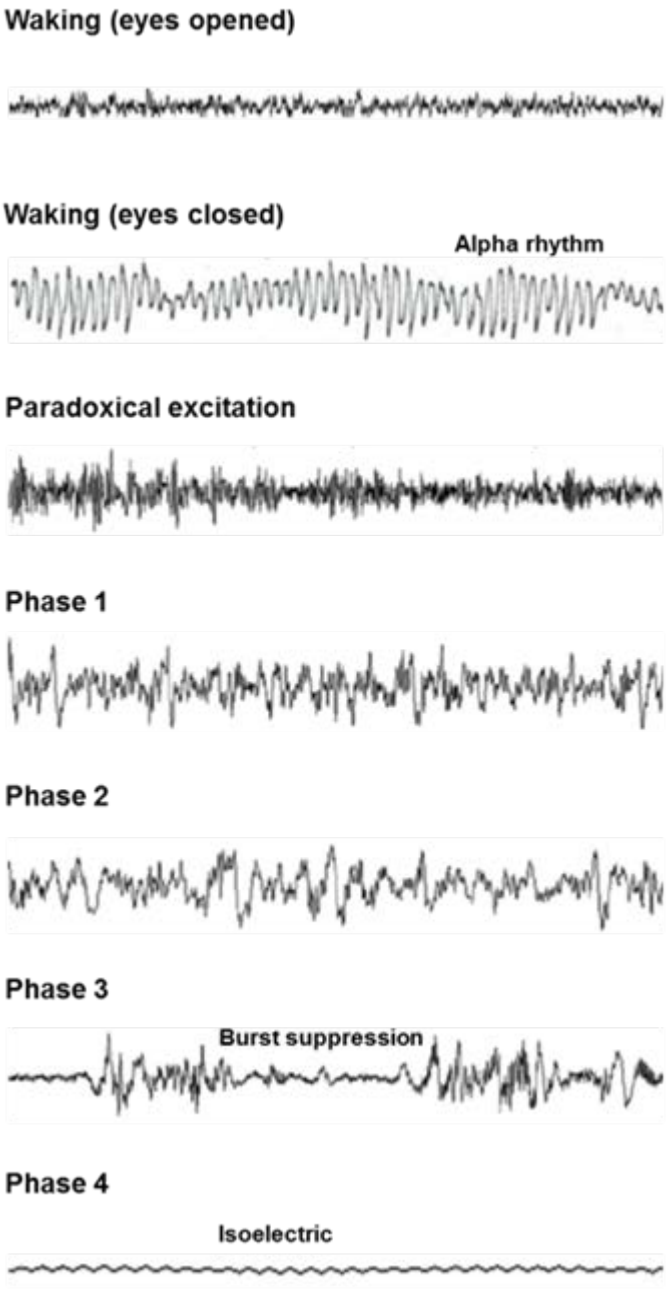

Figure 1.14 EEG of each phase of general anesthesia. Adapted from (Brown, Purdon, & Van Dort, 2011)).

Intermediate state of general anesthesia (i.e., phase 2) has a decrease beta activity with increase alpha and delta activity increases with anteriorization. Anteriorization is an increase in alpha and delta activity in the anterior regions relative to the posterior regions (Feshchenko, Veselis, & Reinsel, 2004; Tinker, Sharbrough, & Michenfelder , 1977). The EEG of phase 2 maintenance resembles EEG observed in stage N3 sleep or slow-wave sleep. Deeper state of general anesthesia (i.e., phase 3) has flat periods interspersed with periods of alpha and beta activity referred to as burst suppression (Clark & Rosner, 1973).

Profound state of general anesthesia (i.e., phase 4) is characterized by an isoelectric EEG pattern (Bergey, 2006; Claassen , Hirsch, Emerson, & Mayer , 2002). The emergence period is when potent anesthetics agent cease to be delivered and reversal agents are administered to return the patient to waking state (Duke, 2011; Sweeny, 2003). Reversal agents are antagonist agents that block or inhibit the effects of anesthetic agents. Examples of reversal agents are naloxone, methylnaltreone, and flumazenil (Alkire, 2009).

Vital physiological functions must be reestablished as the patient emerges from anesthesia. A patient has emerged from anesthesia when the patient has resumed an adequate performance of vital functions and an adequate level of consciousness. The EEG patterns reestablish are consistent with the waking state.

Compared to the induction phase of anesthesia, the emergence phase of anesthesia takes longer than a few seconds. In general, the EEG during general anesthesia with propofol or potent inhaled volatile agents exhibits high-amplitude, low-frequency EEG

rhythm activity, typically in the delta rhythms frequency band company with decrease low-amplitude, high-frequency EEG rhythm activity, typically in the beta rhythms frequency band (Jagadeesan, Wolfson, Chen, Willingham, & Avidan, 2013).

1.1.6 Effects of Sleep on Electroencephalogram

Sleep is a highly active and dynamic process that modulates spontaneous brain activity, such as EEG, and brain potentials evoked by external stimulation, such as AEPs. Sleep may be reversed through external stimuli. Sleep is composed of two distinct states: (a) nonrapid-eye movement (NREM) and (b) rapid-eye movement (REM) or paradoxical sleep (Silber, et al., 2007). The NREM sleep is further divided into four stages that correspond to the depth of sleep e.g., stages 1 and 2 are light sleep and stage 3 and 4 are deep sleep (see Figure 1.15).

In 2007, Visual Scoring Task Force reclassified the stages of sleep as follows: (a) Stage W (i.e., waking or wakefulness), (b) Stage N1 (i.e., drowsiness and sleep onset), (c) Stage N2 sleep (i.e., light sleep), (d) Stage N3 (i.e., deep sleep or slow-wave sleep), and (e) Stage R (i.e., paradoxical sleep) (Silber, et al., 2007).

Wakefulness or waking state EEG is characterized by high frequency beta EEG rhythms with low amplitude 10 to 30 μV accompanied by high muscular tonus (Pace-Schott & Hobson, 2002). The presences of eye blink artifacts are observed because the eyes are open. In an eyes closed relaxed and resting wakefulness state the EEG measured at the occipital location is characterized by an alpha EEG rhythm with an increased amplitude of 20 to 40 μV compared to the more active eyes open wakefulness state (Morin & Espie, 2012).

Stage N1 sleep is the intermediate state between waking and sleep referred to as drowsiness. Stage N1 EEG is characterized by the occurrence of theta EEG rhythm with a greater amplitude 50 to 100 μV and a decrease in muscular tonus compared to the stage N1 sleep (Morin & Espie, 2012). The presence of slow eye moment is observed during this stage N1 sleep (Iber, Ancoli-Israel, Chesson, & Quan, 2007). The attenuation of the alpha rhythm is considered a valid electrophysiological marker of sleep onset (Silber, et al., 2007). At this stage the subject may fail to respond to audible tones but the threshold required for awakening is low compared to the deeper stages of sleep (Morin & Espie, 2012).

Stage N2 sleep is considered light sleep. It is characterized with basal EEG rhythms below 5 Hz and accompanied by transient EEG events called sleep spindles and K-complexes. Sleep spindles are short lasting EEG events about 0.5 to 3 sec in duration with waxing and waning oscillations rhythms in the sigma (i.e., σ) range, i.e., 11 to 16 Hz and whose maximal amplitude is observed at the central location (Borbély, Hayaishi, Sejnowski, & Altman, 2000; De Gennaro, Ferrara, & Bertini, 2000; McCormick, Nielsen, Nicolas, Ptito, & Montplaisir, 1997). K-complexes are short lasting EEG events about at least 0.5 sec. and optimally observed at the frontal location (e.g., Fz or F4) (Iber, Ancoli-Israel, Chesson, & Quan, 2007). Its shape is described as a negative sharp wave of high amplitude followed by a positive wave.

Stage N3 sleep is the deepest of the NREM sleep stages and has the highest arousal threshold for awakening. It is characterized by slow waves EEG rhythms between 0.5 to 2 Hz (Iber, Ancoli-Israel, Chesson, & Quan, 2007). These slow waves are maximally expressed at the frontal location (Iber, Ancoli-Israel, Chesson, & Quan, 2007).

Stage R referred to as paradoxical sleep because the subject appears to be unresponsive but their EEG resembles the EEG activity of the waking state.

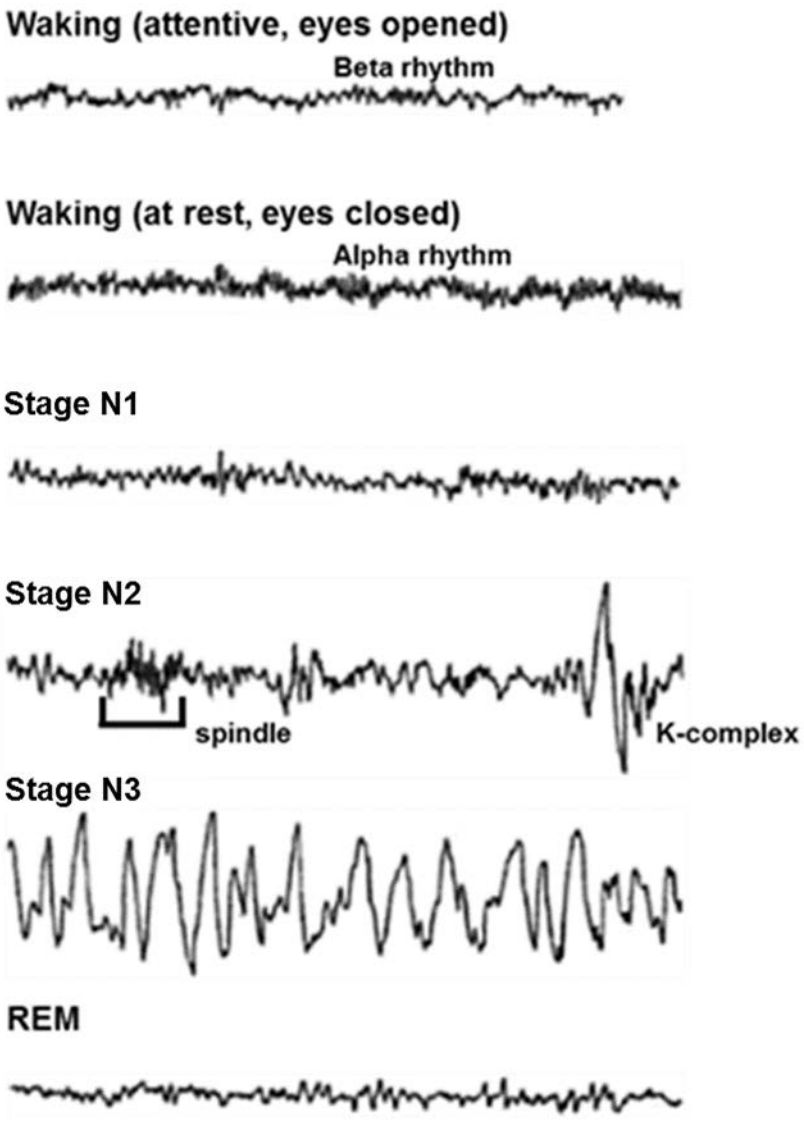

Figure 1.15 EEG of each stage of sleep. Adapted from (Morin & Espie, 2012).

Stage R sleep is characterized by the following main features a mixture of high frequencies in the range of 15 to 30 Hz with a low amplitude less than 50 μV, rapid eye movement, muscular atonia, breath irregularity, and cardiovascular irregularity (Morin & Espie, 2012).The presence of saw-tooth waves, which are trains of sharply or triangular

shaped 2 to 6 Hz waves (Iber, Ancoli-Israel, Chesson, & Quan, 2007). Subjects awaken during REM sleep frequently recall dreaming (Kandel, Schwartz, & Jessell, 2000).

1.2 Evoked Potential

Evoked potentials (i.e., EPs) are classified according to the sensory system that generates the response. EPs have names such as auditory evoked potential, visual evoked potential, somatosensory evoked potential, olfactory evoked potential, and gustatory evoked potential. EPs are further classified according to the origin of the stimulus as exogenous and endogenous: (a) exogenous evoked potentials are elicited by the physical characteristics of the external stimulus and (b) endogenous evoked potentials are elicited by internal brain processes and respond to the significance of the stimulus.

In this study, exogenous auditory evoked potentials (i.e., AEPs or EPs) will be investigated and the term EP will be used interchangeably to refer to auditory evoked potential. Auditory evoked potentials are waveforms also referred to as responses generated by the auditory pathway in response to an external acoustic stimulus; hence AEPs are sometimes referred to as auditory evoked responses (i.e., AERs or EPs).

This neural response elicited by an acoustic stimulus, reflects the activity of auditory neurons along the auditory pathway from cochlea to cortex with the addition of secondary auditory effects. The response is time locked to the onset of the stimulus. This means that each component of the response waveform will be observed at certain time occurrence with respect to the time occurrence of the external stimulus (Thornton & Newton, 1989).

These elicited responses are embedded in spontaneous EEG. This physiological property of generating time locked responses is important for estimating the auditory evoked response from spontaneous EEG. In order to extract the responses embedded in EEG the stimulus is repetitiously presented. The time lock property of each component of the response waveform allows us to use conventional averaging to estimate the response.

Conventional averaging is achieved by segmenting the EEG with respect to the onset of the stimulus then averaging these segments of EEG yielding an auditory evoked response. The generation of an auditory response resembles a deterministic process because a determinant process will evolve in a determined direction given the initial condition, for instance given the onset of a stimulus the determinant process will generate a response.

Spontaneous EEG resembles a signal that is generated by a stochastic process (i.e., random process) because an indeterminant process will evolve in an indetermined direction given the initial condition, for instance given the onset of a stimulus the indeterminate process will generate a signal of random values with respects to time. As the responses of individual stimulus are, add together, the EEG waveforms produced by the indeterminant random process will undergo deconstructive canceling and the response waveforms produced by the determinant process will undergo constructive amplification thus yielding an auditory response (Thornton & Newton, 1989).

Another important property of evoked potential is in regard to the rate of stimulation. At low stimulation rates conventional averaging yields a transient response. A transient response is the response that we have discussed so far. It is a response that has

observable waveform components which reflects the activity of the neurons contained in the auditory pathway.

At high stimulation rates conventional averaging yields a steady-state response. A steady–state response is a composition of overlapped transient responses. At high stimulation rates successive auditory stimuli are applied at a rate that results in the superposition of successive transient responses yielding a response that resembles a periodic response. Responses elicited at high-stimulation rates mask the valuable waveform components of transient responses.

This is a result of the time- lock property of the auditory system but a limitation for the investigation of high rate transient responses. This study employs a deconvolution method to extract transient responses elicited at high stimulation rate, which resolves this limitation – the Continuous Loop Averaging Deconvolution (i.e., CLAD) method.

1.2.1 Neurological Basis for the Generation of Evoked Potential

The ear is divided into three areas: the external (i.e., outer) ear, the middle ear, and the internal (i.e., inner) ear. The external ear, which consists of the pinna, concha, and auditory meatus, focuses the variations in the density of air molecules within a sound wave on to the surface of the tympanic membrane (i.e., eardrum) (Marieb, 1991) (see Figure 1.16). The middle ear, which consists of the tympanic membrane, the ossicles, and tensor tympanic muscles, function to amplify and to transmit the pressure variations on the surface of the tympanic membrane on to the surface of an opening in the cochlea called the vestibular window or the oval window (Bear, Connors, & Paradiso, 2001) (see Figure 1.16).

The compression and rarefaction regions of the sound waves cause the tympanic membrane to vibrate at the same frequency. The tympanic membrane oscillation is amplified and transferred to the oval window by a system of tiny bones called ossicles (Bear, Connors, & Paradiso, 2001) (see Figure 1.16). The greater the intensity of the sound wave the greater the tympanic membrane is displaced.

One of the major functions of the middle ear is to match the impedance of the air medium to the impedance of the cochlear fluid medium (Marieb, 1991; Guyton & Hall, 2006). Impedance is an intrinsic property of medium and it is the resistance to motion of a medium (Guyton & Hall, 2006). Air has low impedance compared to the high impedance of the cochlear fluid. The middle ear creates a pressure gain that matches the low impedance of the sound wave on the surface of the tympanic membrane to the high impedance requirements of the fluid in the inner ear.

The pressure gains achieved by the middle ear can be attributed to two important features such as, the differences in area between the tympanic membrane versus the area of the oval window and the lever action of the ossicles on the oval window (Marieb, 1991) (see Figure 1.16). The structurally the tympanic membrane is 17 to 20 times larger than the oval window which makes the force per unit area exerted on the on the oval window 20 times greater (Marieb, 1991). This increase in force per unit area is one of the contributors applied to overcoming the impedance of the cochlear fluid.

Another contributor is the ossicle system of the middle ear. The ossicle system is made of three small interconnected bones called the malleus, incus, and stapes (Marieb, 1991). These tiny bones connect the tympanic membrane to the oval window.

The vibrations of the tympanic membrane are amplified as they pass through the malleus, incus, and stapes. As sound strikes the tympanic membrane, the variations in pressure are transmitted through the tiny bones to the oval window.

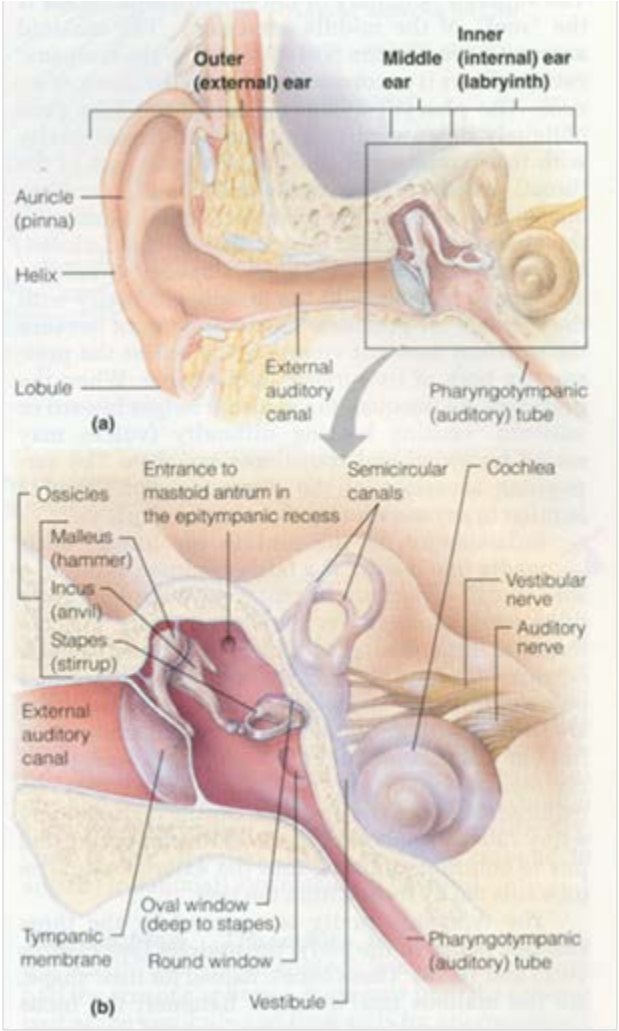

Figure 1.16 Structures of the Ear. Adapted from (Marieb, 1991).

Through the lever action created by the structure of the interconnect bone the oscillatory forces originating at the tympanic are amplified on to the oval window (Guyton & Hall, 2006).

Sound transmission is regulated within ossicle system of the middle ear by an active mechanism consisting of two small muscles one is attached to the malleus called the tensor tympani muscle and it is innervated by cranial nerve V, and the other is attached to the stapes called the stapedius muscle and it is innervated by cranial nerve VII (Bear, Connors, & Paradiso, 2001).

When theses muscle contract the tiny bones of the ossicle system become more ridged causing sound conduction into the inner ear to reduce (Bear, Connors, & Paradiso, 2001). The tensioning of these small muscles protects the ear from loud sounds by reducing the conductive capability of the ossicle system.

The cochlea is a spiral-tube structure located in the inner ear that transforms the oscillatory forces applied to the oval window into small electrical impulses. The cochlear incompressible fluid is set into motion by the oscillatory forces applied on to oval window of the cochlea.

An unwrapped cochlea may reach the length of 35 mm (Bear, Connors, & Paradiso, 2001). The cross-sectional view of an unwrapped cochlea reveals three fluid-filled chambers: the scala vestibuli, the scala media, and the scala tympani (Bear, Connors, & Paradiso, 2001) (see Figure 1.17).

Separating the scala vestibuli from the scala media is a membrane called the Reissner's membrane and separating the scala tympani from the scala media is a membrane called the basilar membrane (Bear, Connors, & Paradiso, 2001). Residing on the top surface of the basilar membrane is the organ of Corti (see Figure 1.17) (Marieb, 1991). This structure contains auditory receptor neurons called cochlear hair cells (Bear,

Connors, & Paradiso, 2001) (see Figure 1.17). Hair cells are embedded in the basilar membrane and make contact with a structure that resides above the organ of Corti called the tectorial membrane (see Figure 1.17).

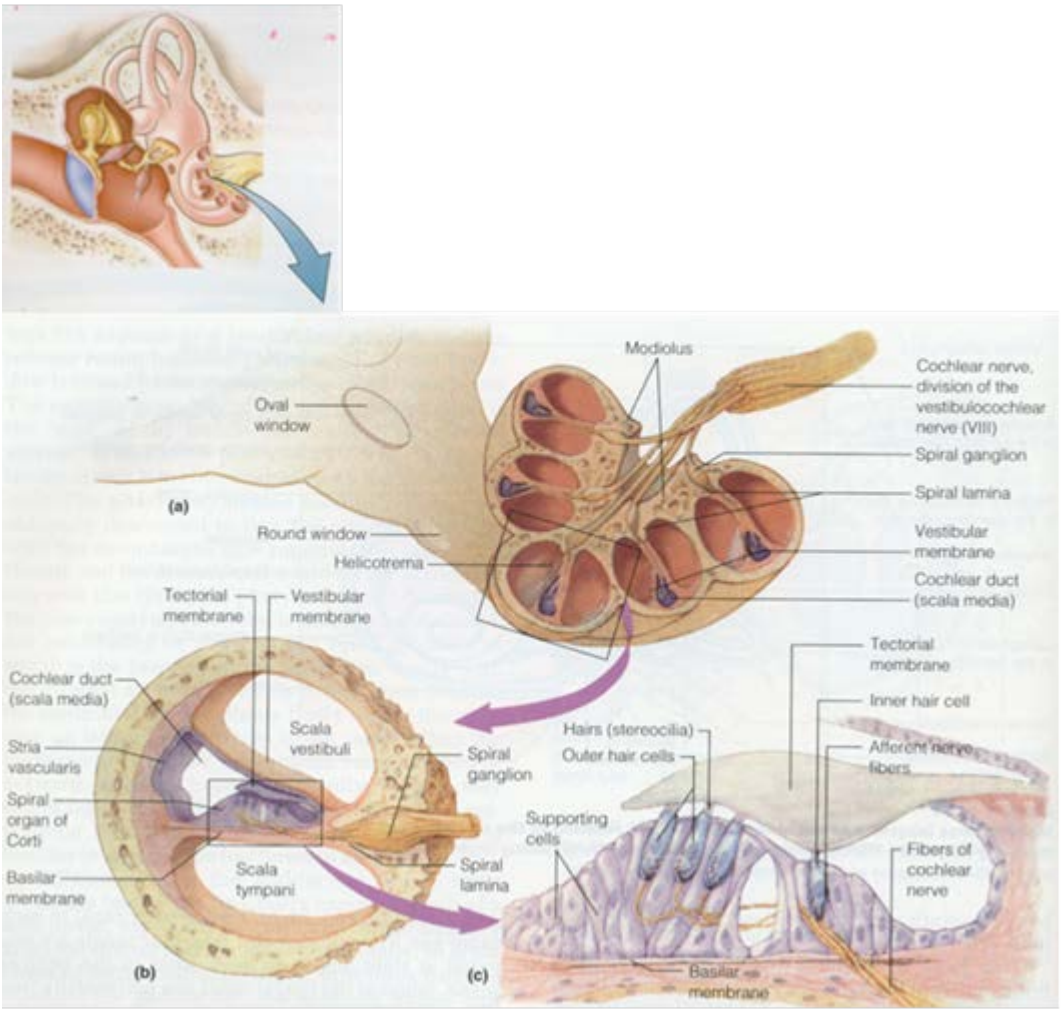

Figure 1.17 Structures of the cochlea. Adapted from (Bear, Connors, & Paradiso, 2001 and Marieb, 1991).

Located at the apex of the cochlea is the helicotrema which is a membrane hole that unites the scala tympani with the scala vestibuli and seals off the scala (see Figure 1.14) (Bear, Connors, & Paradiso, 2001). Conversely, located at the base of the cochlea the scala vestibule is united with the oval window and the scala tympani is united to the round window a second opening of the cochlea below the oval window (see Figure 1.14).

Each chamber of the cochlea contains an incompressible fluid. The scala media contains a fluid called the endolymph and the scala vestibuli and the scala tympani contain a fluid called the perilymph (Bear, Connors, & Paradiso, 2001). Sound waves are focused and amplified by the external and middle ear into the inner ear. For example, a sound is produced by a vibrating body that causes the medium surrounding it to vibrate and produce pressure waves.

These waves have high-pressure compression regions and low-pressure rarefaction regions. The external ear focuses the pressure wave on to the tympanic membrane. The tympanic membrane is induced to vibrate by the compression and rarefaction of the sound's pressure wave. These vibrations are amplified as they conduct through the malleus, incus, and stapes of the ossicle system.

The ossicle system focuses and amplifies the sound's pressure wave onto the oval window of the cochlea, by matching the impedance of the sound wave medium to the medium of the incompressible cochlear fluid (see Figure 1.18). As the stapes of the ossicle lever system applies force on the surface area of the oval window, the pressure is greater on the applied force side of the oval window compare to the pressure on the other side.

The pressure difference between one side of the oval window and the other side of the oval window form a pressure gradient. In contrast, if the direction of the applied force is reversed then the direction of the pressure gradient is reversed. This continual change in direction of the pressure gradient induces pressure waves that travel through the incompressible fluid within the chambers of the cochlea (see Figure 1.18). As a force

is applied to the surface of the oval window, it displaces the perilymph fluid within the scala vestibuli and since the Reissner's membrane is flexible, it displaces the endolymph fluid within the scala media.

The displacement of the endolymph makes the basilar membrane generate a wave that originates at the base and propagates toward the apex (see Figure 1.18). The structures of the basilar membrane will response with maximal amplitude of displacement according to the frequency of the pressure wave (Bear, Connors, & Paradiso, 2001).

The distance the wave propagates through the basilar membrane from the base to the apex depends on the frequency of the pressure wave (Gelfand, 2009; Guyton & Hall, 2006) (see Figure 1.18). The response of the basilar membrane to the frequency of the pressure wave is determined by two structural properties. For instance, the basilar membrane is narrower towards the base than towards the apex and the basilar membrane is stiffer toward the base than towards the apex (Marieb, 1991).

For example, if the frequency of the pressure wave is high then the stiffer base will resonate or vibrate greater at this location of the basilar membrane. This will dissipate most of the pressure wave energy at this region of the basilar membrane and the wave will not continue to propagate towards the more flexible apex area.

Due to the decreasing stiffness of the basilar membrane as a wave travels from base of the membrane to apex of the membrane sounds of certain frequencies and intensities cause local maximum of the wave amplitude to occur along the basilar membrane (Bear, Connors, & Paradiso, 2001; Marieb, 1991; Gelfand, 2009) (see Figure

1.18). Therefore, the response of the basilar membrane establishes a spatial code in which different locations of membrane are maximally deformed by different sound frequencies.

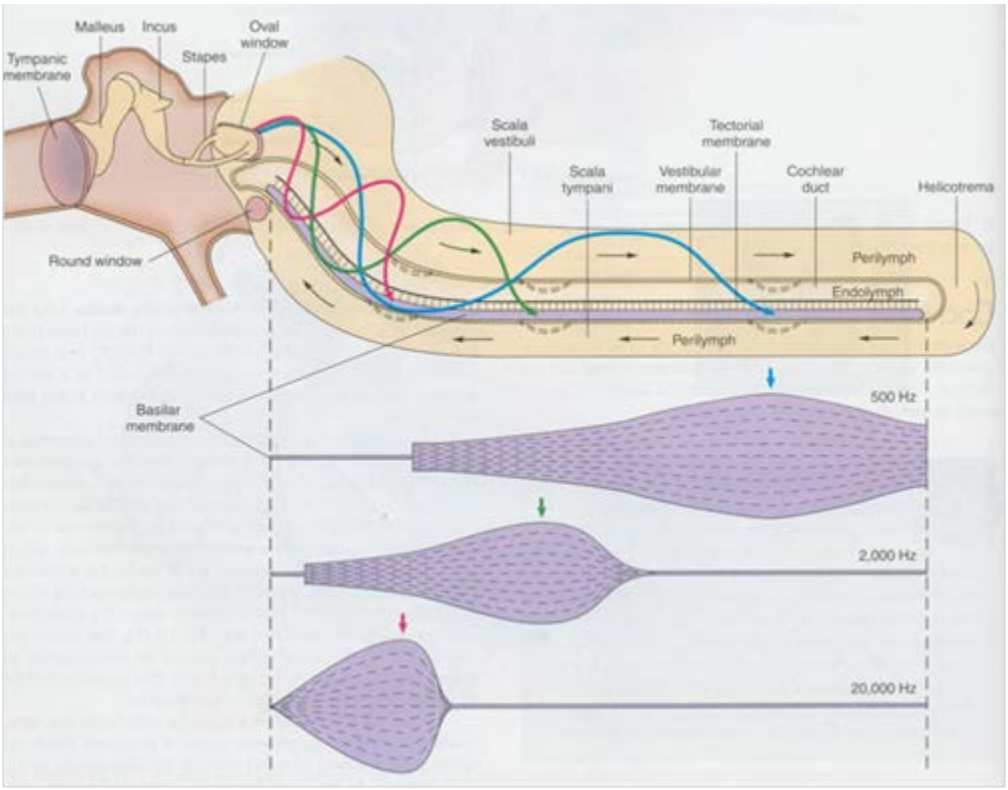

Figure 1.18 Basilar membrane decomposing frequency content of sound. Adapted from (Fox, 2004).

This topographical mapping of frequency is referred to as tonotopy. Tonotopy is conserved throughout much of the auditory system, including the auditory cortex (Gelfand, 2009; Bear, Connors, & Paradiso, 2001). The organ of Corti is set a top of the basilar membrane.

It is composed of many supporting cells and several rows of cochlear hair cells such as the inner hair cells and the out hair cells. Hair cells derived their name from hair like processes, called stereocilia, that protrude from the apical end of the cell. Coiled about the base of the hair cells are afferent fibers of the cochlear nerve (Marieb, 1991).

The cochlear nerve is a division of the vestibule cochlear nerve, which is referred to as cranial nerve VIII (Bear, Connors, & Paradiso, 2001). The stereocilia of inner hair cells protrude into the endolymph and the stereocilia of outer hair cells protrude into the tectorial membrane above them

The motion of a propagating wave traveling along the basilar membrane initiates a vertical displacement. Since the hair cells are anchored to different positions between the basilar membrane and the tectorial membrane, a shearing motion is induced between the basilar membrane and the tectorial membrane (Bear, Connors, & Paradiso, 2001).

The hair cells located closest to the oval window are stimulated by high frequency pressure waves and the hair cells located at the cochlear apex are stimulated by low frequency pressure waves (Bear, Connors, & Paradiso, 2001) (see Figure 1.19).

Additionally, the frequency of the pressure wave directly determines the rate of membrane potential changes that take place in the hair cells and the frequency of signaling that take place by the cochlear nerve fibers. The tension is applied to the stereocilia induces theses hair cells to generated small electrical impulses (Bear, Connors, & Paradiso, 2001).

This motion bends the anchored hair cells and stimulates the hair cells to produce receptor potential in the hair cells. The stimulation of hair cells within the organ of Corti of the cochlea causes the generation of nerve impulses which passes into the pons of the brain (Marieb, 1991; Bear, Connors, & Paradiso, 2001; Gelfand, 2009).

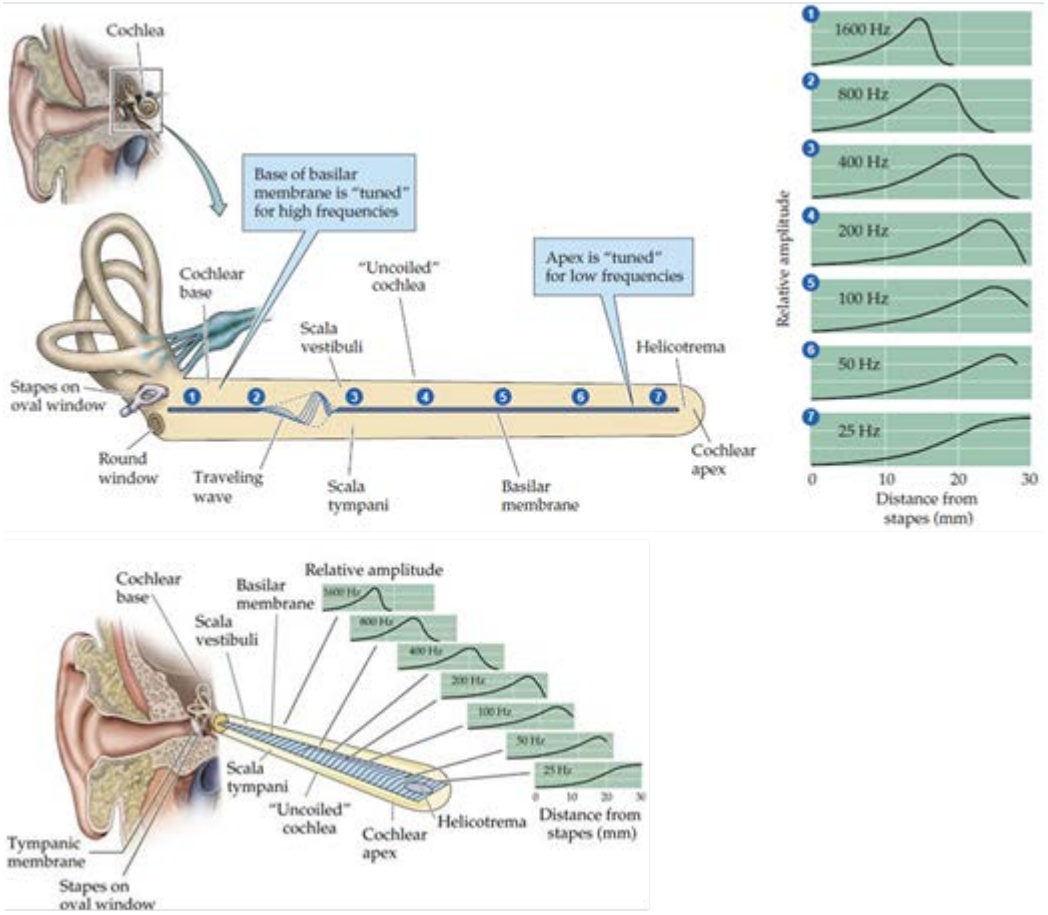

Figure 1.19 Tonotopy of basilar membrane. Adapted from (Purves, 2004).

The impulses that are generated at the cochlea pass through the spiral ganglion along the afferent fibers of the cochlear nerve into three main divisions of the cochlear nucleus within the medulla (Gelfand, 2009; Marieb, 1991; Guyton & Hall, 2006) (see Figure 1.20). The axons originating from the cochlea innervate both the dorsal cochlear nucleus and the ventral cochlear nucleus (Bear, Connors, & Paradiso, 2001; Marieb, 1991). These nuclei are located ipsilateral with respect to the cochlea that innervates it (see Figure 1.20).

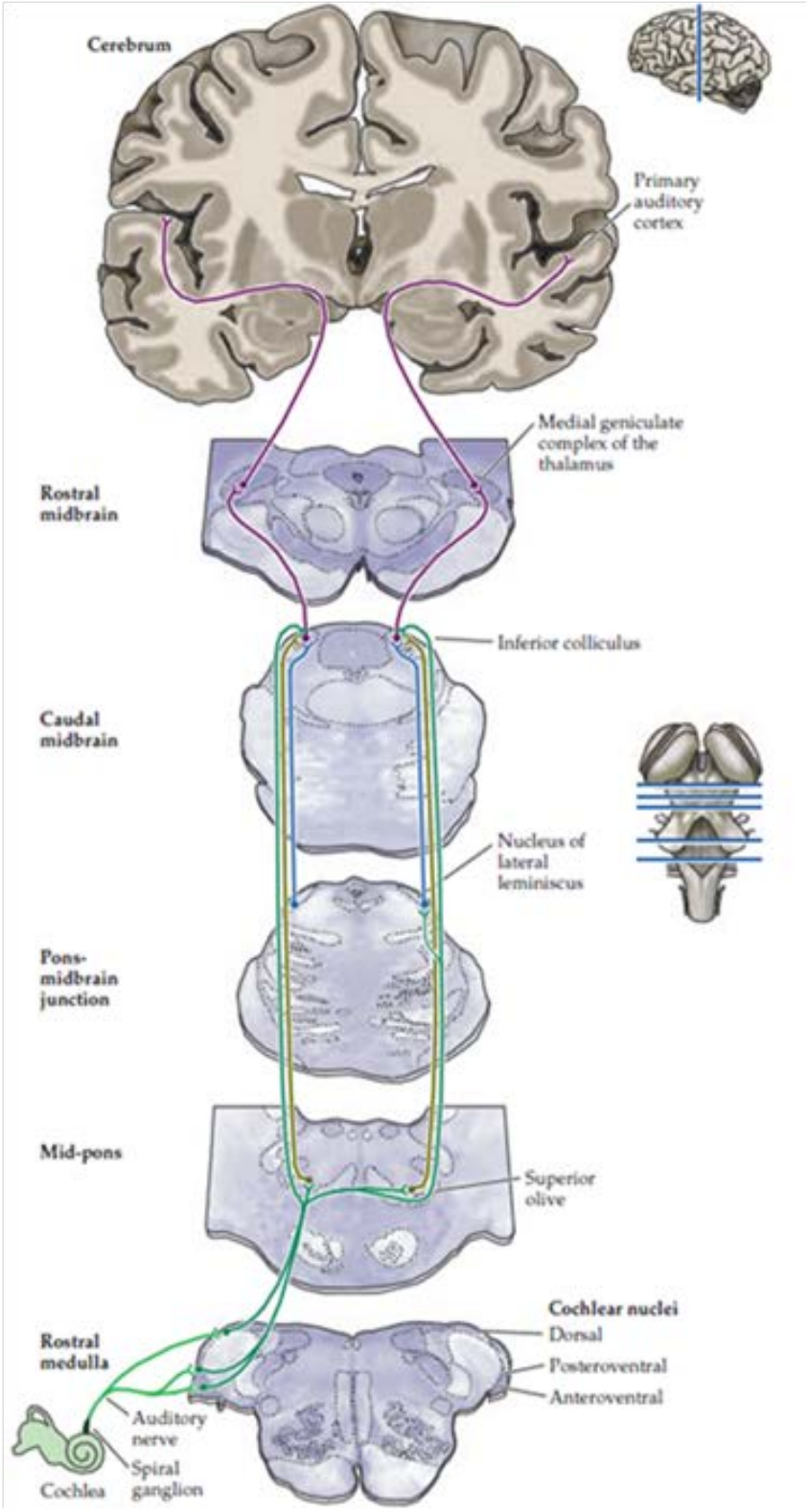

Figure 1.20 The auditory pathway. Adapted from (Purves, 2004)

Neurons from the ventral cochlear nucleus have axons that project into the superior olive on both sides of the brainstem (Bear, Connors, & Paradiso, 2001). From there axons from the superior olive project through the lateral lemniscus tract and innervate the inferior colliculus, which is located in the midbrain (Kandel, Schwartz, & Jessell, 2000) (see Figure 1.20).

The inferior colliculus is the auditory reflex center of the midbrain (Bear, Connors, & Paradiso, 2001; Kandel, Schwartz, & Jessell, 2000) (see Figure 1.20). In contrast, axons originating from the dorsal cochlear nucleus follow similar path as the axons that originate from the ventral cochlear nucleus with the exception that the axons originating from the dorsal cochlear nucleus bypass the superior olive (Marieb, 1991; Kandel, Schwartz, & Jessell, 2000) .

From there neurons located in the inferior colliculus project axons to the medial geniculate body of the thalamus (Bear, Connors, & Paradiso, 2001; Kandel, Schwartz, & Jessell, 2000) (see Figure 1.20). Neurons located in the medial geniculate body project axons to the auditory cortex located on the temporal lobe (Marieb, 1991; Bear, Connors, & Paradiso, 2001) (see Figure 1.20 and Figure 1.21).

The waveform of an evoked potential is dependent on the stimulus that evoked the response. There are two general categories of responses formed by the auditory system with respect to stimulation rate: (a) low stimulation rate transient responses and (b) high stimulation rate steady-state responses.

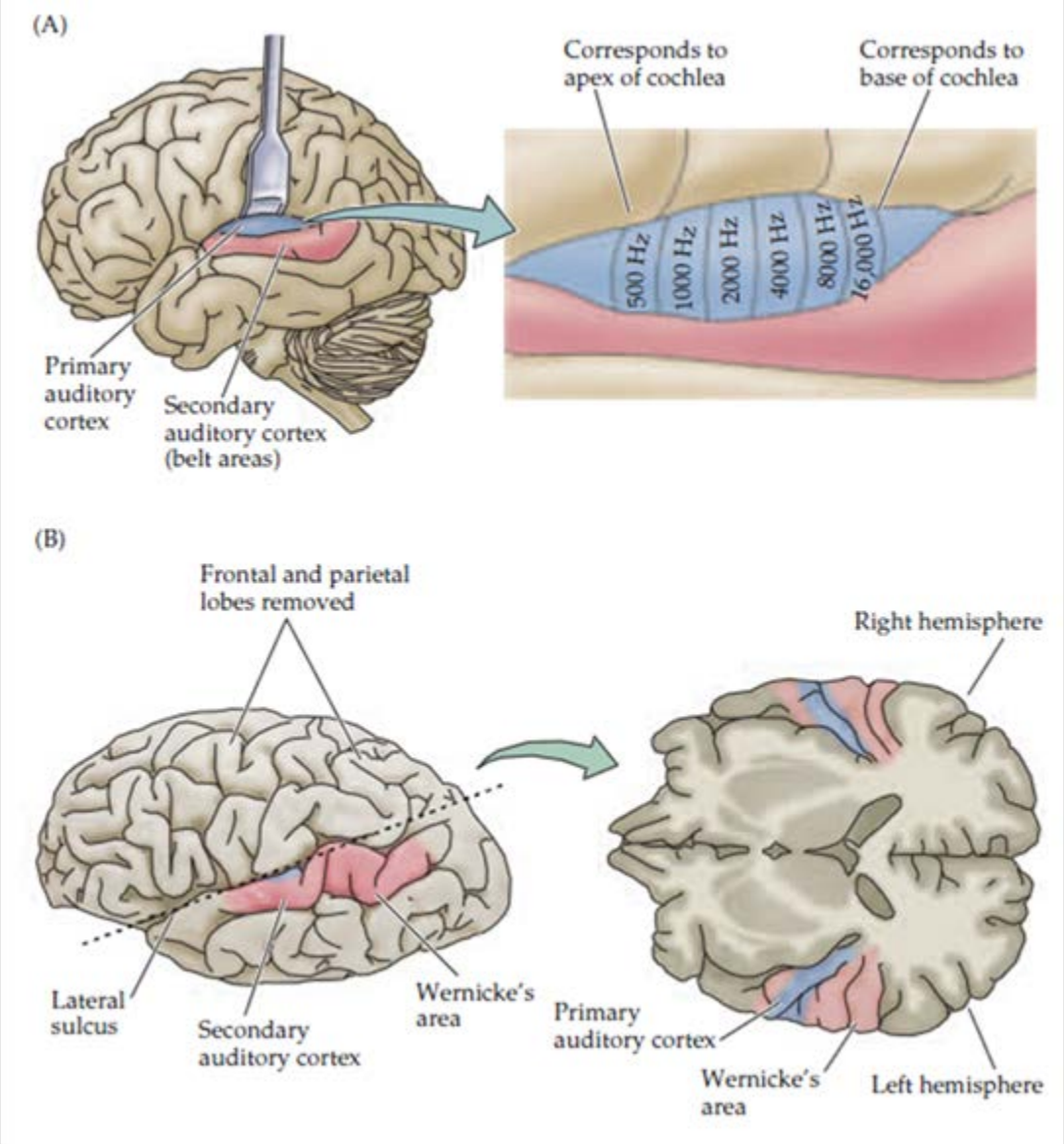

Figure 1.21 Tonotopy of auditory cortex. Adapted from (Purves, 2004).

1.2.2 Genesis of Evoked Potential

1.2.2.1Transient Response

Transient auditory evoked responses are divided into three temporal segments: the auditory brainstem response (i.e., ABR) having a peak latency from 0 to 10 msec. after

stimulus onset (see Figure 1.23, the middle-latency response (i.e., MLR) having a peak latency from 10 to 80 msec. (Atcherson & Stoody, 2012) (see Figure 1.25) after stimulus onset, and the long-latency response (i.e., LLR) having a peak latency from 80 to 500 msec. after stimulus onset (Davis, 1976; Picton, Hillyard, Krausz, & Galambos, 1974; Melcher, 2009) (see Figure 1.26).

The three segments of the auditory evoked response is subdivided into wave components. Each wave component within the temporal segments is identified according to the latency of their peaks with respect to the onset of the stimulus: the auditory brainstem response components (I, II, III, and IV/V), the middle-latency response components (No, Po, Na, Pa, Nb and Pb), and the long-latency response components (N1, P2, and N2) (Atcherson & Stoody, 2012; Ferraro & Durrant, 2009) (see Figure 1.22).

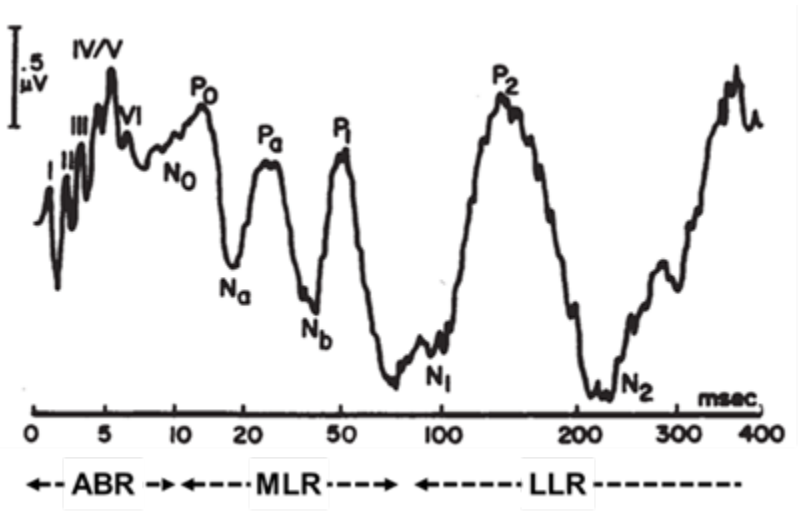

Figure 1.22 Transient auditory evoked response in logarithmic time scale. Adapted from (Michelini, Arslan, & Pedrielli, 1982).

The generators of the auditory brainstem response are as follows: Wave I of the auditory brainstem response is believed to originate from the distal portion the eighth cranial nerve (Moller & Jannetta, 1981) (see Figure 1.24).

Wave II of the auditory brainstem response is believed to originate from the proximal portion of the eighth cranial nerve as it enters the brainstem (Moller & Jannetta, 1981) (see Figure 1.24).

Wave III of the auditory brainstem response is believed to originate from the activity of secondary neurons in or near the cochlear nucleus and in the caudal portion of the auditory (Buchwald & Huang, 1975) (see Figure 1.24).

Wave IV of the auditory brainstem response is believed to originate from the pontine third order neurons commonly located in the superior olivary complex, however additional contributions may come from the cochlear nucleus and nucleus of lateral lemniscus (Roeser, Valente, & Hosford-Dunn, 2007) (see Figure 1.24) .

Wave V of the auditory brainstem response is believed to originate from the inferior colliculus (Buchwald & Huang, 1975; Picton, Woods, Baribeau-Braun, & Healey, 1977) (see Figure 1.24).

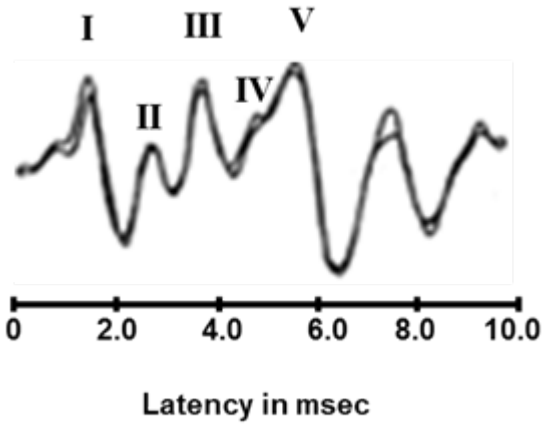

Figure 1.23 Early-latency auditory evoked response. Adapted from (Teasdale, 2001).

The inferior colliculus received more than ninety nine percent of the axons that pass through the lateral lemniscus originate from the lower auditory brainstem regions (Roeser, Valente, & Hosford-Dunn, 2007) (see Figure 1.24).

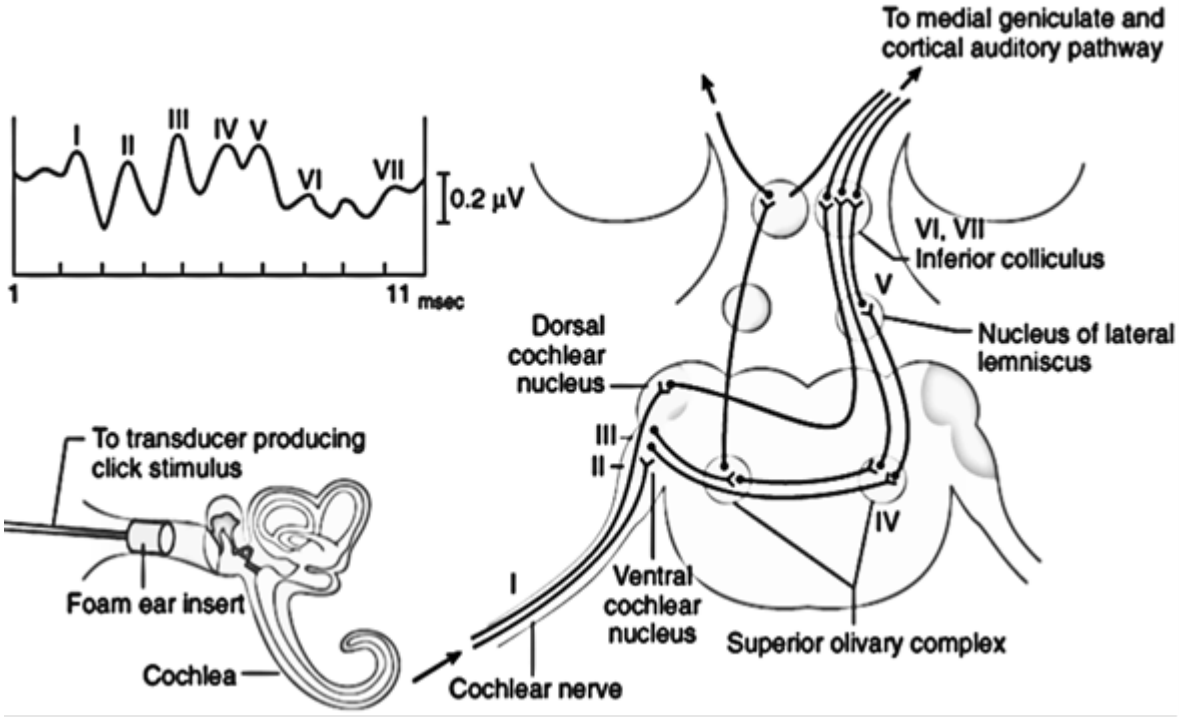

Figure 1.24 Source of the auditory brain stem response potentials. Adapted from (Miller, 2009).

As shown in Figure 1.25, the middle-latency response arises after the ABR and it occurs within the range of 10 and 50 msec. after the onset of the acoustic stimulus. It is believed that the MLR is generated by the combination of multiple generators.

The generators to the MLR waveform are held to be the thalamocortical pathways as the greater contributor and the inferior colliculus and reticular formation as the lesser contributor (Kraus, McGee, Littman, Nicol, & King, 1994). MLR are closely related to the arousal state of the patient; since the thalamocortical, pathways and the reticular

formation are known to modulate the general state of arousal and receptiveness to sensory (Kraus, Therese, & Cornperatore, 1989).

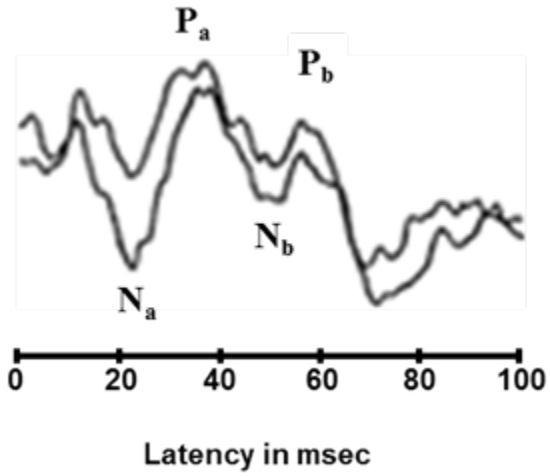

Figure 1.25 Middle-latency evoked response. Adapted from (Teasdale, 2001).

Furthermore, animal and human studies have suggested that MLR is attributed to complex interactions from multiple sites (Knight & Brailowsky, 1990). The animal studies indicate that the thalamocortical pathway's primary and the non-primary components generate the MLR waveform (Kaga, Hink, Shinoda, & Suzuki, 1980; Knight & Brailowsky, 1990; Kraus & McGee, 1993; McGee, Kraus, Killion, Rosenberg, & King, 1993).

Additionally, data from near-field intracranial studies in humans, from computer tomography and magnetic resonance imaging (i.e., MRI) of brain lesions, and from neuromagnetic studies in adults indicate Pa to be generated bilaterally within the primary auditory cortices (Jacobson & Newman, 1990; Ozdamar, Kraus, & Curry, 1982) (see Figure 1.20 and Figure 1.21).

In addition, Jacobson and Newman (1990) examined topographic brain maps to discern the physiological origins of the MLR suggesting that a minimum of two systems which include bilateral systems that are located in the posterior temporal lobes, and deeper midline generator system generate the Pa component of the MLR (see Figure 1.20 and Figure 1.21).

In cats, Kaga et al (1980) produced strong evidence indicating that Pa is distributed overlying the primary auditory cortex on the scalp. The generators of the long-latency response (i.e., LLR) potentials have not been completely determined due to the multiplicity and complexity of the central auditory pathway.

Vaughan and Ritter (1970) proposed Sylvian area near the auditory cortex as the origin of the LLR (see Figure 1.21).

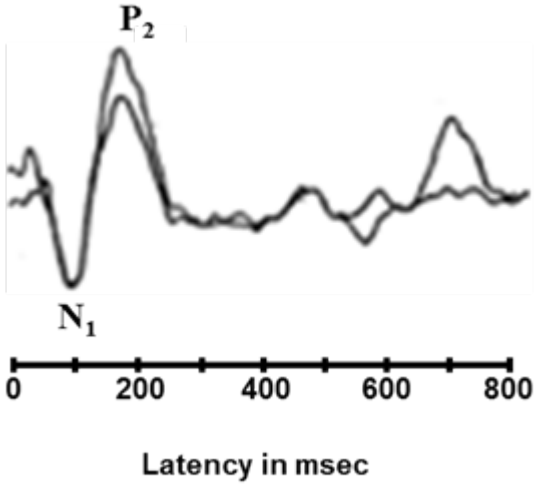

Figure 1.26 Late-latency auditory evoked response. Adapted from (Teasdale, 2001).

Davis, Davis, Loomis, Harvey, and Hobart, (1939) after recording in multiple locations on the scalp, found that the maximum amplitude for LLR is located from the midline over the frontal regions thereby implicating the frontal lobe as the origins for the LLR.

Moreover, Picton et al (1974) suggested that the origin of the LLR was a region in the association cortex of the frontal lobe (see Figure 1.21). Studies have indicated that the N1 and P2 component of the LLR are sensitive to intensity and frequency of auditory stimuli (Adler & Adler, 1991; Adler & Adler, 1989). Moreover, the amplitudes of N1 and P2 are larger with lower frequency stimuli (Picton, Hillyard, Krausz, & Galambos, 1974).

1.2.2.2 Steady State Response

ASSRs are elicited when stimulation rates are above 10 Hz. Auditory steady-state responses (i.e., ASSRs) have relatively consistent phase relation with respect to the superposition of transient responses due to the time locking property of the auditory system. Galambos, Makeig, & Talmachoff (1981) showed that 40 Hz ASSRs are composed of the superposition of the Na-Pa components of the middle latency response evoked by clicks and short duration tone burst presented every 25 msec..

ASSR is considered a phase-locked response that locks the phase of its response to the phase of the time occurrence of the stimulus; hence, the relatively consistent phase relation of the superposition of the transient response produces an ASSR having a fundamental frequency (i.e., resonant frequency) equal to the stimulation rate.

In contrast to transient responses, which are analyzed with respect to component amplitude and latency, auditory steady-state responses are analyzed with respect to its magnitude and phase in the frequency domain. Using the Fourier Transform, ASSRs are transformed from the time domain to the frequency domain. In the frequency domain, the magnitude of the ASSR is represented as a magnitude spectrum.

The ASSR magnitude spectrum is the magnitude of the ASSR with respect to each frequency component. The Fourier transform is a mathematical operation that decomposes a signal into its constituent resonant frequency components, referred to as the frequency spectrum. Each value of the ASSR frequency spectrum is a complex number that represents the magnitude and phase value for each frequency component.

Spectral methods such as phase vectors referred to as phasors are used to analyze ASSRs. A phasors is a phase vector that describes the magnitude and phase angle of each frequency component in the frequency spectrum by using a vector.

Phasor analysis allows the response of different ASSRs to be compared with respects to the length (i.e., magnitude) and direction (i.e., phase angle) of the vector (see Figure 1.27).

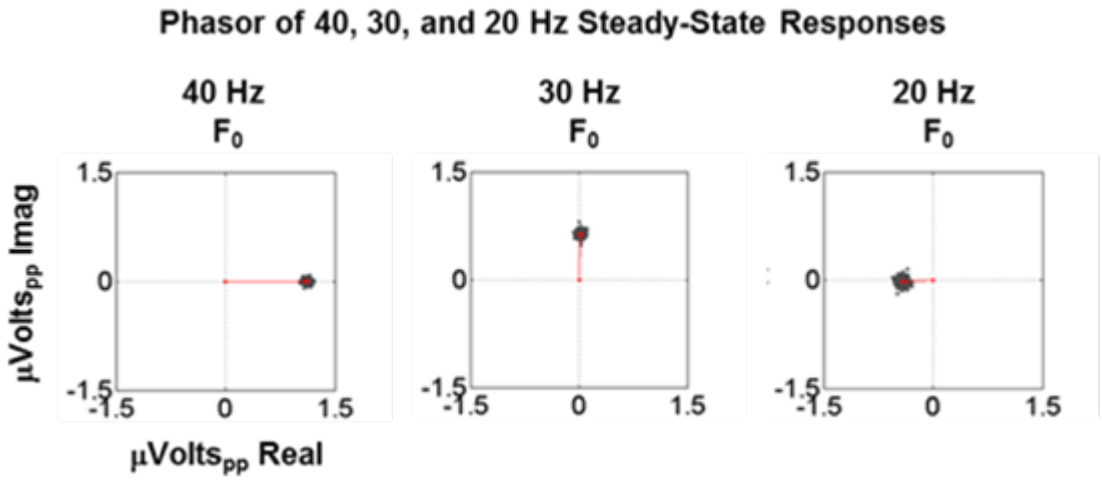

Figure 1.27 The 20, 30, and 40 Hz steady-state response phasor.

A limitation of ASSRs is the inability to clearly observe the components that reflect the activity of the auditory system. They do however indicate the resonance of the auditory system to stimulation rate, indicate any global changes occurring to the process

that generates the resonance of the ASSRs and indicate global changes to the transient responses.

Galambos et al. (1981) showed that auditory steady state responses elicited at 40-Hz rates generated the largest amplitudes and that the amplitude of the 40-Hz ASSR decreased as stimulus intensity was reduced. Galambos et al. suggested that ASSRs are the superposition of the Na-Pa components from the middle latency response evoked by clicks and short duration tone burst presented every 25 msec. (see Figure 1.28).

ASSRs may be elicited by amplitude or frequency modulated pure-tone signals. These stimulus signals are designed with low-carrier frequency and higher depths of modulation. The appropriate modulation frequency to elicit a steady-state response will be dependents on the state of arousal of the subject. Lower modulation frequencies, e.g., 40-Hz, tend to be sensitive to state of arousal than are higher frequencies, e.g., 80-Hz.

Higher modulation frequencies elicit more robust responses in adults who are asleep, and infants (Atcherson & Stoody, 2012). Responses from lower modulation frequencies develop from sources towards the central structures of the brain, whereas responses from higher modulation frequencies develop from sources towards the peripheral auditory nerve and brain stem structures (Gulya, Minor, & Poe, 2010). ASSRs do not provide as much information in the time domain as do TERs therefore ASSR are traditionally analyzed in the frequency domain.

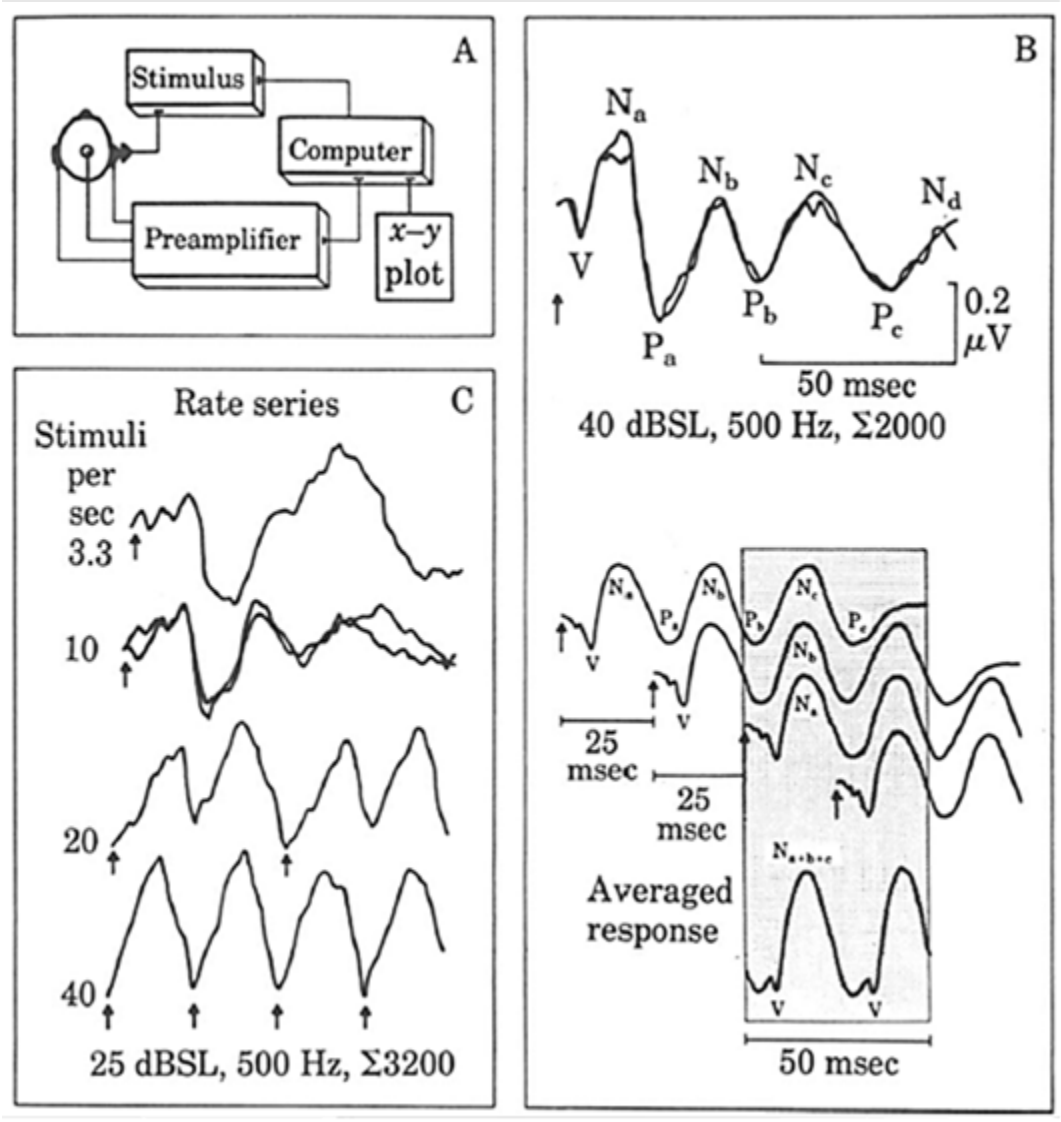

Figure 1.28 The 40 Hz steady-state response synthesis. (A) Diagram of auditory response extraction. Sweeps of auditory stimuli are delivered to the right ear of the subject. The auditory system response that is embedded in the EEG is amplified then acquired by the computer for averaging. (B) Upper diagram, shows the auditory evoked response elicited by a 500 Hz tone burst delivered at a stimulation rate of 10 per sec, arrow indicate time occurrence of stimulus. Lower diagram, shows the synthesis suggested by Galambos et al. (1981), that the sum of several overlapping MLR waveforms express the 40 Hz response when presented at 25 msec. The inset box shows the magnitude and phase of the 40 Hz response component is the sum of the magnitude and phase of the multiple overlapped response components (e.g., Na, Nb, and Nc). (C) Shows auditory evoked responses from one subject elicited by 500 Hz tone burst delivered at different stimulation rates, including the 40 Hz rate shown in (B) in order to compare the synthesis shown in (B) to the actual synthesis of the single wave of the 40 Hz response from multiple waves of responses elicited by lower stimulation rate. Adapted from (Galambos, Makeig, & Talmachoff, 1981).

1.2.3 Simultaneous Deconvolution of the Transient and Steady-State Response

In this study, we present a deconvolution method that permits the extraction of both high rate transient and steady-state response from one data acquisition session. Transient responses provide valuable information about the auditory processing of the auditory system however transient responses can only be extracted at low stimulation rates.

At high stimulation rates conventional averaging yields a response made from the superposition of transient responses (i.e., the convolution of transient responses). The response formed by the convolution of transient responses is called a convolved response. A continuous series of stimuli is referred to as a stimuli sequence.

The duration between two stimuli is referred to as inter-stimulus interval (i.e., ISI). Stimuli sequences have a variety of properties. These properties determine the type of convolved responses produced by the auditory system. Low rate stimuli sequences have large ISI values. High rate stimuli sequences have small ISI values.

Stimuli sequences that have a constant ISI are called isochronic stimuli sequences. ASSRs are elicited by high-rate, isochronic stimuli sequences (see Figure 1.28). Stimuli sequences that do not have a constant ISI are called jittered stimuli sequences (Delgado & Ozdamar, 2004).

A convention used to determine how different a jittered stimuli sequence is from an isochronic stimuli sequence is the jitter factor of the stimuli sequence. The jittered factor is the ratio of the largest ISI value divided by the lowest ISI value of the sequence.

For instance, the jittered factor of an isochronic stimuli sequence is JF = 1.0 the value will increase with increase jitter.

The Continuous Loop Averaging Deconvolution (i.e., CLAD) method deconvolves transient responses from convolved responses elicited by a special class of jittered sequences called CLAD sequences. CLAD sequences are jittered sequences that form solvable set of equations (Delgado & Ozdamar, 2004).

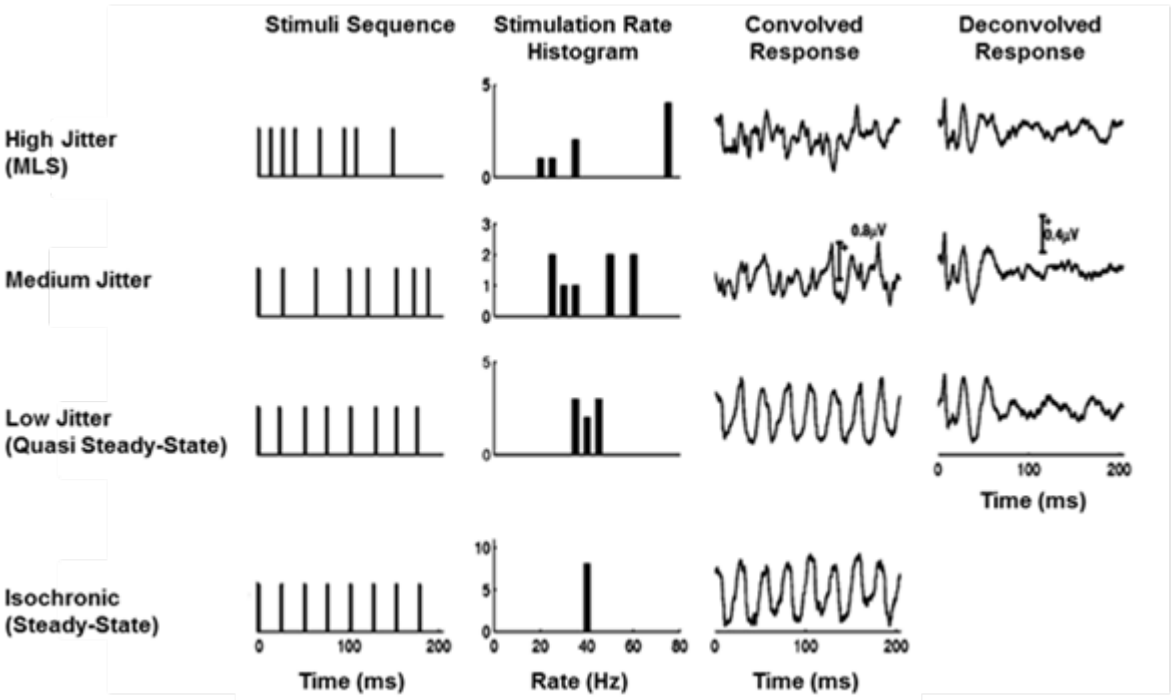

Figure 1.29 Steady-state and transient responses are elicited by low-jittered sequences. Adapted from (Bohórquez & Ozdamar, 2008)

In this study, a unique class of CLAD sequences is employed to extract both transient and steady-state responses from one data acquisition session called low-jittered, CLAD sequences (Bohórquez & Ozdamar, 2008) (see Figure 1.29).

These specially designed sequences evoked convolved responses that approximate to closely to ASSRs. These responses are called quasi steady-state responses (i.e., QSSR)

to distinguish them from the steady-state responses elicited from isochronic sequences (Bohórquez & Ozdamar, 2008). QSSRs provide as much value as ASSRs in that they indicate the resonance of the auditory system to stimulation rate, indicate any global changes occurring to the process that generates the resonance of the QSSRs and indicate global changes to the transient responses.

An advantage of QSSRs versus ASSRs is the capability to extract the transient responses from the quasi steady-state responses. These sequences permit the analysis of the auditory processing effect on both the transient components and the steady-state magnitude and phase under the same conditions because the both type of responses are elicited under one data acquisition session.

In time domain, the auditory system convolves the transient responses elicited by the stimuli sequence. This overlapping process performed by the auditory system can be represented as the convolution between transient response, $y_{TR}(n)$ and the sequence of stimuli, $s(n)$. However, before the "noise free" convolved signal reaches the recording amplifiers, other spontaneous activity is added, $\eta(n)$, such as electroencephalography and electromyography activity etc..

In the frequency domain, this convolution process is equivalent to the multiplication of the transient response spectrum with the sequence spectrum. Conventional averaging of responses elicited by low-jittered CLAD stimuli sequence yields the quasi steady state response, $\hat{y}_{QSSR}(n)$ (see Figure 1.29). The formation of the quasi steady state response by the auditory system is described as the convolution of

transient response by the low-jittered CLAD stimuli sequence summed with additive noise (Bohórquez & Ozdamar, 2008) (see Equation 1.9 and Figure 1.29 (b)).

The time domain convolution expressed in Equation 1.9. Convolution in the time domain is expressed as multiplication in the frequency domain (Ozdamar & Bohorquez, 2006) (see Equation 1.10 and 1.11). The transient response is deconvolved from the quasi steady state response by dividing the frequency spectrum of the quasi steady state response by the frequency spectrum of the low-jittered CLAD stimuli sequence (see Equation 1.12 and 1.13 and see Figure 1.27).

The last term of Equation 1.13 represents the noise shaping factor of the sequence. If magnitude of $|1/S(f\_k)|$ is less than one the noise component at the frequency will be amplified (Ozdamar & Bohorquez, 2006).

$$\hat{y}_{QSSR}(n) = y_{TR}(n) * s(n) + \eta(n) \tag{1.9}$$

$$\hat{Y}_{QSSR}(f_k) = FT\{\hat{y}_{QSSR}(n)\} \tag{1.10}$$

$$\hat{Y}_{QSSR}(f_k) = \hat{Y}_{TR}(f_k) \cdot S(f_k) + \eta(f_k) \tag{1.11}$$

$$\hat{y}_{TR}(n) = FT^{-1}\left\{\frac{\hat{Y}_{QSSR}(f_k)}{S(f_k)}\right\} \tag{1.12}$$

$$\hat{y}_{TR}(n) = y_{TR}(n) + FT^{-1}\left\{\frac{\eta(f_k)}{S(f_k)}\right\} \tag{1.13}$$

In time domain, the convolution of the transient responses with the stimuli sequence caused by the auditory system can be undone by solving the set of equations, which are formed by the CLAD sequence. In the frequency domain, this is equivalent of

dividing the transient response spectrum by the CLAD sequence spectrum (see Figure 1.30).

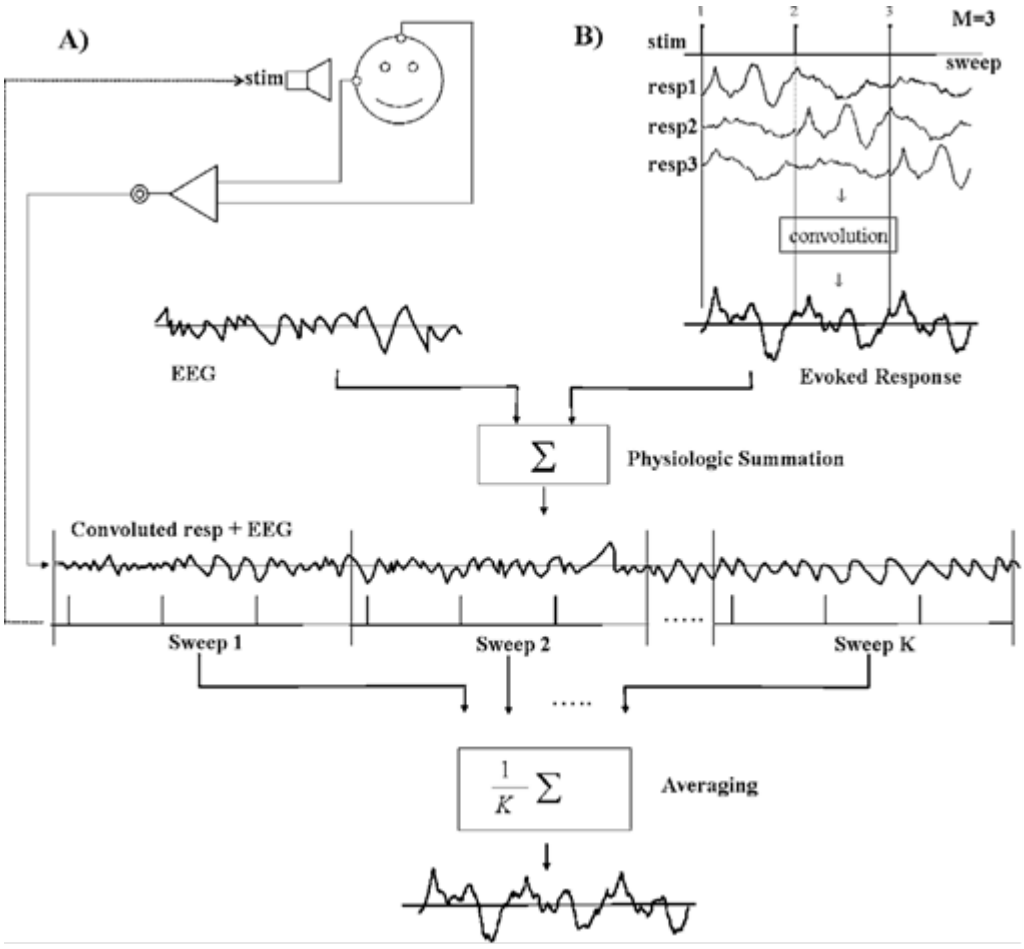

Figure 1.30 Quasi steady-state response as synthesized by the auditory system. Adapted from (Özdamar & Bohórquez, 2006).

However, steady-state responses elicited by isochronic sequences cannot be deconvolved because the stimuli sequences do not form solvable sets equations. In the frequency, stimuli sequences that do not form solvable sets of equations will contain one or more values of zeros in the frequency spectrum.

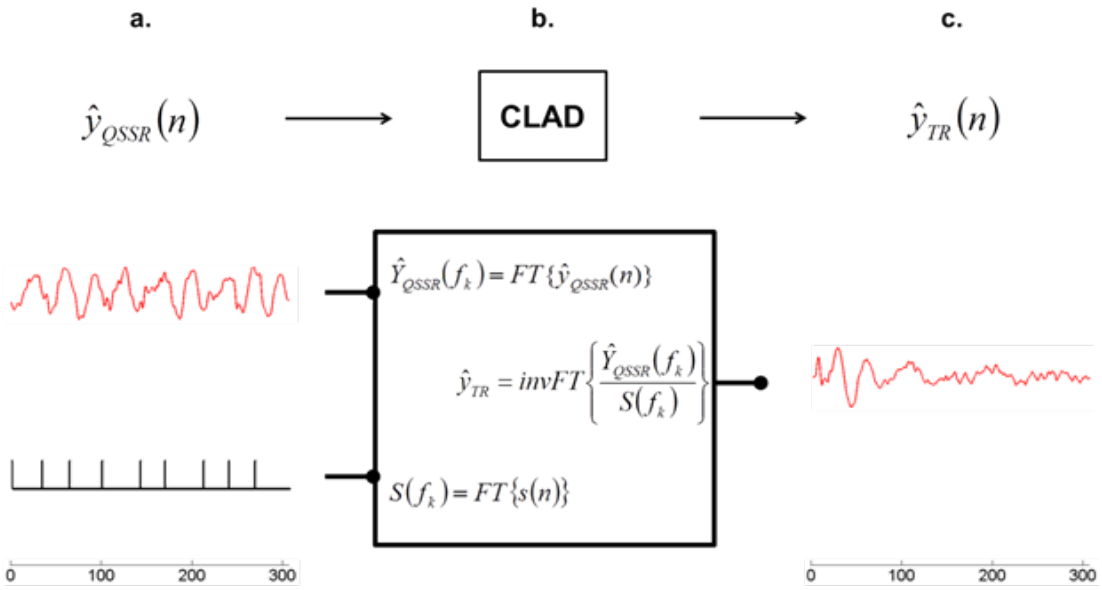

Figure 1.31 CLAD deconvolution of a transient from a quasi steady-state response.

1.2.4 Effects of Anesthesia on Evoked Potential

General anesthesia effects evoked potentials. Specifically, for this study, general anesthesia effects the components of auditory evoked potentials, by causing dose related (Thornton, et al., 1988) and anesthetic agent related changes. These changes caused by general anesthesia are attempting to suppress the arousal caused by surgical or other stimulation. The state of the patient is a result of the balance between arousal caused by surgical or other stimulation and central nervous system suppression caused by anesthetic agents (Thornton, et al., 1988).

Thornton et al. (1988) suggested the term depth of anesthesia should be used to express the net state of the central nervous system resulting from this balance. Studies have suggested that auditory evoked potentials can be used to assess the depth of anesthesia. Thornton et al. (1985) showed that certain intravenous agents produce

changes in AEPs equitable with changes produced by inhalation agents in AEPs (see Figure 1.31). These agent's effects were dose related.

Thornton et al. (1985) binaurally delivered acoustic click stimulation at a rate of 6 clicks per second, duration of the stimulation sequence was 80 ms, intensity of click at 75 dB. It was inferred from the diagram that the AEPs were recorded from the vertex, i.e., Cz location according to 10-20 international system. Etomidate group was infused starting with etomidate 0.01 mg kg-1 min-1 and increased in four equal increments to 0.05 mg kg-1 min-1. Each infusion rate was maintained for 10 min. In the saline group, equivalent volumes of saline were infused over the same time period. For both etomidate and saline group artificial ventilation was maintained with 70% nitrous oxide in oxygen.

Thornton et al. (1985) showed the Pa and Nb components produce by his stimulation sequence increased in latency and decrease in magnitude linearly with increasing concentration of etomidate anesthetic agent. Etomidate showed changes similar to those observed in inhaled agents halothane and enflurane (Thornton, et al., 1983). All three agents showed changes of a similar magnitude over an approximately equipotent range, i.e., etomidate plasma concentration range from 0 to 0.66 \µg ml-1 equates with halothane percent volume concentration range from 0 to 1.3% or enflurane percent volume concentration range from 0 to 2.5% (see Figure 1.31).

Thornton et al. (1985) attempts to equate the MAC value of the intravenous anesthetic agent etomidate through the following formulation if plasma concentration of etomidate when the patient's state is approaches just arousable is 0.14-0.2 µg ml-1 (Doenicke, Loffler, Kugler, Suttmann, & Grote, 1982; Schüttler, Schwilden, & Stoekel,

1983) and if this etomidate awake concentration is equitable to MAC awake for inhalation anesthetics agents, which is MAC awake = 0.6 (Stoelting, Longnecker, & Eger, 1970), then we can calculate an equivalent MAC value of etomidate of 0.2-0.3 µg ml-1 plasma concentration to be equatbale to the halothane MAC value of 0.75 or to the enflurane MAC value of 1.68 (Eger, 1974).

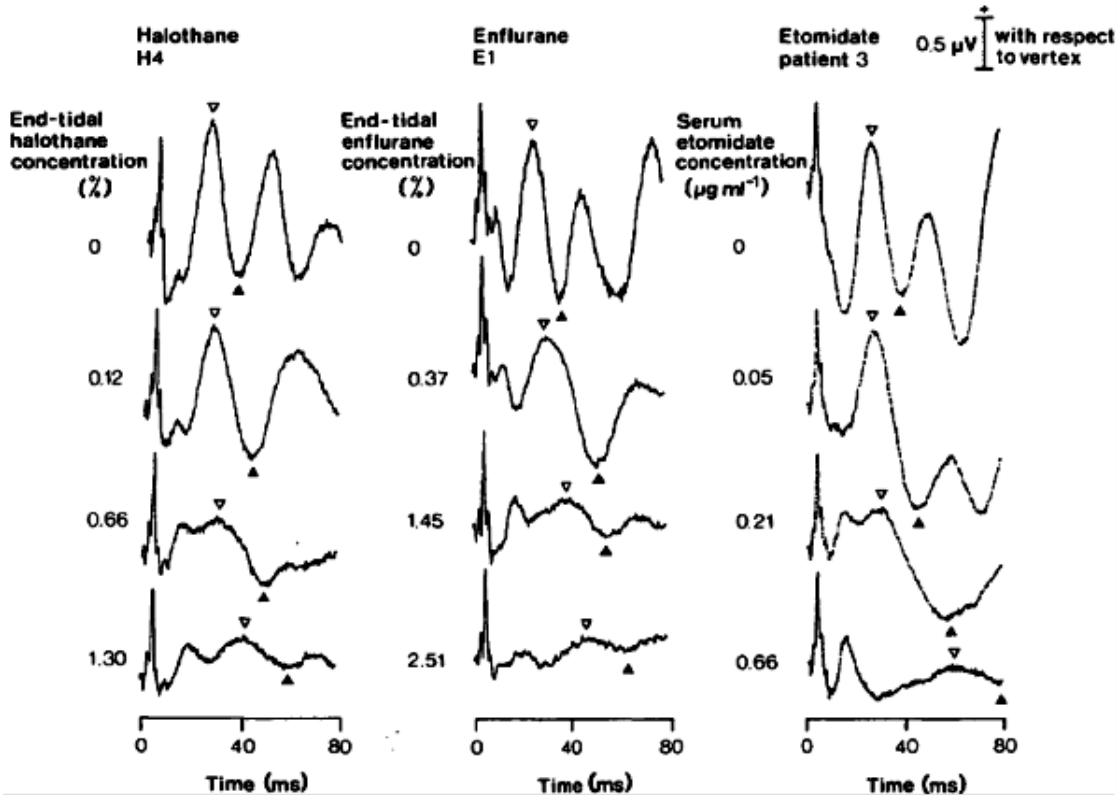

Figure 1.32 Transient evoked responses of inhaled and intravenous anesthesia. Adapted from (Thornton, Heneghan, Navaratnarajah, Bateman, & Jones, 1985).

Schwender et al. (1995) binaurally delivered acoustic click stimulation at a stimulation rate of 9.3 Hz, duration of the stimulation sequence was inferred from articles diagram to be 100 msec., intensity of click at 70 dB. The AEPs were recorded at Cz and A1/A2 with ground at Fpz. Sevoflurane group received sevoflurane at increasing concentrations from 0.5 to 2.0 vol %. Shown in Figure 1.33, the sevoflurane

concentration was measured at the expired concentration intervals 0.5, 1.0, 1.5, and 2.0. Artificial ventilation was maintained with oxygen only.

Schwender et al. (1995) observed that with increasing end-expiratory sevoflurane concentrations the Na, Pa, and Nb AEP components showed an increase in latency and a decrease in magnitude (see Figure 1.32). Schwender et al. (1995) stated that similar findings were shown for middle latency response components with the inhaled anesthetic agents isoflurane, enflurane, and halothane (Thornton C., Heneghan, James, & Jones, 1984; Heneghan, Thornton, Navaratnarajah, & Jones, 1987; Thornton, et al., 1983).

Schwender et al. (1995) observed that at equipotent concentrations isoflurane, enflurane, and halothane effected the middle-latency response components to the same extent as sevoflurane. Also, Schwender et al. (1995) observed that regression analyses under increasing end-expiratory sevoflurane concentrations are comparable with slopes under halothane, enflurane, and isoflurane at equipotent (i.e., equi-MAC) end-expiratory concentrations suggesting this indicates that these inhaled anesthetic agents have comparable anesthetic MAC potencies with regard to middle latency responses suppression halothane (Thornton C. , Heneghan, James, & Jones, 1984; Heneghan, Thornton, Navaratnarajah, & Jones, 1987; Thornton, et al., 1983).

At sevoflurane concentrations of approximately 1.5 - 2.0 vol % (i.e., 0.75 to 1.0 MAC), middle latency responses components were severely attenuated or abolished. Schwender et al. (1995) suggests that because the middle latency response it primarily generated from the primary auditory cortex of the temporal lobe one may conclude that

during sevoflurane concentrations of 1.5 - 2.0 vol % the auditory processing of the primary auditory cortex is suppressed.

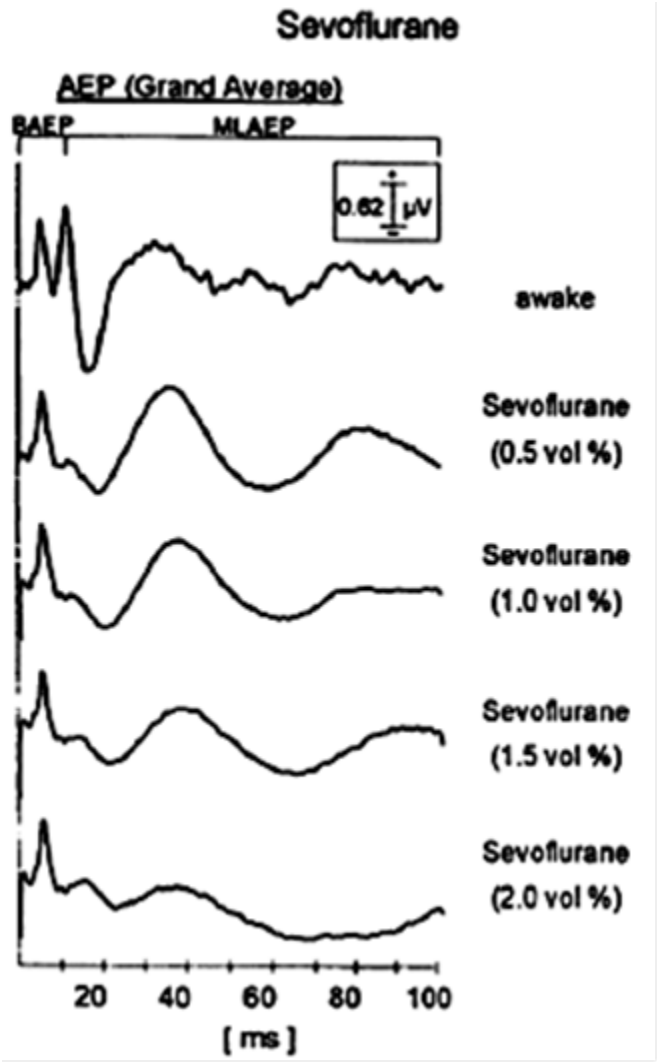

Figure 1.33 Transient evoked responses of sevoflurane inhaled anesthesia. Adapted from (Schwender, et al., 1995).

Plourde et al. (1990) binaurally delivered tone-bursts of 500 Hz, 15 msec. duration, 5 msec. rise/fall, at a rate of 40 per sec, duration of the stimulation sequence was 1490 msec., intensity of click at 90 dB. The ASSR was recorded from Fz, Cz, and Pz electrode locations all locations were referenced to M2 electrode location. The ground electrode location was not indicated.

In contrast to the previously mentioned studies the inhaled anesthetic agents in Plourde et al. (1990) were to administration at clinically adequate for surgery. For isoflurane with nitrous oxide group, the mean end-tidal expired isoflurane was 0.57 vol % and nitrous was 61 vol % (see Figure 1.33). For isoflurane only group, the mean end-tidal level was 1.04%. Plourde et al. (1990) showed that isoflurane effected phase of the ASSR but that no significant effect was due to the interaction of nitrous oxide.

Shown in Figure 1.34, Plourde et al. (1990) demonstrated that the magnitude of the 40 Hz ASSR is reduced to 5 to 50% compared to control values with isoflurane or isoflurane with nitrous oxide. Plourde et al. (1990) indicated that his result replicate the same result observed by (Hogan, 1987) who showed that the magnitude of the 40 Hz ASSRs is reduced by 78% during isoflurane with nitrous oxide.

Further Plourde et al. (1990) states these result are comparable end-tidal expired isoflurane concentrations a 50% reduction of the magnitude of the transient middle-latency AEP for isoflurane with nitrous oxide observed by Heneghan, Thornton, Navaratnarajah, and Jones (1987). Plourde et al. (1990) suggests that ASSRs are more susceptible to anesthetic agents than the transient response because the increase in latency and decrease in magnitude cause by anesthetic agent on the middle latency responses with transient responses interference with the formation of ASSR, which depend on the successive overlapping of transient responses.

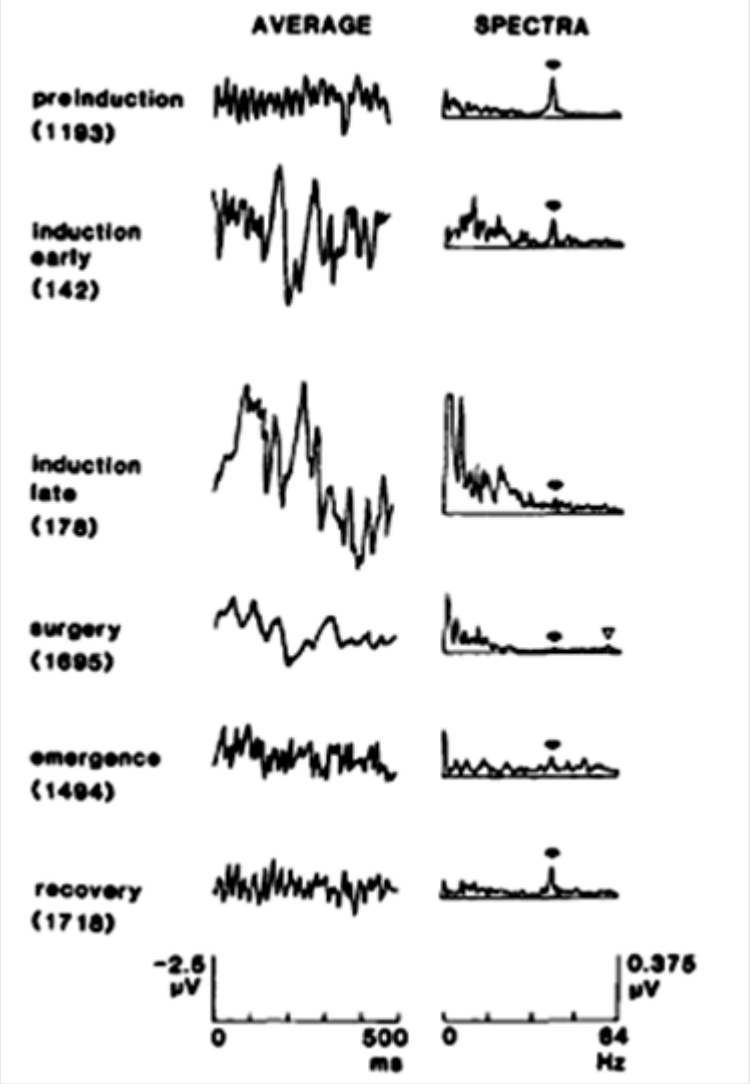

Figure 1.34 Auditory steady-state responses at different anesthesia end-points. Average unfiltered time-series waveform (left) and magnitude spectra (right) under anesthesia. Adapted from (Plourde & Picton, 1990).

1.2.5 Effects of Sleep on Evoked Potential

Sleep is an active and dynamic process that effects spontaneous brain activity, such as EEG, and brain potentials evoked by external stimulation, such as AEPs (Castro-Llanos, Bohórquez, McNeer, & Özdamar, 2013). Various states of sleep can be explored by external sensory stimulation during sleep (Millan, Ozdamar, & Bohorquez, 2006). Studies conducted on human models during sleep have suggested that evoked potentials,

although altered, still carries information as to semantic meaning (Bastuji, Perrin, & Garcia-Larrea, 2002).

PET imaging has shown specific region of the auditory cortex preserve their activation to either simple sounds, e.g., tones or complex sounds, e.g., a subject's name, identically during both sleep and wakefulness (Portas, et al., 2000). While studies indicate that the auditory pathway preserves some of it auditory processes during the sleep state the literature is still unclear about the effects of sleep on specific

AEP components. Mendel and Goldstein (1971) originally suggested that the components of the middle latency response remain stable during the in wakefulness and in various stages of sleep (Mendel & Goldstein, 1971). Mendel (1974) suggested there existed little difference in REM and stage 2 sleep compared to stage N3 sleep in the latency and amplitude of MLR components (Mendel, 1974). Brown & Shallop (1982) suggested that the Pb and Pc component of the MLR decreased in amplitude during sleep, as did (Mendel & Goldstein, 1971).

In young children, i.e., ages 5 to 7 yr, the Pa component of the MLR is sleep state dependent, and in adults, amplitude of the Pa component is largest during REM sleep and smallest during sleep stage N3 (Okitzu, 1984; Osterhammel, Shallop, & Terkildsen, 1985). Kraus et al. (1985) observed that from infancy, i.e., from age 1 to 6 months, to adolescence, i.e., age 12 years, the detectability of MLR during sleep increases monotonically from 20% in infancy to 90% (Kraus, Smith, Reed, Stein, & Cartee, 1985).

Animal model have shown a similar trend if increase MLR detectability with age (Kraus, Smith, & McGee, 1987a; Kraus, Smith, McGee, Stein, & Cartee, 1987b; Kraus,

Smith, & McGee, 1988). Both human and animal maturational changes appear to indicate that the increased detectability of MLRs are caused by an underlying systematic process and that these changes in detectability may be correlated to different developmental time courses for the MLR generators (Kraus, Smith, & McGee, 1988). The MLR has been shown to have multiple generators, reflecting both primary and non-primary auditory pathways (McGee, Kraus, Comperatore, & Nicol , 1991; McGee, Littman, Kraus, & Nicol, 1992).

Kraus & McGee (1992) provide an explanation for the increased detectability of MLRs with respect to maturation, MLR generators have sleep state dependent generators that develop early. Then during the first 10 to 12 years of life other sleep state-resistant MLR generators develop. These later-developing generators dominate the generation of the adult MLR, which shows only minimal changes with sleep state (Kraus & McGee, 1992) .

The effects of sleep on the amplitude of the 40 Hz ASSR show a 50% reduction in response amplitude when transitioning from wakefulness to sleep (Brown & Shallop, 1982; Cohen, Rickards, & Clark, 1991; Galambos, Makeig, & Talmachoff, 1981; Jerger, Chmiel, Frost, & Coker, 1986; Linden, Campbell, Hamel, & Picton , 1985; Picton, John , Purcell , & Plourde, 2003; Shallop & Osterhammel, 1983; Suzuki, Kobayashi, & Umegaki , 1994).

Brown and Shallop (1982) and Shallop and Osterhammel (1983) observed the amplitude of responses recorded during sleep state to one third of the amplitude of responses recorded during the wakefulness state. Klein (1983) also had similar

observation the amplitude of the steady state response was smaller during sleep than wakefulness. Millan (2006) studied high rate 40 Hz transient responses sleep under. Millan delivered monoaural clicks measured from Cz-M1 and Cz-M2 grounded at Fpz. Millan (2006) observed that for the 40 Hz MLR the Na-Pa complex remained stable and the Nb-Pb complex showed a clear reduction in amplitude with regard to sleep depth of subject. Also, Pb declined as with increase in sleep stages. Millan (2006) suggested that for the 40 Hz the Pa-Na-Pb would be useful in for assessing sleep.

Erwin & Buchwald (1986) delivered acoustic click stimulation at a stimulation rate of 1 Hz, intensity of click at 40 dB HL during sleep. The auditory responses were recorded at Cz midline with a linked mastoid reference. The auditory responses were bandpass filtered from 10 to 3000 Hz. Erwin et al. observed no significant changes for the magnitude of Pa for sleep stages N2, N3 or REM (see Figure 1.34). Erwin et al. did an analysis comparing awake which he classified as the mean of stage W and N1 to sleep, which he classified as the mean of stage N2, and N3. From awake to sleep, he found that the latency for Pa significantly increases, albeit small, and the magnitude of Pb is significantly attenuate or even abolished (see Figure 1.34). While Erwin et al. did not measure the N1 component; however it can be observed from Figure 1.34 that the N1 component shows a larger negativity in stages N2 and N3.

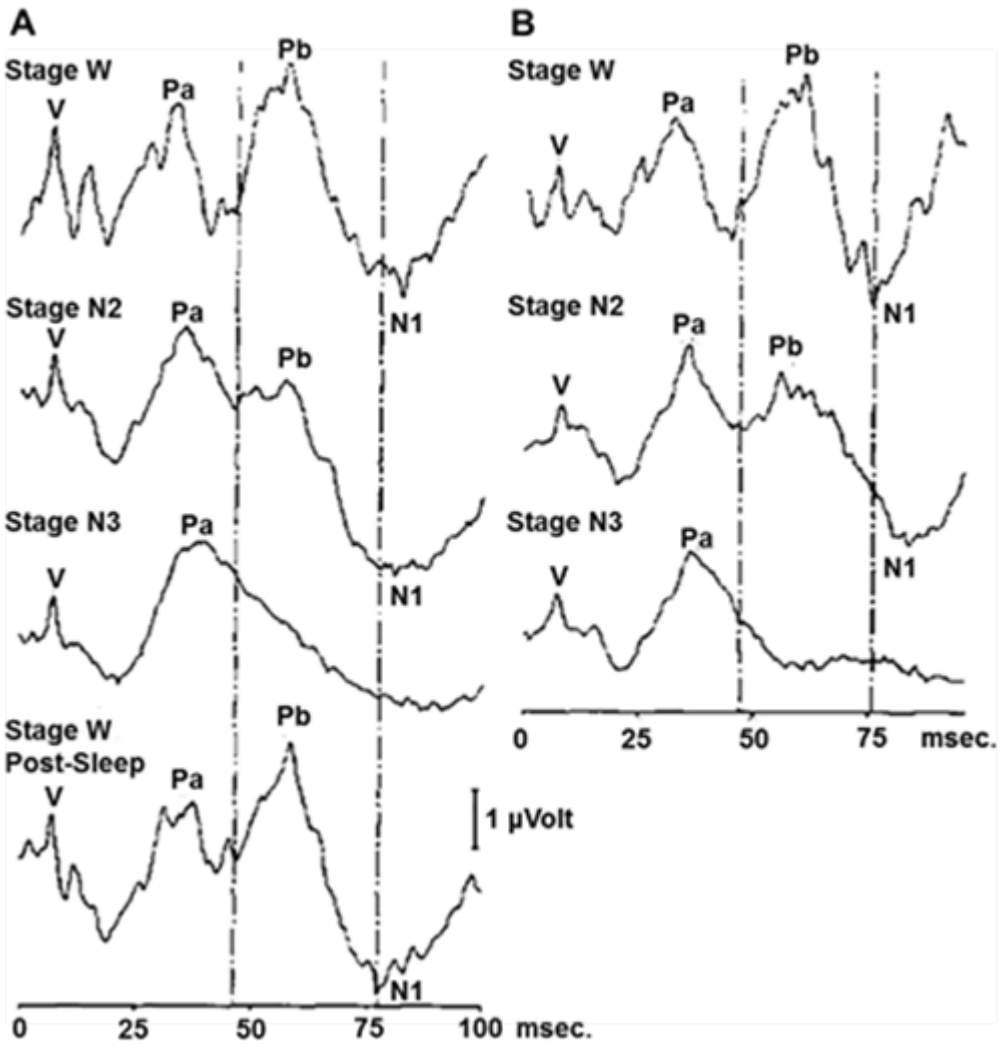

Figure 1.35 Transient response at different stages of sleep. Averaged auditory evoked response of one subject from two sessions recorded three months apart. The first session is column A and the next session column is B. Adapted from (Erwin & Buchwald, 1986)

Deiber, Ibanez, Bastuji, Fischer, & Mauguiere (1989) delivered acoustic clicks randomly between 190 and 290 msec., intensity of click at 60 dB HL during sleep. The auditory responses were recorded at Fpz mediofront with a right shoulder subcutaneous needle reference. The auditory responses were bandpass filtered from 10 to 200 Hz. As shown in Figure 1.35, Deiber, et al. observed that the latency of Na and Pa increases from stage II (i.e., stage N2) to stage IV (i.e., stage N3) and decrease in REM.

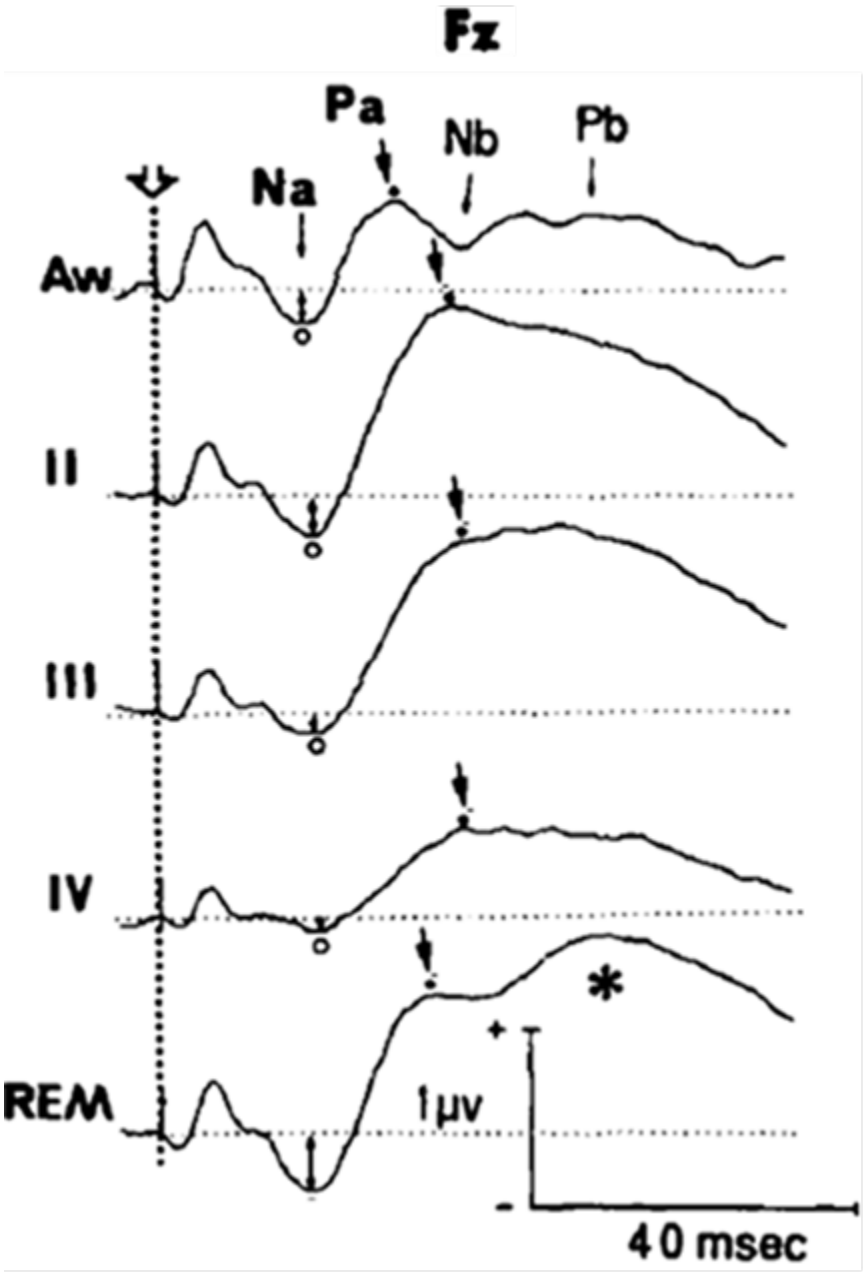

Figure 1.36 Grand mean of auditory middle-latency responses of ten subjects. Each sleep stage is labeled as follows: awake state (Aw), NREM sleep (II, III, and IV), and REM sleep (REM, down). Adapted from (Deiber, Ibanez, Bastuji, Fischer, & Mauguiere, 1989)

Chapter 2 METHODS

2.1 Subjects and Procedures

Anesthesia: This study was conducted with the approval of the University of Miami's institutional review boards and the approval of the Jackson Memorial Hospital's Human Subject Research office. Patients with a history of auditory conditions or with medical conditions were excluded from participating in this study. General anesthesia was administered according to the Standards for Care guidelines established by the American Society of Anesthesiologists (i.e., ASA). Anesthesiologists maintained patients at adequate anesthetic levels by administering both intravenous and inhalation anesthetic agents.

For the purpose of processing at a later time, the vital signals and anesthetic concentration were recorded by an integrated anesthesia management system called Picis. The auditory stimulus and instrument settings were the same for all patients; moreover, these conditions were held identical for both anesthesia and control (i.e., wake condition). Sevoflurane was specifically investigated in this study (i.e., IUPAC name: 1,1,1,3,3,3-Hexafluoro-2-(fluoromethoxy)propane, Structural formula: CH2F-O-CH(CF3)-CF3).

From five patients, the auditory transient and steady-state responses, and the EEG spectral descriptors were acquired during general anesthesia. The decision to conduct this research through a real environment such as a surgical theatre and not a controlled environment such as a research laboratory posed two challenges: (a) Medical devices

used for surgery inputted instrument noise into the biosignals during acquisition and (b) The administration of the anesthetic agent was not a controlled research variable.

Anesthesia was administered to ensure the patients did not experience unintended intraoperative awareness. The administration of anesthesia varied with respects to the minute-to-minute requirements of the surgical procedure. As a consequence, each patient had a unique trajectory of anesthesia administration for surgery. It is common in laboratory settings to refine the parameters in order to investigate the research variables of a study. For ethical reasons, this is not possible in a working surgical environment. In this context, the research was not permitted to influence any aspect of the anesthesia and only serve as spectators acquiring data. This leads to the challenge of having the rate of administration and concentration of anesthetic agent as a research variable that is not controlled by this study.

Sleep: This study was conducted with the approval of the University of Miami's institutional review boards. Subjects with a history of auditory or medical conditions were excluded. Sleep end-points were determined according to American Academy of Sleep Medicine (i.e., AASM) manual for the scoring of sleep and associated events. The auditory stimulus and instrument settings were the same for all subjects; moreover, these conditions were held identical for both sleep and control (i.e., wake condition).

Subjects attempted one hour of sleep on a bed inside an audiometric examination suite. The audiometric suite isolated acoustic sounds and electromagnetic interference (i.e., EMI). From fourteen subjects, the auditory transient and steady-state responses and EEG spectral descriptors were acquired during the first hour of sleep. An inherent

challenge for the subjects was the continuous auditory stimulation delivered while entering sleep.

2.2 Stimulus Design

The effect of auditory stimulation in anesthesia was investigated by using the 20, 30, and 40 Hz rates. Compared to the auditory response elicited by the 20 and 40 Hz rates, the 30 Hz response showed notable performance during changes in anesthetic levels, in regards to cortical and non-cortical potentials. Also, the responses elicited by the 40 Hz rate during changes in anesthesia levels were previously investigated (McNeer, Bohórquez, & Özdamar, 2009).

The 30 Hz rate was investigated further in the Neurosensory Engineering Laboratory in the University of Miami. Here parameters could be refined as needed in order to investigate the research variables; this is the sleep study. For the sleep study, a more optimized version of the 30 Hz low-jittered stimuli sequence used in the anesthesia study was designed having improved spectral noise performance, such as preserving lower frequency components.

For both anesthesia and sleep, this section presents the stimulation paradigm which describes the method used to deliver the auditory stimulation to each subject. Also, this section presents the properties of each stimuli sequence, such as (a) the time occurrence of each stimulus; (b) the histogram distribution of the inter-stimulus interval; and (c) the noise amplification due to the sequence.

2.2.1 Anesthesia Auditory Stimuli

The stimulation paradigm used in the anesthesia study investigated the effects of anesthesia on evoked potential elicited by 20, 30, and 40 Hz low-jittered stimuli sequences. Shown in Figure 2.1 was the designed auditory stimulus for the anesthesia study. The auditory stimulus, which lasted 4,710.4 msec., was a composite of five stimulation regions and one silence region (i.e., control).

The regions were arranged in series as follows 5, 20, 30, 40 Hz, and silence region. The 5 Hz region, which lasted 614.4 msec., was a series of three identical 5 Hz isochronic stimuli sequences; each 5 Hz isochronic stimuli sequences lasted 204.8 msec.. This 5 Hz stimuli sequence had one stimulus that occurred at 0 msec. with respect to the 204.8 msec. sequence length.

The 20, 30, and 40 Hz regions, which each lasted 1,228.8 msec., were each a series of four identical stimuli sequences, each sequence lasted 307.2 msec.. The 20 Hz stimuli sequence had six stimuli that occurred at 0, 55.4, 99.4, 141.8, 201.8, and 259.4 msec. with respect to the 307.2 msec. sequence length.

The 30 Hz stimuli sequence had nine stimuli that occurred at 0, 37.6, 68.8, 98.4, 132.8, 160.8, 200.8 228.8, and 268.8 msec. with respect to the 307.2 msec. sequence length. The 40 Hz stimuli sequence had twelve stimuli that occurred at 0, 21.6, 49.6, 73.6, 99.2, 120.8, 145.6 174.4, 196.0, 225.6, 255.2, and 277.6 msec. with respect to the 307.2 msec. sequence length.

The silence region, which lasted 409.6 msec., did not contain stimuli sequences. It was a 409.6 msec. period of silence. The auditory stimulus had a total duration of 4,710.4 msec.

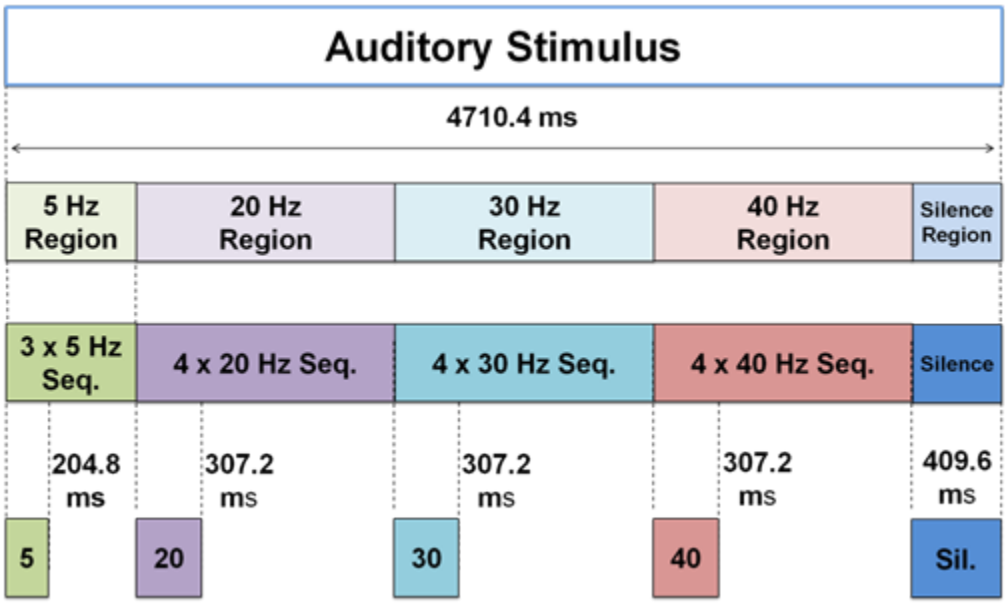

Figure 2.1 The auditory stimulus used in the anesthesia study. The composite auditory stimulus train is 4710.4 msec. long and is comprised of five distinct regions (i.e., four stimuli and one silence). Each region is subdivided into individual sweeps as shown. The 5 Hz region contains three isochronic stimuli sequences, each 204.8 msec. long. The 20, 30, and 40 Hz regions, for each stimulation rate, contain four low jittered CLAD stimuli sequences and each sequence was 307.2 msec. long as shown. The silence region did not contain any stimuli and was 409.6 msec. long.

Jitter Factor (i.e., JF) is a measure of how much a jittered stimuli sequence will differ from an isochronic stimuli sequence. The jittered factor for isochronic stimuli sequences is 1.0. In regards to the 20, 30, and 40 jittered stimuli sequences used in this study the jittered factor values are respectively 1.415, 1.429, and 1.370.

Shown in Figure 2.2, is the sequence of stimuli, rate histogram and noise amplification factor for each sequence. These rates were designed to have little or no overlap in their rate histogram. Due to their noise amplification factors, the spectral

frequencies below 13 Hz were removed in the deconvolution of the auditory transient responses.

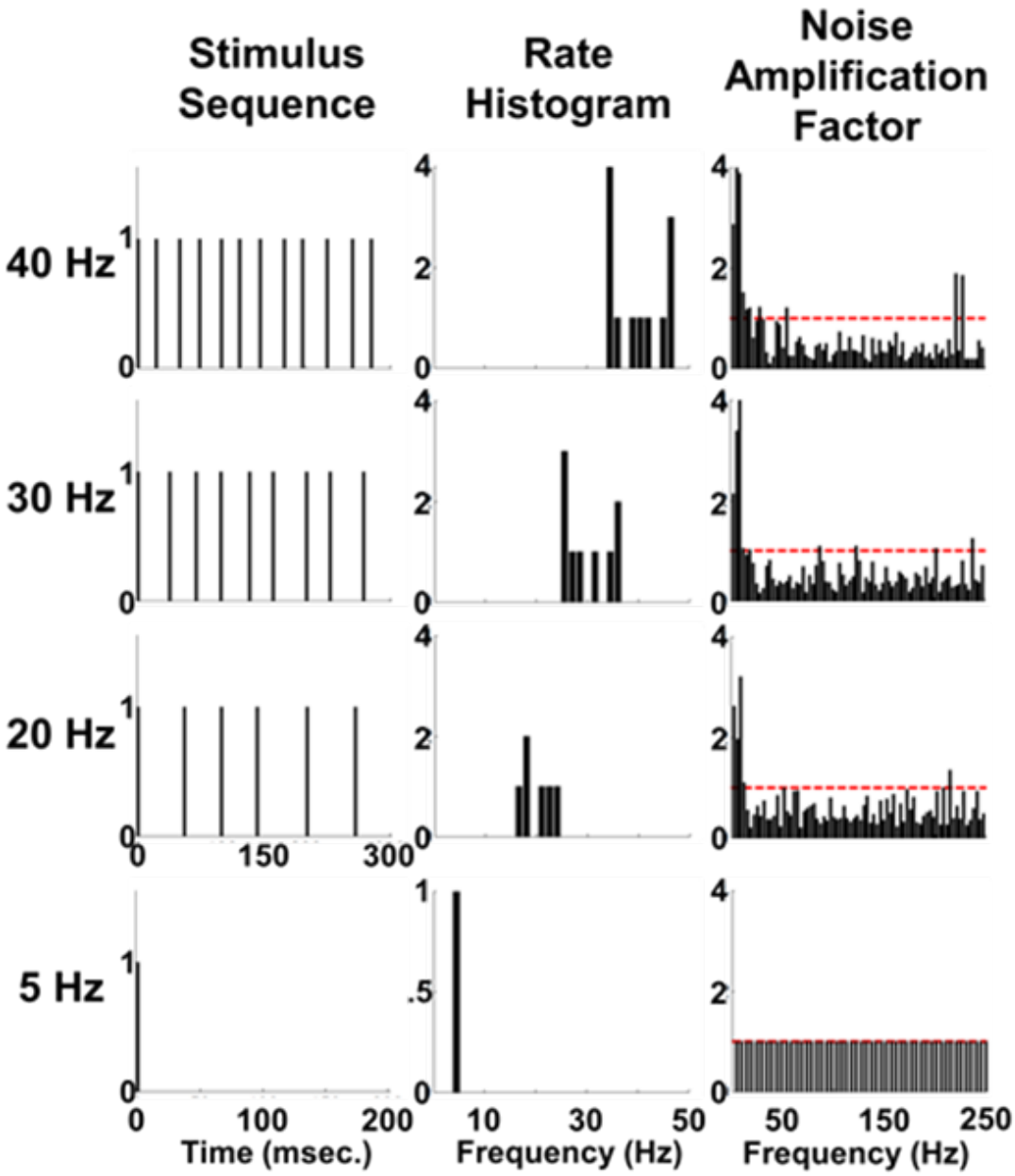

Figure 2.2 Characteristics of the auditory sequence of stimuli. Row 1 shows the time occurrence of each auditory stimulus. Row 2 show the histogram distribution describing the inter-stimulus intervals that comprise the sequence. Row 3 shows the noise amplification property of the sequence design.

2.2.2 Sleep Auditory Stimuli

The sleep study stimulation paradigm investigated the effects of sleep on auditory evoked responses. The auditory stimulus used in the sleep study investigated the effects of sleep stages on the 5 and 30 Hz rates using silence as the control.

The 30 Hz sequence used for the sleep study was designed with improved noise performance and with a longer duration of stimulus regions. Due to its performance in the anesthesia study, the modified 30 Hz sequence was investigated as a prospective sequence for probing the effects that sleep stages have on high-rate auditory responses.

Shown in Figure 2.3 is the designed auditory stimulus for the sleep study. The auditory stimulus, which lasted 36,864 msec., was a composite of two stimulation regions and one silence region (i.e., control). The regions were arranged in series as follows 5, 30 Hz, and silence region.

The 5 Hz region, which lasted 12,288 msec., was a series of sixty identical 5 Hz isochronic stimuli sequences, each 5 Hz isochronic stimuli sequence lasted 204.8 msec.. This stimuli sequence had one stimulus that occurs at 0 msec. with respect to the 204.8 msec. sequence length.

The 30 Hz region, which lasted 12,288 msec., was a series of forty identical stimuli sequences, each sequence lasted 307.2 msec.. The 30 Hz stimuli sequence had nine stimuli that occur at 0, 32.8, 63.20, 99.2, 141.6, 168.8, 211.2, 239.2 and 268.0 msec. with respect to the 307.2 msec. sequence length.

The silence region, which lasted 12,288 msec., did not contain auditory stimuli. It was a 12,288 msec. period of silence. The auditory stimulus had a total duration of 36,864 msec. The jittered factor of the new 30 Hz low-jittered stimuli sequences was 1.559.

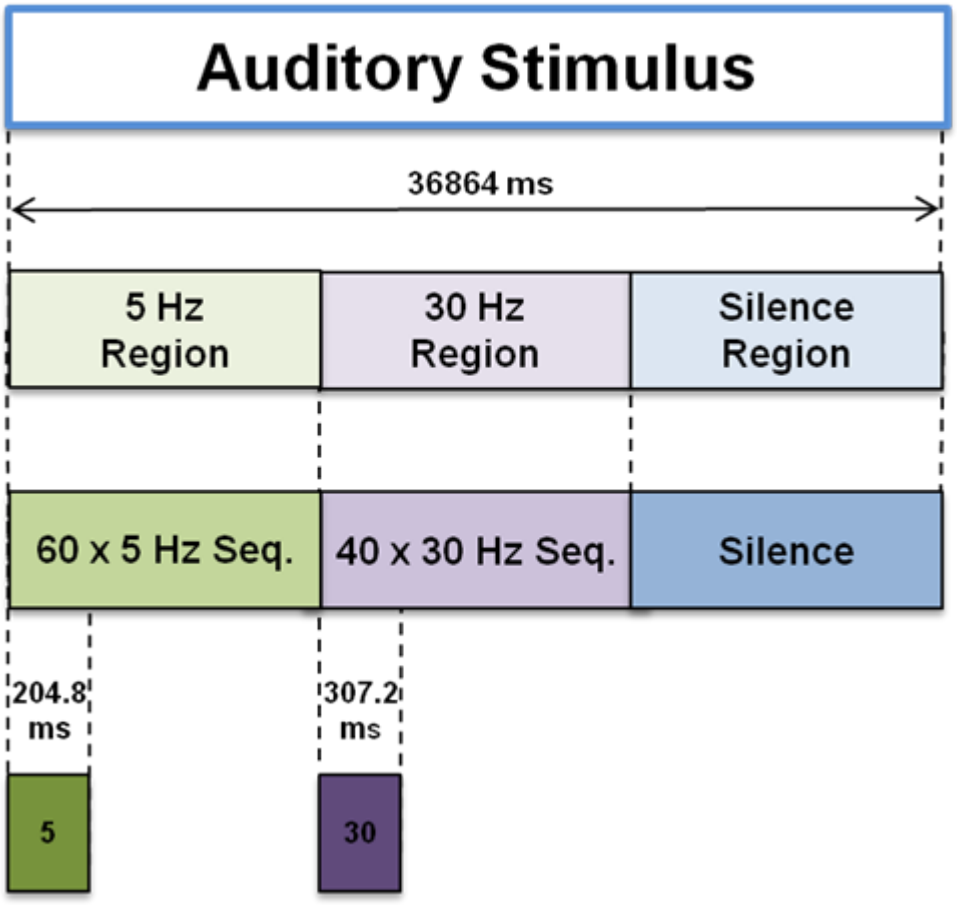

Figure 2.3 The auditory stimulus used in the sleep study. Auditory stimulus is comprised of three auditory stimulus regions: (a) A 5 Hz stimulus region containing sixty individual 5 Hz stimuli sequences, (b) A 30 Hz stimulus region containing forty individual 30 Hz low jittered stimuli sequences and (c) Silence region.

Shown in Figure 2.4, is the sequence of stimuli, rate histogram and noise amplification factor for each sequence. These rates had no overlap in their rate histogram. Due to their noise amplification factors, the spectral frequencies below 5 Hz were removed in the deconvolution of the auditory transient responses.

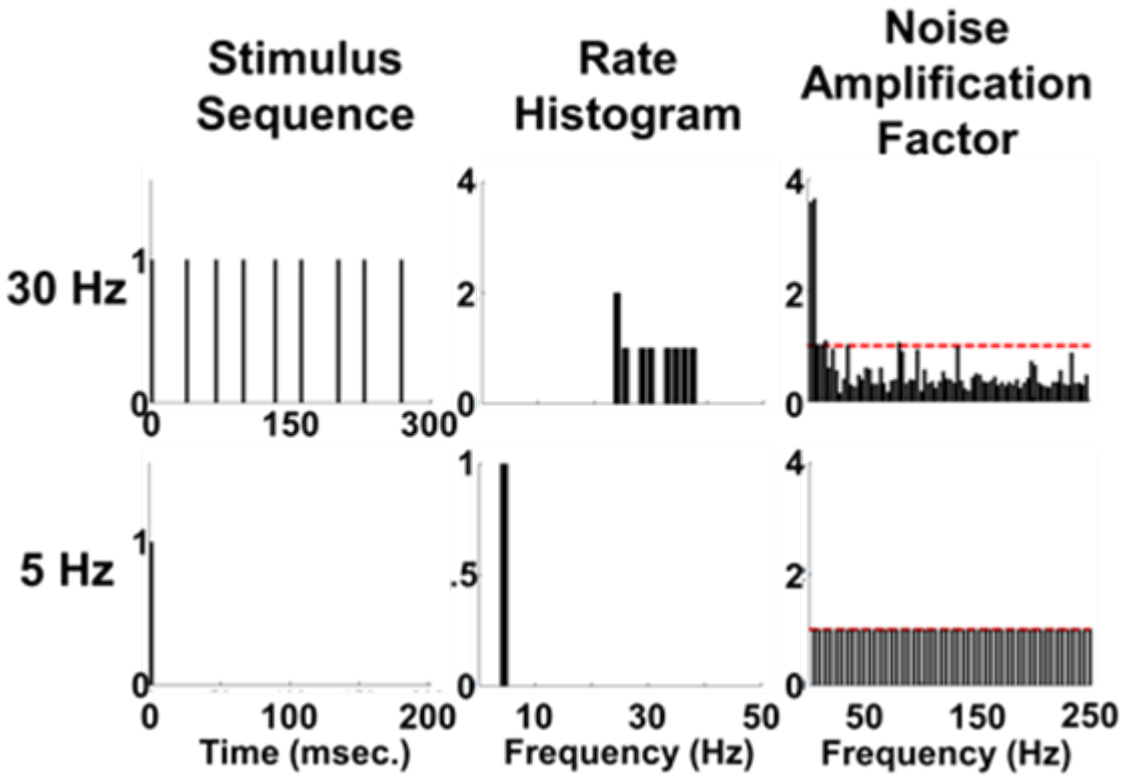

Figure 2.4 Characteristics of the auditory sequence of stimuli. Row 1 shows the time occurrence of each auditory stimulus. Row 2 show the histogram distribution describing the inter-stimulus intervals that comprise the sequence. Row 3 show the noise amplification property of the sequence design.

2.3 Acquisition

To compare the anesthesia and sleep study, the instrument settings used for signal acquisition were identical with the exception of amplifier gain. Both studies acquired signals from electrodes placed in the frontal region. The inactive electrode was placed on the right mastoid, for the anesthesia study, and on the right auricle, for the sleep study. For both anesthesia and sleep, this section presents the acquisition parameters such as intensity (i.e., sound level of acoustic clicks), electrode montage, channel derivatives, and instrument settings during acquisition, filter settings, and artifact rejection method.

2.3.1 Data Acquisition Anesthesia Study

The designed auditory stimulus was delivered at 70 dB nHL intensity (i.e., level 82 dB SPL, calibrated with 2 mL acoustic coupler using the precision sound level meter Quest Model 1800) to the right ear using insert earphone (i.e., ER-3A Ethmotic Research, Elk Grove Village, IL). To mitigate the effects of electromagnetic interference the electrode leads were weaved. EEG was recorded using the Intelligent Hearing Systems (i.e., IHS) acquisition instrument, called SmartEPCAM.

Shown in Figure 2.5 is the electrode placement, which used the 10-20 international system of electrode placement, was as follows: (a) Fz was positive, (b) right mastoid (i.e., M2) was negative, and (c) Fpz forehead was ground. The channel derivative used to record the EEG was Fz-M2.

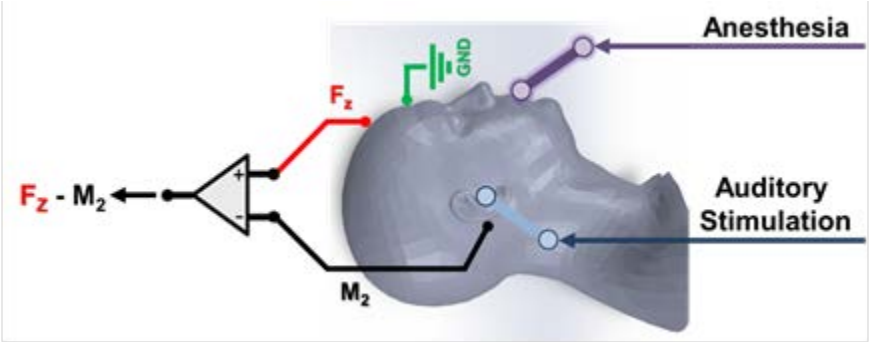

Figure 2.5 Data collection of anesthesia study. Shown is the electrode montage used to record EEG: (a) Fz and Oz (i.e., positive), (b) M2 (i.e., negative, right mastoid), and (c) forehead (i.e., ground reference). The auditory stimulus was delivered to the right ear as shown. Inhaled anesthetic (i.e., sevoflurane) was administered through intubation as shown. The electrode derivatives used to measure were Fz-M2 and Oz-M2 as shown.

The recordings were amplified (i.e., gain 100,000), band-pass filtered from 1 to 1500 Hz (i.e., 6dB/octave roll-off), and digitized (i.e., 16 bits, 200 μsec. sampling period). Typically 1000 repetitions of the auditory stimulus are attempted to be acquired.

The signal was divided into segments called sweeps. The sweeps were processed by artifact rejection software used to visually reject sweeps. The sweeps were demeaned for all auditory responses. The 20, 30 and 40 Hz auditory evoked responses were zero-phase filtered using linear-phase digital filters with a bandpass from 13 to 1500 Hz.

2.3.2Data Acquisition Sleep Study

The designed auditory stimulus for the sleep study was delivered monaurally to the right ear at 60 dB nHL intensity, while for the anesthesia study it was delivered monaurally to the right ear at 70 dB nHL intensity. A modified version of the AASM referential electrode montage was used both to visually score the signals sweeps and to extract the evoked responses.

Shown in Figure 2.6 are the recording channels used in the sleep study such as Cz-A1, Cz-A2, Fz-A2, Oz-A2, E1-A2, E2-A2, and EMG1-EMG2. The ground electrode was placed on the forehead Fpz. The sleep study used the same instrument settings as the anesthesia study, except for the amplification (i.e., gain 50,000) used in the sleep study. Typically a minimum of 1000 repetitions of the auditory stimulus were attempted to be acquired. The signal was divided into segments called sweeps. The sweeps were processed by sleep scoring software used to visually score the sleep stage of the sweeps and visually reject sweeps containing artifacts.

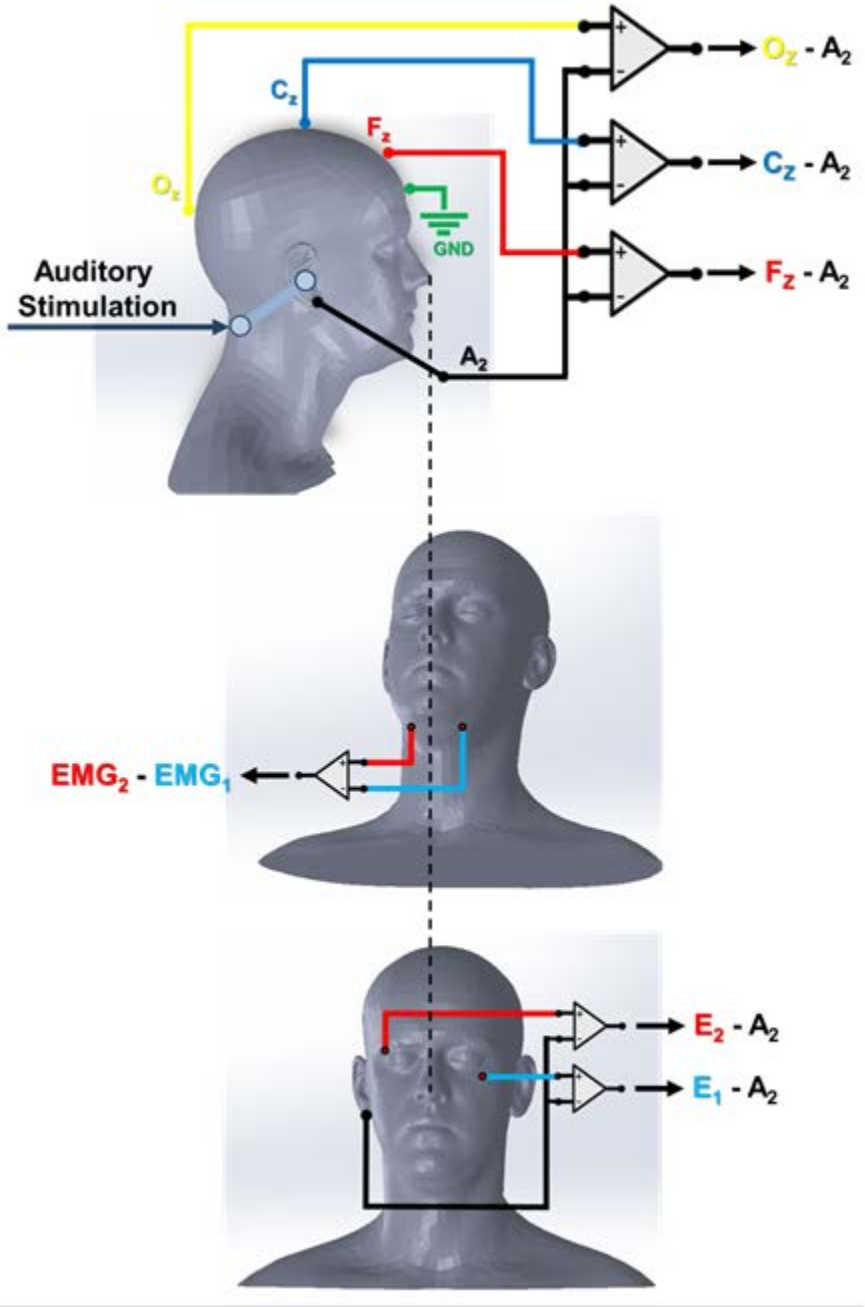

Figure 2.6 Data collection of sleep study. Shown is the electrode montage used to record EEG: (a) Fz (positive), (b) A2 (i.e., negative, right earlobe), (c) A1 (i.e., negative, left earlobe), and (d) forehead (i.e., ground reference). Additional electrodes were for sleep stage scoring.

The sweeps were demeaned for all auditory responses. The 30 Hz auditory evoked responses were zero-phase filtered using linear-phase digital filters at a bandpass from 5 to 1500 Hz.

2.4 Processing

The acquired data was arranged into data structures to analyze the interactions between the features. For the anesthesia study the acquired data was arranged into units referred to as packages that stitch together the various anesthesia data (i.e., Picis, EEG, and EP data) to the same timeline. This arrangement made it possible to preform time series analysis (e.g., trend analysis). The data for anesthesia was not structured in the same manner as sleep. Anesthesia, compared to sleep, does not have clearly defined stages. Therefore, time-series analysis methods were more fitting for processing the anesthesia data, such as trend analysis for EEG spectral descriptors and moving average for auditory evoked responses (i.e., EPs). As sleep has clearly defined stages (i.e., sleep stages) grouped analysis methods were more fitting to process the sleep data, such methodologies that are with respect to sleep stages for both EEG spectral descriptors and auditory evoked responses.

For consistency, these EEG and EP features estimated from anesthesia and sleep were computed using the same parameters as used in the anesthesia study. The acquired data was processed to estimate the spectral descriptors. This section presents the estimation procedure of the power spectral density and the estimation procedure of the spectral descriptors, which was estimated from the power spectral density. It presents the settings used to estimate these features. Also, this section presents the estimation procedure of the auditory evoked responses and includes the settings used to estimate both transient responses via CLAD and the phasors of the steady-state responses. It presents the estimation procedure of the grand mean of the 5 Hz moving average of the anesthesia.

2.4.1 Data Structuring Strategy Anesthesia: Moving Average, Trends

After acquisition, the EEG was divided into segments that corresponded to the onset and duration of the auditory stimulus (i.e., 4,710.4 msec.). After the segmentation of the EEG with respects to auditory stimulus the contaminated segments were artifact rejected using visual rejection of segments. After artifact rejection, the accepted segments were divided according to a sorting scheme presented in this section with respects to time occurrence. This process turns the resulting signal into a time-series signal and allows for time-series methods of analysis.

The integrated anesthesia management system (i.e., Picis) captures physiologic data measured by medical devices recording it at rate of one sample per 60,000 msec. (i.e., one sample per 1 min.). The IHS acquisition system captures discrete voltages samples that comprised the EEG signal from surface electrodes at a rate of 300,000 samples per 60,000 milliseconds. The rate-limiting factor was the sample rate of the Picis system. A data structuring strategy was designed to match the data from the two systems to one time-point occurrence. The acquired data from acquisition system and the acquired data from Picis system were organized into discrete one-minute data structures with respects to the interval of time for each Picis sample point, termed packages.

A package is a data structure that holds all the data from both the Picis and acquisitions system that represent one 60,000 milliseconds of data. The two systems are time synchronized and all time related information is converted to seconds. Each package represents one minute (i.e., 60,000 msec.) of data. The data selected to be written to the packages is any segments of EEG that is acquired from the time-point that marks the

previous minute to the time-point that marks the current minute, but not including time-point that marks the current minute. All segments that have time occurrences that are greater than or equal to the lower limit of the minute time-point and are less than the upper limit of the minute time-point are selected and written into the package data structure. This process makes all the acquired data directly comparable via the same time occurrence and allows for methods of direct comparison to be applied directly to the data.

To account for the dynamic of sevoflurane anesthetic agents a fifteen-point moving average is performed on the data, points refer to packages in this case. The time series method selected for the analysis of this data was the trend analysis. The parameters of the trend analysis were a ten-point windows length with a fifty percent overlap between consecutive windows. The ten-point window length was estimated to be the minimal window length that yielded response. The windows are overlapped by fifty percent to reduce redundancy between adjacent EP responses. The sets of packages produced by the trend analysis were then used to perform the EP and EEG analysis.

2.4.2 Data Structuring Sleep Strategy: Sleep Staging

After acquisition, the EEG was divided into segments that corresponded to the onset and duration of the auditory train stimulation. After the segmentation of the EEG with respects to auditory trains the segments were scored with respect to each of the sleep stages. For accurate manual sleep scoring, an EEG scoring aid software was developed. This software was feature rich in time- and frequency- domain analysis tools. It allowed the user to easily inquire about the signal under study by either exploring its time series

properties or probing its underlying spectral content. Once completed a second, independent, blinded-assessment of scores was performed.

This software was used to reject segments with artifacts or segments that contained more than one sleep stage. After visual scoring and artifact rejecting, the accepted segments are divided according to sleep stage. All parameters measured in this study were grouped with respects to the defined sleep stages.

The analysis of the EEG and EP features with respects to sleep stages in the sleep study draws a contrast to the analysis of the EEG and EP features with respect to time in the anesthesia study. The results of the sleep study provide a perspective or a deeper analysis of the limitations and of the value in discrimination of the anesthesia study features because sleep has well defined end-points (i.e., sleep stages).

Rules of Sleep Stage Scoring: The scoring of sleep stages follows the specifications and rules provided in the American Academy of Sleep Medicine (i.e., AASM) manual for the scoring of sleep and associated events (Conrad, Ancoli-Israel, & Chesson, 2007). The AASM manual recommends the following new terminology for stages of sleep: stage W (i.e., Wakefulness), stage N1, stage N2, stage N3, and stage R. The new terminology classifies stage N3 as slow wave sleep and replaces stage 3 and stage 4 from the original Rechtschaffen and Kales classification of sleep stages (see Rechtschaffen and Kales, 1968).

Scoring is performed on 30 second duration sequential segments of EEG (Conrad, Ancoli-Israel, & Chesson, 2007). In this study, the scores are assigned to the EEG segment of the auditory stimulus length (i.e., 36 seconds). If more than two stages are

present in one segment, then the stage with the greatest portion of the segment is assigned (Conrad, Ancoli-Israel, & Chesson, 2007). It should be noted that the AASM manual uses the term epoch to define a segment of EEG. The rules for visually scoring each sleep stage are described in detail in the AASM manual (Conrad, Ancoli-Israel, & Chesson, 2007) briefly the rules are as follows:

Stage W

- Epochs are scored as stage W when alpha rhythm in occipital region is present for more than 50% of the epoch.
- In the event that alpha rhythm is not observed in epochs then epochs are scored as Stage W if the following features are observed in epochs
    - Eye blinks these are typically within in 0.5 - 2 Hz
    - Reading eye movement, which is denoted by a slow phase of conjugated eye movement in one direction followed by a rapid returning movement in the opposite direction
    - Irregular eye movement, which is denoted by irregular rapid phase of conjugated eye movement. This eye movement is typically observed with chin muscle tone

Stage N1

- Epochs are scored as stage N1 when for subjects with initial alpha rhythm commence showing an attenuation of alpha rhythm that is replaced by low amplitude, mixture of frequency EEG present for more than 50% of the epoch.

- Epochs are scored as stage N1 when for subjects that did not show an initial alpha rhythm show any of the following

    - Slowing of background EEG activity compared to the activity observed in stage W that is greater than or equal to 1 Hz and the presence of activity at a frequency range from 4 to 7 Hz

    - Vertex shaped wave in EEG, which are waves that are sharply defined of duration less than 0.5 seconds. To score stage N1, vertex waves are not required but may be present

    - Slow eye movements

Stage N2

- Epochs are scored as stage N2 when during the first half of the current epoch or the last half of the previous epoch shows any of the following.

    - One or more K complexes are observed that are unassociated with arousal

    - One or more sleep spindle trains are observed

- Continue to score as stage N2 when the previous epoch has K complex that is unassociated with arousal or sleep spindles and the following is observed in the current epoch

    - Low magnitude, mixture of frequency EEG activity and epochs do not show K complexes or sleep spindles

- End scoring as stage N2 when any of the following happens

    - A transition to stage W, stage N3, or stage R

    - An arousal

    - A major body movement that is followed by slow eye movement and low magnitude mixture of frequency EEG

Stage N3

- Epochs are scored as stage N3 when slow wave activity is present for 20 % or more of the epoch. Slow wave activity is denoted by waveforms with a peak-to-peak magnitude of greater than 75 μVolts and with frequency of 0.5 to 2 Hz in the frontal region

Sleep stages were assigned to EEG epochs in the following manner. Two investigators independently assigned the sleep stages to the acquired EEG epochs. Both investigators compared their assigned sleep stages of their EEG epochs. For epochs whose scores differed, both investigators, by referring to rules set by the AASM scoring guideline, questioned the accuracy of the scored stage. EEG epochs having an

inconclusive score were excluded. Epochs that have short burst of arousal or artifacts of contamination during sleep were removed.

2.4.3 Spectral Descriptors Processing: Anesthesia and Sleep

Power Spectrum: In this study, the Welch estimation method was used to compute the power spectrum density (i.e., PSD) of the acquire EEG signal. The Welch power spectrum is estimated by dividing the acquired EEG signal (i.e., 60,000 msec.) into smaller equal length segments of 2000 msec. duration. A short window length such as 2000 msec. was used to approximate stationary conditions – a requirement of Fourier transform. To each segment, a normalized window called Blackman window was applied to reduce spectral leakage. The Welch method reduces variance in the power spectrum by increasing the number of observations via overlapping of the segments. However, the reduction in variance is limited by the correlation between segments. This study used fifty percent overlap between segments. This is widely used for its good trade-off between reduction in variance and correlation between segments. The frequency range (i.e., bandwidth) was from 0.8 to 48 Hz with a frequency resolution of 0.3052 Hz. These parameters were used to make our study comparable to existing work.

Spectral Entropy: In this study the spectral entropy was used as a spectral descriptor of the Welch power spectral density obtained from the acquired EEG signal. Spectral entropy was computed by applying the Shannon entropy function to the power spectrum. It scores the uniformness of the power distributed. Since the Shannon entropy function operates over a probability distribution, the power spectrum was transformed into a probability mass function. This is done by dividing power spectrum by the sum of

the power in the power spectrum. After power spectrum was transformed into a probability mass function the Shannon entropy was computed. This is done by product of the probability distribution and natural logarithm of the probability distribution. The result was normalized the maximum entropy of the probability distribution then multiplied by negative one. The maximum entropy was the natural logarithm of the length of the probability distribution. The resulting value was the Shannon entropy of the power spectrum - the spectral entropy (i.e., SE).

Spectral Edge Frequency: In this study the spectral edge frequency was used as a spectral descriptor of the Welch power spectral density obtained from the acquired EEG signal. Spectral Edge Frequency (i.e., SEF) marked the frequency indicating ninety-percentile boundary power spectrum. For efficiency, the power spectrum was transformed into a probability mass function by dividing power spectrum by the sum of power in the power spectrum. A left cumulative sum of the probability distribution was computed. This represents the cumulative distribution function, which was a different form of viewing the results of the probability function. From the cumulative distribution function, the values were summed until the desired percentage was reached, which for the cumulative distribution function was the probability .90. The argument associated to the value or nearest value within one frequency resolution of the ninety-percentile boundary was the spectral edge frequency. Ninety percent was selected for comparison to existing work.

Median Frequency: In this study the median frequency was used as a spectral descriptor of the Welch power spectral density obtained from the acquired EEG signal. Median Frequency (i.e., MF) was the frequency of the power density spectrum that marks

the central tendency of the distribution. It was computed similar to spectral edge frequency with the exception that median frequency used the fifty-percentile boundary. This was represented in the cumulative distribution function as the probability of .50.

Power Ratio and Total Power: In this study the power ratio (i.e., PR) and total power (i.e., TP) was used as a spectral descriptor of the Welch power spectral density obtained from the acquired EEG signal. The power ratio was the ratio of power of each classical EEG rhythms to the total power of power spectrum. This ratio was a probability of EEG rhythm and together the power ratios represented the probability distribution of the classical EEG rhythms. The total power was the sum of all power values. Total power values may be viewed as a supplement for deep understanding of the power ratio descriptor.

In this study the intervals of the classical EEG rhythm were as follows: (a) 1 Hz < delta rhythm ≤ 4 Hz, (b) 4 Hz < theta rhythm ≤ 8 Hz, (c) 8 Hz < alpha rhythm ≤ 13 Hz, (d) 13 Hz < beta rhythm ≤ 30 Hz, and (e) 30 Hz < gamma rhythm ≤ 48 Hz. The intervals were arranged in this form to prevent overlapping and so that the sum of the power ratios would be equal to one. The total power was computed by taking the sum of the power values contained by the power spectrum. The power for each interval of the classical EEG rhythm was summed. Each summed interval was divided by the total power of the spectrum. The resulting values are the power ratios of the of the power spectrum.

2.4.4 Auditory Evoked Response Processing: Anesthesia and Sleep

Continuous Loop Averaging Deconvolution: In this study, low-jittered continuous loop averaging deconvolution (i.e., CLAD) sequences were delivered to

subjects. Low-jittered CLAD sequences were capable of simultaneously extracting both transient and steady-state responses from the same EEG segment. The EEG segments undergo digital filtering to obtain the frequencies that are within physiological interest and avoid frequencies where noise amplification characteristics of the sequence exist: (a) 13 to 1500 Hz for the anesthesia study and (b) 5 to 1500 Hz for the sleep study. After digital filtering, the EEG segment was divided with respects to the time occurrence of the auditory sequence into sweeps. Conventional averaging of sweeps yields a convolved response. This convolved response approximated to the steady-state response as such it is termed quasi-steady-state response (i.e., QSSR). To estimate the transient response, the Fourier transform of the QSSR is divided by the Fourier transform of the low-jittered sequence (for details see Özdamar and Bohórquez, 2006).

Phasor Analysis of Quasi Steady-State Response: The phasor corresponding to the stimulation rate was used as an estimator of the steady-state response. The magnitude and phase of this phasor was analyzed: (a) for each QSSR extracted from the moving average for anesthesia study and (b) for each sleep stage for sleep study. The QSSR was estimated via conventional averaging of sweeps. The Fourier transform of the QSSR was computed and from this transform the coefficient corresponding to the stimulation frequency was extracted - the phasor. This coefficient was a complex number, and from this complex number both the magnitude and phase was computed.

2.5 Analysis

The anesthesia study used time-series methods of analysis. The EEG spectral descriptors and Picis data were analyzed using trend analysis, while the auditory evoked

response were analyzed using moving average analysis. The correlation between delta and alpha power ratio was a deeper analysis of the observed relation between these two spectral descriptors during anesthesia.

For the analysis of EP, the moving average evoked potentials section describes the transient response analysis via using a moving average study of the response-to-response transitions. The beta entrainment section was a deeper analysis of beta oscillations observed in 20, 30, and 40 Hz transient responses. The phasor analysis of QSSRs describes the analysis for the 20, 30, and 40 Hz QSSRs that were extracted using the moving average procedure.

The sleep study used group analysis that is an analysis with respects to changes in sleep stages. The spectral analysis section describes the group analysis of the spectral descriptors and a pivot of the group analysis that investigates via spectral descriptors the effects of stimulation on EEG. The auditory evoked potential analysis describes the analysis of the transient responses and the phasors responses for each sleep stage.

2.5.1 Trend Analysis: Anesthesia

Electroencephalographic Spectral Descriptors and Picis Data of Anesthesia: The trend of the spectral descriptors and PICIS (i.e., physiological) data were arranged for comparison in a grid layout. The format of the grid layout sets each patient into a column and each measure either spectral descriptor or PICIS data into a row. In this grid structure changes occurring between patients are shown across columns and changes in occurring between measures are shown across rows. The vertical axis of the trends was from the minimum measure value of all patients to the maximum measure value of all

patients. The horizontal axis was at different scales according to the duration for each surgery.

Correlation between Delta and Alpha Power Ratio: In this study the correlation coefficient was used to analyze the relationship between delta and alpha rhythm observed in the power ratio of anesthesia. The correlation coefficient measures the degree of a linear relationship between two signals. It measures the degree to which the change in a set of variables is related. The correlation was measured between: (a) delta power ratio and alpha power ratio trend, (b) sevoflurane and alpha power ratio trend, and (c) sevoflurane and delta power ratio trend. The trends of the measures are arranged from comparison in a grid layout. The format of the grid layout sets each patient into a column and each set of measures in a row. In this grid structure changes occurring between patients were shown across columns and changes in occurring between measures was shown across rows. For each patient and for each set of trends under study the correlation coefficient was provided. At the beginning of each row the total of the coefficients for all patients was provided. In this form both the individual patients (i.e., particular) value and the for-all patients (i.e., global) value of the correlation coefficient were investigated simultaneously.

Moving Average Evoked Potentials: Moving Average (i.e., MA) method was developed in this study to extract multiple responses from one set of sweeps. MA method allows one to view the response-to-response transition (i.e., variation) of the set. A response was extracted from a specified number of sweeps referred to as a window. A window was a set of sweeps and represented the likelihood of the response's waveform. This window was shifted forward by a specific number of sweeps. If the number of

sweeps that the window was shifted forward was less than the window size then the location of the newly shifted window will overlap with the location of the previous window. The size of a window and percent overlap of windows were two properties of MA analysis and influence the scope of the analysis. By applying the MA analysis method for extracting multiple responses from one total data set of sweeps the transition and transformation of the response waveform can be observed by investigating the intermediate responses. This method can be used to analyze transient responses, and phasors of steady-state responses.

The MA method consists of the following steps:

(a) A set window size of sweeps (i.e., 10 min) was conventionally averaged to estimate the convolved response that was associated with the specified window of sweeps. The result was stored into memory for later viewing.

(b) The window of sweeps was shifted forward by fifty percent of the size of the trend window causing an overlap between the previous and adjacent window of sweeps. This new window of sweeps was conventionally averaged to estimate the convolved response that was associated with the shifted window of sweeps. The result was stored into memory with the previous response.

(c) The steps from (a) to (b) were repeated until the end of acquired sweeps was reached.

The MA method for the transient response and steady-state response were similar. For the MA analysis of the transient response, the CLAD method was used to extract the

transient response from the stored convolved responses. The convolved responses were the quasi steady-state responses. From these quasi steady-state responses the phasors were computed.

Grand Mean of 5 Hz Transient Responses of Anesthesia: The grand mean of the 5 Hz transient responses was used to estimate the global changes of maintenance anesthesia. These responses were not high-pass filtered. As far as we know at this time auditory evoked response are not analyzed with frequency bands including the very low frequencies (i.e., 1 to 25 Hz); the literature systematically high-pass filtered the middle latency responses. In order to contrast our results to previous studies, an additional set of responses that were filtered to conventional filter settings of previous studies were estimated. The filter settings used were from Thorton et al. 1985 (i.e., 25 to 2500 Hz). A split buffer analysis was applied to the grand mean of the 5 Hz transient response to assess the signal-to-noise quality.

Beta entrainment: The responses for the 20, 30, and 40 Hz transient responses extracted using moving average showed a beta entrainment. To measure the power of beta entrainment in the responses the beta frequency interval in the responses were determined. A power spectrum for each response was calculated then the power in the determined beta frequency band was measured. The power of beta entrainment for each of the responses extracted using the moving average was plotted forming a trace indicating the activity of beta entrainment from response to response. The power of beta entrainment from the response was computed by computing the power spectrum for each response. From the power spectrum sum the power within the beta entrainment frequency

interval, this was determined from data a posterior analysis to be either 17.0898 Hz or 19.531 Hz.

Quasi Steady-State Response Phasor Analysis: In this study, the trends of the quasi steady-state responses were analyzed by extracting the phasor from these responses. The trends of the phasors are arranged for comparison in a grid layout. The format of the grid layout sets each subject into a column and sets each phasor in a row. In this grid structure, changes occurring between patients were shown across columns and changes in stimulation rate of the phasor are shown across rows. For each trend of the phasor, the mean magnitude and phase of the trends was provided. Each phasor for each QSSR was provided and the mean QSSR phasor was provided. To show the change in magnitude due to stimulation rate across the rows a red circle set to the radius of the magnitude was provide. The change in radius will represent the change in magnitude. All phasors were shown in a scale from 0.00 to 0.55 μVolts.

2.5.2 Stage Analysis: Sleep

In this study, the stage analysis was a paired-wise comparison of sleep stages. The paired-wise comparison of five sleep stages requires the choice of two sleep stages for each comparison, which yields six combinations: (W vs. N1), (W vs. N2), (W vs. N3), (N1 vs. N2), (N1 vs. N3), and (N2 vs. N3). For each of the six mentioned combinations, a statistical test was conducted to evaluate the limitations in separating between sleep stages. The premise for the statistical test was that each sleep stage was assumed to be equal. The test would reveal the sleep stages that the feature was unable to separate. A

two-tailed, two sample Student's t-test using a significance level of 5% (i.e., $\alpha = .05$) was used as the statistical test.

Spectral Descriptor Analysis: For spectral descriptors each set of values for each descriptor of each sleep stage was arranged with respects to each combination. A Student's t-test was conducted for each combination. This procedure was conducted at for each stimulation rate under each channel.

The p-value of the Student's t-test was arranged into a grid layout to each row was the group of spectral descriptors and the columns are the group of sleep stage combinations. The p-values displayed in the grid layout were of three significant figures and any value less than 0.001 was displayed as zero. The grid layout arrangement of p-values was done for each stimulation rate. This structured arranging of the values allows trends embedded in results to be more pronounce.

To further observe trends embedded in results, the results were represented in terms of significant or no-significant difference. The results of significant or no-significant difference are color coded as green or red, respectively. The spectral descriptor that was able to separate between all sleep-stage combinations was colored a light green. All procedures mentioned thus far were performed for both Fz-A2 and Cz-A2 channel derivatives.

The procedure described evaluates the ability of the spectral descriptors to separate between sleep stages for each stimulation rate. It was possible to pivot the analysis in order to evaluate the ability of the spectral descriptors to separate between stimulation rates for each sleep stage.

To evaluate the limitations in separating between stimulation rates for sleep stage of each spectral descriptor a paired-wise comparison of three stimulation rates was conducted. The paired-wise comparison of three stimulation rates required the choice of two stimulation rates for each comparison, which yields three combinations: (5Hz vs. Sil), (30Hz vs. Sil), and (5Hz vs. 30Hz). The premise was that each stimulation rate was assumed to be equal.

The test will reveal the stimulation rates that the spectral descriptors were unable to separate. A two-tailed, two sample Student's t-test using a significance level of 5% (i.e., $\alpha = .05$) was used as the statistical test. The p-values were arranged into a grid layout where the rows were the spectral descriptors and the columns were stimulation rate combinations. One asterisk was shown if the p-values was less than or equal to $\alpha = 0.05$, two if it was less than or equal to $\alpha = 0.01$. To further observe trends embedded in results, the results are represented in terms of significant or no-significant difference. The results of significant or no-significant difference are color coded as green or gray, respectively. All procedures mention were done for both Fz-A2 and Cz-A2.

Auditory Evoked Potential Analysis: For transient responses, each set of values (i.e., component magnitude or latency) for each response of each sleep stage was arranged with respects to each combination. The magnitude and latency were measured at specific locations for each response (see Figure 2.7). These values were used for the statistical analysis to evaluate the ability of the responses to separate between sleep stages.

A Student's t-test was conducted for each combination. The statistical analysis of each combination was conducted at for each stimulation rate for both channels. The results of significant (i.e., Yes) or no-significant (i.e., No) difference are arranged into a grid. The rows of the grid were the magnitude and latency and the columns the sleep stage combinations.

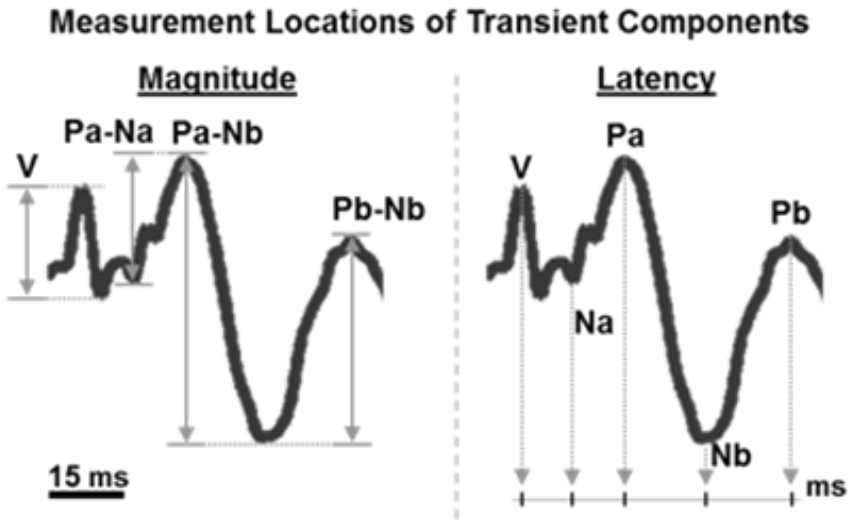

Figure 2.7 Relative magnitude and latency measurement points.

For the steady-state responses, the phasor magnitude and phase angle was measured. For analysis each set of values for each phasor of each sleep stage was arranged with respects to each combination for the statistical analysis to evaluate the ability of the responses to separate between sleep stages. The results of significant (i.e., Yes) or no-significant (i.e., No) difference were arranged into a grid where rows were magnitude and phase of phasor and columns were sleep stage combinations.

Chapter 3 RESULTS

3.1 Study 1. Anesthesia

The anesthesia study results presented are as follows: (a) the Picis measurements extracted via trend analysis; (b) the spectral descriptors of the electroencephalographic (i.e., EEG) signal extracted via trend analysis; (c) the transient auditory evoked responses extracted via moving average analysis; and (d) the phasor of steady-state responses extracted via moving average analysis. For each measured feature, a brief definition of each feature was provided followed by a concise explanation of the most relevant observations of the results. The results for Picis measurements were as follows: breathing (i.e., spontaneous breathing), anesthetic agent (i.e., expired concentration of anesthetic agent), bispectral index (i.e., BIS), heart rate, and core body temperature. The results for spectral descriptors were as follows: total power (i.e., TP), power ratio (i.e., PR), median frequency (i.e., MF), spectral edge frequency (i.e., SEF), and spectral entropy (i.e., SE). The results for the transient responses were for the 5, 20, 30, and 40 Hz responses, while the results for the steady-state responses were for the 20, 30, and 40 Hz response phasors.

3.1.1 Physiological: Vitals Measurements and Bispectral Index

The trend analysis was performed on the physiological signals acquired during surgery using the Picis system. The plots showing the trends of the physiological measurements were arranged in a grid layout. Each column of the grid was one patient receiving general anesthesia. Each row was one physiological measurement.

Breathing: Spontaneous respiration rate measured the number of spontaneous breaths in one minute that were initiated and terminated by the patient during mechanical ventilation (see Figure 3.1, row1 and Table 3.2). Only P23 and P26 showed spontaneous breathing activity: P23 underwent a long surgery (i.e., about 5 hours) and showed breathing activity and increased heart rate when the sevoflurane levels decreased; P26 also presented spontaneous breathing activity and increased heart rate when the he became animated, making audible glottal sounds, groaning, contracting his abdomen and arms. Ledowski et al. 2006 defined clinical reaction, which indicates light anesthesia, as the first reaction by patient, such as movement, coughing, and eye opening. This episode observed from P26 was referred to as clinical reaction.

Anesthetic agent: The expired concentration was an indirect way of estimating brain anesthetic concentrations; at equilibrium, alveolar and brain concentrations are assumed to be equal. The anesthetic agent used for all patients was sevoflurane except for P17 who received both sevoflurane and nitrous oxide. Figure 3.1, row 2, and Table 3.2, showed the expired concentration of the anesthetic agents. The figure showed the different administration strategies used by the anesthesiologists; this feature was not controlled in the present study, for ethical reasons. Having the administered concentration as an uncontrolled variable hindered the analysis of the parameters, but reflected more realistic conditions encountered by anesthesiologists actively monitoring the patient.

Bispectral index: The bispectral index (i.e., BIS) was measured during surgery for all patients. BIS, via processed EEG, indicates the effect of anesthesia and guides anesthetic dosing. Sustaining the patient in the BIS range between 40 and 60 is the recommended operating procedure to prevent unexpected awareness. Shown in Figure

3.1, row 3, and Table 3.2, is the BIS for each patient. The BIS was maintained in the recommended range. The BIS for P26 began with a sharp rise, peaked, and descended steadily until the time occurrence when P26 exhibited clinical reaction (see Figure 3.1). The BIS of P26 did not show any exceptional pattern suggesting that P26 would become animated.

Heart rate: Heart rate measured the number of heartbeats in one minute and may act as an indirect indication of the status of the autonomic system. Shown in Figure 3.1, row 4, and Table 3.2, is the heart rate for each patient. Patients P25, P17, and P22 had similar, stable heart rate traces. The heart rate for P23 had a very slow trend that increased as the sevoflurane decreased gradually; notice the time-compressed time-scale on Figure 3.1. P26 showed a very fast rise in heart rate concomitant with the clinical reaction.

Core body temperature: Core body temperature was measured in surgery to monitor intraoperative hypothermia as anesthesia is suggested to produce a dose-dependent reduction in the core temperature. Shown in Figure 3.1, row 5, and Table 3.2, is the core body temperature for each patient. Except for P26, all patients showed a gradual increase in core body temperature. P26 showed a gradual temperature drop followed by a fast, profound drop in body temperature concomitant with the clinical reaction.

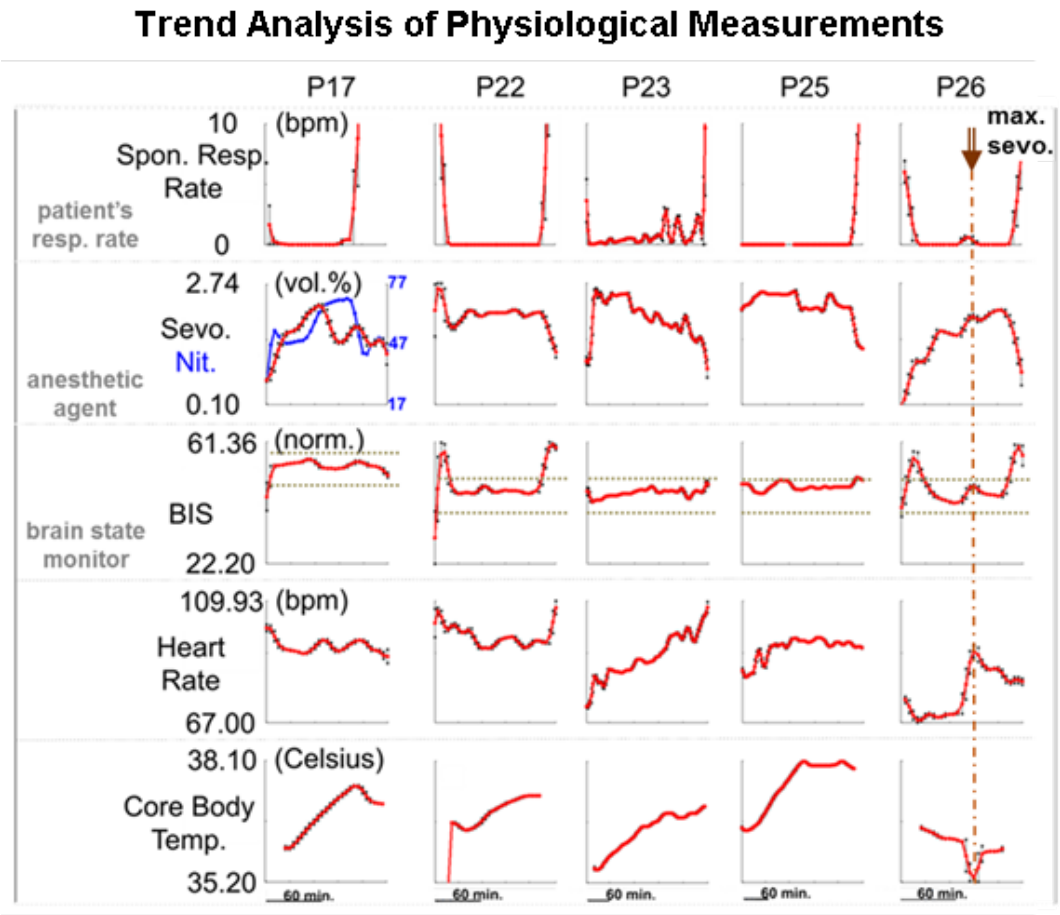

Figure 3.1 Trend of physiological measure. Spontaneous respiration rate measures the respiration rate of patient (row 1). Anesthetic concentration measures expired concentration of anesthetic (row 2). Bispectral index is presented for reference (row 3). Heart rate measures beats per minute of heart (row 4). Core body temperature measures core temperature of patient (row 5). Note that each plot is set to different time scales. The dashed line, labeled max sevo., indicates the peak of response by the anesthesiologist to the clinical reaction.

3.1.2 Electroencephalogram: Spectral Descriptors

A trend analysis was performed on the spectral descriptors of the electroencephalogram (i.e., EEG) acquired during surgery. Shown in Figure 3.2 are the trends of the spectral descriptors arranged in a grid layout. Each column of the grid is one patient receiving general anesthesia. Each row is one spectral descriptor.

Total power: Total power measured the sum of the power contained in the power spectrum, and it is indicative of the total synchronization of neural activity underlying the observed EEG. Shown in Figure 3.2, row 3, and Table 3.2, is the total power of EEG under anesthesia for each patient. In P17, P22, and P25, a rather constant rate of anesthetic agent was observed. These patients showed similar trends such as a constant rate of change in total power. P23 showed large fluctuations in the total power, indicating occurrences of higher neural synchronization in neural activity underlying the EEG. P26 showed a gradual rise in the total power, indicating a gradual rise in the synchronization in neural activity underlying the EEG.

Power ratio: Power ratio is the ratio of power in each of the classical EEG frequency bands. Shown in Figure 3.2, row 4, and Table 3.2, is the power ratio of EEG under anesthesia for each patient. It should be noted that the power ratio exposes the contribution by the EEG frequencies (i.e., EEG rhythms) underlying the values observed in total power. For P23 the greatest contributor to total power is the delta rhythm (0.74) followed by reduced theta (0.18) activity and a suppressed higher frequency bands. Also, the power ratios of P25 presented delta dominance with stable power ratios organized in decreasing order as delta (0.44), theta (0.27), alpha (0.19), beta and gamma. P17 showed delta power (0.38), theta (0.31), alpha (0.21) and reduced beat and gamma. P22 presented theta power dominance with power ratios of delta (0.29), theta (0.35), and alpha (0.26), yet remained clustered. For P26, the patient with clinical reaction, the underlying driver to the total power was the alpha (0.41). Alpha of P26 was greater than delta (0.25) and theta (0.24). A feature of anesthesia observed in the power ratio trend was the delta power ratio was higher than the alpha power ratio. The delta was higher than alpha for all

surgeries that did not show an event of clinical reaction such as P17, P22, P23, and P25. Compared to the total power, the power ratio provides more details which expounded details about the underlying arousal (i.e., alpha) or suppression (i.e., delta) process.

Median frequency: Median frequency indicates the central tendency of the power spectrum. If delta and alpha rhythms in anesthesia EEG were the major contributors that formed the spectrum, then the median frequency indicated the net balance of these two processes. Shown in Figure 3.2, row 5, and Table 3.2, is the median frequency of EEG under anesthesia for each patient. Sorting the patients by increasing order of median frequency yielded the following order, P23 (2.23 Hz), P25 (5.17 Hz), P22 (5.96 Hz), P17 (5.98 Hz) and P26 (8.15 Hz). Notice that this order mostly corresponded to the order obtained by sorting the patients by decreasing delta and by increasing alpha power ratio. Power ratio seemed to have a faster response to changes than median frequency.

Spectral edge frequency: Spectral edge frequency denotes the frequency value marking where ninety percent of the total power spectrum lay. Shown in Figure 3.2, row 6, and Table 3.2, is the spectral edge frequency of EEG under anesthesia for each patient. This parameter does not correlate well neither with the power ratios nor our subjective empirical assessment of the patients anesthetic depths. For example, P26 had lower value (12.86 Hz) than P22 (13.18 Hz). The spectral edge frequency was not as sensitive to the alpha rhythms as was median frequency.

Spectral entropy: Spectral entropy measures the irregularity and complexity (i.e., uniform-ness) of the power spectrum. A value of one is a perfectly uniform distribution (i.e., extremely wide distribution) while a value of zero was a perfectly Dirac distribution

(i.e., extremely narrow distribution). Shown in Figure 3.2, row 7, and Table 3.2, is the spectral entropy of EEG under anesthesia for each patient. P23 presented the lowest average value (0.62) with some fluctuations in agreement with the predominant delta power ratio and the observation that this patient was deeply anesthetized.

In the remaining patients the mean entropy values remained around 0.76 which is considered as light anesthesia in some of the literature. However, P26 who had the clinical reaction presented lower entropy values (0.763) than P22 (0.781) who underwent an eventless procedure. Yet, the spectral entropy decreased when an increase of anesthetic agent was administered after the clinical reaction.

Shown in Table 3.1 were some highlighted spectral features and the order of patient level based on values measured from feature. The arrows next to feature indicated whether the values of the feature were either increasing ↑ or decreasing ↓. The patients were arranged according to feature values in the direction of decreasing anesthetic depth for the feature. A more in-depth analysis (i.e., discrimination analysis) is presented later.

Table 3.1 Anesthetic Level According to Features

Feature Direction	Patient's Level Order Based on Feature
BIS (↑)	P23, P25, P26, P22, P17
Total Power (↓)	P26, P23, P25, P22, P17
Delta Power Ratio (↓)	P23, P25, P17, P22, P26
Alpha Power Ratio (↑)	P23, P25, P17, P22, P26
Theta Power Ratio (↑)	P23, P26, P25, P17, P22
Median Freq. (↑)	P23, P25, P22, P17, P26

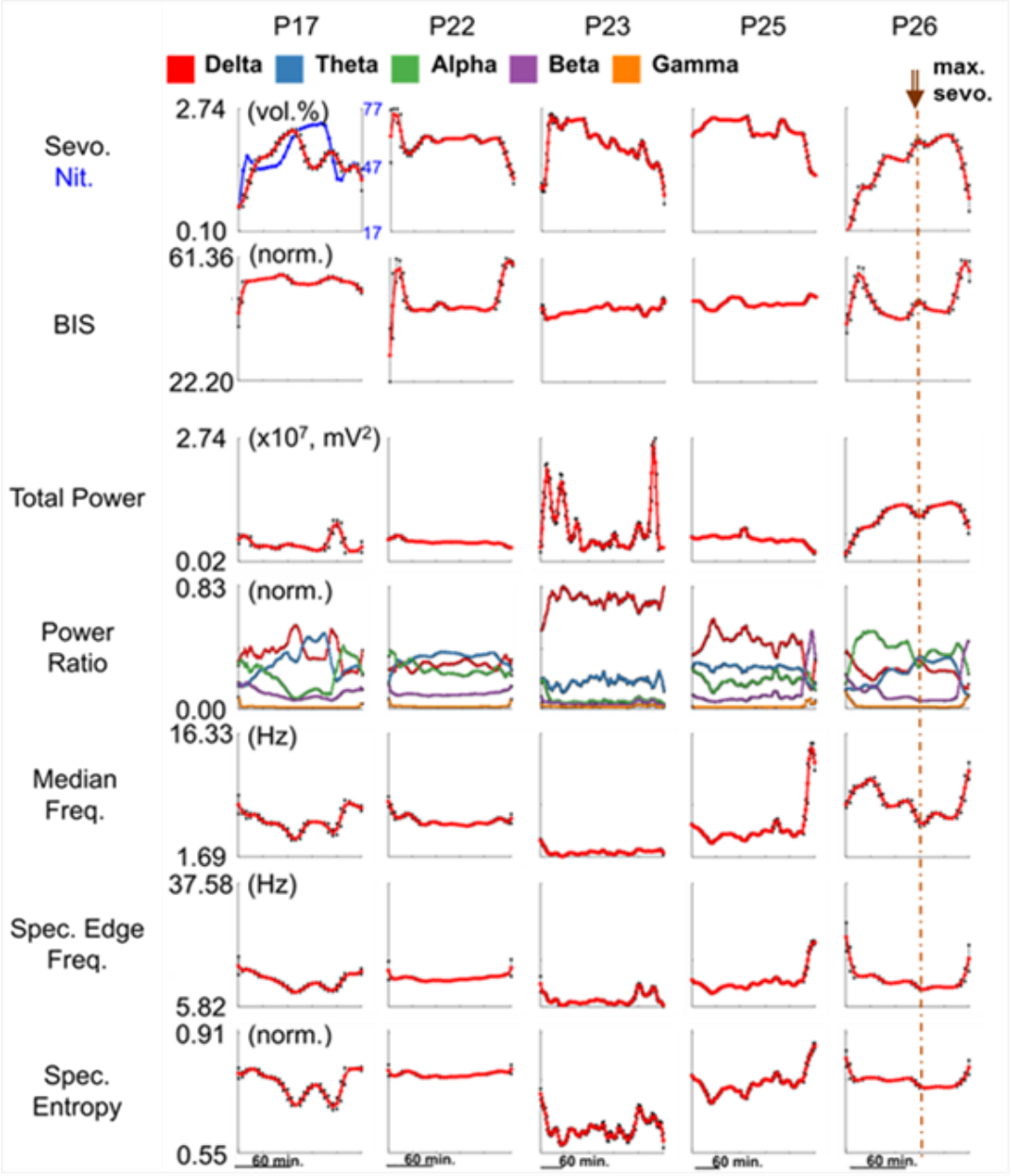

Figure 3.2 Trend of spectral descriptor. Row 1 shows changes in anesthetic concentration. Row 2 shows changes in bispectral index as reference. Row 3 shows total power. Row 4 shows the power ratio. Row 5 shows the median frequency. Row 5 shows the spectral edge frequency. Row 6 shows the spectral entropy. Note that each plot is set to different time scales. The dashed line, labeled max sevo. indicates the peak of response by the anesthesiologist to the clinical reaction.

Table 3.2 Mean and Standard Deviation of Spectral Descriptor Trend Analysis

	Subject				
	P17	P22	P23	P25	P26
	(n = 31)	(n = 37)	(n = 75)	(n = 68)	(n = 31)
Measurement	M (SD)	M (SD)	M (SD)	M (SD)	M (SD)
Physiological					
Spontaneous Respiration	5.16 (8.61)	2.86 (6.21)	1.08 (2.44)	1.33 (2.44)	1.61 (3.80)
Sevoflurane	1.62 (0.39)	2.03 (0.24)	1.98 (0.42)	2.19 (0.40)	1.80 (0.54)
Nitrous Oxide	36.92 (0.46)	0.00 (0.00)	0.00 (0.00)	0.00 (0.00)	0.00 (0.00)
Bispectral Index	53.38 (2.18)	47.66 (5.73)	45.03 (1.25)	47.13 (1.26)	47.14 (3.46)
Heart Rate	93.98 (2.41)	97.63 (3.69)	90.12 (7.82)	94.20 (4.78)	88.80 (10.96)
Core BodyTemperature	36.92 (0.46)	33.80 (9.11)	36.49 (0.44)	37.52 (0.58)	37.24 (0.92)
Spectral Descriptors					
Total Power	4.04E+06 (1.50E+06)	4.50E+06 (0.52E+06)	7.60E+06 (5.32E+06)	5.15E+06 (0.88E+6)	10E+06 (2.96E+06)
Delta Power Ratio	0.380 (0.078)	0.294 (0.023)	0.739 (0.046)	0.444 (0.094)	0.253 (0.044)
Theta Power Ratio	0.314 (0.099)	0.346 (0.033)	0.178 (0.027)	0.270 (0.034)	0.239 (0.080)
Alpha Power Ratio	0.207 (0.102)	0.261 (0.038)	0.048 (0.026)	0.188 (0.034)	0.406 (0.067)
Beta Power Ratio	0.093 (0.033)	0.093 (0.011)	0.028 (0.011)	0.093 (0.093)	0.094 (0.064)
Gamma Power Ratio	0.006 (0.004)	0.006 (0.004)	0.007 (0.004)	0.006 (0.010)	0.007 (0.013)
Median Frequency	5.977 (1.191)	5.956 (0.594)	2.227 (0.302)	5.175 (2.381)	8.154 (1.698)
Spectral Edge Frequency	12.551 (1.952)	13.184 (0.732)	7.658 (1.376)	12.250 (2.684)	12.865 (2.801)
Spectral Entropy	0.752 (0.039)	0.781 (0.007)	0.616 (0.030)	0.754 (0.035)	0.763 (0.020)

Shown in Figure 3.3 and Table 3.3 is an assessment of spectral descriptor discrimination ability. Each patient was a distinct, unique case of general anesthesia. A subjective empirical assessment with respects to the outcome of patient results and as indicated by previous studies in anesthesia categorically placed the level of anesthesia for each patient into subgroups. This was according to the relative distance between patient and other patient members in study, such as P26 the patient that had the clinical reaction was in a lighter level while P23 (i.e., a long surgery) was maintained at deeper levels. This observed patient level was further sustained by categories defined in the results of previous studies mentioned in the discussion section.

The discrimination ability of a descriptor (i.e, feature) was good if it separated patients that were presumed at different anesthetic levels. For each spectral descriptor, each patient's value was normalized by dividing it by the maximum in the set of patients. The normalization allowed for feature comparison using the same scale (i.e., from 0 to 1).

Total power and theta power ratio preformed modestly in separating between the patient levels.

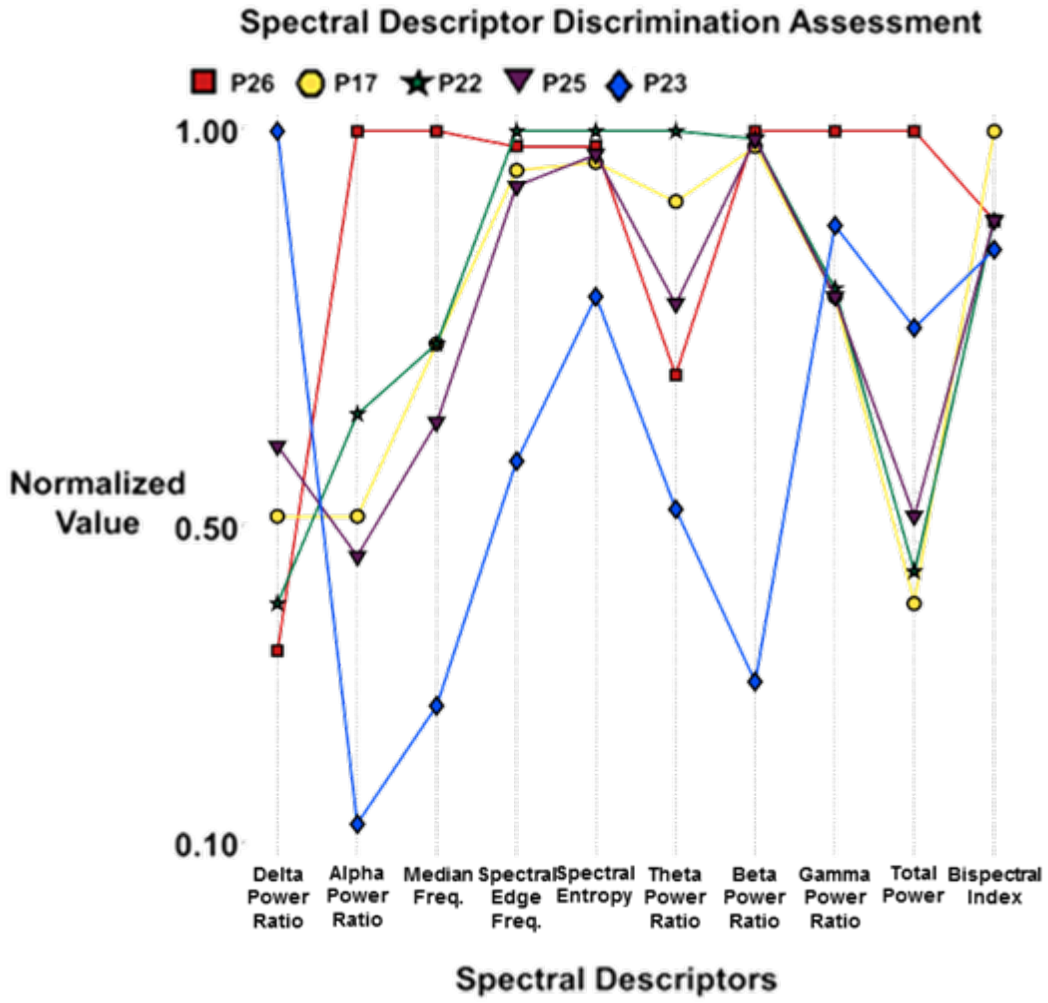

Figure 3.3 Discrimination assessment of anesthesia levels by spectral descriptors. Each column is a spectral descriptor. Each trace is a patient of unique anesthesia level. The spectral descriptors order and separate the patients with respects to anesthetic level. For each feature (i.e., column), the feature value of each patient was normalized by the max feature value of the set of patients.

Delta and alpha power ratio separated well the patient levels showing an agreeable spread between patients. The delta power ratio ordered the patients levels as P26, P22, P17 P25, and P23 while the alpha ratio ordered the patient levels as equal to the delta power ratio but in reverse order. The performance of median frequency follows

after that of alpha power ratio showing a similar ordering of patient levels as the ordering shown by alpha power ratio with the exception of P22 and P17, which were equal. Also, for median frequency the range from lowest to highest normalized value is the next largest after the range of alpha power ratio. Spectral edge frequency spectral entropy, and gamma power ratio did not perform well – showing closely clustered values. Beta power ratio showed a weak performance in discrimination between patient levels. The bispectral index, which is the descriptor with most widespread use, showed a weak performance in did not separate well the patient levels.

Table 3.3 Results of Spectral Descriptor Discrimination Assessment

	Subject				
	P17	P22	P23	P25	P26
Spectral Descriptors	Normalized	Normalized	Normalized	Normalized	Normalized
Total Power	0.40	0.44	0.75	0.51	1.00
Delta Power Ratio	0.51	0.40	1.00	0.60	0.34
Theta Power Ratio	0.91	1.00	0.52	0.78	0.69
Alpha Power Ratio	0.51	0.64	0.12	0.46	1.00
Beta Power Ratio	0.98	0.99	0.30	0.99	1.00
Gamma Power Ratio	0.79	0.80	0.88	0.79	1.00
Median Frequency	0.73	0.73	0.27	0.63	1.00
Spectral Edge Frequency	0.95	1.00	0.58	0.93	0.98
Spectral Entropy	0.96	1.00	0.79	0.97	0.98
Bispectral Index	1.00	0.89	0.85	0.89	0.89

Shown in Figure 3.4 is a diagram that depicts the performance of the spectral descriptors in regards to its discrimination of anesthetic levels. The descriptors were grouped into circles, where the inner circle denotes a better performance than the outer circle. To distinguish further a gray gradient is used to indicate similarity in performance

between adjacent circles. The delta and alpha power ratio discriminated better than the remaining descriptors. Both delta and alpha power ratio showed the greatest dispersion between patients and ordered the patients according to the empirically assessed depth of anesthesia. After delta and alpha power ratio discrimination power, the median frequency followed showing a similar performance to the alpha power ratio in spread and patient order with the exception of P17 and P22.

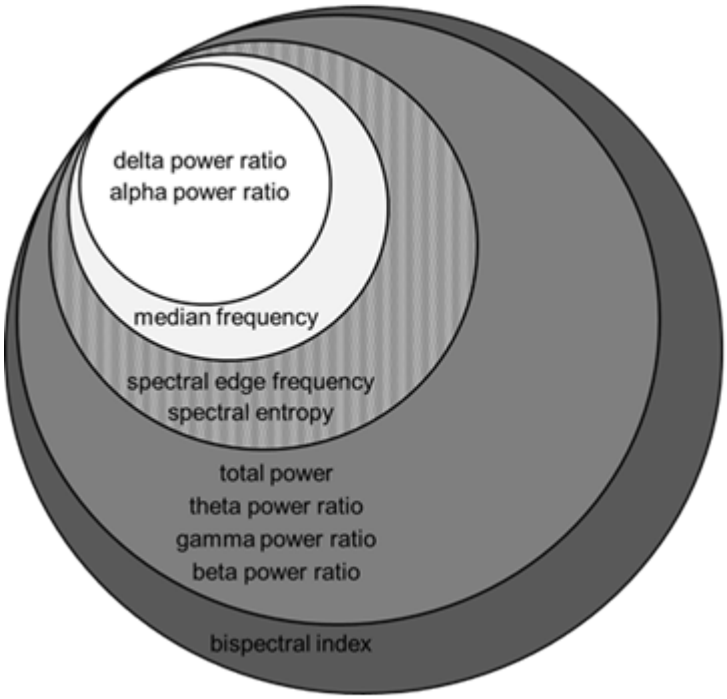

Figure 3.4 Summary of spectral descriptor discrimination performance. The performance is arranged into groups where the inner circle represents better performance than the outer circle. The gradient of the gray color further denotes the similarity in performance to adjacent groups.

Spectral edge frequency and spectral entropy only showed a modest performance and appreciably was less than of the delta and alpha power ratio or median frequency. The descriptors placed in the outer circles weakly discriminated anesthetic depth. The bispectral index, which is the outermost circle showed the least power of separation. These descriptors neither ordered the patients into the empirically assessed depth of

anesthesia nor separated the patients with sufficient dispersion compared to the other descriptors.

Correlation of delta to alpha power ratio: The power ratio for delta and alpha appeared to move in tandem opposed directions. Shown in Figure 3.5, the correlation between delta and alpha was measured using correlation coefficient.

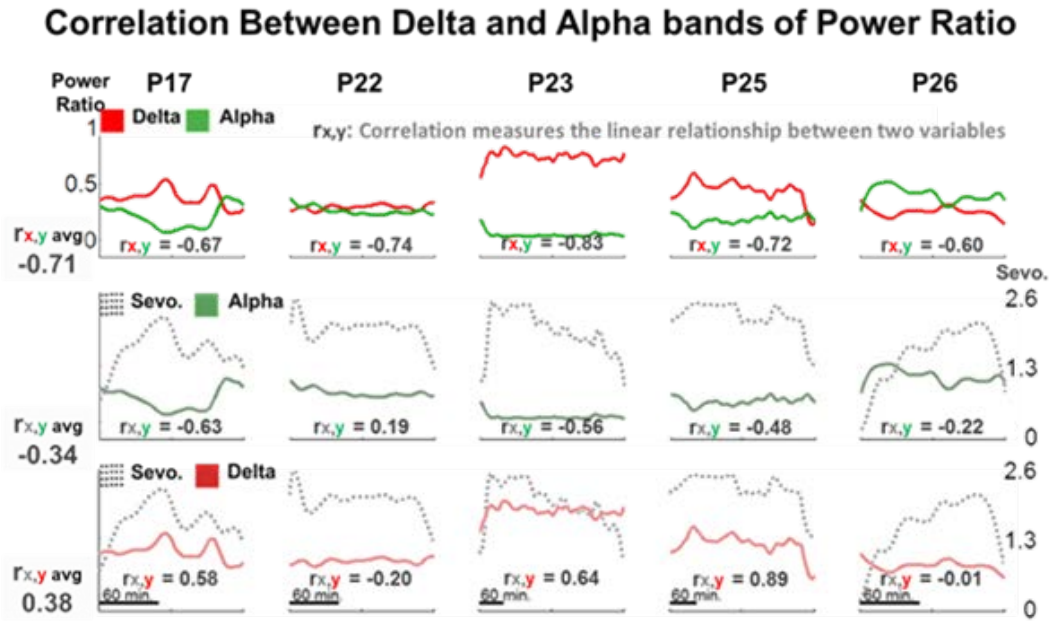

Figure 3.5 The relationship between delta and alpha power ratio in anesthesia. Each column is one patient. At the front of each row is the mean correlation coefficient value of the set of individual correlation coefficient in the columns. Row 1 shows the trends of delta (red) and alpha (green) power ratio. At the bottom of each plot is the correlation coefficient between delta and alpha power ratio. Row 2 shows the trends of sevoflurane (gray) and alpha power ratio. At the bottom of each plot is the correlation coefficient between sevoflurane and alpha power ratio. Row 2 shows the trends of sevoflurane and delta power ratio. At the bottom of each plot is the correlation coefficient between sevoflurane and delta power ratio.

The correlation coefficient of delta to alpha showed that alpha has a negative correlation to delta – an increase in delta exhibited a decrease in alpha. The correlation coefficient of alpha to sevoflurane showed that alpha is weakly and negatively correlated to

sevoflurane. The correlation coefficient of delta to sevoflurane showed that delta was weakly and positively correlated to sevoflurane (see Figure 3.5). The correlation coefficient indicated that alpha had a negative correlation to delta and that an increase in sevoflurane would simultaneously drive delta power ratio to increase and drive alpha power ratio to decrease. The negative correlation between delta to alpha power ratio of P23 (- 0.83) was greater than P26 (- 0.60). The correlation between anesthetic concentration to delta power ratio was smallest for P26 (- 0.01) while P23 (+ 0.64) showed the second largest of the group.

3.1.3 Evoked Potential: Transient Response

The transient responses extracted via moving average corresponded to the time sample points of the other measured features, such as spectral descriptors, physiological measures, and phasors. This facilitated the investigation and comparison all measured features with respects to the same time sample point.

Moving average 5 Hz transient response - Observed waveforms: Shown in Figure A.1 is the 5 Hz transient response extracted using the moving average (i.e., MA) MA used a 10-point window length and 50% overlap between windows. Each column of the figure represents the transient responses extracted of one patient and the rows represent the response extracted from one of the overlapping windows of the moving average which is indexed. Figure A.1 shows the effects of anesthesia on the morphology of the transient responses.

The waveforms underwent considerable changes that arise and dissipate with time. Regardless of the variability between waveforms, the evoked potentials can be

classified as following two main patterns: either one dominant peak response or two dominant peaks response (see Figure 3.6 and Table 3.4).

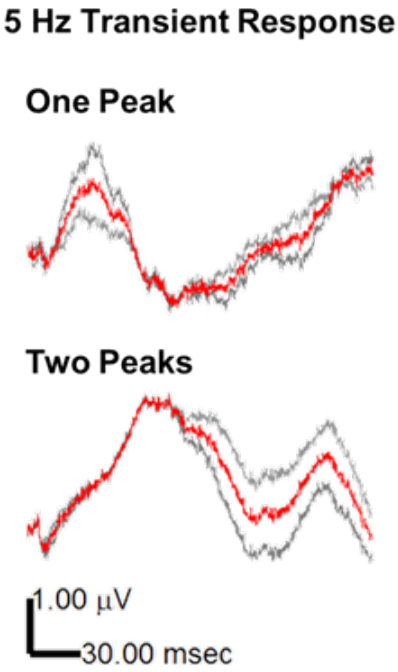

Figure 3.6 Transient response pattern observed in 5 Hz transient response via MA.

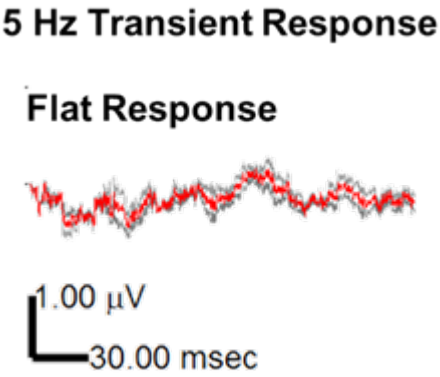

Figure 3.7 Flat response pattern observed in 5 Hz transient response via MA.

Throughout the extracted responses, second wrapping of transient responses was observed (see Figure A.1 and Table 3.4). Second wrapping causes a time shift of the transient components. This shift makes it difficult to identify the components of the

auditory response and makes it difficult to measure the magnitude and latency of transient components (see Figure 3.8).

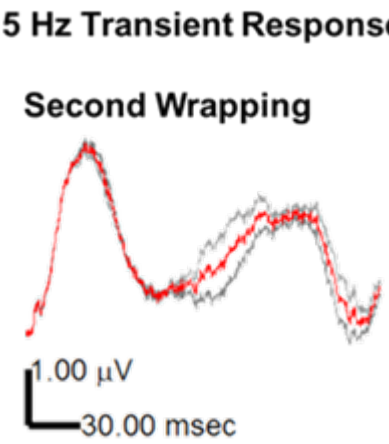

Figure 3.8 Second wrapping observed in 5 Hz transient responses via MA.

Table 3.4 Percent of Observed Responses in 5 Hz Transient Responses by Moving Average.

	Subject				
	P17	P22	P23	P25	P26
5 Hz Waveform	Percentage	Percentage	Percentage	Percentage	Percentage
Second Wrapping	61.3	64.9	17.3	30.9	61.3
One Dominant Peak	12.9	16.2	16.0	13.2	3.2
Two Dominant Peaks	9.7	0.0	2.7	19.1	9.7
Flat Response	9.7	2.7	24.0	5.8	3.2
Other Response Type	0.0	5.4	2.7	10.7	19.4
EMG	6.5	10.8	37.3	20.3	3.2

Moving average 5 Hz transient response – Range measurement: The effects of second wrapping prevented the direct measurement of the transient components in the conventional form; however, the transient components were measured in an indirect form by measuring the range of the response. Through this procedure the responses can be

investigated. The range was measured as the difference between the most positive and most negative peak of the response. Shown in Figure 3.9 is the measured range for each 5 Hz transient responses extracted via the moving average method.

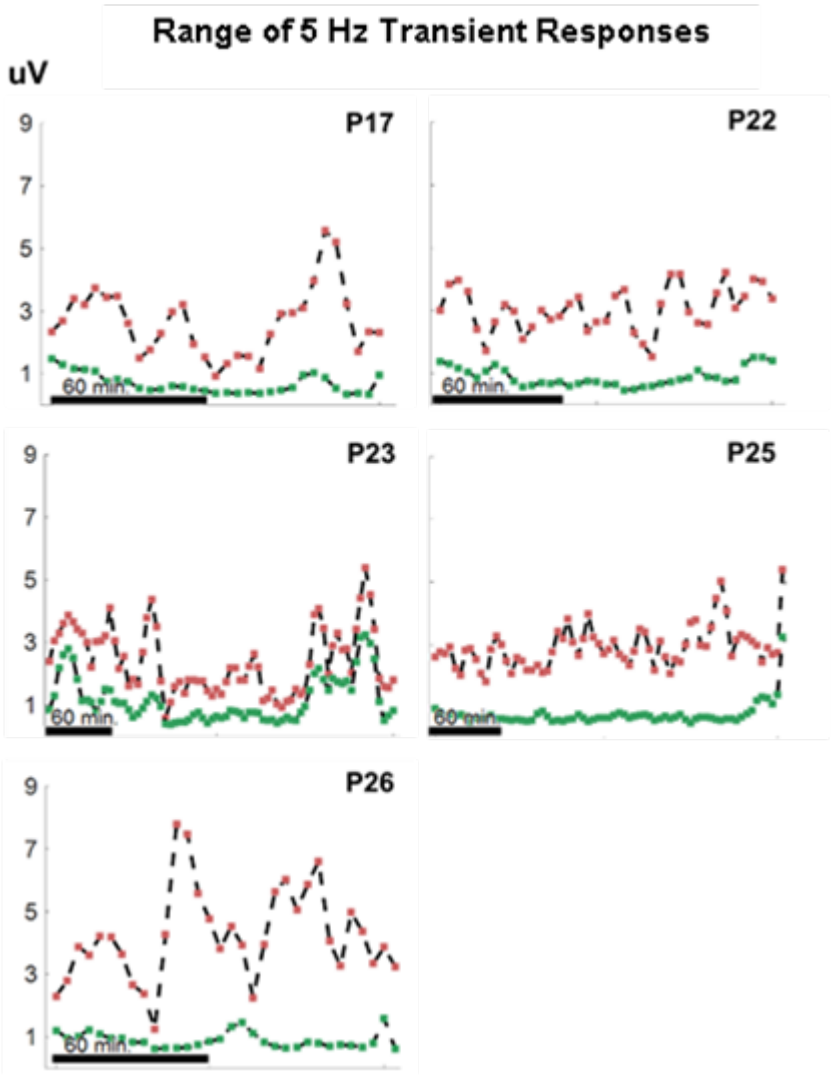

Figure 3.9 Measured range of each 5 Hz transient response in moving average. The range measured of the 5 Hz transient responses from the moving average (red) and the range for the high-pass filtered 5 Hz transient responses from the moving average (green).

Also, the measured range for each 5 Hz transient responses that were filtered with respects to conventional filter settings (i.e., bandpass filter from 25 to 1500 Hz). The

range measured from the filtered responses produced traces that showed slight changes, less activity, and an attenuated magnitude with respects to the rise and fall of the waveform. By contrast, the range measured from the responses that were not filtered showed prominent changes under anesthesia as evident by the magnitude of the traces.

Moving average 5 Hz transient response – Discrimination Assessment: Shown in Figure 3.10, A. and Table 3.5 is an assessment of 5 Hz transient response discrimination ability via the measured range for each transient response. The measured range for each patient was normalized by dividing it by the maximum among set of patients. The normalization allows for the comparison of the features by placing all values for each patient on the same scale (i.e., from 0 to 1).

The 5 Hz transient response showed a modest separation between patients ordering the patients as follows P26, P22, P25 P17, and P23. The 5 Hz transient response separated P23 deeply anesthetized patient from P26 who had the clinical reaction. Figure 3.10, B. and Table 3.5 showed the discrimination assessment for the 5 Hz transient responses under conventional filter settings. The responses under conventional filter settings show a lower power of discrimination. The responses did not separate P23 and P26 to opposite ends of the discrimination axis and closely clusters P22 and P26.

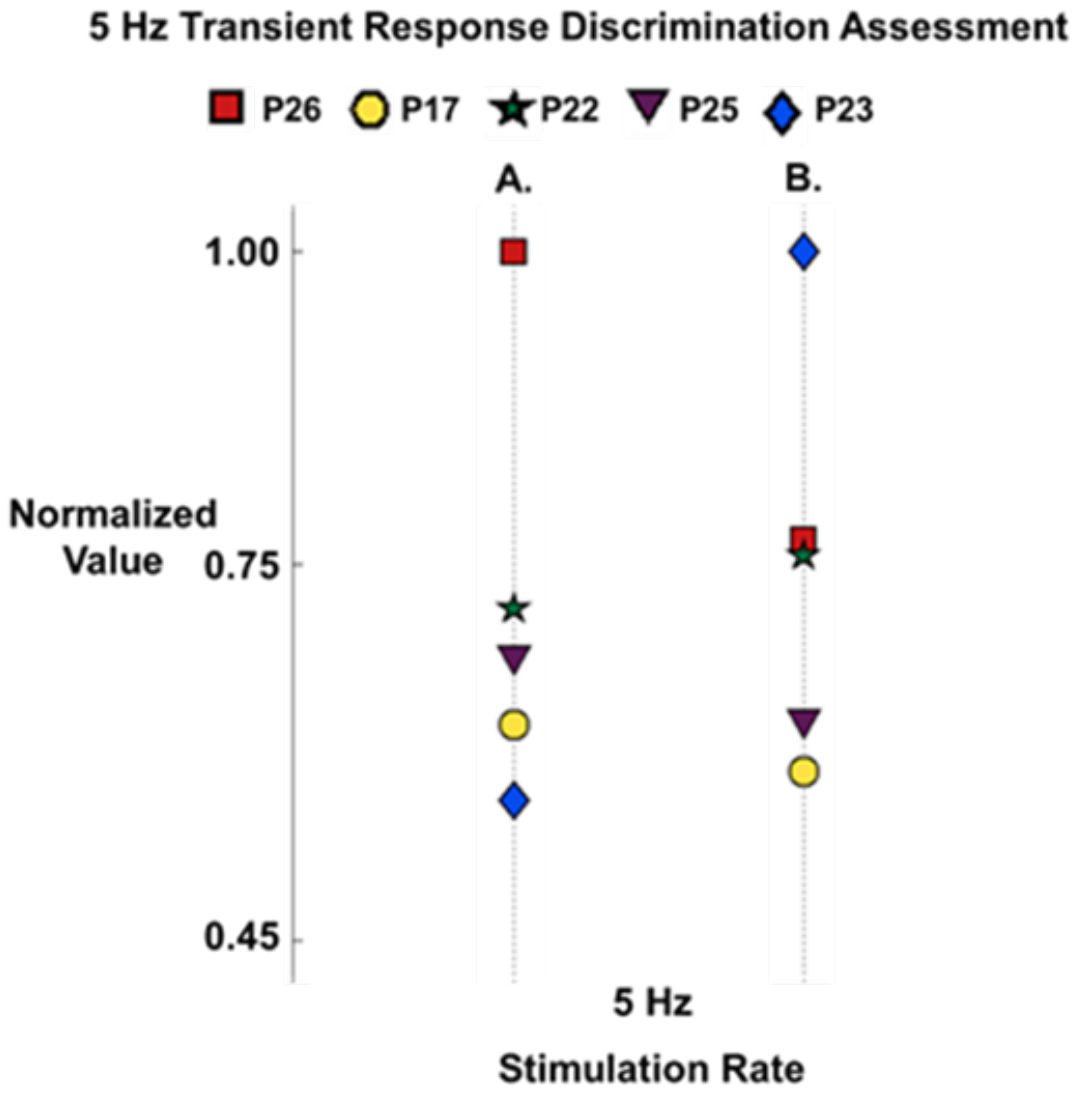

Figure 3.10 Discrimination assessment of anesthesia levels by 5 Hz transient response. The discrimination assessment computed for this study (column A.) and computed using the conventional filter (i.e., bandpass filtered from 25 to 1500 Hz) (column B.).

Table 3.5 Results for 5 Hz Transient Response Discrimination Assessment

	Subject				
	P17	P22	P23	P25	P26
5 Hz	M (SD)	M (SD)	M (SD)	M (SD)	M (SD)
Our Study	2.48 (0.83)	2.95 (0.78)	2.10 (0.98)	2.58 (0.58)	4.15 (1.52)
Conventional Filter	0.68 (0.32)	0.88 (0.30)	1.16 (0.73)	0.73 (0.18)	0.89 (0.25)
5 Hz	Normalized	Normalized	Normalized	Normalized	Normalized
Our Study	0.623	0.715	0.563	0.677	1.000
Conventional Filter	0.585	0.757	1.000	0.626	0.770

Grand mean of moving average 5 Hz response: The grand mean of moving average responses for 5 Hz responses was computed. Shown in Figure 3.11, are the grand mean of the 5 Hz transient responses extracted using moving average. The responses are plotted in the order of decreasing median frequency: P26, P17, P22, P25, and P23. The responses for patients P26, P17, and P22 showed a larger waveform magnitude by contrast patients P23 and P25 showed attenuated waveforms. Patients P23 and P25 had a greater anesthetic depth than patients P26, P17, and P22.

Also, the responses showed an increase in attenuation, from P25 to P23, suggesting the suppression of the auditory responses had increased. Shown in Figure 3.11, are the grand mean of the 5 Hz transient responses under conventional filter settings. The low frequency signals (i.e., slow wave potentials) that were affected by anesthesia are eliminated under conventional filtering. After conventional filtering, the responses, as suggested in the moving average analysis of the 5 Hz responses, continue to

appear attenuated and show small effect due to anesthesia. The gray traces are the split-buffer average traces. The split-buffer traces for both grand mean indicate good signal-to-noise ratio.

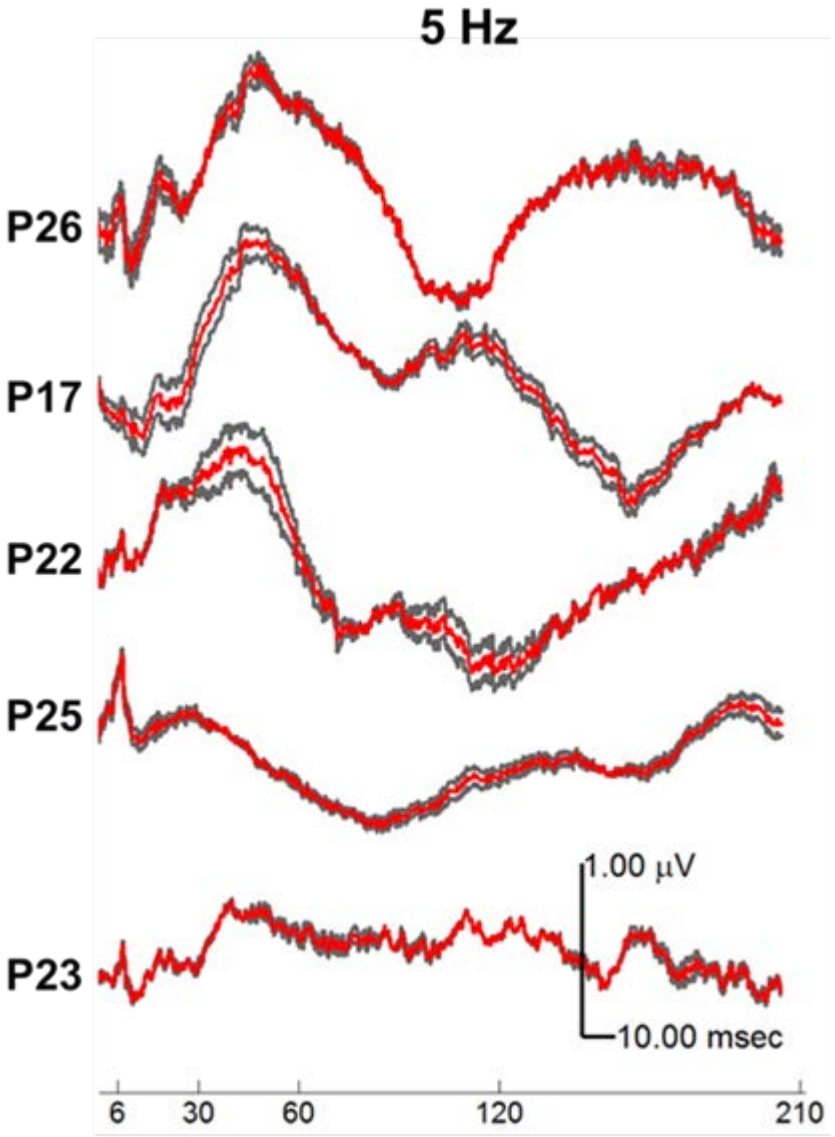

Figure 3.11 Grand mean of 5 Hz transient responses via MA. The red trace is the mean response and the gray trace is the mean of the split buffer of sweeps.

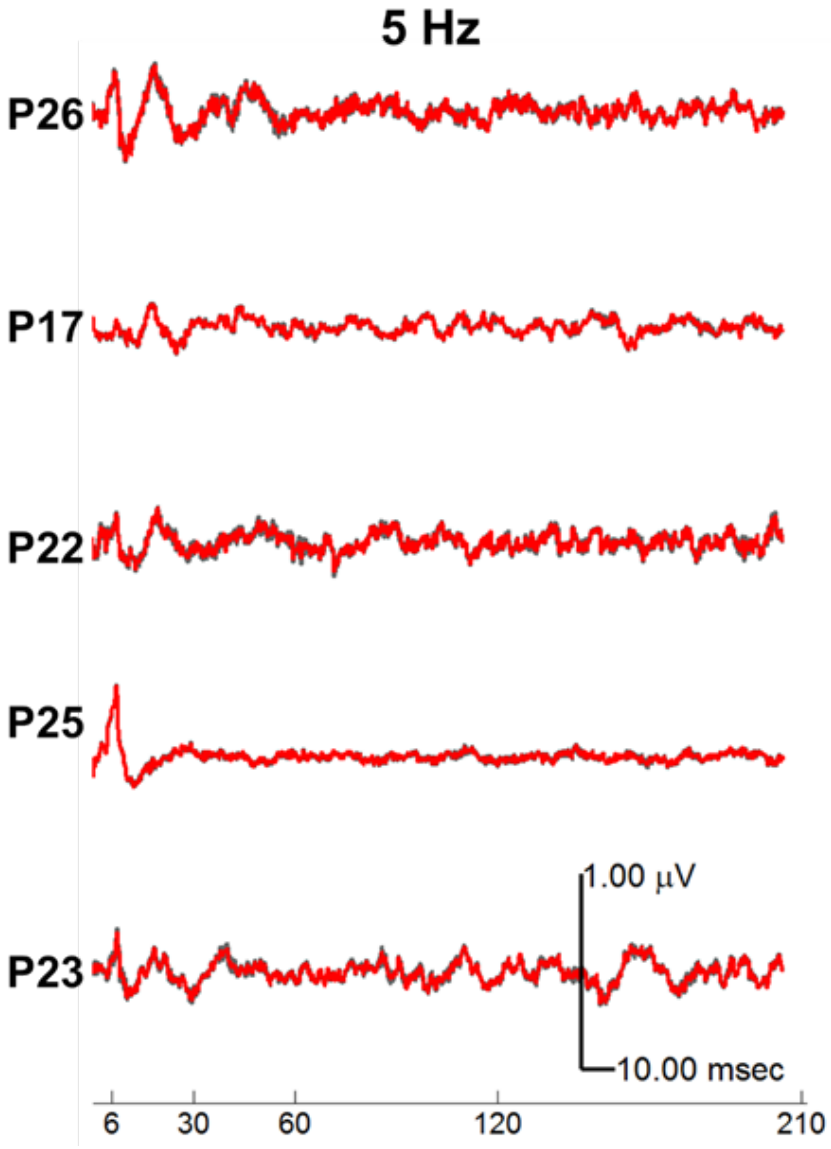

Figure 3.12 Grand mean of high-pass filtered 5 Hz transient responses via MA. The red trace is the mean response and the gray trace is the mean of the split buffer of sweeps.

Moving Average 20, 30 and 40 Hz transient response: Shown in Figure A1.2-4 the 20, 30, and 40 Hz transient responses extracted using the moving average. Each column represents the transient responses extracted of one patient. Each row represents the response extracted from one of the overlapping windows via moving average which is indexed. Figure A1.2-4 shows the effects of anesthesia on the morphology of the transient responses at rates higher than 5 Hz. Beta oscillations with considerable phase

consistency were observed in the 20, 30, and 40 Hz deconvolved transient responses. The beta oscillations were observed for all patients and all stimulation rates: 20 Hz, 30 Hz and 40 Hz. Some oscillations embedded in the responses were robust, such as P22 from index 14 (75 min.) to 16 (85 min.), P26 from index 5 (30 min.) to 9 (50 min.).

The majority of the responses resembled a stable form, such as P17 from index 18 (95 min.) to 20 (105 min.), P22 from index 26 (135 min.) to 27 (140 min.), P23 from index 44 (225 min.) to 46 (235 min.), P25 from index 6 (35 min.) to 9 (50 min.), and P26 from index 2 (15 min.) to 4 (25 min.). The amplitude of the oscillations varied vary from small to larger, such as P17 index 27 (140 min.) and P23 index 28 (145 min.). Also, for 20 30 and 40 Hz stimulation rates the transient response show the similar phase of oscillation (about 5 cycles in 307.2 msec. yields 16.276 Hz) that was not observed in the 5 Hz.

Beta entrainment power: The anesthesia transient responses showed prevalent beta oscillatory activity. This beta activity was embedded in the transient auditory responses during anesthesia (see Figure A1.2-4). The power of the dominant frequency within the beta range was measured (see Figure 3.13and Table 3.6). The prevailing oscillation frequency for P17, P23, P25, and P26 was 17.0898 Hz, and for P22 was 19.531 Hz.

Shown in Figure 3.13 is the power of beta entrainment of each stimulation rate for each patient. The power of beta entrainment indicated the stability of the beta oscillation embedded in 20, 30, and 40 Hz transient responses. Patient P22 had a robust oscillation frequency at 17.0898 Hz, but the frequency at 19.531 Hz was greatest. For the patients

P23 and P25, the deeper patients of the group of patients, there was less fluctuations and more flat regions in the beta entrainment power trace.

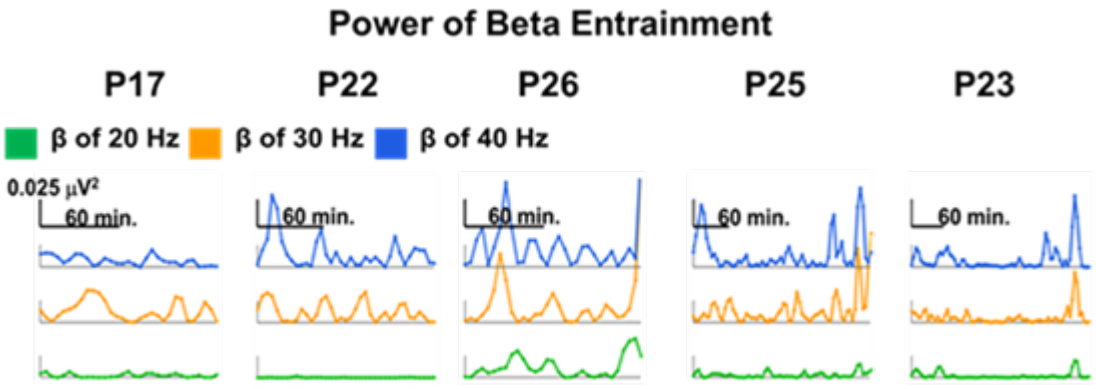

Figure 3.13 Power of beta entrainment in 20, 30, and 40 Hz transient response. The power of the beta entrainment measures the synchrony of the underlying beta oscillations that were observed in the 20, 30, and 40 Hz responses.

Table 3.6 Results for the Power of Beta Entrainment in 20, 30, and 40 Hz Transient Responses

Power of Beta Entrainment					
	P17	P22	P23	P25	P26
	(n = 31)	(n = 37)	(n = 75)	(n = 68)	(n = 31)
Simulation Rate	M (SD)	M (SD)	M (SD)	M (SD)	M (SD)
20 Hz	0.0019 (0.0017)	0.0002 (0.0003)	0.0018 (0.0031)	0.0025 (0.0025)	0.0096 (0.0098)
30 Hz	0.0103 (0.0089)	0.0095 (0.0085)	0.0046 (0.0072)	0.0113 (0.0146)	0.0166 (0.0286)
40 Hz	0.0058 (0.0043)	0.0126 (0.0141)	0.0069 (0.0108)	0.0120 (0.0160)	0.0187 (0.0222)

The higher stimulation rate transient responses (e.g., 30Hz and 40Hz), compared to the lower (e.g., 20 Hz), showed more variations in beta entrainment power for all patietns. The 30 Hz transient response showed reasonably good activity with respect to changes in anesthesia, especially P17.

The 20 Hz power of beta entrainment showed less activity for P17, P22, P25, and P23 with the exception of P26 (see Figure 3.13 and Table 3.6). For P26, the beta oscillation in 20 Hz transient response was greater than comparable patients.

Beta entrainment power – Discrimination Assessment: Shown in Figure 3.14 and Table 3.7 is an assessment of beta entrainment discrimination ability.

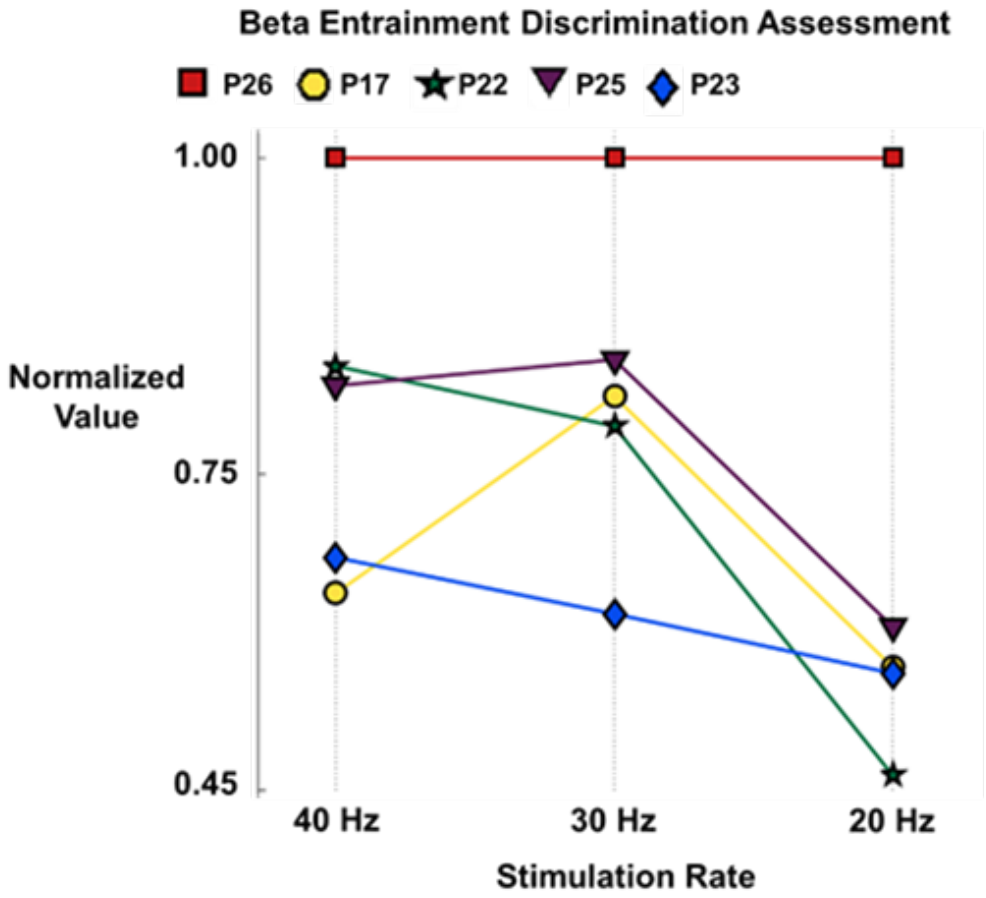

Figure 3.14 Discrimination assessment of anesthesia levels by beta entrainment.

For each spectral descriptor, the patient's value was normalized by dividing it by the maximum among the set of patients. The normalization allowed the features to be compared at the same scale (i.e., from 0 to 1). The beta entrainment measured from the 40 Hz transient response preformed modestly in separating between the patients. It

clustered P22 and P25 closely and it clustered P17 and P23 closely. It did not perform well as the 30Hz. The beta entrainment measured from the 30 Hz transient response separated well the patients spreading widely P23 from P26. It showed that the 30 Hz clusters closely P17, P22, and P25. The beta entrainment measured from the 20 Hz transient response dispersed the P26 from the remaining patients the furthest in comparison to the other stimulation rates. It did not distinguish between P17 and P23 and placed P22 at the opposite end of the discrimination axis.

Table 3.7 Results for Beta Entrainment Discrimination Assessment

	Subject				
	P17	P22	P23	P25	P26
Stimulation Rate	Normalized	Normalized	Normalized	Normalized	Normalized
40 Hz	0.312	0.671	0.368	0.640	1.000
30 Hz	0.623	0.576	0.279	0.681	1.000
20 Hz	0.195	0.024	0.185	0.259	1.000

3.1.4 Evoked Potential: Steady-State Response

The trend analysis was performed on the phasors. The plots showing the trends of the phasors are arranged in a grid layout. Each column of the grid is one patient. Each row is a stimulation rate of the phasor.

Phasors of 20, 30, and 40 Hz steady-state response: A phasor is a phase vector that describes the magnitude and phase angle of a frequency component in the frequency spectrum by using a vector. Shown in Figure 3.15 is the magnitude and phase angle for

the 20, 30, and 40 Hz steady-state response phasors. The phasor were estimated from the fundamental frequency (i.e., stimulation rate) of the steady-state response.

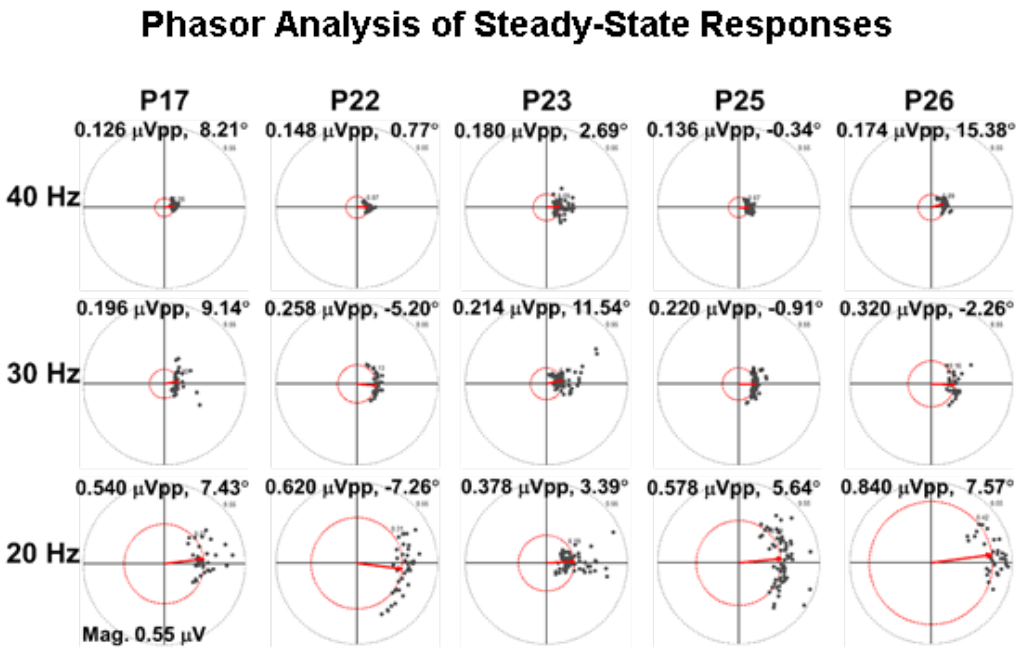

Figure 3.15 Trend of magnitude and phase for steady-state phasor. The top of each phasor plot is the numeric value for the magnitude and phase of phasor. The columns are each patient. The rows are each stimulation rate of phasor. The gray circular axis is set at 0.55 µV. For visual purposes, a red axis is drawn and set at the magnitude value of the phasor. The gray dots represent individual phasor instances acquired during surgery and used to compute the mean phasor (red arrow).

The magnitude of the phasors increased with decrease of stimulation rate. The 40 Hz phasor amplitudes are less than ten percent compared to typical awake subject (see Figure 1.27) and showed a stable phase. The 30 Hz phasor showed more phase dispersion than 40 Hz and a slight higher amplitude.

Compared to 30 and 40Hz, the 20 Hz phasor showed higher amplitude. The 20 Hz phasor amplitude was larger than the 30 and 40 Hz amplitudes. The patients were arranged with respects to the amplitude of the 20 Hz phasors in decreasing order as

follow: P26, P22, P25, P17, and P23. This arrangement showed a separate between the more deep (i.e., P23) and the patient who showed clinical reaction (i.e., P26).

Shown in Figure 3.16 and Table 3.8 is an assessment of 20, 30 and 40 Hz phasor magnitudes discrimination ability.

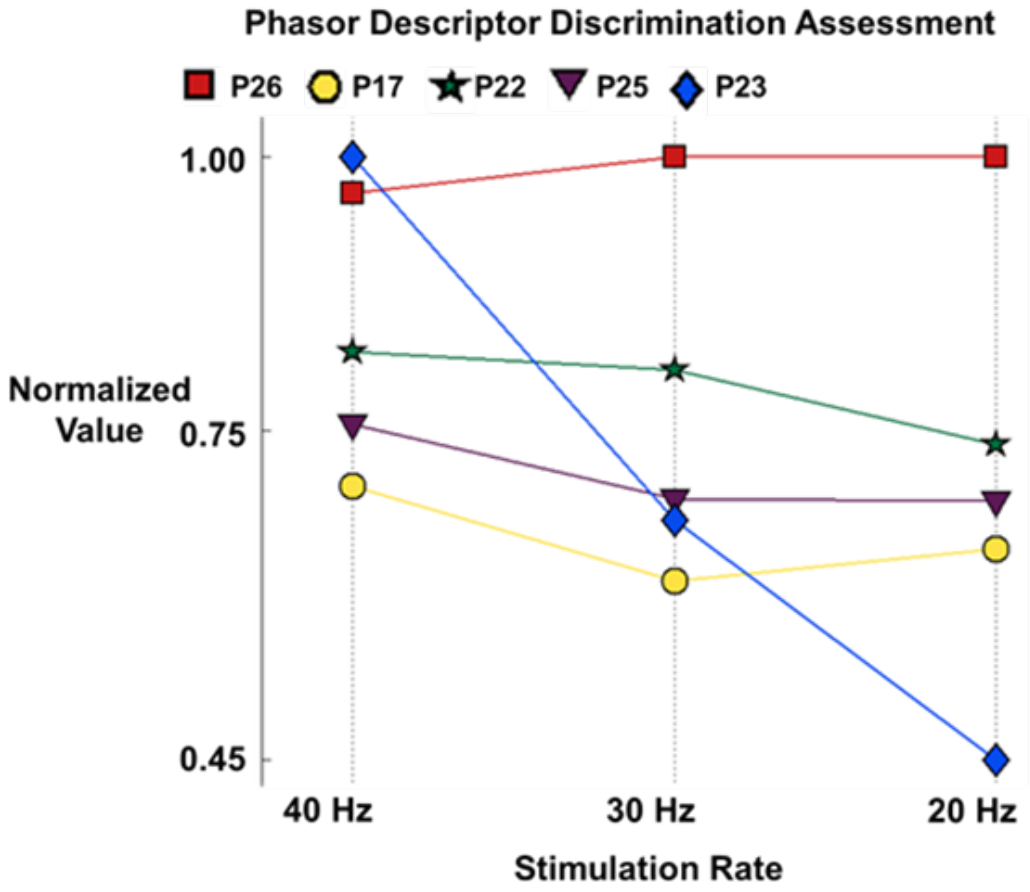

Figure 3.16 Discrimination assessment of anesthesia levels by steady-state phasors. The magnitude of the phasors for each patient is normalized by dividing it by the maximum among the set of patients. The normalization allowed the features to be compared at the same scale (i.e., from 0 to 1).

It was observed that with decreasing stimulation rate the phasors tend to increase in the separate between P23 (i.e., deeply anesthetized patient) and P26 (i.e., patient that showed clinical reaction). The 40 Hz phasor ordered the patients as P23, P26, P22, P25, and P17 closely clustering P23 (i.e., deep) and P26 (i.e., light). The 30 Hz phasor separated P23 from P26 more than the 40 Hz phasor and ordered the patients as P26, P22, P25, P23, and P17. The 20 Hz phasor showed the greatest separation of between P23 and P26 ordering the patients as P17 P26, P22 P25, P17 and P23. The 20 Hz phasor preformed similar to the 5 Hz transient response and showed a similar ordering of patients as 5 Hz transient response.

Table 3.8 Results for Phasor Discrimination Assessment

	Subject				
	P17	P22	P23	P25	P26
Stimulation Rate	Normalized	Normalized	Normalized	Normalized	Normalized
40 Hz	0.700	0.822	1.000	0.756	0.967
30 Hz	0.613	0.806	0.669	0.688	1.000
20 Hz	0.643	0.738	0.450	0.686	1.000

3.2 Study 2. Sleep

The sleep study results presented in this section are as follows: (a) the spectral descriptors for electroencephalographic signal; (b) the transient responses extracted for each sleep stage; and (c) the phasor of steady-state response extracted for each sleep

stage. For each measured feature, a brief definition of the feature is provided followed by a concise explanation of the most relevant observations of the results. The spectral descriptors presented are: total power (i.e., TP), power ratio (i.e., PR), median frequency (i.e., MF), spectral edge frequency (i.e., SEF), and spectral entropy (i.e., SE). Transient responses for 5 and 30 Hz recorded from the channel Fz-A2 and Cz-A2 are presented. Also, presented are the magnitude and latency results of the transient responses. For each sleep stage, the grand mean of the transient responses are presented. The results for the phasors of the 30 Hz steady-state responses are presented.

3.2.1 Sleep Stage: Measurement and Evaluation

A total of 14 subjects participated in the sleep study. Shown in Figure 3.17 are the hypnogram results for each subject. A hypnogram is a graphical representation of stages of sleep. In the hypnogram plot, the vertical axis denotes the sleep stages while the horizontal axis denotes the epoch. The subjects showed a diverse distribution of sleep stages. It was not expected that each subject would yield an equal number stages for each sleep stage condition. The number of sleep stages is a function of the sleep load and homeostatic drive of each subject. As continuous auditory stimulation works counter to fascinating the onset of sleep. It may have affected the number of sleep stages yielded by each subject, particularly for entering the deeper stages.

In order to prevent one subject from contributing undue influence in the population average the number of sweeps of each subject was limited to a maximum of 1200 sweeps for 5 Hz and 800 sweeps for 30 Hz, while a minimum of 540 sweeps for 5 Hz and 360 sweeps for 30 Hz. This led subject-to-subject variability in weights to

approximate to equally weighted distribution of subject contribution (see Table 3.9). Therefore, the equal weighting the subject's contribution and the reduction in variability

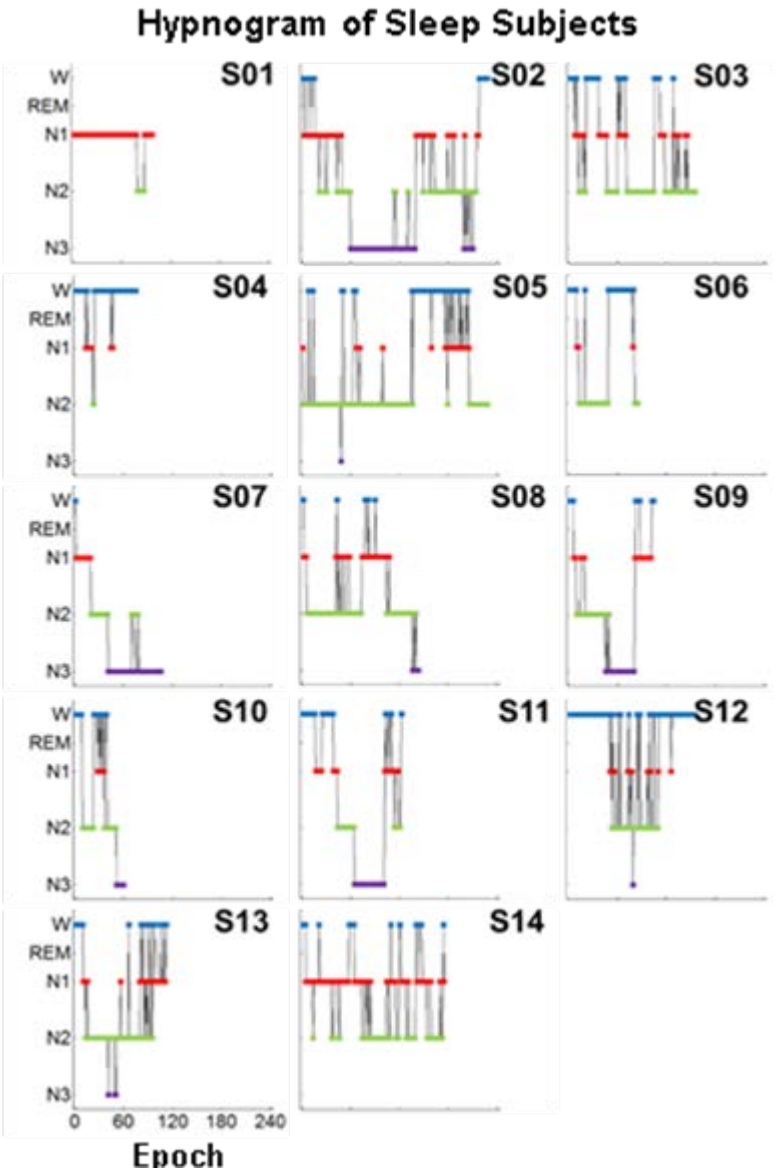

Figure 3.17 The hypnograms of subjects. A color is assigned to each sleep stage: W (blue), N1 (red), N2 (green), and N3 (purple).

by taking the population average leads to less bias by a subject's individual contribution to the mean (i.e., unweighted average).

Shown in Table 3.9 is the number of sleep stages yield by each subject. Column one is the original number of sleep stages and column two is the modified number of sleep stages use to evaluate the performance of the parameters measured in sleep. The modification of the sleep stage count was to ensure that an individual subject would not unduly contribute more than another subject when representing the population.

Table 3.9 Count of Sleep Stage Epochs for each Subject

	Original Count Sleep Stage				Modified Count Sleep Stage			
Subjects	W	N1	N2	N3	W	N1	N2	N3
FzA2/CzA2								
S01	0/0	88/0	9/0	0/0	0/0	20/0	9/0	0/0
S02	23/0	59/0	65/0	81/0	20/0	20/0	20/0	20/0
S03	40	34	81	0	20	20	20	0
S04	63	10	2	0	20	10	0	0
S05	60	22	145	1	20	20	20	0
S06	41	4	40	0	20	0	20	0
S07	1	18	26	61	0	18	20	20
S08	8	37	92	6	0	20	20	0
S09	14	23	33	34	14	20	20	20
S10	20	4	26	10	20	0	20	10
S11	38	23	25	37	20	20	20	20
S12	106	10	38	1	20	10	20	0
S13	18	25	66	3	18	20	20	0
S14	21	93	61	0	20	20	20	0
FzA2 Total	453	450	709	234	**212**	**218**	**249**	**90**
CzA2 Total	430	303	635	153	**192**	**178**	**220**	**70**

For statistical analysis of parameters under sleep, a two-tailed, two sample Student's t-test using a significance level of 5% (i.e., $\alpha = .05$) was used as the statistical

test. This analysis evaluated if the parameter under study (i.e., spectral descriptor, transient responses, or phasors) can discriminate between sleep stages. This analysis tested if there existed a difference exists between the following pairing of sleep stages (i.e., W vs. N1, W vs N2, W vs. N3, N1 vs. N2, and N2 vs. N3) and was applied to all parameters in this study.

3.2.2 Electroencephalogram: Spectral Descriptors

In terms of auditory stimulation, the spectral descriptors showed the same discrimination performance – no significant difference found in regards to the discrimination ability under different auditory stimulation. Further, Fz-A2 showed better discrimination than Cz-A2. Due to redundancy only 5 Hz will be presented. EEG spectral descriptors were analyzed via sleep stages. A detailed analysis of the effect of stimulation on EEG spectrum is presented in section 3.2.3.

Power Ratio: The power ratios of EEG were grouped, for each sleep stage, in from ascending order from delta to gamma: Delta (1 - 4 Hz, red), Theta (4 - 8 Hz, blue), Alpha (8 - 13 Hz, green), and Beta (13 - 30 Hz, purple), and Gamma (30 - 48 Hz, orange). Shown in Figure 3.18 are the changes to the EEG power ratio (i.e., power ratio distribution) for both Fz-A2 and Cz-A2. As expected, the waking stage of sleep showed a broad distribution and became narrow from stage N1 to stage N3 due to the effect of sleep on EEG. The delta band of the power ratio increased in a monotonic and linear-like form, from waking (i.e., stage W) to stage N3. The higher-frequency power ratios attenuated as the delta power ratio monotonically increased. By stage N3, the delta power

ratio showed greatest value of the set of power ratios and the higher-frequency power ratios showed least value. Cz-A2 showed a higher alpha power ratio value in waking, than Fz-A2 showed. The EEG power ratios were observed to change their values with respects to sleep stages.

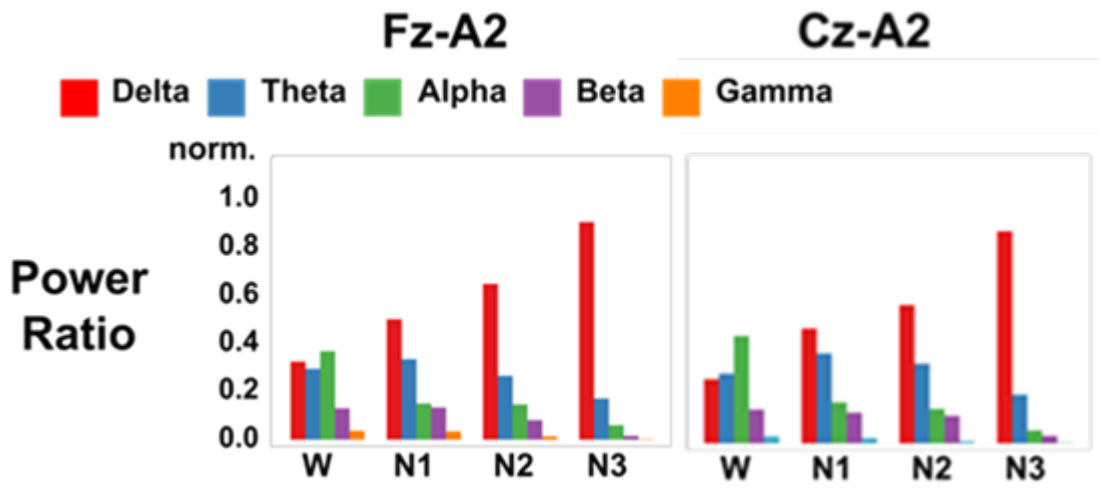

Figure 3.18 The power ratios from delta to gamma grouped by sleep stages in FzA2 and CzA2. Each group shows the effect of a sleep stage on the power ratio of EEG arranged into a distribution as bins of classical EEG bands.

To contrast to grouping the power ratios by sleep stage, the power ratios were grouped by EEG bands. Shown in Figure 3.19, the power ratios of EEG were grouped, for each EEG band, in from ascending order from stage W to N3. The delta power ratio significantly increased in a monotonic linear-like form W (0.28 ± (0.09)) to N3 (0.79 ± (0.074)). The theta power ratio decreased significantly from W (0.26 ± (0.07)) to N3 (0.148 ± (0.043)) and from N1 (0.29 ± (0.064)) to N3 (0.15 ± (0.04)) and N2 (0.23 ± (0.06)).

The alpha power ratio decreased significantly from W (0.319 ± (0.09)) to N1 (0.13 ± (0.03)), N2 (0.13 ± (0.04)), and N3 (0.05 ± (0.03)). Also, it significantly

decreased from N1 (0.13 ± (0.03)) to N3 (0.05 ± (0.03)) and from N2 (0.13 ± (0.04)) to N3 (0.05 ± (0.03).

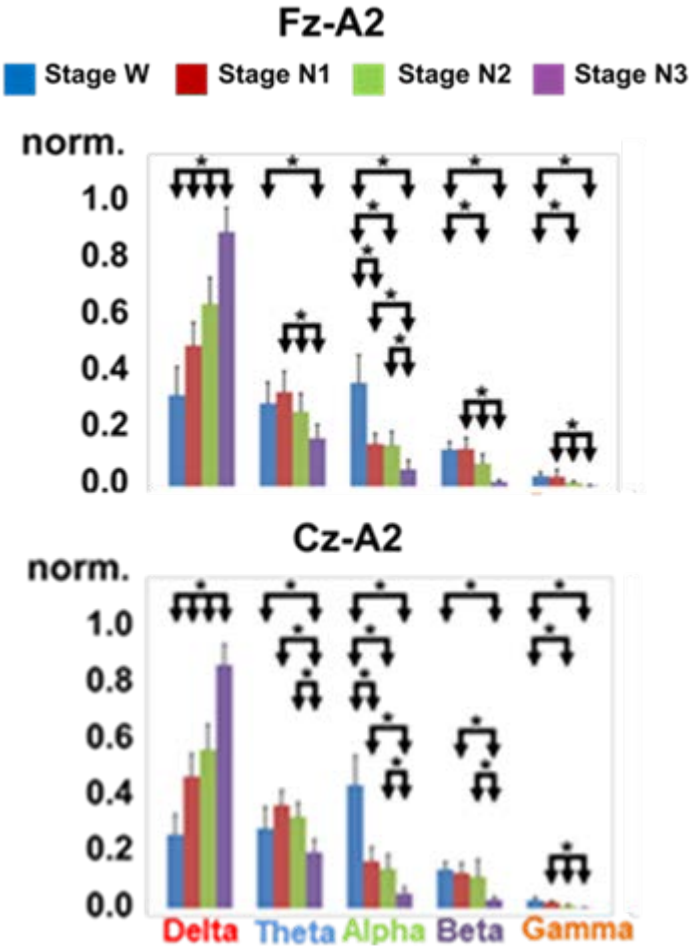

Figure 3.19 The power ratios grouped by EEG bands from stage W to N3 in FzA2 and CzA2. The power ratio of EEG is grouped by classical EEG bands and arranged in order of sleep stage (stage W, stage N1, stage N2 and stage N3) (± St.Dev., *, Significantly Different ($p<0.05$)).

The beta power ratio significantly decreased from W (0.11 ± (0.024)) to N2 (0.07 ± (0.03)) and N3 (0.01 ± (0.006)) and from N1 (0.12 ± (0.03)) to N2 (0.07 ± (0.03)) and N3 (0.01 ± (0.006)). The gamma power ratio significantly decreased from W (0.032 ± (0.012)) to N2 (0.011 ± (0.005)) to N3 (0.002 ± (0.001)) and from N1 (0.030 ± (0.022)) to N2 (0.011 ± (0.005)) and to N3 (0.002 ± (0.001)). Power ratio for channel CzA2

showed similar values to FzA2 with the following exceptions: (a) the Cz-A2 theta power ratio was not significant from W to N2, and (b) the Cz-A2 beta power ratio was not significant from W to N2 and from N1 to N2. As shown in Table 3.13, the ability of the power ratio to discriminate was less when it discriminated between the early stages of sleep such as stage W and N1. The alpha power ratio discriminated greater in the early stages, but discriminated less in deeper sleep stages. For the power ratio, the delta power ratio, for all sleep stages, showed significant difference. The delta power ratio discriminated between all sleep stages and its value increased in a linear-like manner, from stage W to N3.

Total Power: Shown in Figure 3.20 is the total power arranged in order from waking to stage N3 for channel Fz-A2 and Cz-A2.

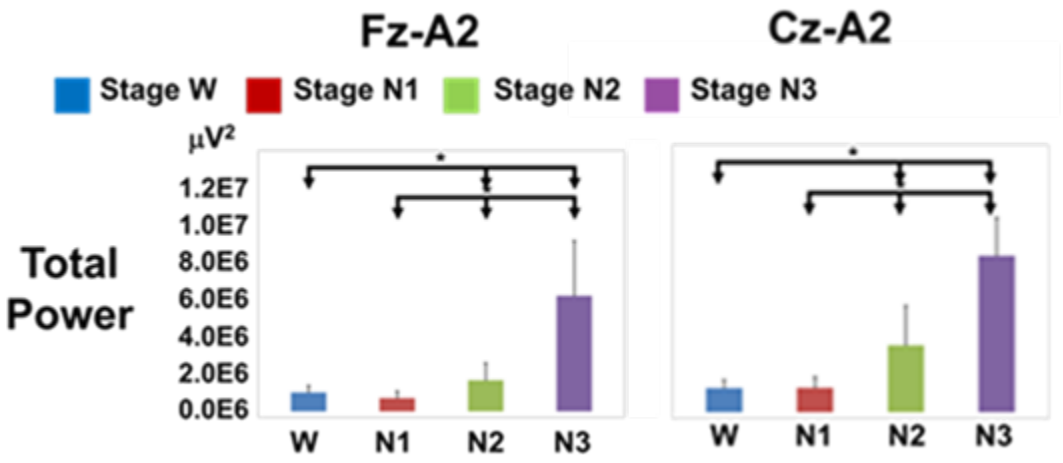

Figure 3.20 The total power of EEG for each sleep stage in FzA2 and CzA2 (± St.Dev., *, Significantly Different ($p<0.05$)).

The total power modestly increased from W to N2 ($8.9\times10^5 \pm (3.1\times10^5)$ to $1.5\times10^6 \pm (8.0\times10^5)$). Then it showed a steep increase from N2 to N3 ($1.5\times10^6 \pm (8.0\times10^5)$ to $5.4\times10^6 \pm (2.6\times10^6)$). Total power showed a significant difference between

all sleep stages, except between stage W and N1 (see Table 3.10 to Table 3.13). Total power for Cz-A2 showed similar values to FzA2: (a) modestly increased from W to N2 ($1.1\times10^6 \pm (3.6\times10^5)$ to $3.1\times10^6 \pm (1.8\times10^6)$), (b) steeply increased from N2 to N3 ($3.1\times10^6 \pm (1.8\times10^6)$ to $7.2\times10^6 \pm (1.7\times10^6)$), and (c) was significantly difference between all sleep stages, except between stage W and N1. CzA2 showed a slightly greater value in N2 and N3 compared to FzA2.

Spectral Edge Frequency: Shown in Figure 3.21 is the spectral edge frequency arranged in order from waking to stage N3 for channel FzA2.

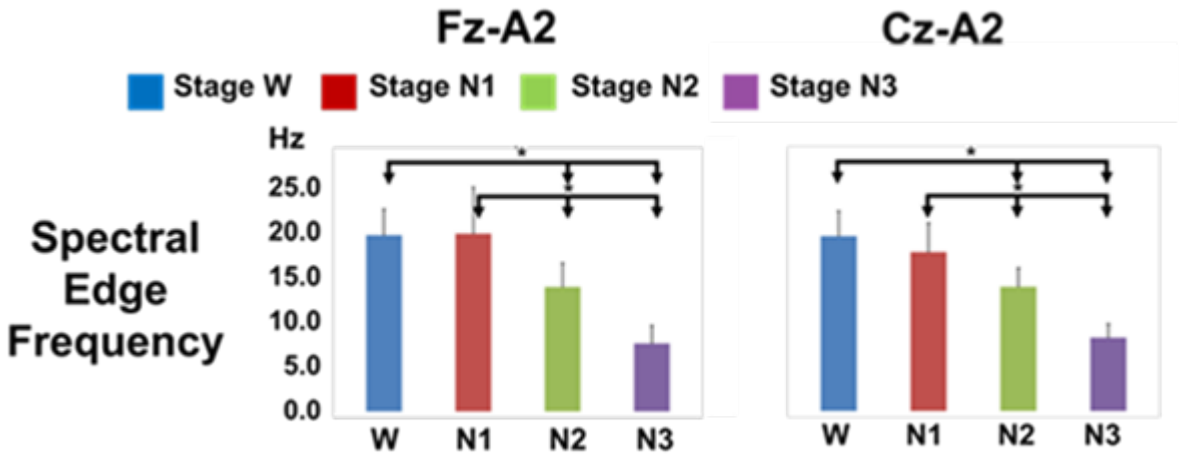

Figure 3.21 The spectral edge frequency of EEG for each sleep stage in FzA2 and CzA2. (± St.Dev., *, Significantly Different ($p<0.05$)).

The spectral edge frequency showed a stable value for W and N1 (~ 17.1 Hz) then it significantly decreased in N2 (12.08 ± (2.31) Hz) and in N3 (6.60 ± (1.72) Hz). The spectral edge frequency for Cz-A2 showed a significant steady decrease from N1 to N3 (15.37 ± (2.79) to 7.08 ± (1.33) Hz) and slight decrease was observed from W to N1 (16.91 ± (2.43) to 15.37 ± (2.79)) that was not found to be statistically significant.

Median Frequency: shown in Figure 3.22 is the median frequency arranged in order from waking to stage N3 for channel Fz-A2. The median frequency significantly decreased in a monotonic linear-like form W (7.23 ± (1.28) Hz) to N3 (2.22 ± (0.402) Hz). The median frequency discriminated between all sleep stages. The median frequency for Cz-A2 significantly decreased from W (8.00 ± (1.19)) to N2 (4.51 ± (0.94)) and N3 (2.42 ± (0.47)) and significantly decreased from N2 to N3 (4.51 ± (0.94) to 2.42 ± (0.47)). The median frequency for Cz-A2 showed a significant difference between all sleep stages, except between stage N1 and N2.

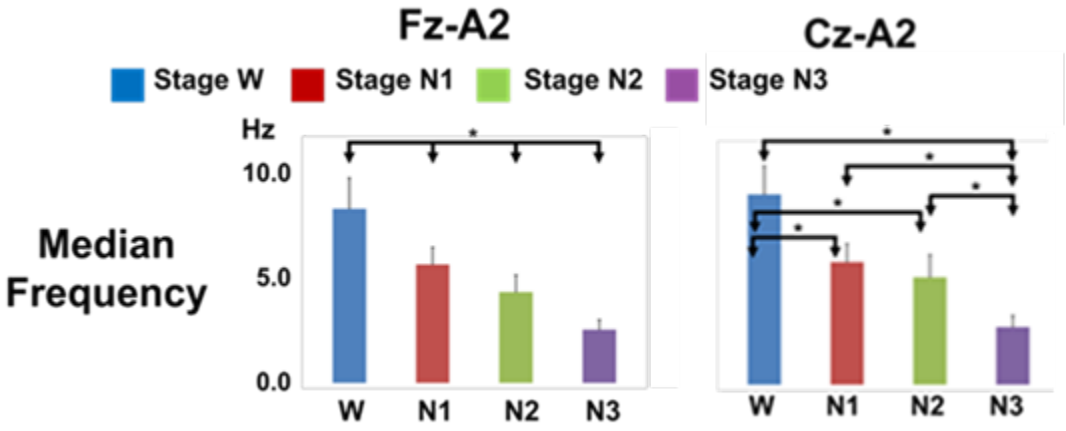

Figure 3.22 The median frequency of EEG for each sleep stage in FzA2 and CzA2. (± St.Dev., *, Significantly Different ($p<0.05$)).

Spectral Entropy: Shown in Figure 3.23 is the spectral entropy arranged in order from W to N3 for channel Fz-A2. It showed stable values for W and N1 (~ 0.78) then it significantly decreased in N2 (0.71 ± (0.036)) and in N3 (0.59 ± (0.059)). Spectral entropy discriminated well between all sleep-stage pairs, but not between stage W and N1 (see Table 3.11 to 3.13). Cz-A2 preformed similar to Fz-A2 with a slightly greater value in W and N3 for Cz-A2 than Fz-A2 and slight lesser value in N1 for Cz-A2 than Fz-A2.

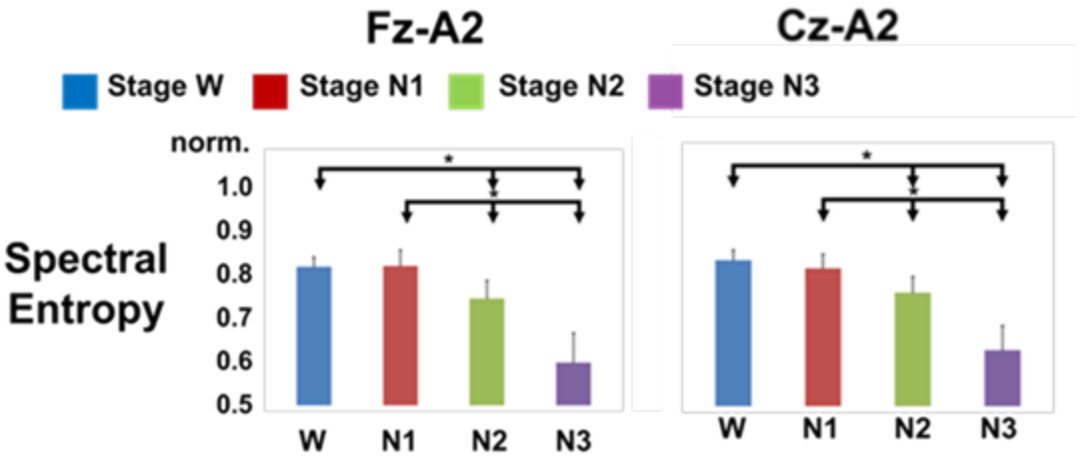

Figure 3.23 The spectral entropy of EEG for each sleep stage in FzA2 and CzA2. (± St.Dev., *, Significantly Different ($p<0.05$)).

Table 3.10 Results for Spectral Descriptors for each Stimulation Rate in Fz-A2

	Sleep			
	Stage W	Stage N1	Stage N2	Stage N3
	(n = 212)	(n = 218)	(n = 240)	(n = 90)
Spectral Descriptor	M (SD)	M (SD)	M (SD)	M (SD)
5Hz Stimulation				
Delta Power Ratio	0.281 (0.088)	0.434 (0.072)	0.562 (0.082)	0.785 (0.074)
Theta Power Ratio	0.256 (0.066)	0.290 (0.064)	0.230 (0.057)	0.148 (0.043)
Alpha Power Ratio	0.319 (0.085)	0.130 (0.032)	0.126 (0.042)	0.052 (0.029)
Beta Power Ratio	0.113 (0.024)	0.116 (0.034)	0.070 (0.028)	0.013 (0.006)
Gamma Power Ratio	0.032 (0.012)	0.030 (0.022)	0.011 (0.005)	0.002 (0.001)
Total Power	8.9E +5 (3.1E +5)	6.2E +5 (3.3E +5)	1.5E +6 (8.0E +5)	5.4E +6 (2.6E +6)
Spec. Edge Freq.	17.112 (2.499)	17.244 (4.517)	12.083 (2.306)	6.604 (1.723)
Median Freq.	7.232 (1.275)	4.924 (0.706)	3.774 (0.696)	2.216 (0.402)
Spec. Entropy	0.777 (0.019)	0.778 (0.032)	0.714 (0.036)	0.585 (0.059)
30Hz Stimulation				
Delta Power Ratio	0.264 (0.078)	0.429 (0.068)	0.575 (0.075)	0.797 (0.059)
Theta Power Ratio	0.261 (0.065)	0.291 (0.072)	0.218 (0.048)	0.140 (0.036)
Alpha Power Ratio	0.327 (0.089)	0.130 (0.033)	0.127 (0.041)	0.048 (0.025)
Beta Power Ratio	0.117 (0.037)	0.121 (0.030)	0.070 (0.027)	0.013 (0.005)
Gamma Power Ratio	0.031 (0.011)	0.030 (0.022)	0.011 (0.004)	0.002 (0.002)
Total Power	8.3E +5 (3.2E +5)	5.7E +5 (3.1E +5)	1.6E +6 (8.9E +5)	5.7E +6 (2.4E +6)
Spec. Edge Freq.	17.309 (3.048)	17.757 (4.440)	11.979 (1.857)	6.516 (1.499)
Median Freq.	7.453 (1.139)	4.969 (0.650)	3.657 (0.634)	2.112 (0.303)
Spec. Entropy	0.783 (0.029)	0.784 (0.026)	0.708 (0.033)	0.581 (0.049)
Silence				
Delta Power Ratio	0.296 (0.096)	0.435 (0.075)	0.601 (0.091)	0.800 (0.067)
Theta Power Ratio	0.276 (0.069)	0.300 (0.073)	0.228 (0.031)	0.141 (0.041)
Alpha Power Ratio	0.285 (0.093)	0.130 (0.038)	0.107 (0.038)	0.047 (0.025)
Beta Power Ratio	0.112 (0.029)	0.106 (0.034)	0.054 (0.025)	0.011 (0.005)
Gamma Power Ratio	0.032 (0.012)	0.028 (0.023)	0.010 (0.004)	0.002 (0.001)
Total Power	8.5E +5 (4.0E +5)	6.6E +5 (3.2E +5)	1.8E +6 (4.6E +5)	6.0E +6 (3.0E +6)
Spec. Edge Freq.	17.228 (2.696)	16.390 (4.753)	10.654 (2.358)	6.238 (1.527)
Median Freq.	6.936 (1.072)	4.906 (0.758)	3.439 (0.687)	2.115 (0.324)
Spec. Entropy	0.781 (0.024)	0.770 (0.032)	0.690 (0.055)	0.575 (0.056)

Table 3.11 Student t-Test p-Values of Spectral Descriptors for each Stimulation Rate in Fz-A2

Spectral Descriptor	W vs. N1	W vs. N2	W vs. N3	N1 vs. N2	N1 vs. N3	N2 vs. N3
5Hz Stimulation						
Delta Power Ratio	0.000	0.000	0.000	0.000	0.000	0.000
Theta Power Ratio	0.213	0.318	0.005	0.020	0.000	0.010
Alpha Power Ratio	0.000	0.000	0.000	0.794	0.000	0.002
Beta Power Ratio	0.822	0.001	0.000	0.001	0.000	0.000
Gamma Power Ratio	0.814	0.000	0.000	0.006	0.015	0.002
Total Power	0.057	0.037	0.000	0.003	0.000	0.000
Spec. Edge Freq.	0.933	0.000	0.000	0.001	0.000	0.000
Median Freq.	0.000	0.000	0.000	0.000	0.000	0.000
Spec. Entropy	0.900	0.000	0.000	0.000	0.000	0.000
30Hz Stimulation						
Delta Power Ratio	0.000	0.000	0.000	0.000	0.000	0.000
Theta Power Ratio	0.313	0.073	0.002	0.006	0.001	0.005
Alpha Power Ratio	0.000	0.000	0.000	0.842	0.000	0.001
Beta Power Ratio	0.774	0.002	0.000	0.000	0.000	0.000
Gamma Power Ratio	0.879	0.000	0.000	0.005	0.017	0.000
Total Power	0.065	0.009	0.000	0.001	0.000	0.000
Spec. Edge Freq.	0.782	0.000	0.000	0.000	0.000	0.000
Median Freq.	0.000	0.000	0.000	0.000	0.000	0.000
Spec. Entropy	0.930	0.000	0.000	0.000	0.000	0.000
Silence						
Delta Power Ratio	0.002	0.000	0.000	0.002	0.000	0.004
Theta Power Ratio	0.464	0.169	0.002	0.015	0.000	0.005
Alpha Power Ratio	0.000	0.002	0.000	0.270	0.001	0.018
Beta Power Ratio	0.721	0.003	0.000	0.008	0.000	0.005
Gamma Power Ratio	0.721	0.003	0.000	0.008	0.000	0.005
Total Power	0.250	0.002	0.000	0.000	0.000	0.014
Spec. Edge Freq.	0.645	0.001	0.000	0.024	0.000	0.008
Median Freq.	0.000	0.000	0.000	0.002	0.000	0.005
Spec. Entropy	0.431	0.001	0.000	0.002	0.000	0.011

Table 3.12 Measurement Results for Spectral Descriptors for each Stimulation Rate in Cz-A2

	Sleep			
	Stage W	Stage N1	Stage N2	Stage N3
	(n = 192)	(n = 178)	(n = 220)	(n = 70)
Spectral Descriptor	M (SD)	M (SD)	M (SD)	M (SD)
5Hz Stimulation				
Delta Power Ratio	0.227 (0.063)	0.408 (0.070)	0.491 (0.079)	0.753 (0.064)
Theta Power Ratio	0.247 (0.066)	0.319 (0.045)	0.282 (0.045)	0.173 (0.040)
Alpha Power Ratio	0.381 (0.092)	0.146 (0.044)	0.122 (0.045)	0.046 (0.021)
Beta Power Ratio	0.120 (0.024)	0.109 (0.031)	0.098 (0.052)	0.026 (0.010)
Gamma Power Ratio	0.025 (0.010)	0.019 (0.004)	0.007 (0.003)	0.002 (0.001)
Total Power	1.1E+6 (3.6E+5)	1.1E+6 (4.9E+5)	3.1E+6 (1.8E+6)	7.2E+6 (1.7E+6)
Spec. Edge Freq.	16.914 (2.428)	15.363 (2.794)	12.023 (1.793)	7.084 (1.326)
Median Freq.	8.001 (1.185)	5.149 (0.770)	4.514 (0.943)	2.422 (0.472)
Spec. Entropy	0.784 (0.020)	0.768 (0.027)	0.721 (0.031)	0.609 (0.047)
30Hz Stimulation				
Delta Power Ratio	0.213 (0.057)	0.410 (0.063)	0.487 (0.084)	0.760 (0.063)
Theta Power Ratio	0.252 (0.058)	0.322 (0.041)	0.269 (0.044)	0.169 (0.043)
Alpha Power Ratio	0.389 (0.083)	0.133 (0.034)	0.130 (0.048)	0.043 (0.020)
Beta Power Ratio	0.122 (0.030)	0.115 (0.026)	0.106 (0.052)	0.026 (0.012)
Gamma Power Ratio	0.024 (0.008)	0.020 (0.004)	0.008 (0.003)	0.002 (0.000)
Total Power	1.1E+6 (1.2E+5)	1.0E+6 (1.6E+5)	2.9E+6 (6.1E+5)	8.1E+6 (5.8E+5)
Spec. Edge Freq.	17.044 (2.408)	15.958 (2.452)	12.526 (1.923)	6.939 (1.430)
Median Freq.	8.190 (1.054)	5.074 (0.695)	4.544 (0.978)	2.453 (0.429)
Spec. Entropy	0.786 (0.020)	0.774 (0.024)	0.728 (0.034)	0.607 (0.045)
Silence				
Delta Power Ratio	0.245 (0.050)	0.399 (0.066)	0.535 (0.075)	0.771 (0.055)
Theta Power Ratio	0.268 (0.063)	0.345 (0.050)	0.295 (0.027)	0.163 (0.036)
Alpha Power Ratio	0.346 (0.071)	0.137 (0.046)	0.094 (0.035)	0.042 (0.020)
Beta Power Ratio	0.117 (0.027)	0.101 (0.028)	0.068 (0.020)	0.023 (0.005)
Gamma Power Ratio	0.025 (0.010)	0.018 (0.004)	0.008 (0.004)	0.002 (0.001)
Total Power	1.0E+6 (3.7E+5)	1.3E+6 (4.7E+5)	3.9E+6 (1.4E+6)	7.8E+6 (2.5E+6)
Spec. Edge Freq.	16.875 (2.559)	14.675 (2.542)	10.963 (2.192)	6.737 (1.171)
Median Freq.	7.632 (0.875)	5.214 (0.699)	3.960 (0.611)	2.361 (0.393)
Spec. Entropy	0.788 (0.022)	0.761 (0.026)	0.700 (0.043)	0.601 (0.041)

Table 3.13 Student t-Test p-Values of Spectral Descriptors for each Stimulation Rate in Cz-A2

Spectral Descriptor	W vs. N1	W vs. N2	W vs. N3	N1 vs. N2	N1 vs. N3	N2 vs. N3
5Hz Stimulation						
Delta Power Ratio	0.000	0.000	0.000	0.020	0.000	0.000
Theta Power Ratio	0.011	0.168	0.030	0.077	0.000	0.001
Alpha Power Ratio	0.000	0.000	0.000	0.237	0.001	0.007
Beta Power Ratio	0.383	0.248	0.000	0.586	0.000	0.020
Gamma Power Ratio	0.081	0.000	0.001	0.000	0.000	0.007
Total Power	0.943	0.003	0.000	0.004	0.000	0.002
Spec. Edge Freq.	0.202	0.000	0.000	0.004	0.000	0.000
Median Freq.	0.000	0.000	0.000	0.109	0.000	0.001
Spec. Entropy	0.149	0.000	0.000	0.002	0.000	0.000
30Hz Stimulation						
Delta Power Ratio	0.000	0.000	0.000	0.031	0.000	0.000
Theta Power Ratio	0.006	0.454	0.024	0.012	0.000	0.002
Alpha Power Ratio	0.000	0.000	0.000	0.865	0.000	0.004
Beta Power Ratio	0.581	0.410	0.000	0.636	0.000	0.011
Gamma Power Ratio	0.161	0.000	0.000	0.000	0.000	0.001
Total Power	0.776	0.002	0.000	0.002	0.000	0.000
Spec. Edge Freq.	0.331	0.000	0.000	0.002	0.000	0.000
Median Freq.	0.000	0.000	0.000	0.173	0.000	0.001
Spec. Entropy	0.250	0.000	0.000	0.002	0.000	0.000
Silence						
Delta Power Ratio	0.000	0.000	0.000	0.007	0.000	0.002
Theta Power Ratio	0.013	0.445	0.012	0.001	0.000	0.001
Alpha Power Ratio	0.000	0.000	0.000	0.128	0.003	0.042
Beta Power Ratio	0.250	0.303	0.000	0.061	0.000	0.005
Gamma Power Ratio	0.058	0.007	0.001	0.001	0.000	0.018
Total Power	0.250	0.002	0.000	0.000	0.000	0.014
Spec. Edge Freq.	0.096	0.003	0.000	0.028	0.000	0.014
Median Freq.	0.000	0.000	0.000	0.114	0.000	0.005
Spec. Entropy	0.014	0.001	0.000	0.008	0.000	0.016

Shown in Figure 3.24 is a summary of the ability of the spectral descriptors to separate between paired sleep stages. The spectral descriptors yielded the same results for each stimulation rate.

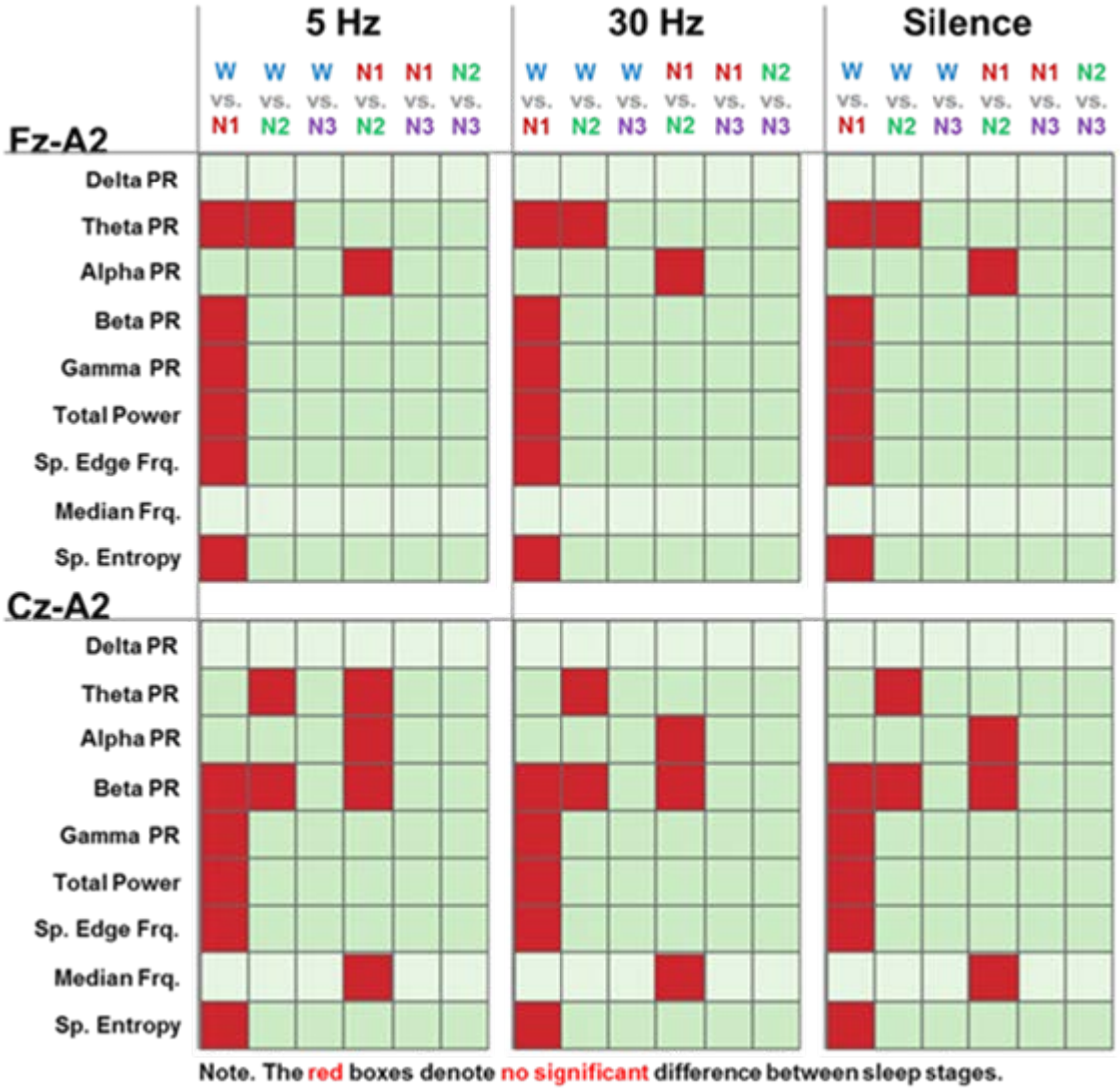

Figure 3.24 Discrimination of sleep stages by spectral descriptors in Fz-A2 and Cz-A2. (Red, Significantly Different ($p<0.05$)).

The change in stimulation did not show a change in the ability of the spectral descriptor to separate between the sleep stages, with the exception of Cz-A2 theta power ratio between N1 and N2.

Shown in Figure 3.25 and Table 3.14 is the spectral descriptor discrimination assessment. For each spectral descriptor, each sleep stage's value was normalized by dividing it by the maximum in the set of sleep stages.

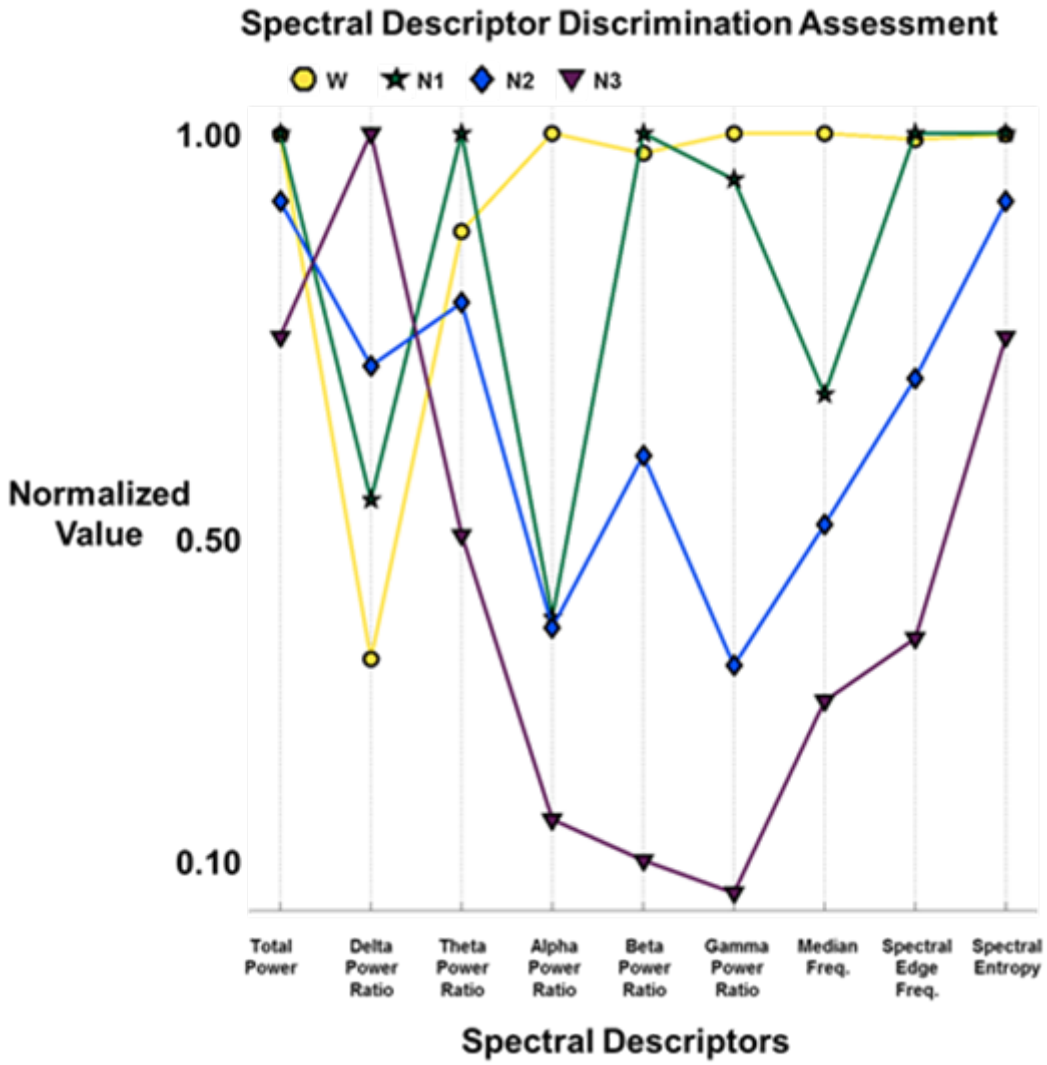

Figure 3.25 Discrimination assessment of sleep stages levels by spectral descriptors. Each column is one spectral descriptor. Each trace is one sleep stage. For comparison within spectral descriptors, the spectral descriptor values of the sleep stages were normalized by the stage subject having the highest spectral descriptor value.

The normalization allowed for feature comparison using the same scale (i.e., from 0 to 1).

Total power showed a low separation power. Total power did not separate W and N1 and

both W and N1 in the same location. It separated W and N3 to the opposite ends of the discrimination axis. In this study W and N1 are considered lighter sleep stages than N2 and N3. Stage N2 is the onset of sleep and stage N3 is the deepest sleep stage. The discrimination assessment showed that for W vs. N1 the discrimination performance of the features decreased.

Table 3.14 Results for Spectral Descriptors Discrimination Assessment

	Sleep Stages			
	W	N1	N2	N3
Spectral Descriptors	Normalized	Normalized	Normalized	Normalized
Total Power	1.00	1.00	0.92	0.75
Delta Power Ratio	0.36	0.55	0.72	1.00
Theta Power Ratio	0.88	1.00	0.79	0.51
Alpha Power Ratio	1.00	0.41	0.40	0.16
Beta Power Ratio	0.98	1.00	0.61	0.11
Gamma Power Ratio	1.00	0.94	0.35	0.07
Median Frequency	1.00	0.68	0.52	0.31
Spectral Edge Frequency	0.99	1.00	0.70	0.38
Spectral Entropy	1.00	1.00	0.92	0.75

Delta power ratio showed a high separation power. Compared to the group of power ratios, delta power ratio separated all the sleep stages. Theta power ratio did not separate W and N3 to opposite ends of the discrimination axis. The alpha power ratio did not separate N1 and N2, but did place W and N3 to opposite end of discrimination axis. Both the beta and gamma power ratios separated the lighter (i.e., W and N1) and deeper stages (i.e., N2 and N3). Gamma power ratio separated W and N3 to opposite ends of discrimination axis.

The median frequency separated all sleep stages. The discrimination assessment showed a high separation between the sleep stages. Median frequency showed a high separation power. Median frequency separated W and N3 to the opposite ends of the discrimination axis. The median frequency widely dispersed W and N1. The spectral edge frequency and spectral entropy did not separate between W and N1, but did separate the remaining sleep stages. It separated W and N3 to opposite ends of the discrimination axis.

Effects of Stimulation on Spectral Descriptors: To evaluate the ability of the spectral descriptors to separate between stimulation rates under each sleep stage an analysis akin to the one previously mentioned was conducted. To evaluate the limitations in separating between stimulation rates a paired-wise comparison of three stimulation rates was conducted. The paired-wise comparison of three stimulation rates required the choice of two stimulation rates for each comparison, which yielded three combinations: (5Hz vs. Sil), (30Hz vs. Sil), and (5Hz vs. 30Hz).

The premise was that each stimulation rate was assumed to be equal. Shown in Table 3.15 are the resulting Student's t-test p-values and significant difference expressed as one asterisk for p-values less than 0.05 and one asterisk for p-values less than 0.01. The spectral descriptors showed the majority of separation in stage N1 between 30 Hz vs. silence and in stage N3 5 Hz vs. 30 Hz. As was expected alpha, as shown by the alpha power ratio, separated between 5 Hz vs. silence and 30 Hz vs. silence. In stage N3 no significant difference was observed. Figure 3.26 showed the results in terms of significant different (green) or no significant different (gray) for each combination of stimulation rates.

In channels Fz-A2 and Cz-A2 the presence of stimulation, compared with silence, significantly incremented the alpha power ratio in stage W. This effect may have been related with attentional effects of the subjects.

Table 3.15 Student t-Test p-Values between each Stimulation Rate of Spectral Descriptors in Fz-A2 and Cz-A2

	W			N1			N2			N3		
	5Hz vs.	30Hz vs.	5Hz vs.	5Hz vs.	30Hz vs.	5Hz vs.	5Hz vs.	30Hz vs.	5Hz vs.	5Hz vs.	30Hz vs.	5Hz vs.
Spectral Descriptor	Sil.	Sil.	30Hz	Sil.	Sil.	30Hz	Sil.	Sil.	30Hz	Sil.	Sil.	30Hz
FzA2												
Delta Power Ratio												
Theta Power Ratio								*			*	*
Alpha Power Ratio	**	*										
Beta Power Ratio				*	**							
Gamma Power Ratio					**			*			*	
Total Power					*							
Spec. Edge Freq.				*	**							
Median Freq.												
Spec. Entropy					**							
CzA2												
Delta Power Ratio	*	**										
Theta Power Ratio								*			*	*
Alpha Power Ratio	*	**					*					**
Beta Power Ratio				*	**							*
Gamma Power Ratio					**		*					*
Total Power				*	**							
Spec. Edge Freq.				*	**							**
Median Freq.	*	**										
Spec. Entropy				*	**							*

Regardless, this entrainment was very small (~ 12%), compared to the effect of the sleep stage which was more than 60%. This alpha entrainment was lost when the subjects move to other sleep stages. A similar entrainment (~ 12%) occurred in the beta power ratio in stage N1.

Cz-A2 was more sensitive to stimulation since the delta power ratio was significantly decreased by about 10% by the presence of stimulation in awake subjects;

the increase on alpha and decrease on delta produced a significant yet small increase of the median frequency (~ 7%).

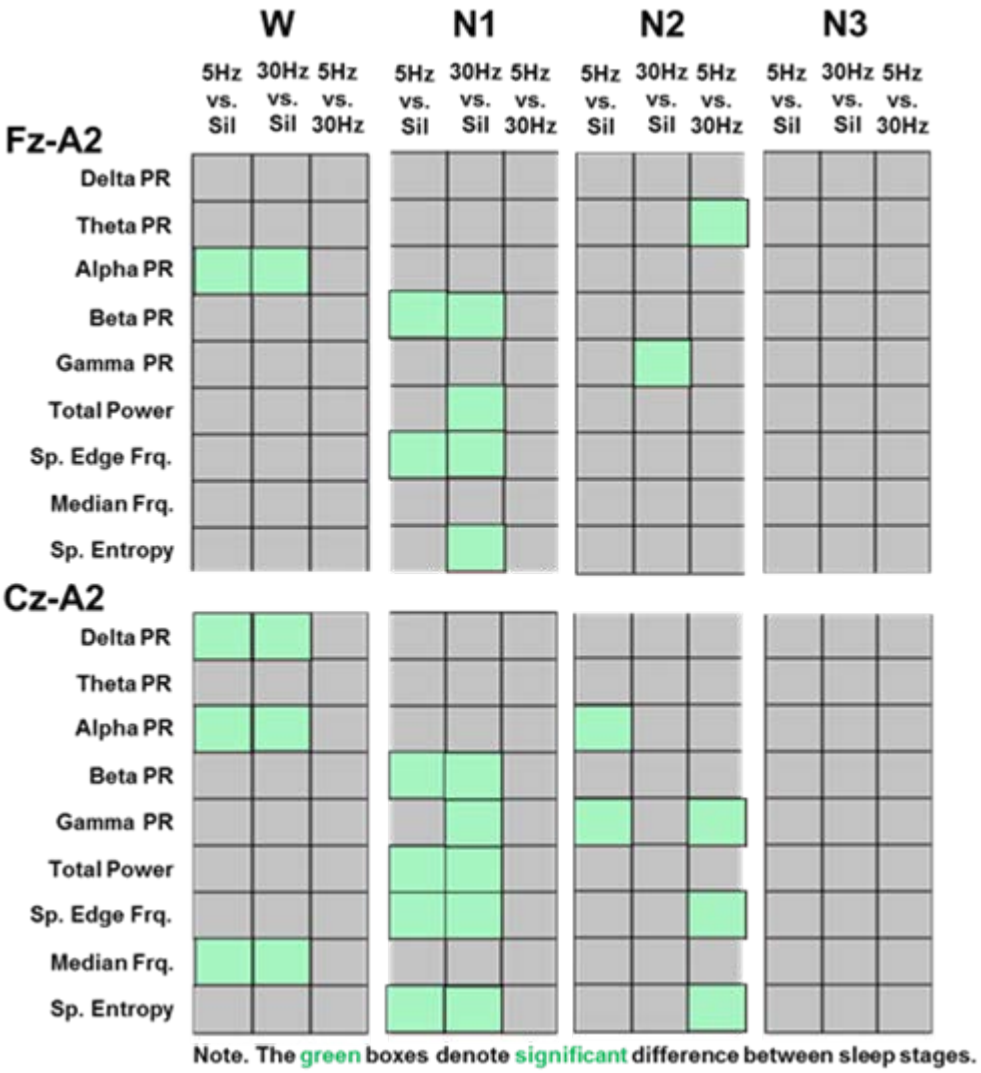

Figure 3.26 Discrimination of auditory stimulation in EEG by spectral descriptors in Fz-A2 and Cz-A2. (Green, Significantly Different ($p<0.05$)).

In stage N2 and for Cz-A2, the 5 Hz stimulation produced an increased alpha power ratio by 30% while in stage W it was only 10%. The gamma power ratio which was already small (0.007) significantly increased from silence to 5 Hz about 13% and from 5 Hz to 30 Hz about 14%; this increment shifted the spectral edge frequency

significantly by about 4% and the spectral entropy by about 1%. In stage N3 the EEG spectrum showed to be insensitive to the presence of auditory stimulation.

3.2.3Evoked Potential: Transient Response

The auditory stimulus was composed of three stimulation regions: 5 Hz, 30 Hz, and silence. The segment of EEG corresponding to the presentation of the individual stimulus sequences are referred to as sweeps (i.e., 5 Hz sweeps, 30Hz sweeps, and Sil. sweeps). The 5 Hz region has sixty 5 Hz sweeps, where each sweep is 204.8 msec. in duration. The 30 Hz region has forty 30 Hz sweeps, where each sweep is 307.2 msec. in duration. The silence region has one sweep of 12,288 msec. For each stimulus region, the sweeps are averaged to estimate the convolved response (i.e., steady-state response). The convolved response was deconvolved to estimate the transient response.

Population average 5 Hz transient response: Shown in Figure 3.27 is the population average for the 5 Hz transient responses during sleep. From awake to N3, the 5 Hz transient responses showed the build-up of a low frequency component between 10 to 100 msec. This build-up of potential was identify as Pα. It may possibly be P1. It occured in the latency range of both Pa and Pb and it was centered about 44 msec. in latency. In awake the Pa and Pb components were clearly distinguishable, however by stage N3 only Pα was distinguishable. In stage W, the Pb component was observed. However, from stage W to N1, the Pb component was attenuated and it was abolished by stages N2 and N3. The N1 component, in stage N3, showed a greater negativity than the other stages. Shown in Figure 3.27 was the gradual slowing of the waveform observed by an increase in magnitude from stage W to N3.

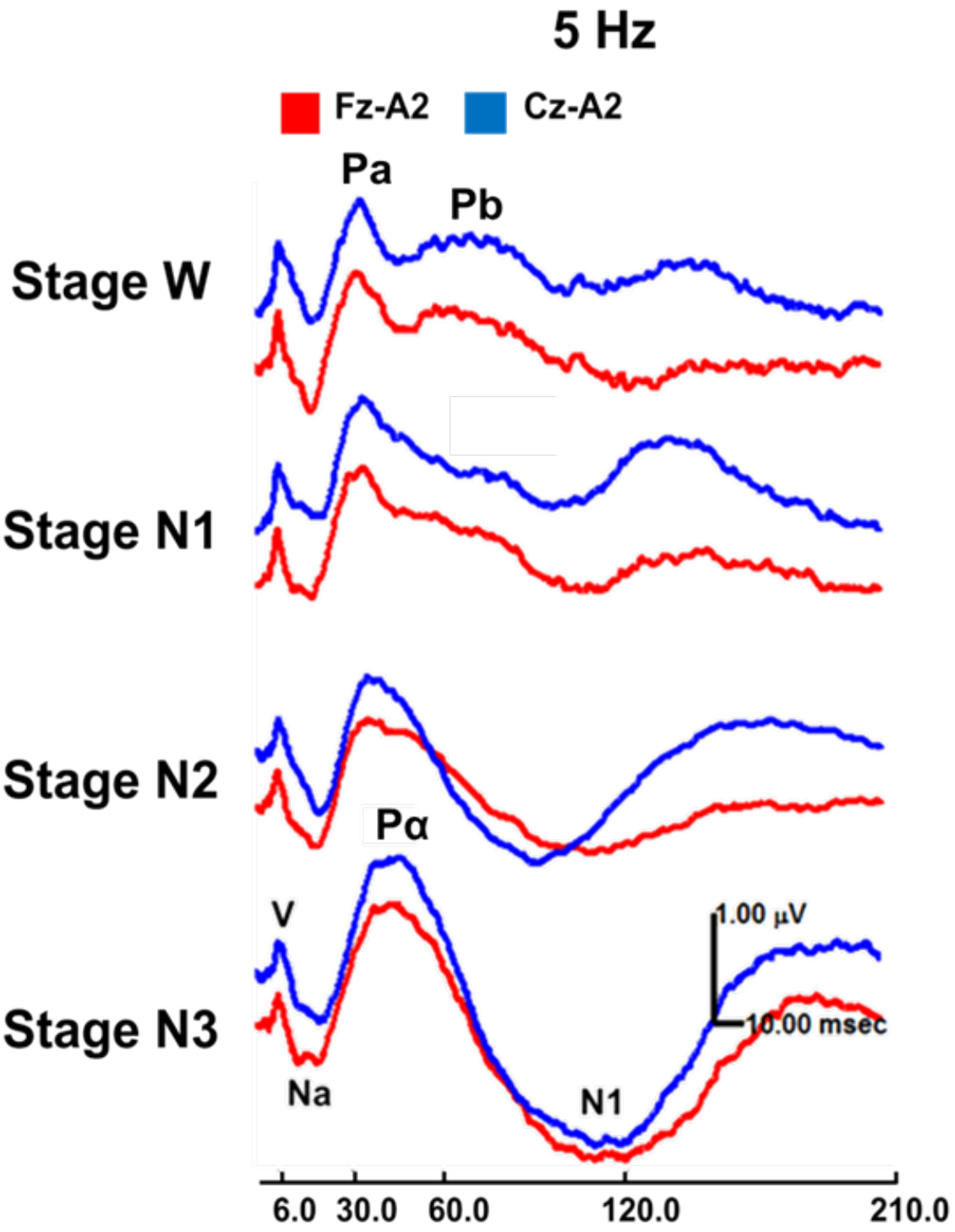

Figure 3.27 The 5 Hz transient response mean for all subjects in Fz-A2 and Cz-A2. Shown for each sleep stage is the mean transient response for all subjects for Fz-A2 (red) and Cz-A2 (blue).

Later portions of the waveform that occurred greater than 45 msec. in the time axis that were observed in stage W were attenuated. This was the Pb component. Also, negative components of the waveform showed a deflection downwards from stage W to N3. This was the N1 component. The observed changes were quantified by measuring the relative magnitude and the latency of the transient components. Shown in Figure 3.28 and Table 3.16 to 3.19, the magnitude and latency of

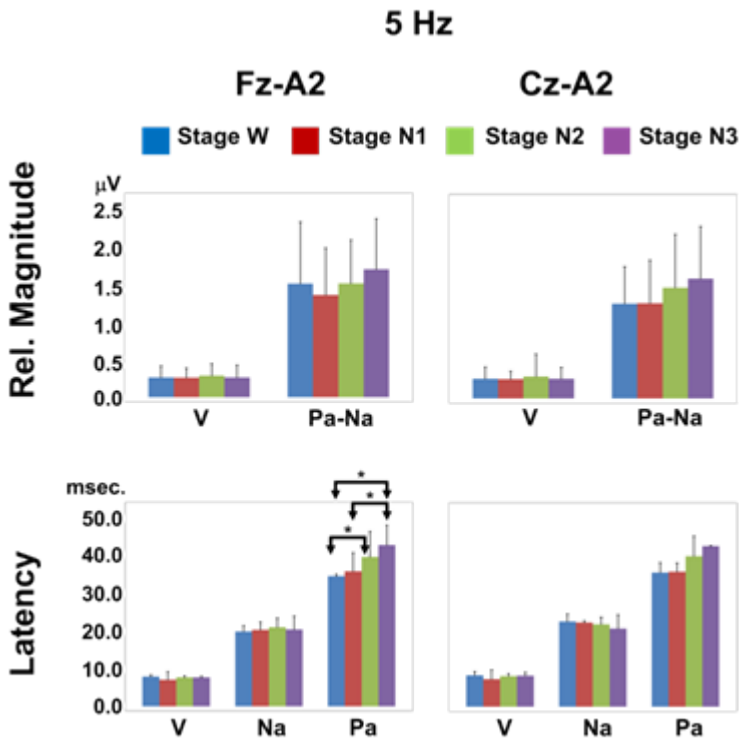

Figure 3.28 Relative magnitude and latency of V, Na, and Pa component of 5 Hz transient response. Shown is row 1 is the relative magnitude V and Pa-Na for channel Fz-A2 and Cz-A2. Shown in row 2 is the latency of V, Na, Pa for the both channels. (± St.Dev., *, Significantly Different ($p<0.05$)).

component V of the 5 Hz transient response for both channels remained consistent between the sleep stages and the relative magnitude showed no differences.

For both the Fz-A2 and Cz-A2 channel, the relative magnitude of Pa-Na did not show a significant difference in change of sleep stages. For Fz-A2, a small decrease was observed from stage W to N1, which was not observed in Cz-A2, followed by a gradual increase from stage N1 to N3 (see Figure 3.28, row 1, Fz-A2).

For channel Fz-A2, the latency of the Na component remained consistent between the sleep stages and the Pa component's latency gradually increased with a significant difference between stage W to N3 and N2 and between stage N1 and N3. For channel Cz-A2 the component latency did not show significant difference.

Shown in Figure 3.29 and Table 3.16 to 3.19, the relative magnitude of component Pα-N1 gradually increased and the latency showed small changes from stage W to N3 for both Fz-A2 and Cz-A2. The latency for Pα remained subtly the same, but the latency for N1 showed more change between sleep stages.

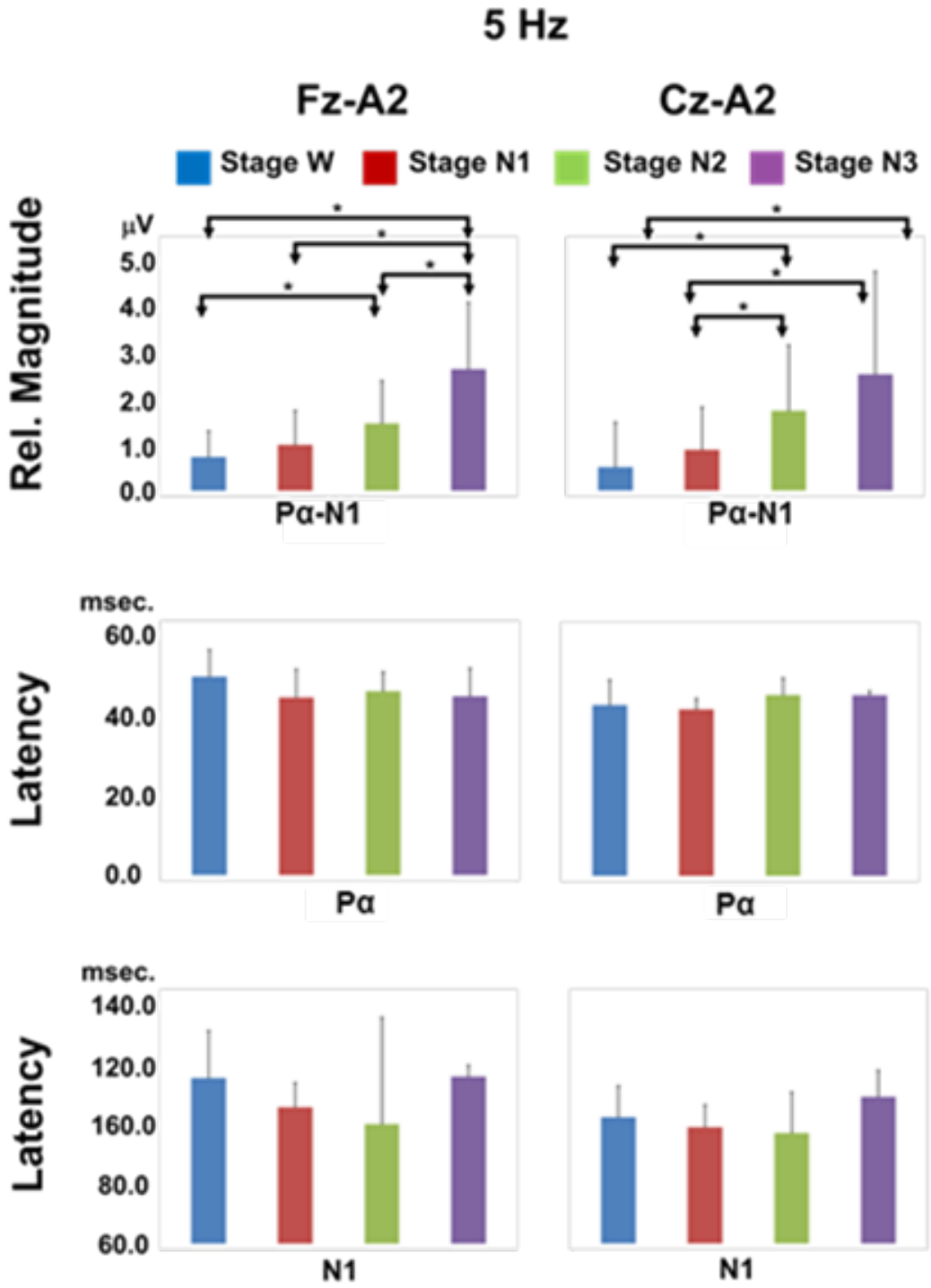

Figure 3.29 Relative magnitude and latency of Pα and N1 component in 5 Hz transient response. Shown is row 1 is the relative magnitude Pα- N1 for channel Fz-A2 and Cz-A2. Shown in row 2 is the latency of Pα for the channels. Shown in row 3 is the latency of N1for the channels. (± St.Dev., *, Significantly Different ($p<0.05$)).

Table 3.16 Results for 5Hz, Fz-A2 Transient Response Components

	Sleep			
	Stage W	Stage N1	Stage N2	Stage N3
	(n = 212)	(n = 218)	(n = 240)	(n = 90)
Component	M (SD)	M (SD)	M (SD)	M (SD)
Relative Magnitude				
V	0.247 (0.143)	0.243 (0.120)	0.269 (0.149)	0.246 (0.155)
Pa-Na	1.423 (0.771)	1.281 (0.589)	1.426 (0.544)	1.603 (0.634)
Pα-N1	0.681 (0.521)	0.923 (0.690)	1.354 (0.861)	2.449 (1.343)
Latency				
V	7.473 (0.393)	6.646 (2.017)	7.277 (0.342)	7.280 (0.228)
Na	18.782 (1.446)	19.150 (2.007)	19.846 (2.266)	19.280 (3.321)
Pa	29.933 (9.437)	33.883 (4.620)	37.462 (6.409)	40.480 (4.933)
Pα	47.945 (6.514)	42.917 (6.825)	44.400 (4.659)	43.200 (6.769)
N1	113.425 (15.242)	104.000 (7.812)	98.571 (34.395)	113.880 (3.660)

Table 3.17 Student t-Test Results for 5Hz, Fz-A2 Transient Response in Sleep

Component	W vs. N1	W vs. N2	W vs. N3	N1 vs. N2	N1 vs. N3	N2 vs. N3
Relative Magnitude						
V	No	No	No	No	No	No
Pa-Na	No	No	No	No	No	No
Pα-N1	No	Yes	Yes	No	Yes	Yes
Latency						
V	No	No	No	No	No	No
Na	No	No	No	No	No	No
Pa	No	Yes	Yes	No	Yes	No
Pα	No	No	No	No	No	No
N1	No	No	No	No	No	No

Table 3.18 Measurement Results for 5Hz, Cz-A2 Transient Response in Sleep

	Sleep			
	Stage W	Stage N1	Stage N2	Stage N3
	(n = 192)	(n = 178)	(n = 220)	(n = 70)
Component	M (SD)	M (SD)	M (SD)	M (SD)
Relative Magnitude				
V	0.247 (0.146)	0.241 (0.099)	0.275 (0.280)	0.248 (0.142)
Pa-Na	1.187 (0.463)	1.191 (0.540)	1.388 (0.668)	1.502 (0.654)
Pα-N1	0.426 (0.814)	0.741 (0.768)	1.447 (1.192)	2.109 (1.864)
Latency				
V	7.145 (2.532)	5.831 (3.366)	6.492 (2.936)	6.200 (3.538)
Na	19.418 (6.678)	17.600 (8.228)	17.462 (7.922)	15.680 (9.257)
Pa	28.000 (13.274)	28.200 (13.316)	31.908 (14.888)	32.200 (18.001)
Pα	41.340 (6.082)	40.280 (2.596)	43.764 (4.039)	43.700 (0.945)
N1	100.740 (10.020)	97.480 (7.174)	95.636 (13.134)	107.300 (8.483)

Table 3.19 Student t-Test Results for 5Hz, Cz-A2 Transient Response in Sleep

Component	W vs. N1	W vs. N2	W vs. N3	N1 vs. N2	N1 vs. N3	N2 vs. N3
Relative Magnitude						
V	No	No	No	No	No	No
Pa-Na	No	No	No	No	No	No
Pα-N1	No	Yes	Yes	Yes	Yes	No
Latency						
V	No	No	No	No	No	No
Na	No	No	No	No	No	No
Pa	No	Yes	Yes	Yes	Yes	No
Pα	No	No	No	No	No	No
N1	No	No	No	No	No	No

Shown in Figure B.1 to B.8 are the transient responses estimated from each subject for each sleep stage and the mean response of the transient responses from all

subjects. The transient response estimated from each subject represents the mean response for that subject and for that sleep stage. The mean transient response for all subjects (i.e., population average) represents the mean response of all subjects for that for that sleep stage. Shown in Figure 3.30, the mean 30 Hz transient response for all subjects showed changes in the components from stage W to N3. Stage N3 showed the response that was the most distinct compared to the other responses. It showed remanence of entrainment as observed by its oscillations.

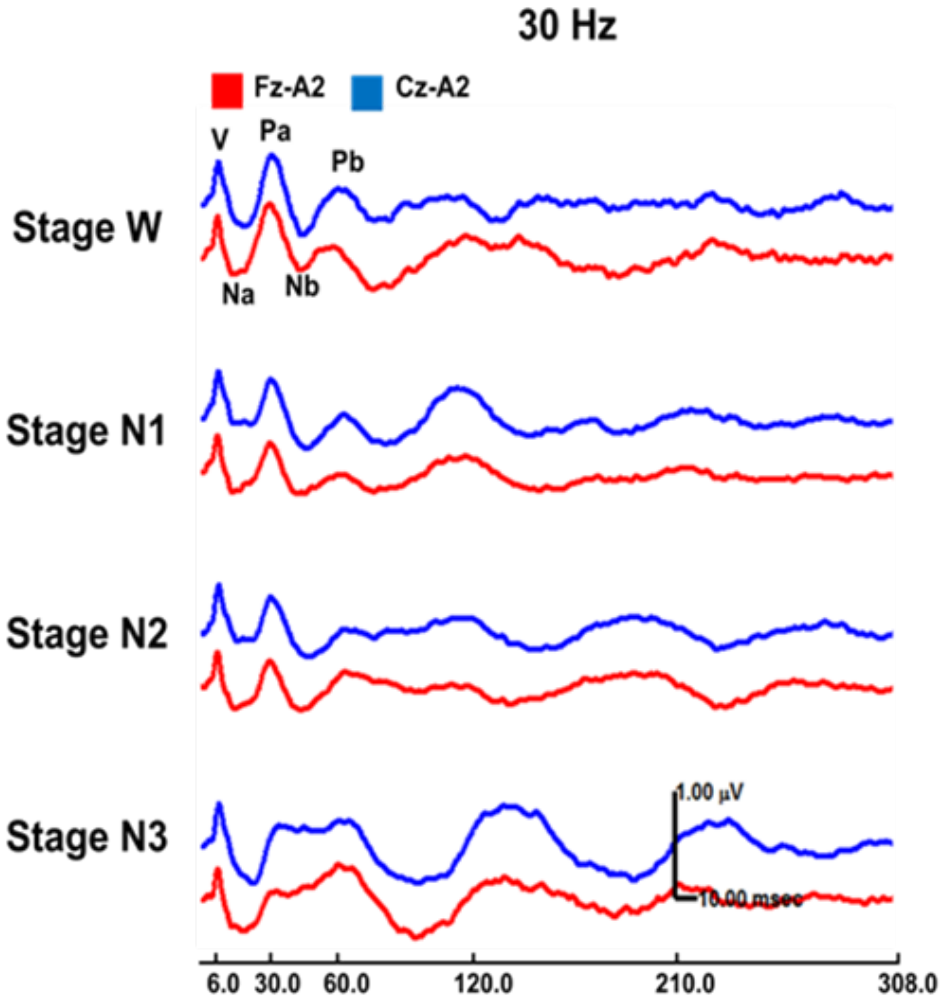

Figure 3.30 The 30 Hz transient response mean for all subjects in Fz-A2 and Cz-A2. Shown for each sleep stage is the mean transient response for all subjects for Fz-A2 (red) and Cz-A2 (blue).

Shown in Figure 3.31 row 1, the relative magnitude for V component showed relatively consistent value from stage W to N3.

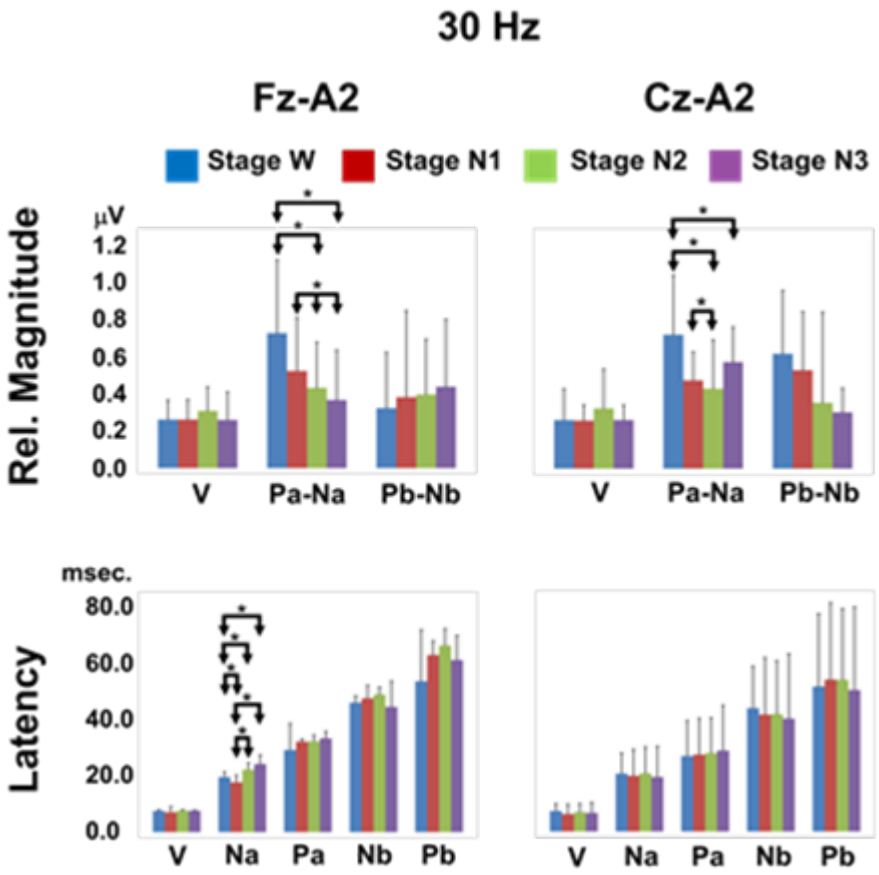

Figure 3.31 Relative magnitude and latency of 30 Hz transient response components. Shown is row 1 is the relative magnitude of transient components for channel Fz-A2 and Cz-A2. Shown in row 2 is the latency of transient components for the channels. (± St.Dev., *, Significantly Different ($p<0.05$)).

The Pa-Na component showed an attenuation in the value from stage W to N3. For Fz-A2, the Pb-Nb component showed a small gradual increase from stage W to N3, in contrast to Pa-Na. For Cz-A2, the relative magnitude for V component was similar between sleep stages. For Cz-A2, the Pa-Na showed the highest value occurring during stage W and the Pa-Na showed a decrease from stage W to N2. For Cz-A2, the relative

magnitude for Pb-Nb gradually decreased from stage W to N3 in contrast to the increase shown from in Fz-A2 stage W to N3.The latency for both Fz-A2 and Cz-A2 increased from component V to component Pb as expected and the difference between sleep stages were small in scale. For Fz-A2, the latency showed a significant difference between sleep stages.

Table 3.20 Measurement Results for 30 Hz, Fz-A2 Transient Response in Sleep

	Sleep			
	Stage W	Stage N1	Stage N2	Stage N3
	(n = 212)	(n = 218)	(n = 240)	(n = 90)
Component	M(SD)	M(SD)	M(SD)	M(SD)
Relative Magnitude				
V	0.248 (0.099)	0.249 (0.103)	0.293 (0.123)	0.247 (0.144)
Pa-Na	0.691 (0.374)	0.497 (0.274)	0.412 (0.234)	0.349 (0.254)
Pb-Nb	0.307 (0.286)	0.363 (0.443)	0.377 (0.282)	0.418 (0.345)
Latency				
V	7.255 (0.401)	6.708 (2.023)	7.323 (0.311)	7.320 (0.110)
Na	18.745 (1.827)	17.000 (2.309)	21.231 (2.375)	23.200 (3.076)
Pa	27.967 (9.026)	30.817 (0.908)	30.954 (2.080)	32.000 (2.354)
Nb	44.145 (2.247)	45.583 (4.508)	46.908 (2.507)	42.680 (8.793)
Pb	51.400 (17.567)	60.400 (4.729)	63.617 (5.705)	58.640 (8.368)

Table 3.21 Student t-Test Results for 30 Hz, Fz-A2 Transient Response in Sleep

Component	W vs. N1	W vs. N2	W vs. N3	N1 vs. N2	N1 vs. N3	N2 vs. N3
Relative Magnitude						
V	No	No	No	No	No	No
Pa-Na	No	Yes	Yes	Yes	Yes	Yes
Pb-Nb	No	No	No	No	No	No
Latency						
V	No	No	No	No	No	No
Na	Yes	Yes	Yes	Yes	Yes	No
Pa	No	No	No	No	No	No
Nb	No	No	No	No	No	No
Pb	No	No	No	No	No	No

Table 3.22 Measurement Results for 30 Hz, Cz-A2 Transient Response in Sleep

	Sleep			
	Stage W	Stage N1	Stage N2	Stage N3
	(n = 192)	(n = 178)	(n = 220)	(n = 70)
Component	M (SD)	M (SD)	M (SD)	M (SD)
Relative Magnitude				
V	0.248 (0.159)	0.246 (0.079)	0.308 (0.201)	0.249 (0.077)
Pa-Na	0.685 (0.305)	0.452 (0.146)	0.410 (0.249)	0.545 (0.179)
Pb-Nb	0.588 (0.323)	0.503 (0.300)	0.337 (0.462)	0.289 (0.122)
Latency				
V	7.018 (2.381)	5.908 (3.381)	6.585 (2.941)	6.360 (3.565)
Na	19.691 (7.046)	19.000 (8.922)	19.846 (8.863)	18.560 (10.375)
Pa	25.700 (12.121)	26.233 (12.311)	26.677 (12.099)	27.600 (15.429)
Nb	42.018 (14.243)	39.833 (19.411)	40.015 (18.123)	38.440 (22.099)
Pb	49.400 (24.721)	51.800 (26.071)	51.650 (24.255)	48.160 (28.370)

Table 3.23 Student t-Test Results for 30 Hz, Cz-A2 Transient Response in Sleep

Component	W vs. N1	W vs. N2	W vs. N3	N1 vs. N2	N1 vs. N3	N2 vs. N3
Relative Magnitude						
V	No	No	No	No	No	No
Pa-Na	No	Yes	Yes	Yes	No	No
Pb-Nb	No	No	No	No	No	No
Latency						
V	No	No	No	No	No	No
Na	No	No	No	No	No	No
Pa	No	No	No	No	No	No
Nb	No	No	No	No	No	No
Pb	No	No	No	No	No	No

3.2.4 Evoked Potential: Steady-State Response

The 30 Hz steady-state response was analyzed by calculating the phasor of the response. The phasor only looks at the contribution made by the steady-state response at the frequency of the stimulation rate (i.e., 30 Hz). Shown in Figure 3.32, row 1, the magnitude of the phasors gradually decreased and showed a small change from stage W to N3 for Fz-A2. For Cz-A2, the magnitude increased from stage W to N1 and decreased from stage N1 to N2 leaving stage N2 and N3 about the same. For both Fz-A2 and Cz-A2, the phase gradually decreased from stage W to N3. Shown in Figure 3.32, row 2, the Cz-A2 phase value was less than the Fz-A2 values in a manner that corresponded to Fz-A2 values. Also, this was observed in Figure 3.32, row 3, the phase of Cz-A2 is group delay compared to the phase of Fz-A2.

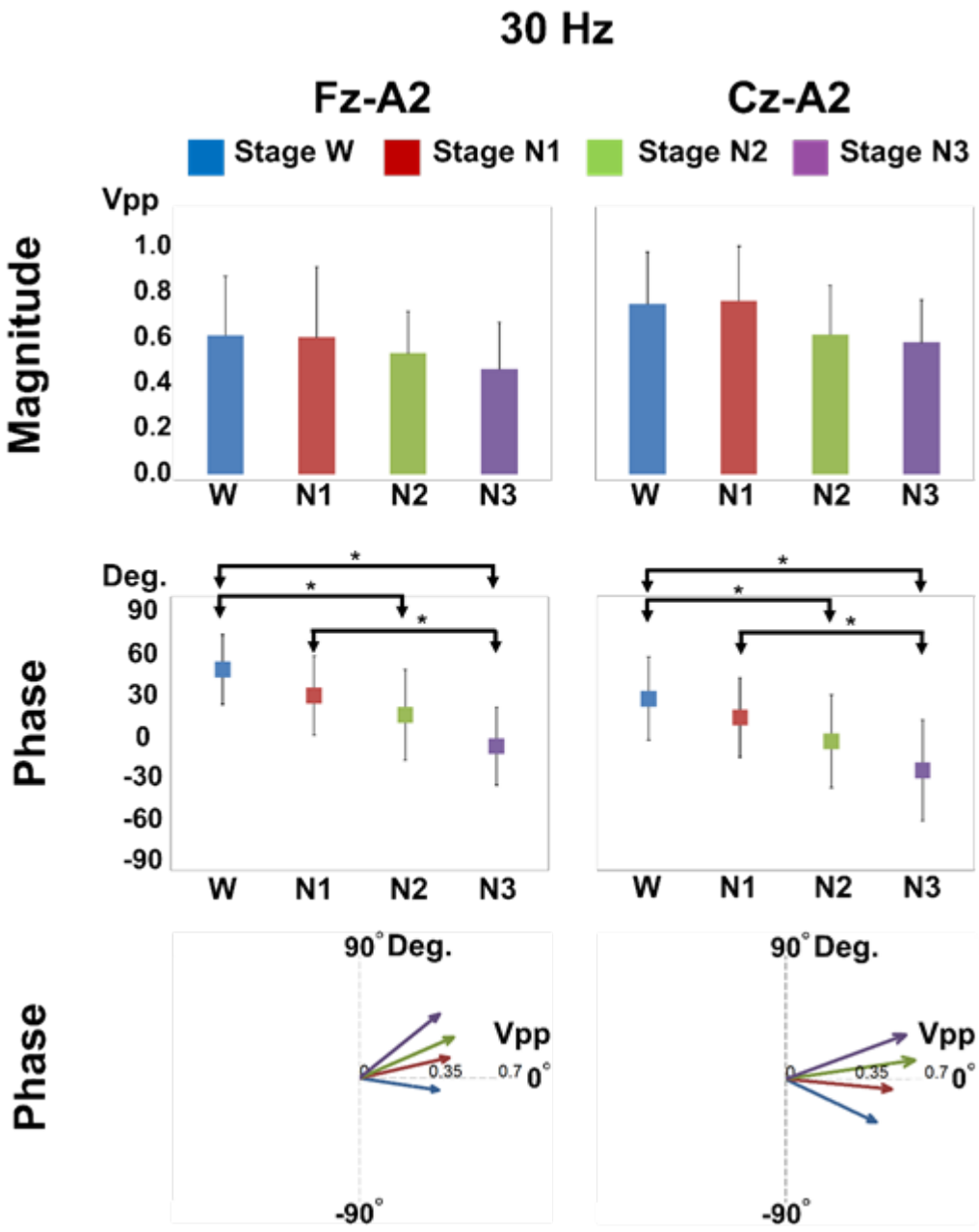

Figure 3.32 The 30 Hz steady-state response phasor magnitude and phase. Shown in row 1 is the magnitude for the steady-state response phasor for channel Fz-A2 and Cz-A2. Shown in row 2 is the phase of the phasor. Shown in row 3 is the phasor (± St.Dev., *, Significantly Different ($p<0.05$)).

Table 3.24 Measurement Results for 30 Hz, Fz-A2 Steady-State Response in Sleep

	Sleep			
	Stage W	Stage N1	Stage N2	Stage N3
	(n = 212)	(n = 218)	(n = 240)	(n = 90)
Phasor	M(SD)	M(SD)	M(SD)	M(SD)
Magnitude	0.533 (0.225)	0.525 (0.268)	0.463 (0.160)	0.404 (0.178)
Phase	44.098 (23.966)	26.221 (27.243)	12.871 (31.176)	-8.660 (26.754)

Table 3.25 Student t-Test Results for 30 Hz, Fz-A2 Steady-State Response in Sleep

Phasor	W vs. N1	W vs. N2	W vs. N3	N1 vs. N2	N1 vs. N3	N2 vs. N3
Magnitude	No	No	No	No	No	No
Phase	No	Yes	Yes	No	Yes	No

Table 3.26 Measurement Results for 30 Hz, Cz-A2 Steady-State Response in Sleep

	Sleep			
	Stage W	Stage N1	Stage N2	Stage N3
	(n = 192)	(n = 178)	(n = 220)	(n = 70)
Phasor	M(SD)	M(SD)	M(SD)	M(SD)
Magnitude	0.652 (0.198)	0.665 (0.207)	0.536 (0.188)	0.506 (0.161)
Phase	23.930 (28.679)	10.844 (27.334)	-5.464 (31.904)	-25.505 (34.756

Table 3.27 Student t-Test Results for 30 Hz, Cz-A2 Steady-State Response in Sleep

Phasor	W vs. N1	W vs. N2	W vs. N3	N1 vs. N2	N1 vs. N3	N2 vs. N3
Magnitude	No	No	No	No	No	No
Phase	No	Yes	Yes	No	Yes	No

Chapter 4 DISCUSSION

4.1 Study 1. Anesthesia

4.1.1 Physiological: Vitals Measurements and Bispectral Index

Heart rate: Heart rate is a valuable physiologic measurement as it is mediated by the autonomic system. While the heart rate increased remarkably during the clinical reaction of P26 it does not appear to be a good indicator of awareness.

Bispectral Index: BIS monitor is the most widely used monitor in anesthesia. Avidan et al. demonstrated BIS-guided anesthetic administration fails to prevent awareness. Incidence of awareness was 7 of 2,861 patients (0.24%) in the BIS group, compared with 2 of 2852 (0.07%). Avidan preformed a more aggressive follow up study in 2011 that shows the same results – BIS-guided anesthesia has more incidence of awareness. Our study shows that, compared to other spectral descriptors, the bispectral index preformed lowest in power of separation between patients having different anesthetic levels. As shown in Figure 3.3 the discrimination assessment of spectral descriptors, BIS clustered patients closely together and did not indicate that the clinical reaction would occur in P26.

4.1.2 Electroencephalogram: Spectral Descriptors

Total Power: Total power showed a low separation power. As observed in the discrimination assessment of the spectral descriptors. Shown in Figure 3.3, total power placed P23 under P26.

In this study P23 and P25 were considered to be the deeper anesthetic levels and P26 was empirically assessed to be the lightest in depth. Total power did not separate P23 and P26 to the opposite ends of the discrimination axis. Drummond, Brann, Perkins, and Wolfe (1991) believe that total power is an unlikely basis for an accurate predictor of imminent arousal. Studies show conflicting findings Plourde and Picton (1990) find that total power increases in anesthesia. However, Drummond et al. and Bührer, Maitre, Ebling, and Stanski, (1987) finds that total power decreases in anesthesia.

Power Ratio: Alpha and delta power ratio showed a high separation power. As observed in the discrimination assessment (see Figure 3.3), the alpha and delta power ratio separated P23 and P26 to opposite ends of the discrimination axis. Also, the alpha and delta power ratio arranged the patients in that order along the discrimination axis, but in opposite directions. The theta, beta, and gamma power ratio showed low separation power. Theta power ratio placed P23 next to P26. Beta power ratio closely clustered the patients near the upper boundary of the discrimination axis. Gamma power ratio closely clustered the patients and place P23 next to P26. Studies involving power ratio have observed that delta power ratio increases in anesthesia and alpha power ratio decreases in anesthesia (see Schmidt, Bischoff, Standl, Lankenau, Hilbert, & am Esch, 2004 and (Kiyama & Takeda, 1997)). Schmidt et al. (2004) investigated the power ratio of certain clinical end-points such as awake, steady-state anesthesia, and first-reaction. Schmidt et al. (2004) observed the delta power ratio decreases from steady-state anesthesia (median 48.0, interquartile range 40 to 55) to first-reaction (median 19.0, interquartile range 10 to 25). From Schmidt's findings and from the results presented in his figures, P23 would be categorized as very deep (mean 0.74), while P26 would be categorized in the range that is

very close to first-reaction (mean 0.25). Schmidt et al. (2004) observed the alpha power ratio increases from steady-state anesthesia (median 22.0, interquartile range 16 to 31) to first-reaction (median 27.0, interquartile range 10 to 20). Following Schmidt's alpha power ratio findings P23 would be categorized as very deep (mean 0.048) and P26 would be categorized as in a state greater than the range of first-reaction state (mean 0.41). The same inverse relationship between delta and alpha observed in this study is observed by Schmidt et al. In this study theta power ratio moved in the opposite direction to Schmidt et al.. Schmidt et al. theta power ratio figure shows a decrease from steady-state anesthesia (median 19, interquartile range 15 to 22) to first-reaction (median 13 interquartile range 12 to 15). In our study theta power ratio increased from deepest to lightest anesthesia patient. Schmidt et al. beta power ratio figure shows that beta power ratio distinguishes the six anesthesia end-points studied. In our study beta power ratio was observed to separate between lightest and deepest anesthesia patients, but did not separate the nuance differences in the remaining patients. The gamma band of the power ratio is not commonly found in studies involving power ratio. It is not mentioned in Schmidt et al.. In our study the gamma power ratio showed a lower separation power than beta power ratio. It did not separate the lightest and deepest patients as much as the beta power ratio did, and it did not separate the nuance differences between the remaining patients as the beta power ratio did not.

Median frequency: Median frequency showed a high separation power. Median frequency separates P23 and P26 to lower and upper boundary respectively of the discrimination axis. It did not separate patients P22 and P17 as did the delta power ratio. However, it may have been the case that P22 and P17 should have been in close

proximity, at least with respects to median frequency. In comparison P23 and P25 was considered to be lower than the other patients. As observed in the discrimination assessment P25 was typically adjacent to P23. The median frequency separated P25 from P22 and P17. In this study the median frequency decreased from P26 to P23. When arranged from highest to lowest median frequency, the five patients are ordered as follows: P26 (mean 8.15), P17 (mean 5.98), P22 (mean 5.96), P25 (mean 5.17), and P23 (mean 2.23). Studies involving median frequency have shown that median frequency is lower in anesthesia (see Plourde & Picton, 1990; Drummond, Brann, Perkins, & Wolfe, 1991; and Kiyama & Takeda, 1997). Schmidt et al. observes similar findings such as a decrease in median frequency from first-reaction (median 11.0, interquartile range 8.0 to 13.0) to steady-state anesthesia (median 3.0, interquartile range 2.5 to 6.0). Drummond et al. found that during the intraoperative state, which is the anesthetized state during surgical stimulation, the population average of the median frequency is 4.6 ± 1.7 Hz and that in the pre-arousal state, which is a state immediately prior to arousal the population average of the median frequency is 8.5 ± 2.2 Hz. Our study observed similar findings. According to Drummond et al. the intraoperative state range is 2.9 to 6.3 Hz by this criterion the following patients P17, P22, P25, and P23 would be categorized as intraoperative state. Also, Drummond et al. observes that the state immediately prior to arousal from anesthesia is in the range of 6.3 to 10.7 Hz; using this criterion patient P26 would be categorized as the state that Drummond refers to as pre-arousal. Drummond et al. (1991) goes further to state that a median frequency value greater than 6 Hz was identified in nine of ten subjects in the state of imminent arousal. These findings

corroborate our findings (see Table 3.2) in that four of the five patients remained less than 6 Hz and patient P26 remained above 6 Hz.

Spectral edge frequency: Spectral edge frequency showed a low separation power. As observed in the discrimination assessment, it did not separate the P23 and P26 to opposite ends of the discrimination axis. The patient values for P22, P26, P25, and P17 were closely clustered. It did disperse P23 widely apart from the remaining patients. The values observed in this study for spectral edge frequency were similar to other studies: P22 (mean 13.18), P26 (mean 12.86), P17 (mean 12.55), P25 (mean 12.25), and P23 (mean 7.66). As observed in the discrimination assessment of the spectral descriptors (see Figure 3.3) compared to the median frequency descriptor the spectral edge frequency descriptor showed a lower power of separation because it did not disperse P23 and P26 to both ends of the discrimination axis.

Plourde and Picton (1990) observe the spectral edge frequency is 13.4 ± 4.5 during surgery. Using this finding by Plourde and Picton (1990) as criterion for classification, P23 would be considered to be in the deepest anesthesia level. The spectral edge values observed in this study were consistent with the values observed in other studies (Plourde & Picton, 1990; Gökahmetoglu, Tercan, Bicer, Aksu, & Boyaci, 2013; and Arndt, Hofmockel, & Benad, 1994; Kiyama & Takeda, 1997, and Gurman, Fajer, Porat, Schily, & Pearlman, 1994). Schwilden and Stoeckel (1987) maintained the opinion that, compared to the median frequency descriptor, the spectral edge frequency descriptor shows a lower discrimination power.

Spectral entropy: Spectral entropy showed a low separation power. Spectral entropy did not separate P23 and P26 to opposite ends of the discrimination axis (see Figure 3.3). It closely clustered the patients in the upper boundary of the discrimination axis and dispersed P23 widely from the cluster. Bein (2006) states that the recommended range of adequate anesthesia in response entropy (i.e., RE) is from 40 to 60.

To compare our spectral entropy results to the response entropy result in Bein (2006), response entropy values were estimated from our spectral entropy values. Viertiö-Oja et al. (2004) provides a spline function that is used to transform the spectral entropy values used in our study to response entropy values. Using the spline function as reference, the equivalent response spectral values for the patients in our study would be as follows: P17 (0.75 is RE=70), P22 (0.78 is RE=75), P23 (0.62 is RE=45), P25 (0.75 is RE=70), and P26 (0.76 is RE=70). According to Bein, P23 would be considered in a deep level of anesthesia because it was located in the lower boundary of the 40 to 60 range for adequate anesthesia. The remaining patients were greater than 60, which was outside the range for adequate anesthesia. Spectral entropy did not separate the remaining patients.

Correlation of delta to alpha power ratio: The correlation coefficient of delta and alpha power ratio was an interesting measure that has not been previously applied to elucidate anesthetic levels. As shown in Figure 3.5, the power ratio for delta and alpha move in tandem opposed directions as shown by the correlation measure. Shown in Figure 3.5, the correlation coefficient between delta and alpha decreases from P23 ($r_{delta,alpha}$ = -0.83) to P26 ($r_{delta,alpha}$ = -0.60). This decrease in lighter anesthetic levels may be associated to a decoupling of the systems driving the delta and alpha power ratio. The correlation coefficient values of the remaining patients were closely cluster. The

correlation coefficient between sevoflurane and alpha and sevoflurane and delta showed low correlation coefficient values. This may suggest that sevoflurane acts on alpha and delta power ratio as an indirect effector.

4.1.3 Evoked Potential: Transient Response

Moving average 5 Hz transient response: In our study the waveform of the 5 Hz transient response were extensively altered by the effects of anesthesia. The grand mean of the 5 Hz transient response showed waveforms were attenuated from P26 to P23. For patients P23 and P25 middle latency components were severely attenuated or abolished. Shown in Figure 3.10, A., is the discrimination assessment for 5 Hz transient responses. The 5 Hz transient responses separated P23 and P26 to opposite ends of the discrimination axis. P26 was widely disperse from the remaining patients suggesting that 5 Hz transient response preformed best for detecting broad difference in anesthetic levels. Shown in Figure 3.10, B., is the discrimination assessment after the 5 Hz responses were filtered (25 to 1500 Hz) according to conventional filter settings. By comparison, the high-pass filtered assessment showed a lower power of discrimination. The assessment with the filtered settings does not separate P23 and P26 to opposite ends of the discrimination axis and dispersed widely P23 from P25.

The effects cause by conventional high-pass filter were apparent in the grand mean of the 5 Hz transient responses (see Figure 3.11 and 3.12), in the moving average ranges (see Figure 3.9) and in the power of separation in the discrimination assessment (see Figure 3.10). All these observations leads us to conclude that anesthesia predominately operate in the low frequency components of the 5 Hz transient responses.

Previous studies apparently were filtering out the most prominent effect. Also, this grand mean of 5 Hz transient responses showed the split buffer traces very close to the mean trace. This close proximity of the split buffer traces of the grand mean of the 5 Hz transient responses indicates a good signal-to-noise quality of the transient responses.

Moving Average 20, 30 and 40 Hz transient response - Beta entrainment: Beta rhythm oscillations were observed in the 20, 30, and 40 Hz de-convolved transient responses of anesthesia. Three different stimulation rates elicited by low-jittered sequences all showed phase-locked, beta-rhythm responses, related to anesthetic levels.

The power of the beta entrainment observed in the transient response was measured and assessed for its discrimination power. Shown in Figure 3.14, the power of separation between P23 and P26 was observed to increase from 40 Hz to 20 Hz as observed by the discrimination assessment of beta entrainment. The power of separation may be associated with decrease in rate of low-jittered sequences. The 40 Hz beta entrainment showed a low power of separation between P22 and P25 or between P17 and P23. The 30 Hz beta entrainment closely clustered P25, P17, and P22. The 20 Hz beta entrainment closely clustered P25, P17, and P23; also, it did not separate P26 and P23 to opposite ends of the discrimination axis. Shown in Figure 3.13, the activity of the power of beta entrainment for 20 Hz in P26 suggested that activity in power of beta entrainment for 20 Hz may have been associated to lighter anesthetic levels. The 20 Hz activity was minimal for the other patients.

The observed beta entrainment may involve GABA-A receptors. Studies have indicated that GABA-A receptor actions are fundamental for beta oscillations to occur,

and blockade of GABA-A receptors leads to the loss of beta rhythm synchronization (Haenschel, Baldeweg, Croft, Whittington, & Gruzelier, 2000; Porjesz, Almasy, Edenberg, Wang, Chorlian, Foroud, ... & Begleiter, 2002).

The observed phase locking of the beta oscillations may be explained by regularity and periodicity in firing of GABA receptors. Inhibitory GABA receptors have been shown to fire with remarkable regularity in burst periodicity and duration that can be observed in many brain sites (Whittington, Traub, Faulkner, Stanford, & Jefferys, 1997; Traub, Whittington, Stanford, & Jefferys, 1996).

The observed beta entrainment may be elicited by actions of sevoflurane on GABA-A receptors. Nishikawa and Harrison (2003) have shown that GABA-A receptors are important in the actions of inhaled agents such as sevoflurane (Bertaccini & Trudell, 2001; Mascia, Trudell, & Harris, 2000; Jenkins, Greenblatt, Faulkner, Bertaccini, Light, Lin, ... & Harrison, 2001; Nishikawa, Jenkins, Paraskevakis, & Harrison, 2002, Jenkins, Andreasen, Trudell, & Harrison, 2002).

The noise amplification of the low jittered sequences required the removal of the low-frequency components. Similar to the issue of the conventional filter settings, the valuable information that resides in the low frequency components of transient response may have been lost by filtering out low frequencies. Despite this limitation observing entrainment was still possible. Increasing the jitter of a sequence, decreases the noise amplification factor in the lower frequencies, but if beta entrainment is a consequence of low-jittered sequences then sequences with higher jitter may disrupt the mechanism eliciting entrainment. This remains to be investigated. It may reveal a greater

understanding of entrainment and its role in a large mechanism that may explain auditory responses in anesthesia.

4.1.4 Evoked Potential: Steady-State Response

As shown by the discrimination assessment of the phasor amplitude (Figure 3.16), there was an improvement in discrimination, associated with a decrease in stimulation rate. The 40 Hz phasor has been studied extensively but has not been explored for lower rate such as 30 Hz or lower. The 40 phasor showed the lowest separation power (i.e., it placed P23 and P26 together). The 30 Hz phasor showed a better separation power than the 40 Hz phasor, but it did not separate to opposite ends of the discrimination assessment, but it closely clustered P23 and P25. The 20 Hz phasor was the one that preformed the best of the group. The 20 Hz phasor separated P23 and P26 to opposite ends of the discrimination axis. It clustered P22 near P17, but did not cluster P23 near P25. Plourde and Picton (1990) suggest that 40 Hz ASSR is a better indicator than EEG for level of anesthesia. Our results contradicted these findings (see Figure 3.16). McNeer et al. (2009) found that 40 Hz ASSR in anesthesia is mainly generated by the overlapping of early components of the transient response. This may explain the low power of separation observed for 40 Hz phasor. The steady-state response of the 40 Hz phasor is mainly effected by early components of the transient responses that overlap to form the steady-state response. Moreover, anesthesia mainly interacted on low-frequency transient response components (i.e., not the early components).

4.1.5 Summary of contributions of this study

To summarize the most notable findings about anesthesia from this body of work were that for electroencephalographic changes during altered levels of consciousness: (a) Delta/alpha power ratio correlation coefficient changes with changes in anesthetic level; (b) BIS does not appear to be an appropriate feature for risk of unintentional awareness. To summarize the most notable new findings about anesthesia from this body of work were that for evoked potentials changes during altered levels of consciousness: (a) 5 Hz responses that are high-passed filtered are not sensitive to change in awareness state; (b) High-rate transient beta entrainment may separate well patients near clinical reaction from patients in general anesthesia, 20 Hz would preforms better; (c) High-rate (30 and 40 Hz) ASSR does not discriminate well, but lower rate (20 Hz) seems to separate well general anesthesia from clinical reaction.

4.2 Study 2. Sleep

As in the results, due to redundancy of results, this section refers to the findings in channel FzA2 and 5 Hz stimulation rate. As observed in the results, channel FzA2 demonstrated better discrimination between sleep stages and the 5 Hz stimulation rate demonstrated the same discrimination performance as the other stimulation rates.

4.2.1 Electroencephalogram: Spectral Descriptors

Total Power: Total power showed a low separation power. As observed in Figure 3.20 by the significant differences and in Figure 3.25 by the discrimination assessment. Total power did not separate W from N1. In the assessment total power placed W and N1

in the same location. It separated W and N3 placing it at the opposite ends of the discrimination axis (see Figure 3.25). Figure 3.20 showed that total power separated N1, N2, and N3. Also, this was shown in the assessment. The dispersion from N2 to N3 was wider than from N1 to N2. From N1 to N3 it showed the largest dispersion. In our study W and N1 were considered lighter sleep stages than N2 and N3. Stage N2 is the onset of sleep and stage N3 is the deepest sleep stage. As observed in the discrimination assessment the distinction between W and N1 was demanding to resolve for the features.

Power Ratio: Delta power ratio showed a high separation power. As observed by the significant difference in Figure 3.19, the delta power ratio separated all sleep stages compared to the other power ratios. The discrimination assessment showed a high separation between the sleep stages as well (see Figure 3.25). Shown in Figure 3.19, the theta power ratio significantly separated between W and N3, but in the assessment it did not separate W and N3 to opposite ends of the discrimination axis. The alpha power ratio did not separate between N1 and N2, but alpha power ratio did separate all of the remaining sleep stage combinations (see Figure 3.19). The assessment showed stages N1, N2, and N3 clustered closely together and stage W widely dispersed (see Figure 3.25). A possible explanation is that alpha rhythms were more pronounced in stage W. Both the beta and gamma power ratios did not separate between W and N1 but did separate all of the remaining sleep stage combinations (see Figure 3.19). In the assessment, beta and gamma power ratio separated the lighter (W and N1) and deeper stages (N2 and N3); however, gamma power ratio dispersed the lighter and deeper stages more than beta. Gamma power ratio separated W and N3 to opposite ends of discrimination axis. Delta power ratio compared to the other power ratios showed the highest power of separation

and showed significant difference between all sleep stages combinations. Fell et al. (1996) found that delta power ratio showed a significant difference between stage N1 and N2 and between stage N2 and N3. Also, Fell et al. found a significant difference between N1, N2, N3, and REM. They did not investigate stage W.

Median frequency: As observed in Figure 3.22 the median frequency significantly separated all sleep stages. The discrimination assessment (Figure 3.25) was perfectly consistent with the statistical analysis showing a high separation between the sleep stages. Median frequency placed W and N3 to lower and upper boundaries and widely dispersed each sleep stage along the discrimination axis. In contrast to the other spectral features, median frequency showed the highest power of separation for W and N1, which were the most demanding stages to resolve.

Spectral edge frequency and spectral entropy: As observed in Figure 3.21 and Figure 3.23 the spectral edge and entropy frequency did not significantly separate between W and N1, but did resolve the remaining combination of sleep stages. The discrimination assessment was consistent with previous observations – features showed weaker discrimination performance in W vs. N1. It did separate between W and N3 to opposite ends of the discrimination axis, and it separated the lighter sleep stages from the deeper sleep stages.

Fell et al. found that spectral edge frequency showed a significant difference between stage N2 and N3 and between N1, N2, N3, and REM. In contrast to our study (see Figure 3.21), Fell et al. did not observe a significant difference between stage N1and N2. Fell et al. found that spectral entropy showed a significant difference between stage

N1 and N2 and between stage N2 and N3. Also, Fell et al. found a significant difference between N1, N2, N3, and REM.

Effects of Stimulation on Spectral Descriptors: Spectral descriptors afforded the opportunity to verify if the stimulation produces EEG entrainment at different sleep stages. The results summarized in Figure 3.26 and Table 3.15 showed the differential effects as a function of the sleep stage and channel being more prominent in wake and N1 while very negligible in stages N2 and N3. The EEG spontaneous activity seemed to become more independent from stimulation at deeper stages.

4.2.2 Evoked Potential Transient Response

5 Hz transient response: As shown in Figure 3.27, the population average of the 5 Hz transient response showed components of the MLR underwent changes with respects to sleep stages. The transition from awake to stage N3 showed the build-up of a low frequency component between 10 to 100 msec. The strengthening of this potential occurred in the latency range of both Pa and Pb with center about 44 msec. in latency. This build-up of potential that was identify as Pα (i.e., possibly P1) along with the N1 component demonstrated notable changes during the transition from W to N3. The components Pa and Pb are clearly distinguishable in W; however, by N3 the potential build-up was maximal and only Pα was distinguishable. The Pb component observed in awake was attenuated from W to N1 and abolished by stages N2 and N3. The N1 component in stage N3 showed a greater negativity than the other stages. The Pa-Na components of the MLRs appeared stable during changes in sleep stages while the Pα-N1 components showed variation of its potentials. The magnitude of Pa-Na did not show

significant difference (see Figure 3.28), but the magnitude for Pα-N1 did show significant differences for the following sleep combinations W vs. N2, W vs. N3, N1 vs. N3, and N2 vs. N3 (see Figure 3.29). Except for the latency of the Pa component, the latency of the transient components (V, Na, Pα, and N1) did not show significant differences. The Pa latency showed significant changes for W vs. N2, N1 vs. N3, and W vs. N3 (see Figure 3.28). As shown in Table 3.16, the latency of component Pa slightly increased from W to N3. The observed Na-Pa stability was similar to that reported in other studies. Millan (2006) found that the Na-Pa complex remains stable showing no major changes in magnitude during sleep. Erwin et al. found no significant changes for Pa during stage 2, 3, 4 or REM. The increase observed in the Pa latency is similar to that observed in other studies. Deiber, et al. (1989) shows that the latency for Na and Pa components tends to increase from stage II (i.e. stage N2) to stage IV (i.e stage N3) and decreases in REM. Erwin and Buchwald (1986) found a significant increase Pa latency from awake (the mean of W and N1) to sleep (i.e., the mean of N1, N2, and N3). Like Erwin et al., we observed the Pb component attenuate or abolish from awake to sleep. However, we observe the Pb attenuated from W to N1 and abolished in N2 and N3. Similarly, Erwin et al. found that the magnitude of Pb significantly decreases from awake (W and N1) to N2 and is abolished from stage 3 to stage 4. The N1 component showed a progressive strengthening in negativity from W to N3 (see Figure 3.27). The increase in negativity (i.e., hyperpolarization) of the N1 component was reflected in the increase in magnitude of Pα-N1 from awake to stage N3 by about 260%. The N1 component became most prominent by stage N2 and became more negative for the subsequent sleep stage, stage N3 (see Figure 3.27). This was reflected, from stage N2 to stage N3, by the increase in

magnitude of Pα-N1 that was about 81%. Erwin et al. elicits his MLR using a lower stimulation rate (i.e. 1 Hz) than our study (i.e. 5 Hz). This lower stimulation led to a pronounced N1 negativity in awake responses. For sleep stages, the paper's figures shows (see Figure 1.34) a larger negativity of the N1 component in stages N2 and N3, however very little (i.e., around 33%) and it was not as pronounced as observed in our results (i.e., around 260%). This may be explained by Erwin et al. filter settings (i.e., bandpass filtered from 10 to 500 Hz) that attenuates the low frequencies.

30 Hz transient response: The waveform of the 30 Hz transient response was altered by the effects of sleep (see Figure 3.30). As shown in Figure 3.31, the magnitude of Pa-Na showed significant changes for all combinations of sleep stages except W vs. N1, but no significant changes for Pb-Nb. The magnitude of Pa-Na decreased from W to N3. The latency of the transient components did not show significant differences with the exception of component Na. The latency of Na showed significant difference for all combinations of stages except N2 vs. N3. It increased from N1 to N3 and slightly decreased from W to N1. In 30 Hz transient response, the Pa-Na component of the MLRs showed a significant decrease in magnitude, and the Pb-Nb did not show a significant change. Compared to 5 Hz transient response, the 30 Hz transient response showed fewer changes with respect to sleep stages.

4.2.3 Evoked Potential: Steady-State Response

As shown in Figure 3.32, the magnitude of the 30 Hz steady-state response phasors did not showed a significant difference between sleep stages; only a decrease trend as the stage deepen. Previous studies involving sleep and steady state potentials use

40 Hz stimulation rate that made drawing reliable comparisons very difficult. In these studies the 40 Hz ASSR response, from waking to NREM sleep, decrease by (a) half (Galambos Makeig, & Talmachoff, 1981) or (b) one-third (Brown & Shallop, 1982). A significant difference for sleep stages was observed in the phase angle of the phasors. For each sleep stage the phase angle of the phasor showed a sleep stage dependent decrease in phase angle, from waking to stage N3 sleep. Jerger et al. (1986) studied the 40 Hz ASSR for waking, stage N1, and stage N2 sleep stages and found that, for the 40 Hz frequency component, the phase coherency remained unaffected by sleep. In our study the phase angle of the 30Hz steady-state response phasor was more indicative of change in sleep than was the magnitude. The phase angles had a significant difference in stage W vs. N3 or stage W vs. N2, and stage N1 vs. N3, but not stage N2 vs. N3 or stage W vs. N1. The steady-state phasor may prove promising for uses in identifying the onset of sleep (Khuwaja, Haghighi, & Hatzinakos, 2015).

4.2.4 Summary of contributions of this study

To summarize the most notable new findings about sleep from this body of work were that for electroencephalographic changes during sleep: (a) Fz-A2 shows a better discrimination power to classify sleep stages; (b) Delta power ratio and median frequency have the best discrimination power - W vs. N1 is more difficult to resolve; and (c) Auditory stimulation significantly change spectral descriptors but the changes are very small compared to the changes due to sleep stages. To summarize the most notable new findings about sleep from this body of work were that for evoked potentials changes during sleep: (a) Fz-A2 shows a better discrimination power to separate sleep stages; (b) 5 Hz responses are very sensitive to sleep stages, like anesthesia, preserving the low

frequencies is critical for observing theses effects; (c) 30 Hz transient responses show entrainment but it may be reduced due to the high-pass filter required by deconvolution; (d) 30 Hz response only stage N3 is can be resolved from the remaining stages; and (e) ASSR phases show sensitivity to stage - can significantly resolve light sleep versus deep sleep.

REFERENCES

Adler, G., & Adler, J. (1989). Influence of stimulus intensity on AEP components in the 80-to 200-millisecond latency range. Audiology, 28(6), 316-324.

Adler, G., & Adler, J. (1991). Auditory stimulus processing at different stimulus intensities as reflected by auditory evoked potentials. Biological Psychiatry, 29(4), 347-356.

Alkire, M. T. (2009). General anaesthesia and consciousness. In S. Laureys, & G. Tononi, (Eds.), The neurology of consciousness. San Diego: Elsevier.

Alkire, M. T., & Gorski, L. A. (2004). Relative amnesic potency of five inhalational anesthetics follows the Meyer-Overton rule. The Journal of the American Society of Anesthesiologists, 101(2), 417-429.

Arndt, V. M., Hofmockel, R., & Benad, G. (1994). EEG changes during propofol-alfentanil-nitrous oxide anesthesia. Anaesthesiologie und Reanimation, 20(5), 126-133.

Atcherson, S. R., & Stoody, T. M. (Eds.). (2012). Auditory electrophysiology: A clinical guide. New York: Thieme Medical Publisher.

Avidan, M. S., Jacobsohn, E., Glick, D., Burnside, B. A., Zhang, L., Villafranca, A., ... & Evers, A. S. (2011). Prevention of intraoperative awareness in a high-risk surgical population. New England Journal of Medicine, 365(7), 591-600.

Avidan, M. S., Zhang, L., Burnside, B. A., Finkel, K. J., Searleman, A. C., Selvidge, J. A., ... & Hantler, C. (2008). Anesthesia awareness and the bispectral index. New England Journal of Medicine, 358(11), 1097-1108.

Barach, P. G., Cullen, B. F., & Stoelting, R. K. (2006). Clinical Anesthesia (5th ed.). Philadelphia: Lippinocott Williams & Wilkins.

Bastuji, H., Perrin, F., & Garcia-Larrea, L. (2002). Semantic analysis of auditory input during sleep: Studies with event related potentials. International Journal of Psychophysiology, 46(3), 243-255.

Bear, M. F., Connors, B. W., & Michael, A. (2001). Paradiso. Neuroscience: Exploring the brain. Philadelphia: Lippinocott Williams & Wilkins.

Bein, B. (2006). Entropy. Best Practice & Research Clinical Anaesthesiology, 20(1), 101-109.

Bergey, G. K. (2006). Refractory status epilepticus: Is EEG burst suppression an appropriate treatment target during drug-induced coma? What is the holy grail?. Epilepsy Currents, 6(4), 119-120.

Bertaccini, E., & Trudell, J. R. (2001). Molecular modeling of ligand-gated ion channels: Progress and challenges. International Review of Neurobiology, 48, 141-166.

Bevan, J. C., Veall, G. R., Macnab, A. J., Ries, C. R., & Marsland, C. (1997). Midazolam premedication delays recovery after propofol without modifying involuntary movements. Anesthesia & Analgesia, 85(1), 50-54.

Bohórquez, J., & Özdamar, Ö. (2008). Generation of the 40-Hz auditory steady-state response (ASSR) explained using convolution. Clinical Neurophysiology, 119(11), 2598-2607.

Borbely, A., Hayaishi, O., Sejnowski, T. J., & Altman, J. S. (2000). The regulation of sleep. Strasbourg: HFSP.

Brown, D., & Shallop, J. K. (1982). A clinically useful 500 Hz evoked response. Nicolet potentials, 1(5), 9-12.

Brown, E. N., Lydic, R., & Schiff, N. D. (2010). General anesthesia, sleep, and coma. New England Journal of Medicine, 363(27), 2638-2650.

Brown, E. N., Purdon, P. L., & Van Dort, C. J. (2011). General anesthesia and altered states of arousal: a systems neuroscience analysis. Annual Review of Neuroscience, 34, 601-628.

Buchwald, J. S., & Huang, C. H. (1975). Far-field acoustic response: origins in the cat. Science, 189(4200), 382-384.

Bührer, M., Maitre, P. O., Ebling, W. F., & Stanski, D. R. (1987). Pharmacological quantitation of midazolam's CNS drug effect in hypnotic doses. The Journal of the American Society of Anesthesiologists, 67(3), A658-A658.

Castro-Llanos, A., Bohórquez, J., McNeer, R. R., & Özdamar, Ö. (2013, May). Feasibility of Evoked Potentials as a Probe for Exploring Sleep. In Biomedical Engineering Conference (SBEC), 2013 29th Southern (pp. 7-8). IEEE.

Claassen, J., Hirsch, L. J., Emerson, R. G., & Mayer, S. A. (2002). Treatment of refractory status epilepticus with pentobarbital, propofol, or midazolam: a systematic review. Epilepsia, 43(2), 146-153.

Clark, D. L., & Rosner, B. S. (1973). Neurophysiologic effects of general anesthetics: The electroencephalogram and sensory evoked responses in man. The Journal of the American Society of Anesthesiologists, 38(6), 564-582.

Cohen, L. T., Rickards, F. W., & Clark, G. M. (1991). A comparison of steady-state evoked potentials to modulated tones in awake and sleeping humans. The Journal of the Acoustical Society of America, 90(5), 2467-2479.

Conrad, I., Ancoli-Israel, S., Chesson, A., & Quan, S. F. (2007). The AASM manual for the scoring of sleep and associated events: rules, terminology and technical specifications. Westchester: American Academy of Sleep Medicine.

Cover, T. M., & Thomas, J. A. (2006). Elements of information theory (2nd ed.). New Jersey: John Wiley & Sons Inc.

Davis, H. (1976). Principles of electric response audiometry. The annals of Otology, Rhinology, and Laryngology, 85(3), 1.

Davis, H., Davis, P. A., Loomis, A. L., Harvey, E. N., & Hobart, G. (1939). Electrical reactions of the human brain to auditory stimulation during sleep. Journal of Neurophysiology, 2(6), 500-514.

Deiber, M. P., Ibanez, V., Bastuji, H., Fischer, C., & Mauguiere, F. (1989). Changes of middle latency auditory evoked potentials during natural sleep in humans. Neurology, 39(6), 806-806.

De Gennaro, L., Ferrara, M., & Bertini, M. (2000). Topographical distribution of spindles: Variations between and within NREM sleep cycles. Sleep Res Online, 3(4), 155-160.

Delgado, R. E., & Ozdamar, O. (2004). Deconvolution of evoked responses obtained at high stimulus rates. The Journal of the Acoustical Society of America, 115(3), 1242-1251.

Doenicke, A., Loffler, B., Kugler, J., Suttmann, H., & Grote, B. (1982). Plasma concentration and EEG after various regimens of etomidate. British journal of anaesthesia, 54(4), 393-400.

Drummond, J. C., Brann, C. A., Perkins, D. E., & Wolfe, D. E. (1991). A comparison of median frequency, spectral edge frequency, a frequency band power ratio, total power, and dominance shift in the determination of depth of anesthesia. Acta Anaesthesiologica Scandinavica, 35(8), 693-699.

Duke, J. (2015). Duke's anesthesia secrets. Amsterdam: Elsevier Health Sciences.

Eger, E. I. (1974). Anesthetic systems: Construction and function. Anesthetic uptake and action. Baltimore: Williams & Wilkins.

Elizabeth M. & Anthony E. (1981). Effects of creativity on developing minds. Science, 100(1), 3-17

Erwin, R., & Buchwald, J. S. (1986). Midlatency auditory evoked responses: Differential effects of sleep in the human. Electroencephalography and Clinical Neurophysiology-Evoked Potentials Section, 65(5), 383-392.

Fell, J., Röschke, J., Mann, K., & Schäffner, C. (1996). Discrimination of sleep stages: A comparison between spectral and nonlinear EEG measures. Electroencephalography and Clinical Neurophysiology, 98(5), 401-410.

Ferraro, J. A., & Durrant, J. D. (1994). Auditory evoked potentials: Overview and basic principles. Handbook of Clinical Audiology, 4, 317-38.

Feshchenko, V. A., Veselis, R. A., & Reinsel, R. A. (2004). Propofol-induced alpha rhythm. Neuropsychobiology, 50(3), 257-266.

Fox, S. I. (2004). Human physiology (8th ed.). New York: McGraw-Hill Company.

Galambos, R., Makeig, S., & Talmachoff, P. J. (1981). A 40-Hz auditory potential recorded from the human scalp. Proceedings of the National Academy of Sciences, 78(4), 2643-2647.

Gelb, A. W., Leslie, K., Stanski, D. R., & Shafer, S. L. (2009). Monitoring the depth of anesthesia. In R. D. Miller (Ed.), Miller's anesthesia. Churchill Livingstone: Elsevier.

Gelfand, S. A. (2009). Essentials of audiology (3rd ed.). New York: Thieme.

Gibbs, F. A., Gibbs, E. L., & Lennox, W. G. (1937). Effect on the electro-encephalogram of certain drugs which influence nervous activity. Archives of Internal Medicine, 60(1), 154-166.

Gökahmetoglu, G., Tercan, E., Bicer, C., Aksu, R., & Boyaci, A. (2013). Comparison of the depth of anesthesia in sevoflurane and halothane anesthesia with bispectral index and 95% spectral edge frequency. Dicle Medical Journal, 40 (3), 350-356.

Gulya, A. J., Minor, L. B., Glasscock, M. E., & Poe, D. (2010). Glasscock-Shambaugh Surgery of the ear. Shelton: People's Medical Publishing House.

Gurman, G. M., Fajer, S., Porat, A., Schily, M., & Pearlman, A. (1994). Use of EEG spectral edge as index of equipotency in a comparison of propofol and isoflurane for maintenance of general anaesthesia. European Journal of Anaesthesiology, 11(6), 443-448.

Guyton, A. C., & Hall, J. E. (2006). Textbook of medical physiology (11th ed.). Pennsylvania: Elsevier.

Haenschel, C., Baldeweg, T., Croft, R. J., Whittington, M., & Gruzelier, J. (2000). Gamma and beta frequency oscillations in response to novel auditory stimuli: A comparison of human electroencephalogram (EEG) data with in vitro models. Proceedings of the National Academy of Sciences, 97(13), 7645-7650.

Heneghan, C. P. H., Thornton, C., Navaratnarajah, M., & Jones, J. G. (1987). Effect of isoflurane on the auditory evoked response in man. British Journal of Anaesthesia, 59(3), 277-282.

Hogan, K. (1987). 40 Hz steady-state evoked potentials (SSEP) during isoflurane-N20 anesthesia. The Journal of the American Society of Anesthesiologists, 67(3), A402-A402.

Iber, C., Ancoli-Israel, S., Chesson, A., & Quan, S. F. (2007). The AASM manual for the scoring of sleep and associated events: Rules, terminology and technical specifications. Westchester: American Academy of Sleep Medicine.

Jacobson, G. P., & Newman, C. W. (1990). The decomposition of the middle latency auditory evoked potential (MLAEP) Pa component into superficial and deep source contributions. Brain Topography, 2(3), 229-236.

Jagadeesan, N., Wolfson, M., Chen, Y., Willingham, M., & Avidan, M. S. (2013). Brain monitoring during general anesthesia. Trends in Anaesthesia and Critical Care, 3(1), 13-18.

Jenkins, A., Andreasen, A., Trudell, J. R., & Harrison, N. L. (2002). Tryptophan scanning mutagenesis in TM4 of the GABA-A receptor α1 subunit: implications for modulation by inhaled anesthetics and ion channel structure. Neuropharmacology, 43(4), 669-678.

Jenkins, A., Greenblatt, E. P., Faulkner, H. J., Bertaccini, E., Light, A., Lin, A., ... & Harrison, N. L. (2001). Evidence for a common binding cavity for three general anesthetics within the GABA-A receptor. Journal of Neuroscience, 21(6), 136.

Jerger, J., Chmiel, R., Frost Jr, J. D., & Coker, N. (1986). Effect of sleep on the auditory steady state evoked potential. Ear and Hearing, 7(4), 240-245.

Kaga, K., Hink, R. F., Shinoda, Y., & Suzuki, J. (1980). Evidence for a primary cortical origin of a middle latency auditory evoked potential in cats. Electroencephalography and Clinical Neurophysiology, 50(3), 254-266.

Siegelbaum, S. A., & Hudspeth, A. J. (2000). Principles of neural science. New York: McGraw-Hill.

Kay, S. M. (1988). Modern spectral estimation. Englewood Cliffs: Prentice.

Khuwaja, G. A., Haghighi, S. J., & Hatzinakos, D. (2015). 40-Hz ASSR fusion classification system for observing sleep patterns. EURASIP Journal on Bioinformatics and Systems Biology, 2015(1), 2.

Kiersey, D. K., Bickford, R. G., & Faulconer, A. (1951). Electro-encephalographic patterns produced by thiopental sodium during surgical operations: description and classification. British Journal of Anaesthesia, (23), 141-152.

Kiyama, S., & Takeda, J. (1997). Effect of extradural analgesia on the paradoxical arousal response of the electroencephalogram. British Journal of Anaesthesia, 79(6), 750-753.

Klein, A. J. (1983). Properties of the brain-stem response slow-wave component: I. Latency, amplitude, and threshold sensitivity. Archives of Otolaryngology, 109(1), 6-12.

Knight , A. (2010). Basics of matlab and beyond. Boca Raton: CRC Press.

Knight, R. T., & Brailowsky, S. (1990). Auditory evoked potentials from the primary auditory cortex of the cat: topographic and pharmacological studies. Electroencephalography and Clinical Neurophysiology/Evoked Potentials Section, 77(3), 225-232.

Kraus, N., & McGee, T. (1992). Electrophysiology of the human auditory system. In The mammalian auditory pathway: Neurophysiology. New York: Springer.

Kraus, N., & McGee, T. (1993). Clinical implications of primary and nonprimary pathway contributions to the middle latency response generating system. Ear and Hearing, 14(1), 36-48.

Kraus, N., McGee, T., Littman, T., Nicol, T., & King, C. (1994). Nonprimary auditory thalamic representation of acoustic change. Journal of Neurophysiology, 72(3), 1270-1277.

Kraus, N., Smith, D. I., & McGee, T. (1987a). Rate and filter effects on the developing middle-latency response. Audiology, 26(5), 257-268.

Kraus, N., Smith, D. I., & McGee, T. (1988). Midline and temporal lobe MLRs in the guinea pig originate from different generator systems: A conceptual framework for new and existing data. Electroencephalography and Clinical Neurophysiology, 70(6), 541-558.

Kraus, N., Smith, D. I., McGee, T., Stein, L., & Cartee, C. (1987b). Development of the middle latency response in an animal model and its relation to the human response. Hearing Research, 27(2), 165-176.

Kraus, N., Smith, D. I., Reed, N. L., Stein, L. K., & Cartee, C. (1985). Auditory middle latency responses in children: Effects of age and diagnostic category. Electroencephalography and Clinical Neurophysiology-Evoked Potentials Section, 62(5), 343-351.

Kraus, N., McGee, T., & Cornperatore, C. (1989). MLRs in children are consistently present during wakefulness, stage 1, and REM sleep. Ear and Hearing, 10(6), 339-345.

Kropotov, J. D. (2009). Qualitative EEG, event related potentials and neuropathy. San Diego: Academic Press.

Ledowski, T., Bromilow, J., Paech, M. J., Storm, H., Hacking, R., & Schug, S. A. (2006). Skin conductance monitoring compared with Bispectral Index® to assess emergence from total iv anaesthesia using propofol and remifentanil. British Journal of Anaesthesia, 97(6), 817-821.

Linden, R. D., Campbell, K. B., Hamel, G., & Picton, T. W. (1985). Human auditory steady state evoked potentials during sleep. Ear and Hearing, 6(3), 167-174.

Marieb, E. N. (1991). Human anatomy and physiology (3rd ed.). Redwood City: The Benjamin-Cummings Publising Company.

Mascia, M. P., Trudell, J. R., & Harris, R. A. (2000). Specific binding sites for alcohols and anesthetics on ligand-gated ion channels. Proceedings of the National Academy of Sciences, 97(16), 9305-9310.

Mashour, G. (2010). Consciousness, awareness, and anesthesia. New York: Cambridge University Press.

McCarthy, M. M., Brown, E. N., & Kopell, N. (2008). Potential network mechanisms mediating electroencephalographic beta rhythm changes during propofol-induced paradoxical excitation. Journal of Neuroscience, 28(50), 13488-13504.

McCormick, L., Nielsen, T., Nicolas, A., Ptito, M., & Montplaisir, J. (1997). Normal sleep topographical distribution of spindles and K-complexes in normal subjects. Sleep, 20(11), 939-941.

McGee, T., Kraus, N., Comperatore, C., & Nicol, T. (1991). Subcortical and cortical components of the MLR generating system. Brain Research, 544(2), 211-220.

McGee, T., Kraus, N., Killion, M., Rosenberg, R., & King, C. (1993). Improving the reliability of the auditory middle latency response by monitoring EEG delta activity. Ear and Hearing, 14(2), 76-84.

McGee, T., Kraus, N., Littman, T., & Nicol, T. (1992). Contributions of medial geniculate body subdivisions to the middle latency response. Hearing Research, 61(1), 147-154.

McNeer, R. R., Bohórquez, J., & Özdamar, Ö. (2009). Influence of auditory stimulation rates on evoked potentials during general anesthesia: Relation between the transient auditory middle-latency response and the 40-Hz auditory steady state response. The Journal of the American Society of Anesthesiologists, 110(5), 1026-1035.

Melcher, J. R. (2009). Auditory evoked potential. In L. R. Squire (Ed.), Encyclopedia of neuroscience. Oxford: Oxford Academic Press.

Mendel, M. I. (1974). Influence of stimulus level and sleep stage on the early components of the averaged electroencephalic response to clicks during all-night sleep. Journal of Speech, Language, and Hearing Research, 17(1), 5-17.

Mendel, M. I., & Goldstein, R. (1971). Early components of the averaged electroencephalic response to constant level clicks during all-night sleep. Journal of Speech, Language, and Hearing Research, 14(4), 829-840.

Michelini, S., Arslan, E., Prosser, S., & Pedrielli, F. (1982). Logarithmic display of auditory evoked potentials. Journal of Biomedical Engineering, 4(1), 62-64.

Millan, J. (2006). Analysis of auditory middle latency responses at low and high stimulus rates during sleep (Doctorial Dissertation). Retrieved from ProQuest

Miller, R. D., Eriksson, L. I., Fleisher, L. A., Wiener-Kronish, J. P., & Young, W. L. (2009). Anesthesia. Amsterdam: Elsevier Health Sciences.

Møller, A. R., & Jannetta, P. J. (1981). Compound action potentials recorded intracranially from the auditory nerve in man. Experimental Neurology, 74(3), 862-874.

Morin, C. M., & Espie, C. A. (Eds.). (2011). The Oxford handbook of sleep and sleep disorders. Oxford: Oxford University Press.

Mulert, C., & Lemieux, L. (Eds.). (2009). EEG-fMRI: physiological basis, technique, and applications. Berlin: Springer Science & Business Media.

Nishikawa, K., & Harrison, N. L. (2003). The actions of sevoflurane and desflurane on the γ-aminobutyric acid receptor type A effects of TM2 mutations in the α and β subunits. The Journal of the American Society of Anesthesiologists, 99(3), 678-684.

Nishikawa, K., Jenkins, A., Paraskevakis, I., & Harrison, N. L. (2002). Volatile anesthetic actions on the GABA A receptors: contrasting effects of α1 (S270) and β2 (N265) point mutations. Neuropharmacology, 42(3), 337-345.

Okitsu, T. (1984). Middle components of the auditory evoked response in young children. Scandinavian Audiology, 13(2), 83-86.

Orser, B. A. (2007). Lifting the fog around anesthesia. Scientific American, 296(6), 54-61.

Osterhammel, P. A., Shallop, J. K., & Terkildsen, K. (1985). The effect of sleep on the auditory brainstem response (ABR) and the middle latency response (MLR). Scandinavian Audiology, 14(1), 47-50.

Özdamar, Ö., & Bohórquez, J. (2006). Signal-to-noise ratio and frequency analysis of continuous loop averaging deconvolution (CLAD) of overlapping evoked potentials. The Journal of the Acoustical Society of America, 119(1), 429-438.

Özdamar, Ö., Kraus, N., & Curry, F. (1982). Auditory brain stem and middle latency responses in a patient with cortical deafness. Electroencephalography and Clinical Neurophysiology, 53(2), 224-230.

Pace-Schott, E. F., & Hobson, J. A. (2002). The neurobiology of sleep: Genetics, cellular physiology and subcortical networks. Nature Reviews Neuroscience, 3(8), 591-605.

Picton, T. W., Hillyard, S. A., Krausz, H. I., & Galambos, R. (1974). Human auditory evoked potentials. I: Evaluation of components. Electroencephalography and Clinical Neurophysiology, 36, 179-190.

Picton, T. W., John, M. S., Purcell, D. W., & Plourde, G. (2003). Human auditory steady-state responses: The effects of recording technique and state of arousal. Anesthesia & Analgesia, 97(5), 1396-1402.

Picton, T. W., Woods, D. L., Baribeau-Braun, J., & Healey, T. M. (1977). Evoked potential audiometry. Journal of Otolaryngology, 6(2), 90-119.

Plonsey, R., & Malmivuo, J. (1995). Bioelectromagnetism: principles and applications of bioelectric and biomagnetic fields. New York: Oxford University Press.

Plourde, G., & Picton, T. W. (1990). Human auditory steady-state response during general anesthesia. Anesthesia & Analgesia, 71(5), 460-468.

Porjesz, B., Almasy, L., Edenberg, H. J., Wang, K., Chorlian, D. B., Foroud, T., ... & Kuperman, S. (2002). Linkage disequilibrium between the beta frequency of the human EEG and a GABA-A receptor gene locus. Proceedings of the National Academy of Sciences, 99(6), 3729-3733.

Portas, C. M., Krakow, K., Allen, P., Josephs, O., Armony, J. L., & Frith, C. D. (2000). Auditory processing across the sleep-wake cycle: simultaneous EEG and fMRI monitoring in humans. Neuron, 28(3), 991-999.

Posner, J. B., & Plum, F. (2007). Plum and Posner's diagnosis of stupor and coma. Oxford: Oxford University Press.

Proakis, J. G. (1996). Digital signal processing: principles, algorithms, and application (3rd ed.). New Jersey: Prentice-Hall

Purves, D., Augustine, G. J., Fitzpatrick, D., Katz, L. C., LaMantia, A., McNamara, J. O., & Williams, S. M. (2004). Neuroscience (3rd ed.). Massachusetts: Sinauer Associates.

Rampil, I. J. (1998). A primer for EEG signal processing in anesthesia. The Journal of the American Society of Anesthesiologists, 89(4), 980-1002.

Rechtschaffen, A., & Kales, A. (1968). A manual of standardized terminology, techniques and scoring system for sleep stages of human subjects. US Department of Health, Education and Welfare, Public Health Service, National Institutes of Health, National Institute of Neurological Diseases and Blindness, Neurological Information Network.

Roeser, R. J., Valente, M., & Hosford-Dunn, H. (2007). Audiology diagnosis (2nd ed.). New York: Thieme Medical Publisher.

Schmidt, G. N., Bischoff, P., Standl, T., Lankenau, G., Hilbert, M., & am Esch, J. S. (2004). Comparative evaluation of Narcotrend™, Bispectral Index™, and classical electroencephalographic variables during induction, maintenance, and emergence of a propofol/remifentanil anesthesia. Anesthesia & Analgesia, 98(5), 1346-1353.

Schwilden, H., Schüttler, J., & Stoekel, H. (1983). Pharmacokinetics as applied to total intravenous anaesthesia. Anaesthesia, 38(S1), 51-52.

Schwender, D., Conzen, P., Klasing, S., Finsterer, U., Poppel, E., & Peter, K. (1995). The effects of anesthesia with increasing end-expiratory concentrations of sevoflurane on midlatency auditory evoked potentials. Anesthesia & Analgesia, 81(4), 817-822.

Schwilden, H., & Stoeckel, H. (1987). Quantitative EEG analysis during anaesthesia with isoflurane in nitrous oxide at 1.3 and 1.5 MAC. British Journal of Anaesthesia, 59(6), 738-745.

Shallop, J. K., & Osterhammel, P. A. (1983). A comparative study of measurements of SN-10 and the 40/sec middle latency responses in newborns. Scandinavian Audiology, 12(2), 91-95.

Shannon, C. (1948). A mathematical theory of communication. Bell System Technical Journal 27, 379–423

The MathWorks. (2013). Signal Processing Toolbox™: User Guide. Natick, MA

Silber, M. H., Ancoli-Israel, S., Bonnet, M. H., Chokroverty, S., Grigg-Damberger, M. M., Hirshkowitz, M., ... & Pressman, M. R. (2007). The visual scoring of sleep in adults. Journal of Clinical Sleep Medicine, 3(2), 121-131.

Sonner, J. M., Antognini, J. F., Dutton, R. C., Flood, P., Gray, A. T., Harris, R. A., ... & Trudell, J. (2003). Inhaled anesthetics and immobility: mechanisms, mysteries, and minimum alveolar anesthetic concentration. Anesthesia & Analgesia, 97(3), 718-740.

Stoelting, R. K., Longnecker, D. E., & Eger, E. I. (1970). Minimum alveolar concentrations in man on awakening from methoxyflurane, halothane, ether and fluroxene anesthesia. Anesthesiology, 33(1), 5-9.

Suzuki, T., Kobayashi, K., & Umegaki, Y. (1994). Effect of natural sleep on auditory steady state responses in adult subjects with normal hearing. Audiology, 33(5), 274-279.

Sweeny, F. (2008). The anesthesia fact book: Everything you need to know before surgery. Cambridge: Da Capo Press.

Tatsumi, K., Hirai, K., Furuya, H., & Okuda, T. (1995). Effects of sevoflurane on the middle latency auditory evoked response and the electroencephalographic power spectrum. Anesthesia & Analgesia, 80(5), 940-943.

Tatum, W. O., Husain, A., & Kaplan, P. W. (2008). Handbook of EEG interpretation. New York: Demos Medical Publishing.

Teasdale, T. (2001). The self-instructional modules in geriatric medicine. (4th ed.). Houstan: Baylor College of Medicine.

Thornton, C., & Newton, D. E. F. (1989). The auditory evoked response: A measure of depth of anaesthesia. Baillière's Clinical Anaesthesiology, 3(3), 559-585.

Thornton, C., Catley, D. M., Jordan, C., Lehane, J. R., Royston, D., & Jones, J. G. (1983). Enflurane anaesthesia causes graded changes in the brainstem and early cortical auditory evoked response in man. British Journal of Anaesthesia, 55(6), 479-486.

Thornton, C., Heneghan, C. P. H., James, M. F. M., & Jones, J. G. (1984). Effects of halothane or enflurane with controlled ventilation on auditory evoked potentials. British Journal of Anaesthesia, 56(4), 315-323.

Thornton, C., Heneghan, C. P. H., Navaratnarajah, M., Bateman, P. E., & Jones, J. G. (1985). Effect of etomidate on the auditory evoked response in man. British Journal of Anaesthesia, 57(6), 554-561.

Thornton, C., Konieczko, K., Jones, J. G., Jordan, C., Dore, C. J., & Heneghan, C. P. H. (1988). Effect of surgical stimulation on the auditory evoked response. British Journal of Anaesthesia, 60(4), 372-378.

Tinker, J. H., Sharbrough, F. W., & Michenfelder, J. D. (1977). Anterior shift of the dominant EEG rhytham during anesthesia in the Java monkey: Correlation with anesthetic potency. Anesthesiology, 46(4), 252-259.

Traub, R. D., Whittington, M. A., Stanford, I. M., & Jefferys, J. G. (1996). A mechanism for generation of long-range synchronous fast oscillations in the cortex. Nature, 383(6601), 621.

Vaughan, H. G., & Ritter, W. (1970). The sources of auditory evoked responses recorded from the human scalp. Electroencephalography and Clinical Neurophysiology, 28(4), 360-367.

Velluti, R. A. (2008). The Auditory System in Sleep. San Diego: Elsevier.

Viertiö-Oja, H., Maja, V., Särkelä, M., Talja, P., Tenkanen, N., Tolvanen- Laakso, H., ... & Meriläinen, P. (2004). Description of the Entropy™ algorithm as applied in the Datex-Ohmeda S/5™ Entropy Module. Acta Anaesthesiologica Scandinavica, 48(2), 154-161.

Welch, P. (1967). The use of fast Fourier transform for the estimation of power spectra: a method based on time averaging over short, modified periodograms. IEEE Transactions on Audio and Electroacoustics, 15(2), 70-73.

Whittington, M. A., Traub, R. D., Faulkner, H. J., Stanford, I. M., & Jefferys, J. G. (1997). Recurrent excitatory postsynaptic potentials induced by synchronized fast cortical oscillations. Proceedings of the National Academy of Sciences, 94(22), 12198-12203.

APPENDIX A Transient Response of Patients in Anesthesia Study

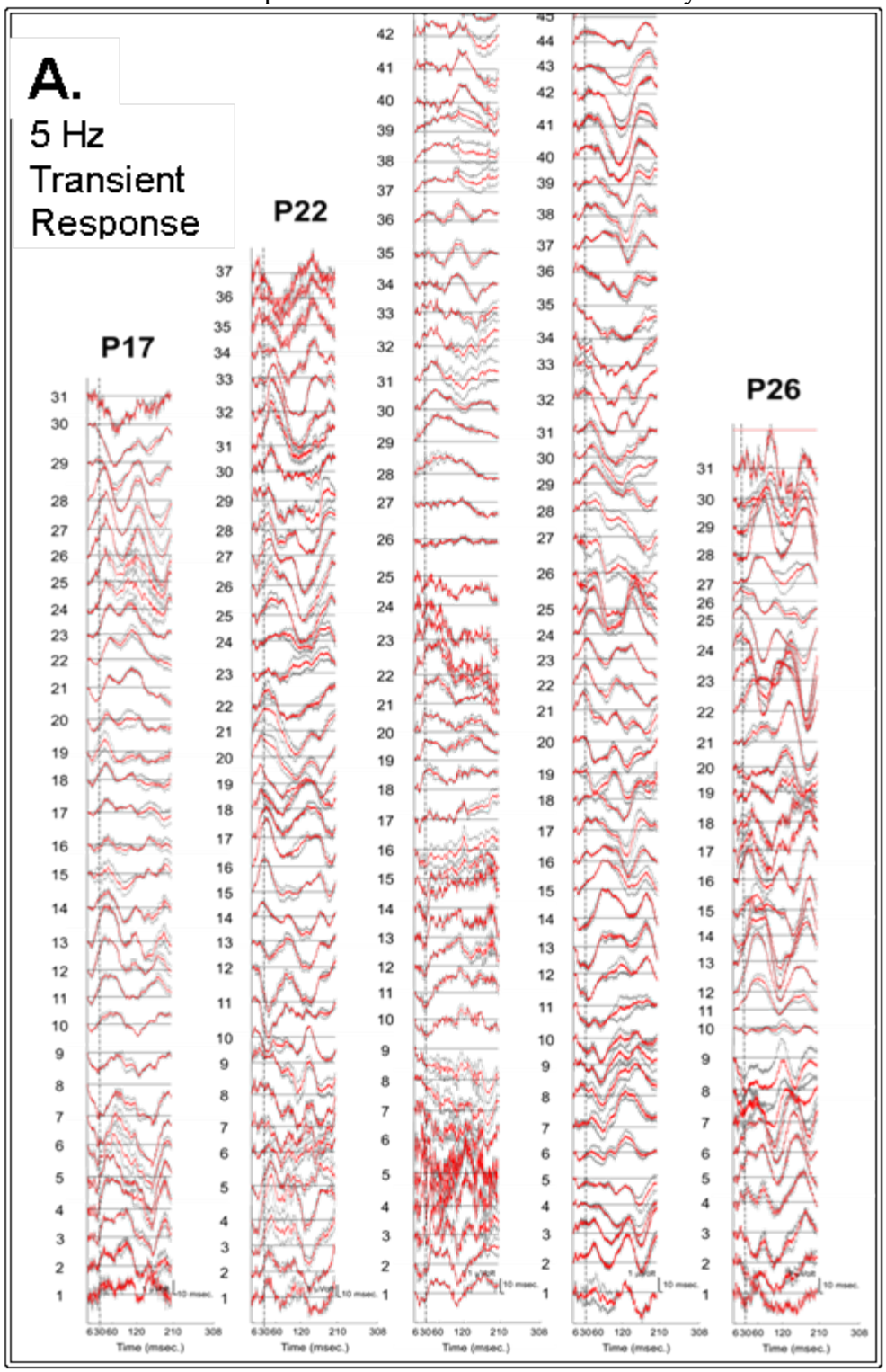

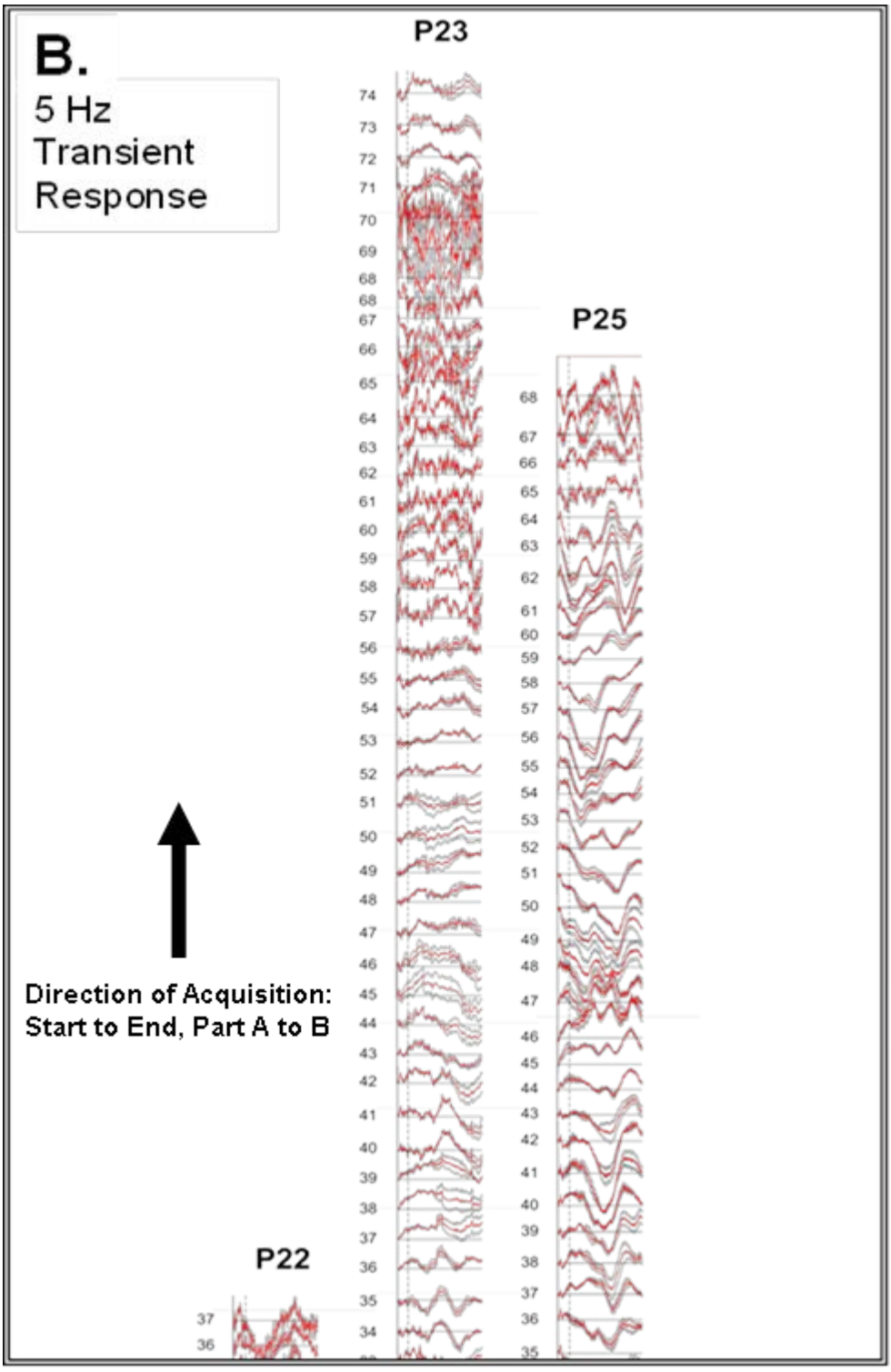

Figure A.1 Trend of 5 Hz transient response. Shown are the transient responses from 10 point, 50 % overlap trend to illustrate effect of anesthesia on responses.

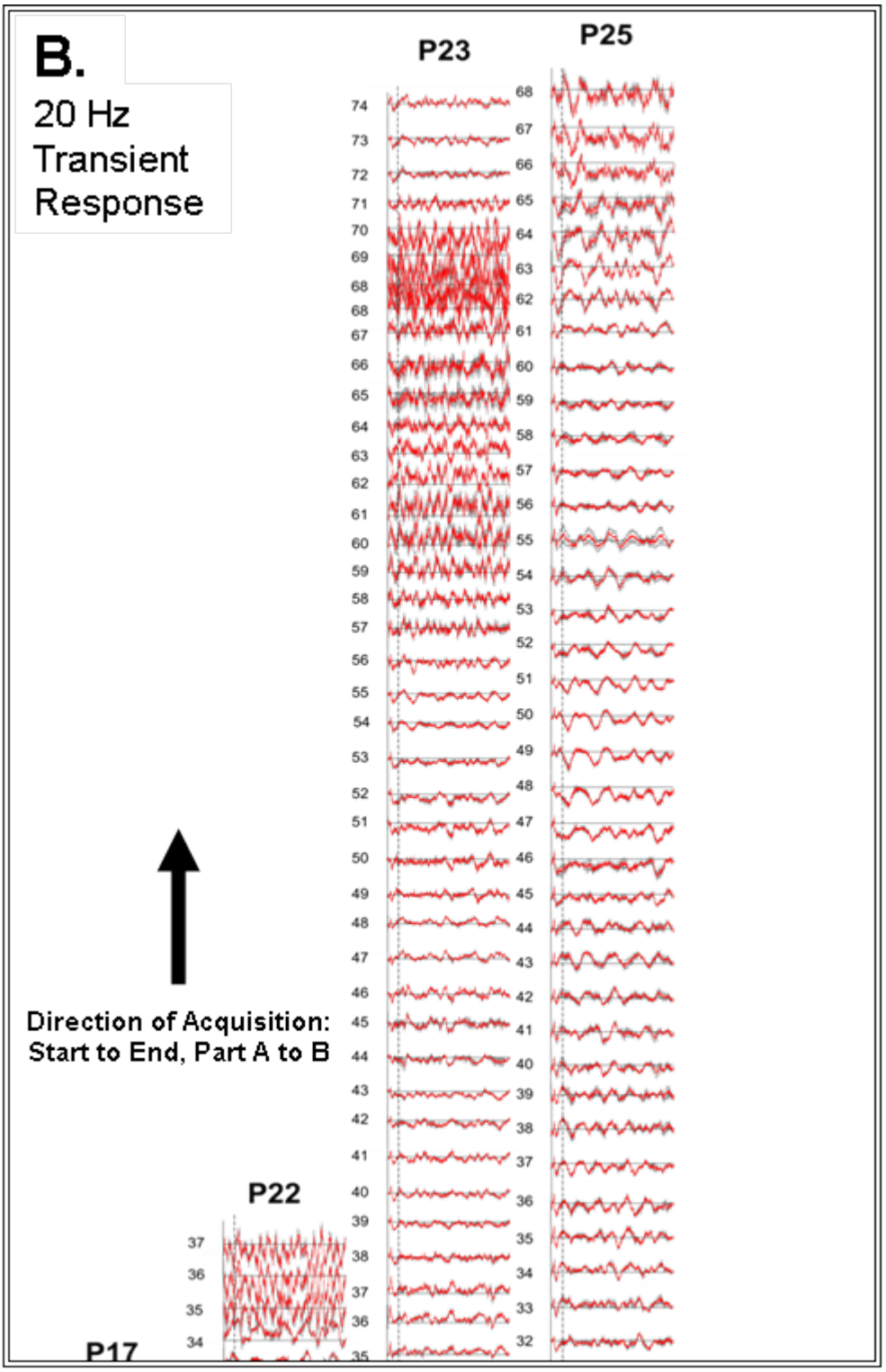

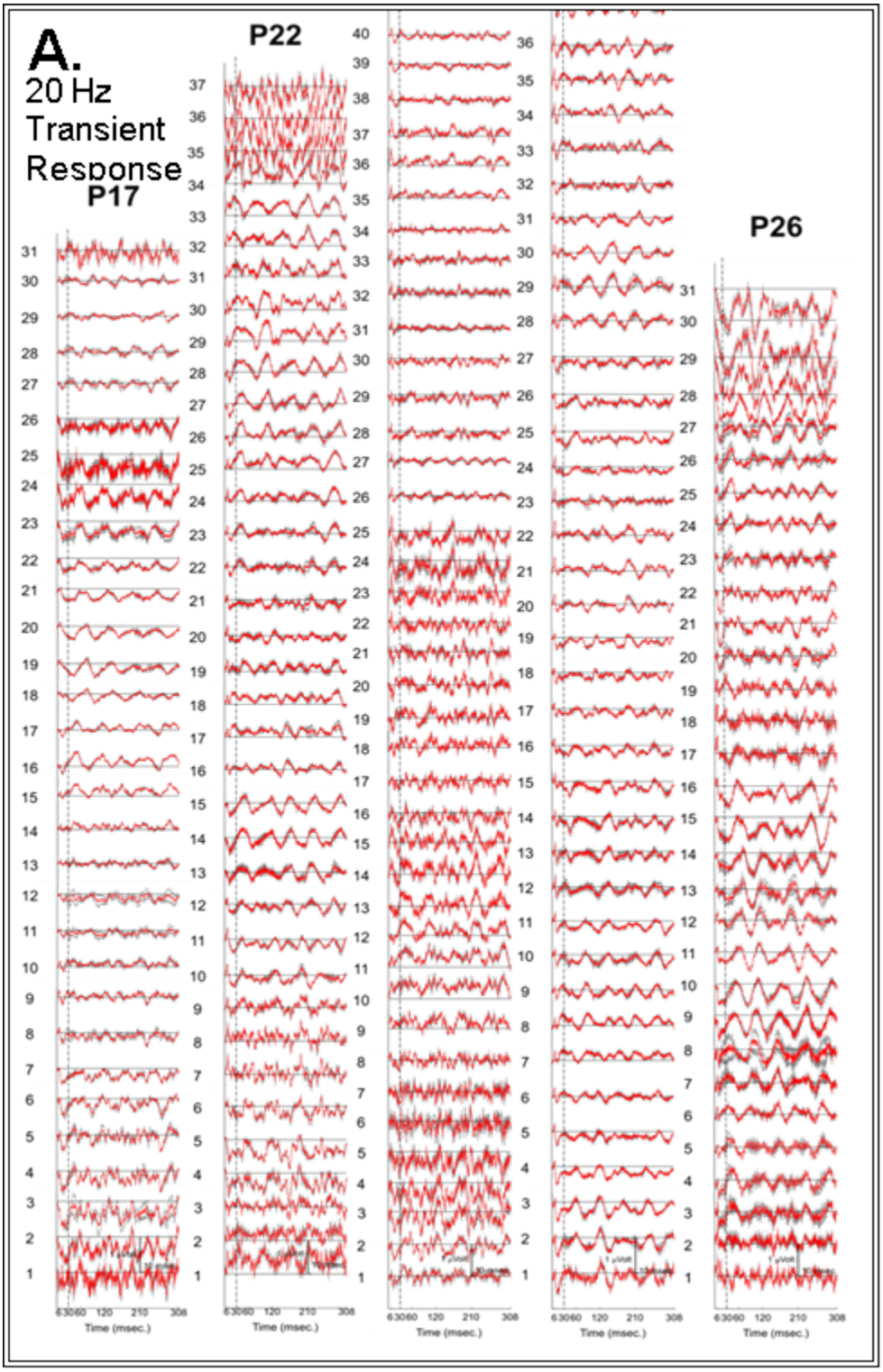

Figure A.2 Trend of 20 Hz transient response. Shown are the transient responses from 10 point, 50 % overlap trend to illustrate effect of anesthesia on responses.

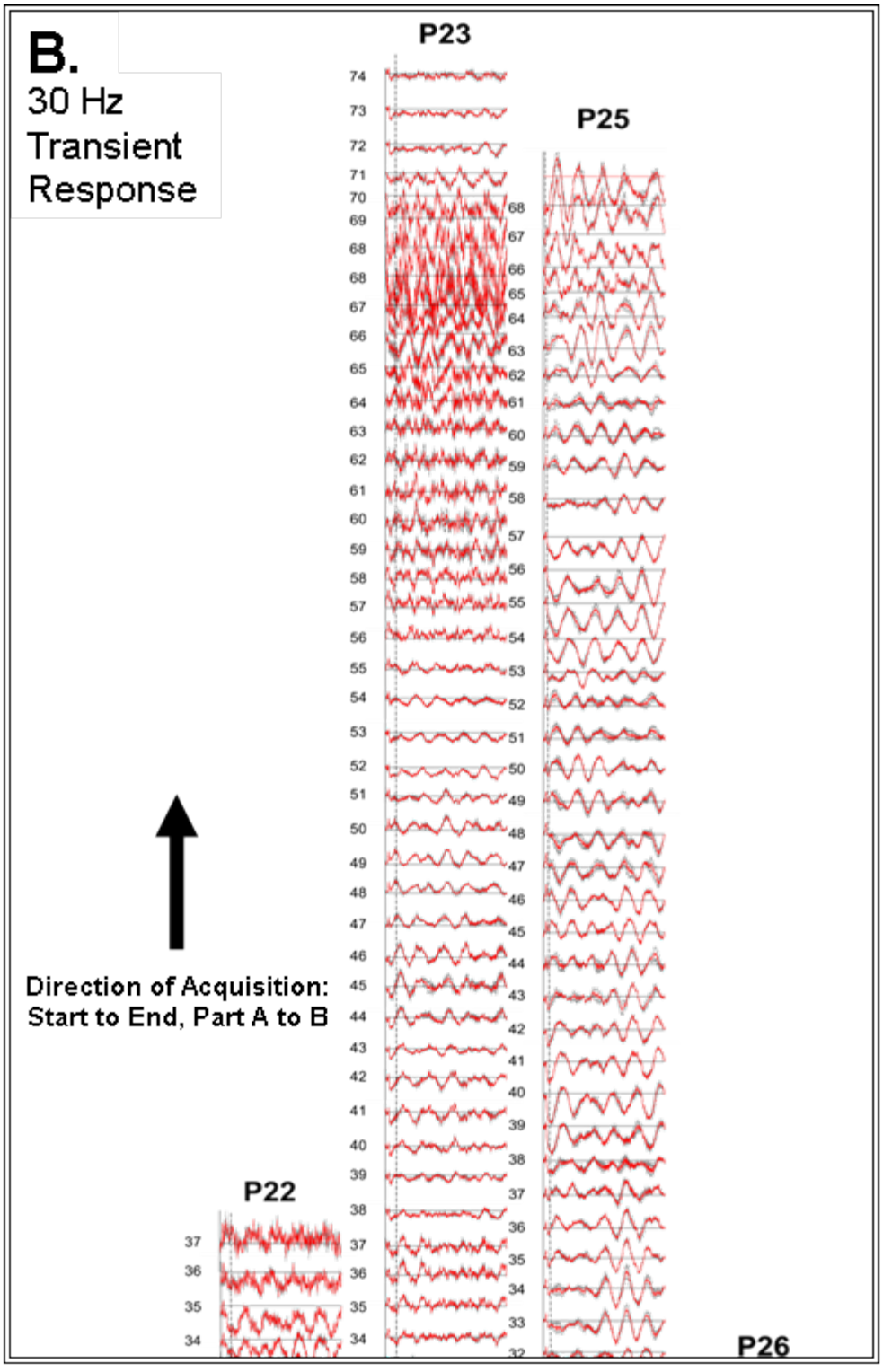

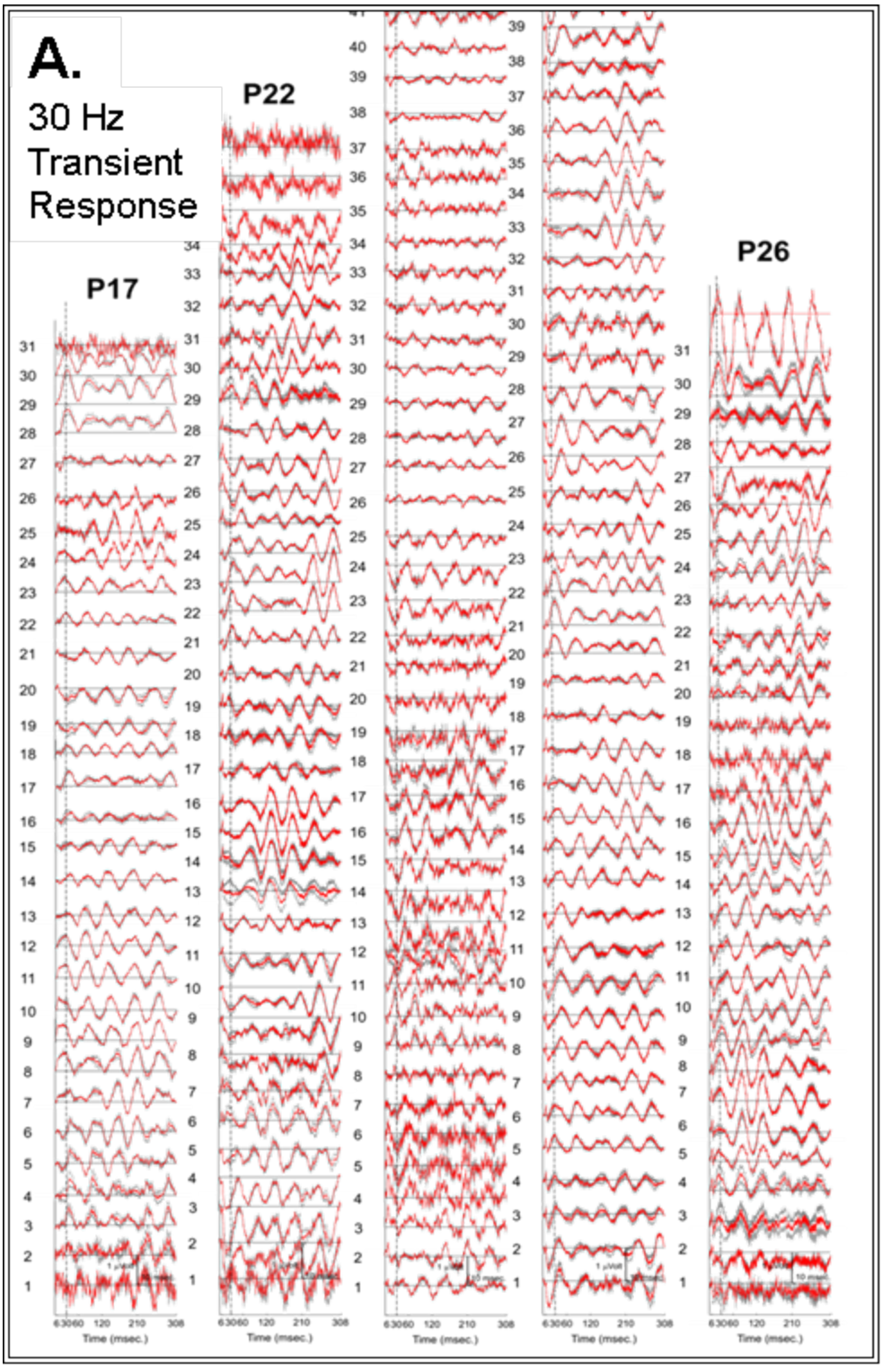

Figure A.3 Trend of 30 Hz transient response. Shown are the transient responses from 10 point, 50 % overlap trend to illustrate effect of anesthesia on responses.

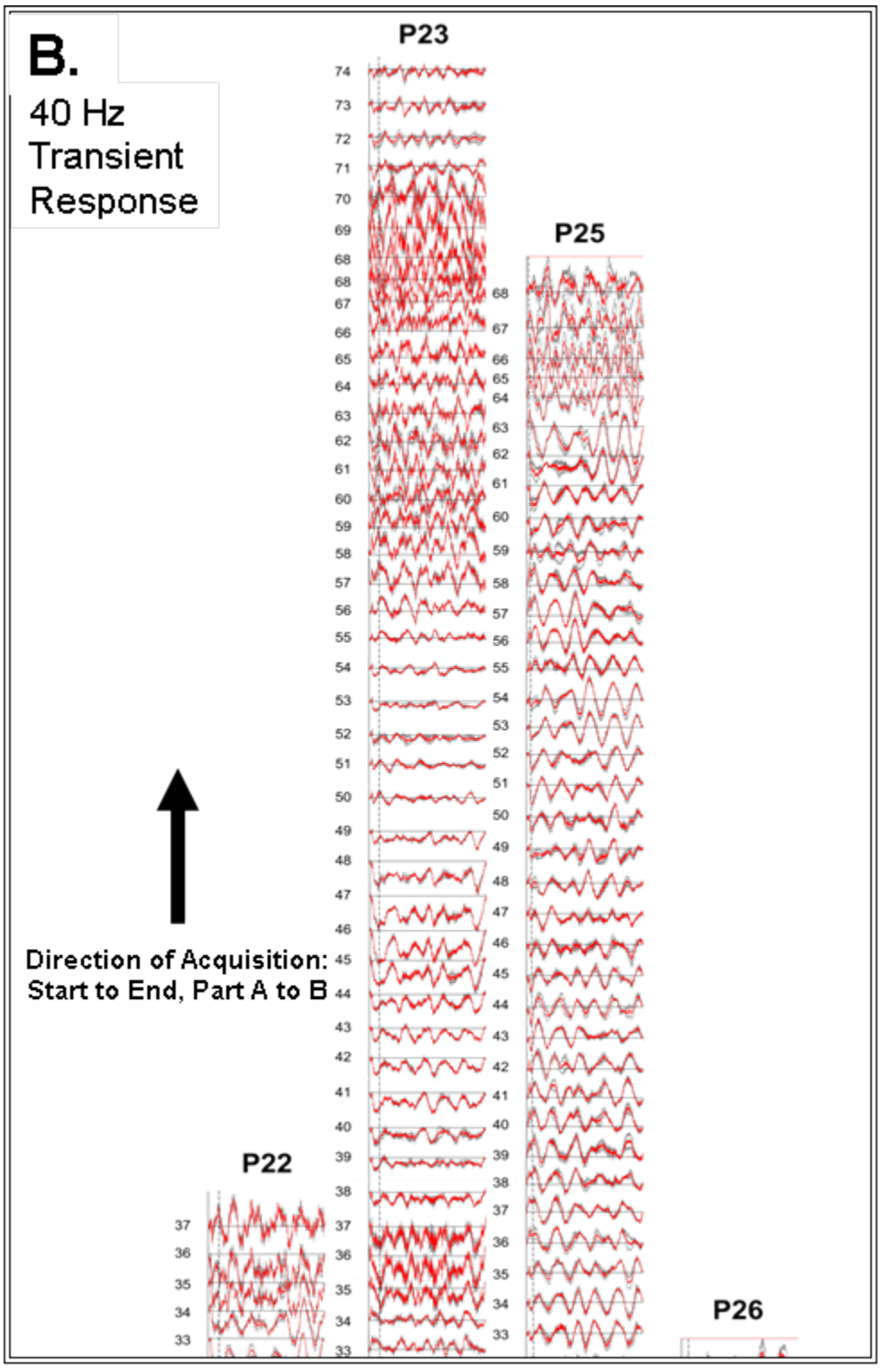

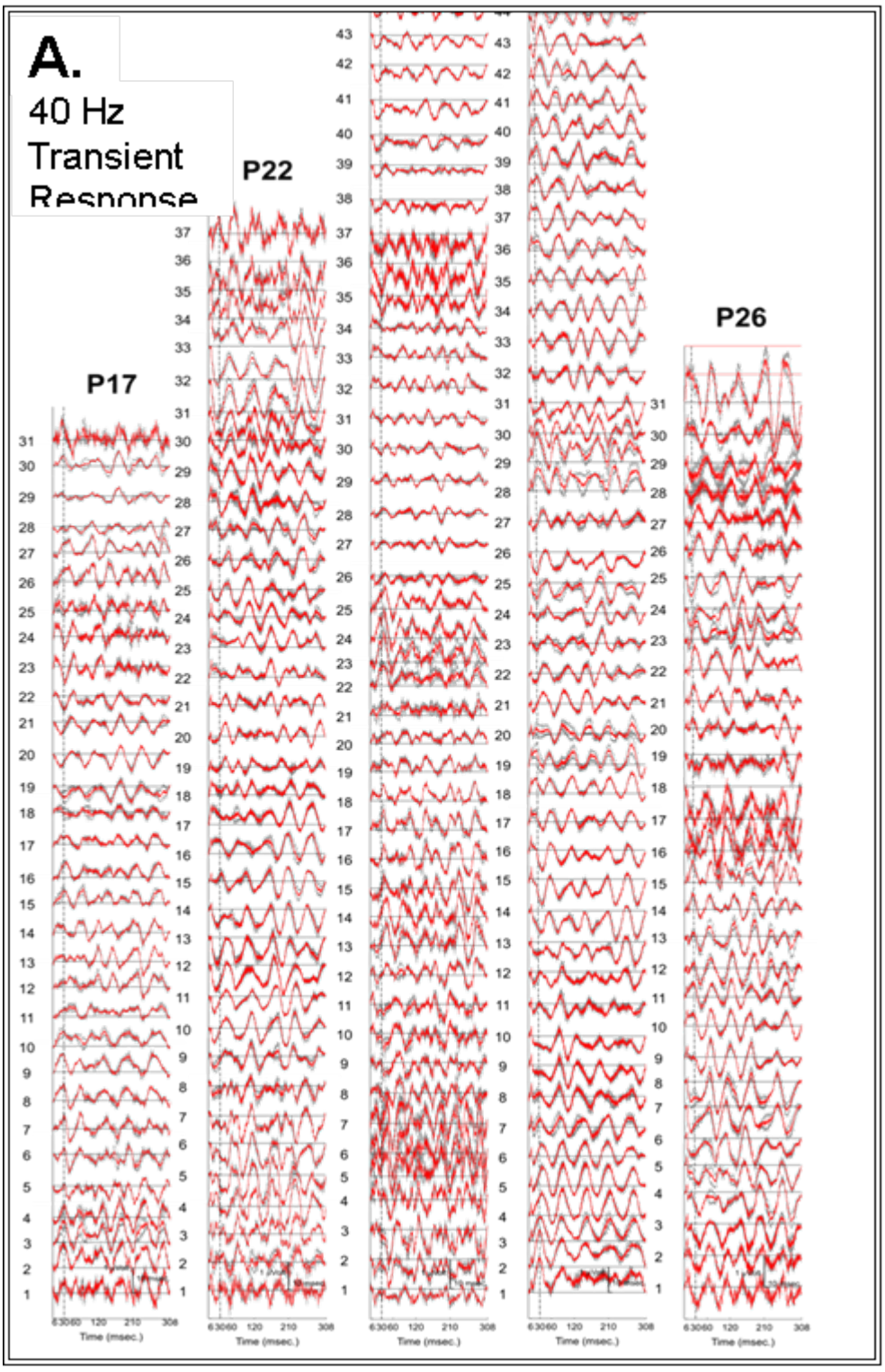

Figure A.4 Trend of 40 Hz transient response. Shown are the transient responses from 10 point, 50 % overlap trend to illustrate effect of anesthesia on responses.

APPENDIX B Transient Response of Subjects in Sleep Study

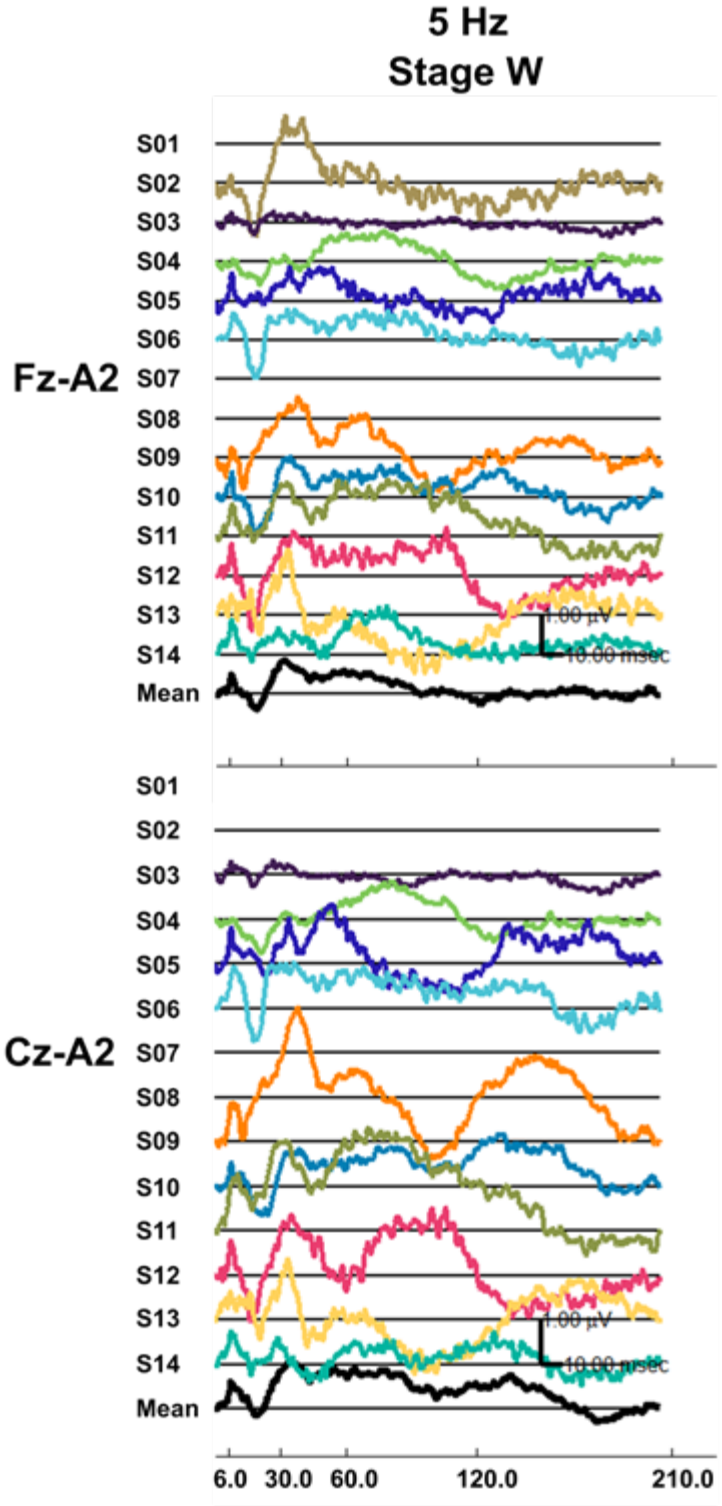

Figure B.1 The 5 Hz Transient Response for each Subject in Stage-W. Shown for each channel is the transient response for each subject and the mean for all subjects.

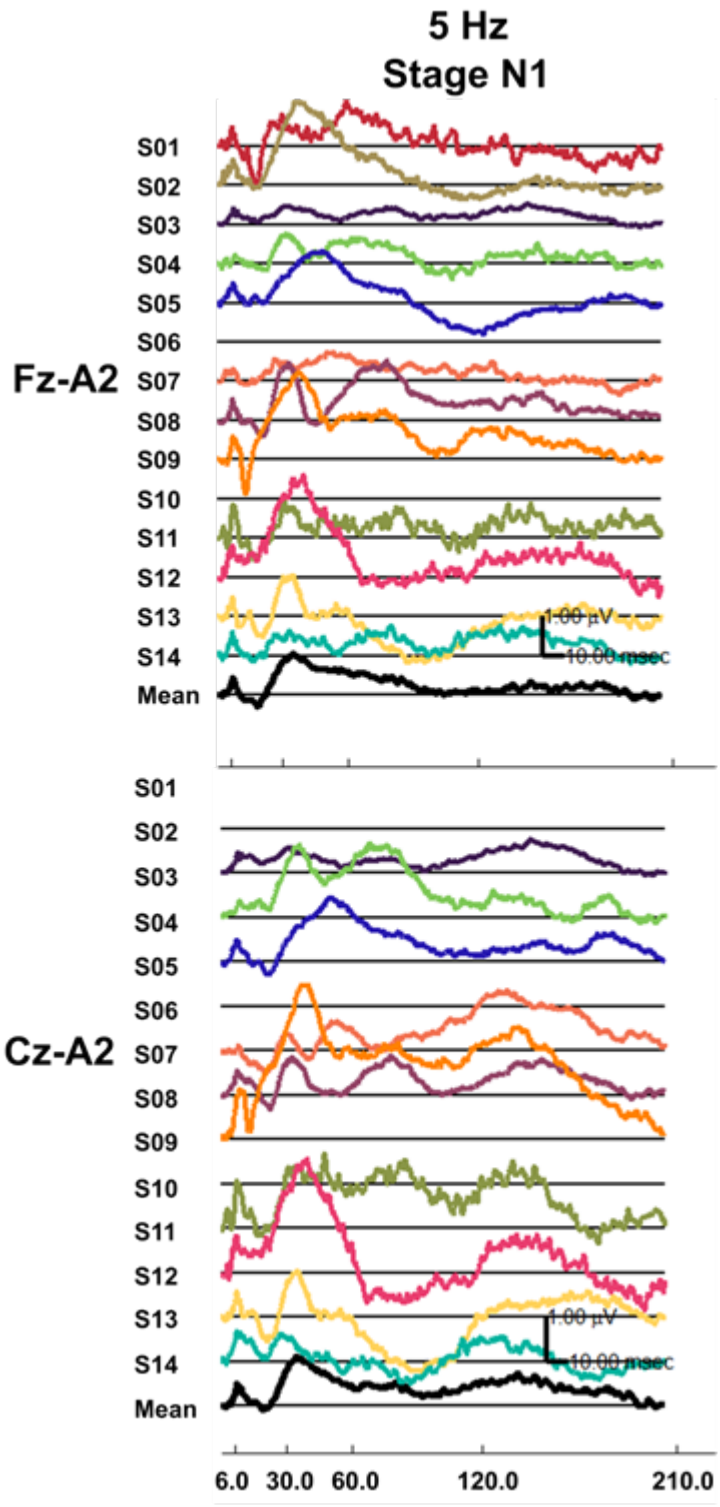

Figure B.2 The 5 Hz Transient Response for each Subject in Stage-N1. Shown for each channel is the transient response for each subject and the mean for all subjects.

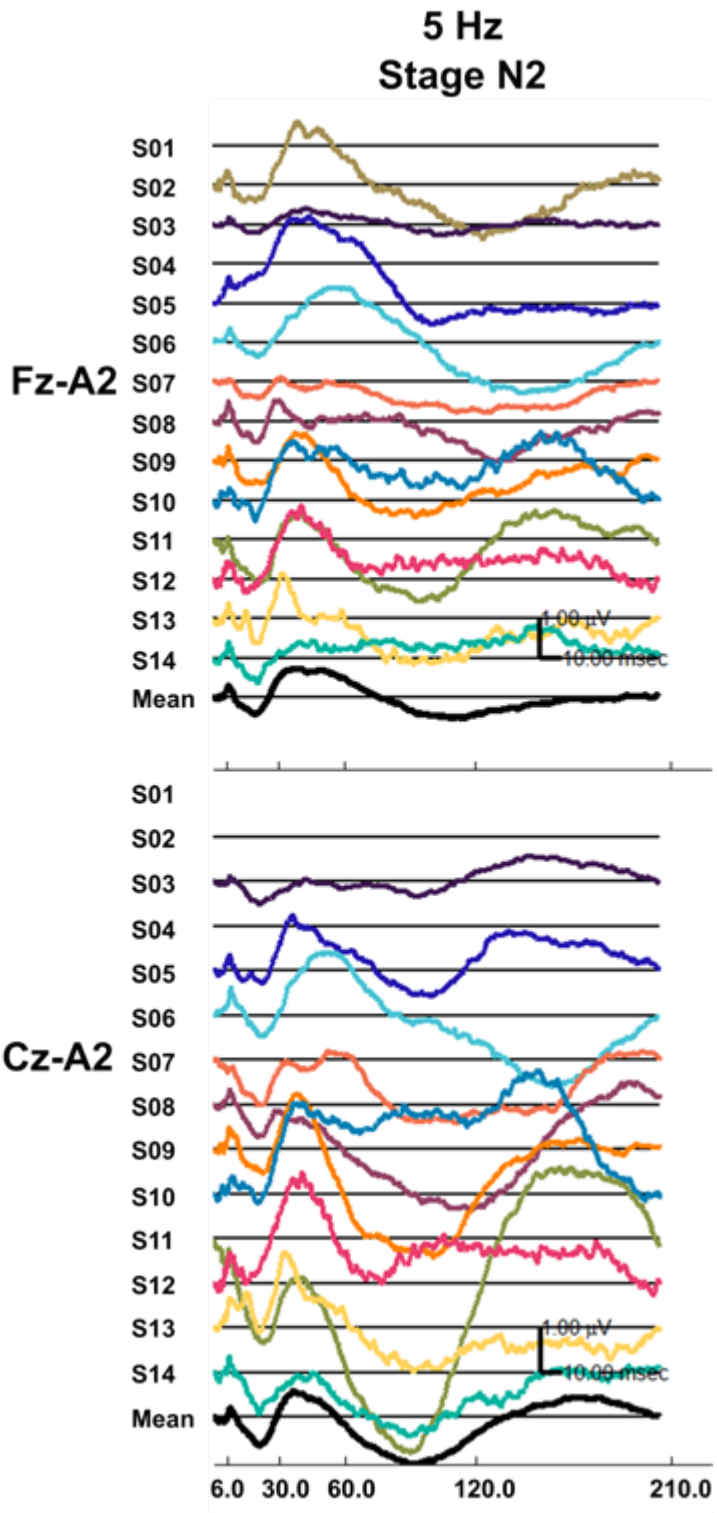

Figure B.3 The 5 Hz Transient Response for each Subject in Stage-N2. Shown for each channel is the transient response for each subject and the mean for all subjects.

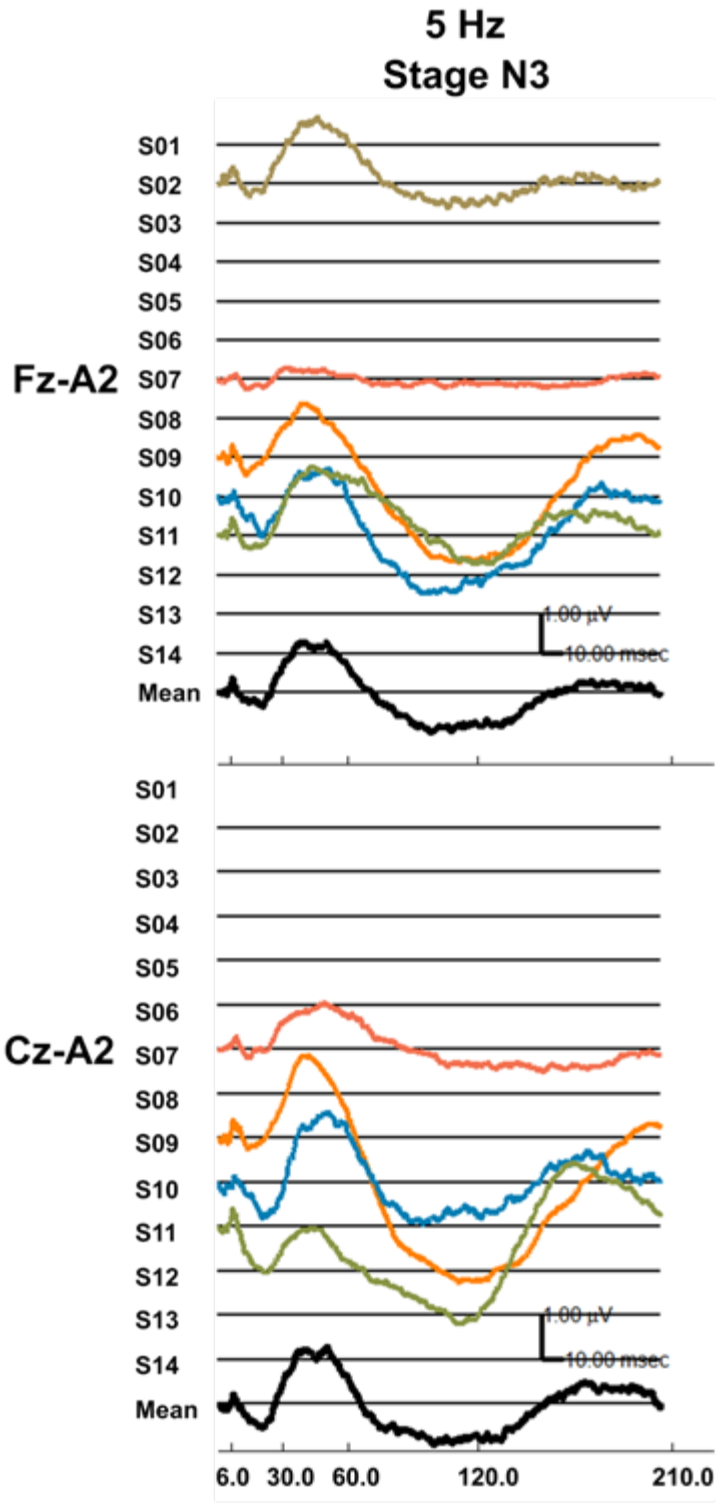

Figure B.4 The 5 Hz Transient Response for each Subject in Stage-N3. Shown for each channel is the transient response for each subject and the mean for all subjects.

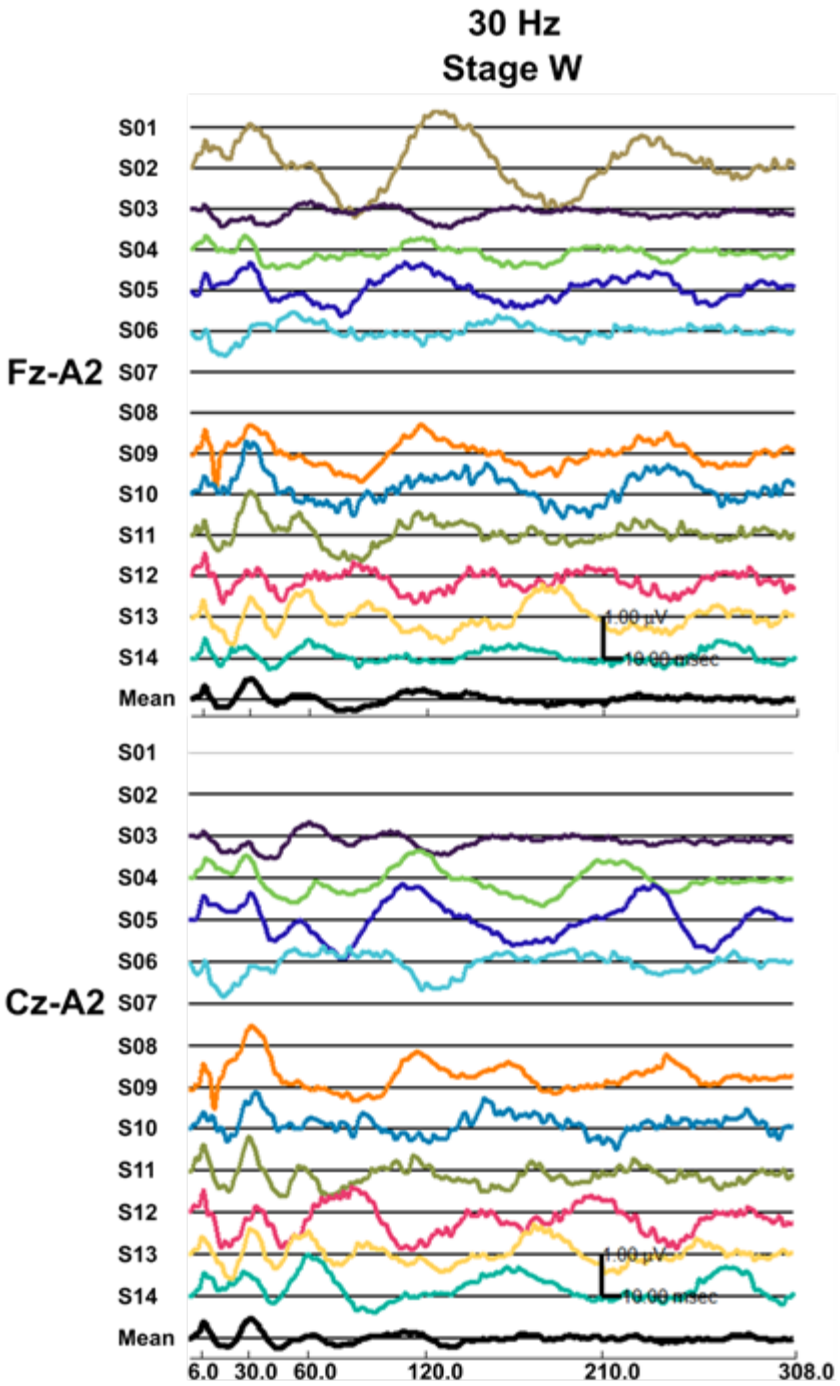

Figure B.5 The 30 Hz Transient Response for each Subject in Stage-W. Shown for each channel is the transient response for each subject and the mean for all subjects.

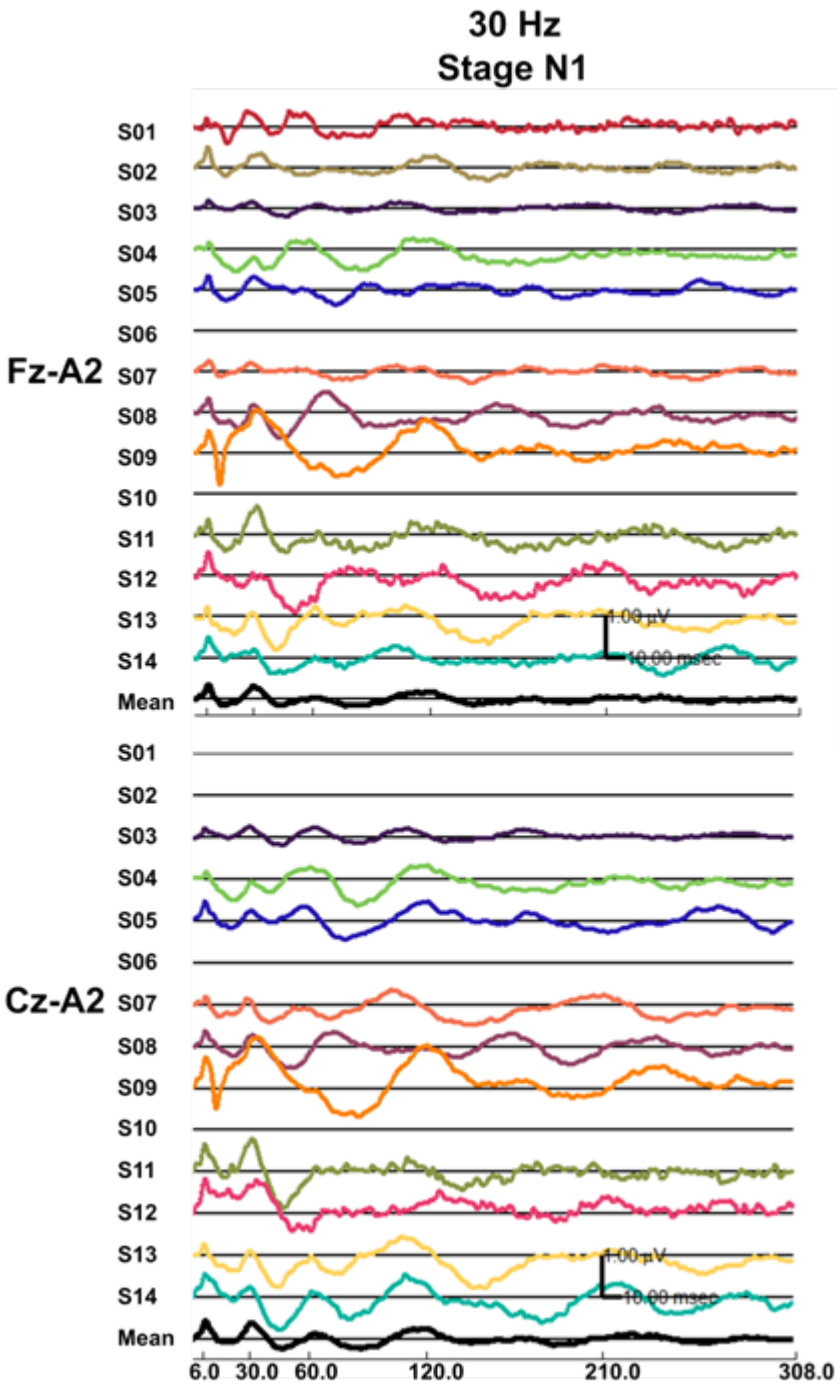

Figure B.6 The 30 Hz Transient Response for each Subject in Stage-N1. Shown for each channel is the transient response for each subject and the mean for all subjects.

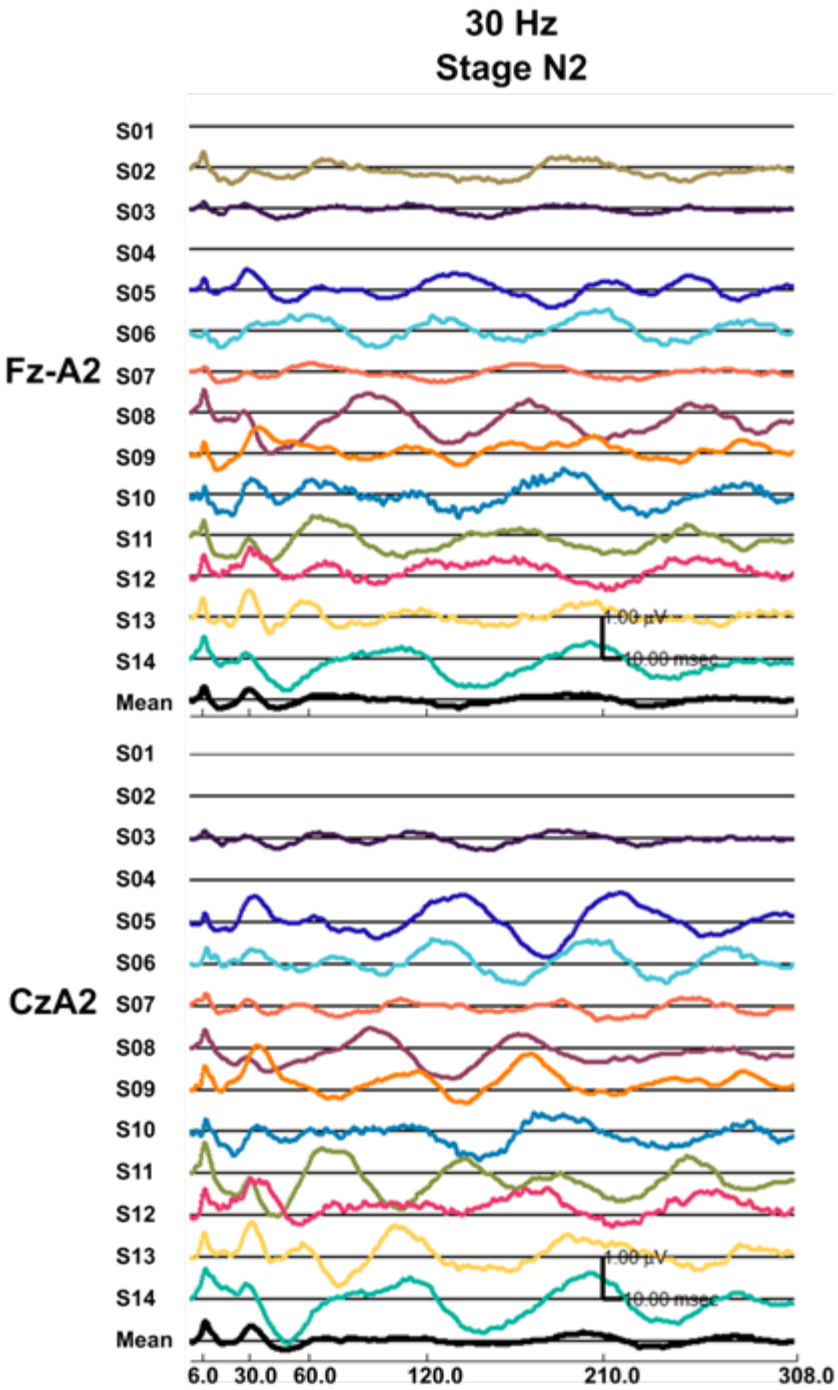

Figure B.7 The 30 Hz Transient Response for each Subject in Stage-N2. Shown for each channel is the transient response for each subject and the mean for all subjects.

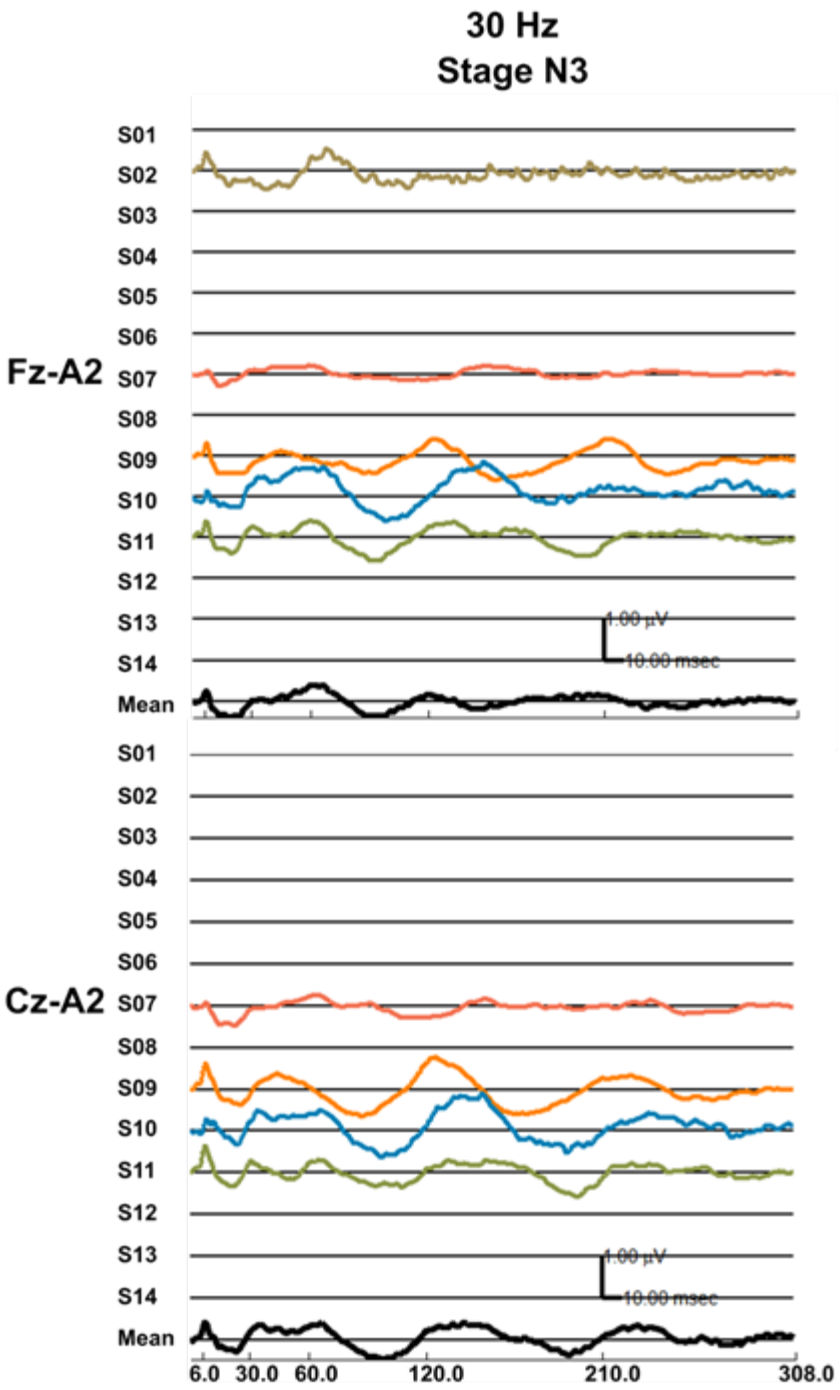

Figure B.8 The 30 Hz Transient Response for each Subject in Stage-N3. Shown for each channel is the transient response for each subject and the mean for all subjects.

APPENDIX C Welch Estimation Method of Power Spectral Density

EEG signal denoted as x(m), having length M, was divided into K overlapping segments, having length N, and each segment was windowed prior to computing the periodogram. The ith segment was defined as

$$x_i = x(m + iD) \qquad m = 0, \ldots, N-1, \qquad i = 0, \ldots, K-1 \tag{1}$$

where D denotes the length of overlap between adjacent windows. No overlap between adjacent windows is where D is equal to N. For the ith windowed segment, the periodogram was given by

$$P_{XX}^{i}(f) = \frac{1}{NU}\left|\sum_{m=0}^{N-1} w(m)\, x_i(m)\, e^{-j2\pi f m}\right|^2 \tag{2}$$

where w(m) is the window function (i.e., Blackman window) used to mitigate spectral leakage to side lobes and U is the power in the window function, given by

$$U = \frac{1}{N}\sum_{m=0}^{N-1} w^2(m) \tag{3}$$

The Welch power spectrum was the average of K periodograms:

$$\hat{P}_{XX}^{W}(f) = \frac{1}{K}\sum_{i=0}^{K-1} P_{XX}^{i}(f) \tag{4}$$

$$\hat{P}(\omega_r)_{A.C.\ Cmpt} \tag{5}$$

APPENDIX D Extended Abstract of Dissertation

MONITORING OF ELECTROENCEPHALOGRAPHIC AND MULTI-RATE AUDITORY EVOKED RESPONSE CHANGES DURING ALTERED LEVELS OF CONSCIOUSNESS

Extended Abstract

Alexander Castro-Llanos

Background: Previous studies in altered levels of consciousness in anesthesia and sleep have been focus only on either EEG or EP analysis. Additionally, studies involving EP only focus on either transient or steady-state responses without deconvolution, with the exception of our lab. The results for monitoring awareness in the field have not been satisfactory, yet research is progressing in preventing intraoperative awareness.

Purpose: To investigate the expression of inherent patterns that are attributed to the features of altered levels of consciousness in both the anesthesia and sleep models as measured via the simultaneous acquisition of both multi-rate auditory evoked responses and electroencephalographic spectral descriptors.

Methods: For anesthesia, a stimulation paradigm composed of 5 Hz isochronic, 20, 30, 40 Hz short low-jittered and silence regions was used. In the sleep study, the stimulus consisted of 5 Hz isochronic, 30 Hz low-jittered and silence region having durations of 61,440 ms for each. Both in anesthesia and sleep, the stimulus was 200 μsec click delivered at 70 dB nHL and 60 dB nHL respectively, delivered monaurally to right ear.

From the anesthesia study, 30 Hz seemed to exhibit stable and regular cortical and non-cortical activity during different levels. The sleep stimulation paradigm is an optimized version of the anesthesia one. It gains a greater number of low frequency components via a newly optimized sequence and a greater number of delivered sweeps per sequence via newly optimized stimulation region.

Physiological data, consisting of spontaneous respiration rate, expired agent concentration, bispectral index, heart rate, and core body temperature, were collected for all the anesthesia patients using a system termed Picis. Picis and EEG data were time synchronized. EEG was continuously acquired from Fz-M2 derivation ground forehead.

The instrument settings were as follows: amplifier set to 100k gain, analog filters set to 1 to 1500 Hz with 6dB/decade roll-off, quantization set to 16 bit precision with 5 kHz sampling rate.

For sleep, identical settings were used with the following exceptions: a.) Fz-A2 and Cz-A2 derivatives, b.) Amplification set to 50k gain, and c.) Additional sleep scoring derivatives Cz-A1, Oz-A2, E1-A2, E2-A2, and chin-EMG.

For accurate sleep **manual** scoring, an EEG scoring aid software was developed. This software was feature rich in time- and frequency- domain analysis tools. It allowed the user to easily inquire about the signal under study either by exploring its time series properties or by probing its underlying spectral content. Once completed a second, independent, blinded-assessment of scores was performed.

For anesthesia and sleep, the following spectral descriptors were computed: total power, power ratio, spectral edge frequency, median frequency, and spectral entropy. To extract both high-rate transient and steady-state responses, continuous loop acquisition deconvolution (CLAD) method was used. For the high-rate stimulation, spectral filtering set to 13-1500 Hz for anesthesia and 5-1500 Hz for sleep was applied during deconvolution.

Also, phasors of the fundamental frequency of the steady-state responses were extracted. Trend analysis was used to analyze the spectral descriptors in anesthesia. Correlation coefficient was used to analyze the apparent relationship of delta and alpha power ratio. Moving average was used to analyze the trend response-to response changes auditory responses. 5 Hz grand mean was used to analyze global changes of maintenance anesthesia. The 5Hz elicited responses were not digitally high-pass filtered.

The 20, 30, and 40 Hz transient responses exhibited Beta entrainment – a phase locked beta rhythm embedded in the responses. The power of this beta entrainment was analyzed for each stimulation rate.

The sleep study measures many of the same attributes measure in the anesthesia study such as, spectral descriptors, transient responses and phasors of steady-state responses. The sleep study investigated these attributes by contrasting between sleep stages for analysis

Results - Anesthesia: Five subjects were collected and fully analyzed. For brevity in this abstract, we have focused on end-boundary subject levels P23 (deeper level) and P26 (lighter level). P26 expressed a clinical reaction event. Ledowski et al. 2006 defines it (an indicator of light anesthesia) as the “first reaction” by patient, such as movement, coughing, and eye opening. Anesthesiologists used different administration strategies; this parameter is an uncontrolled variable, for ethical reasons, but reflects realistic conditions.

BIS values for all subjects were within 40 to 60 - range that is typically recommended to prevent awareness. P26 did not show any exceptional BIS that suggested clinical reaction

would have occurred. Heart rate was an autonomic indicator. P23's heart rate increased as agent concentration decreased. P26 showed a fast rise in heart rate concomitant with the clinical reaction.

EEG spectral descriptors were analyzed using trend analysis. Power ratio indicates each classical EEG rhythms contribution. Except P26, all surgeries showed the delta trend higher than alpha. The power ratios underlying subject levels were for P23 delta (**0.74**), alpha (**0.048**) and for P26 alpha (**0.41**), delta (**0.25**).

Median frequency (MF) is the central tendency of the power spectrum. When subjects were ordered by increasing value of MF, this order corresponded to the subjective depth level from deep to light. The same order was observed using decreasing delta and increasing alpha power ratio.

Spectral edge frequency did not correlate well neither with the power ratios nor our presumed subject anesthetic level. It was less sensitive to the alpha rhythms than median frequency. Ordered by BIS did not arrange the subjects with our presumed subject anesthetic levels. It clustered closely all subjects and did not separate P23 and P26 to both ends of the anesthesia levels.

Spectral entropy measures uniformness, values less than one are less uniform and considered more anesthetic depth. The lowest spectral entropy was observed for P23 (**0.62**). P26 (**0.763)** and rest were about **0.76** considered light anesthesia. P22 (**0.781**) was greater than P26 (**0.763**), yet P22 did not have first reaction.

The power ratio for delta and alpha appeared to move in tandem opposed directions - correlation coefficient was measured. Delta-to-alpha correlation coefficient showed an increase from P23 (**- 0.83**) to P26 (**- 0.60**).

A discrimination assessment of how well the spectral descriptors separate between subject anesthesia levels is summarized in Figure 1. The inner circle denotes better performance; the gray gradient indicates the similarity in performance. The bispectral index showed the least power of separation.

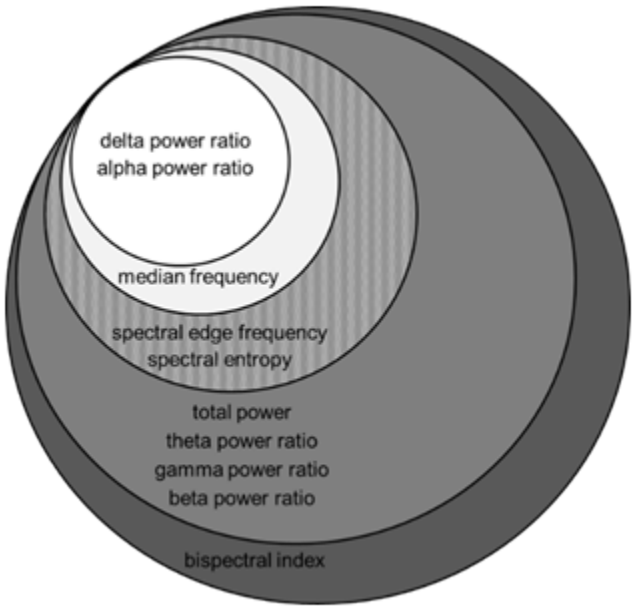

Figure 1. Summary of spectral descriptor discrimination assessment. The performance is arranged into groups where the inner circle represents better performance than the outer circle. The gradient of the gray color further denotes the similarity in performance to adjacent groups.

The 5 Hz evoked transient response were analyzed using moving average analysis (10 point window, 50% overlap same as spectral descriptors). Responses showed two main patterns: response with one dominant or two dominant peak(s). Also, flat responses were observed.

Second-wrapping responses present in the set of extracted responses prevent direct magnitude and latency measurements. Magnitude was measured indirectly via the response range. Additionally, a set of filtered responses were extracted using conventional settings (bandpass filter: 25 to 1500 Hz) as used in previous studies. The trend showed that filtering discards prominent activity caused by anesthesia. The unfiltered responses showed a good separation, but after conventional filtering its power of discrimination lowered to unusable levels.

Shown in Figure 2., the grand mean of the responses indicate global differences in subjects. In the figure the transient responses are arranged in presumed anesthetic depth: P26, P17, P22, P25, and P23. The resulting order placed P26 and P23 to opposite ends. P23 and P25 showed attenuated waveform compared to rest. Note that the order is same as median frequency in decreasing order.

When filtered by conventional settings effects of anesthesia were severely attenuated. The split-buffer traces for both grand mean indicated good signal-to-noise ratio.

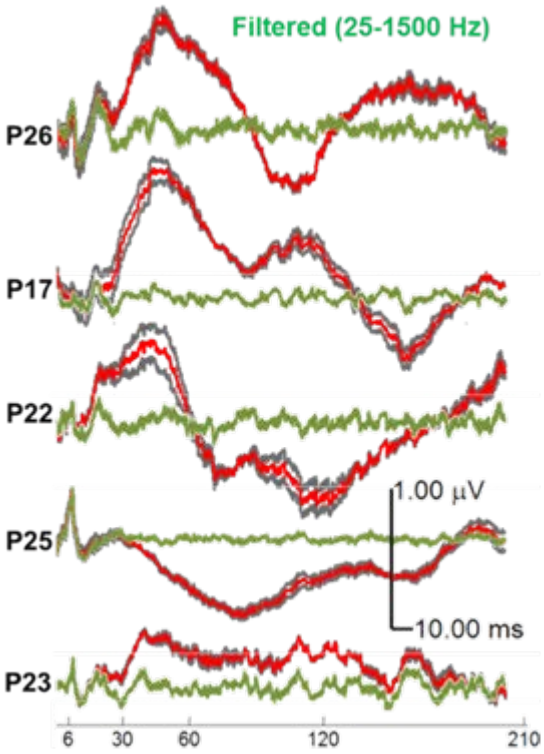

Figure 2. The grand mean of the moving average 5 Hz transient responses. Shown is mean (red), split-buffer (gray), and filtered (green) responses.

The 20, 30, and 40 Hz de-convolved responses showed beta oscillations (17.0 and 19.5 Hz) with considerable phase consistency. Beta entrainment offers the advantage of separating light from deep anesthetic levels, but not for nuance differences. Beta entrainment's separation of P23 and P26 increased as the rate decreased from 40 to 20 Hz. In 20 Hz beta entrainment showed activity for P26 and no activity for P23 or the remaining subjects.

Phasor magnitude for 20, 30, and 40 Hz showed the capacity to separate light from deep anesthetic levels, but not nuance differences. It increased in discrimination as stimulation rate decreased. For 40 Hz phasor the values between P23 (**0.180**) and P26 (**0.174**) showed a small difference contrast by the lower rate 20 Hz which showed a larger difference between P23 (**0.378**) and P26 (**0.840**).

Results - Sleep: Fourteen subjects were collected. Same features in anesthesia are studied in sleep. All statistical tests, will test if there exists a difference between the following pairing of sleep stages (W vs. N1, W vs N2, W vs. N3, N1 vs. N2, and N2 vs. N3).

In terms of auditory stimulation, the spectral descriptors showed the same discrimination performance – no significant difference found in regards to the discrimination ability under different auditory stimulation. Further, Fz-A2 showed better discrimination than

Cz-A2. Due to redundancy only 5 Hz will be presented. EEG spectral descriptors were analyzed via sleep stages.

Shown in Figure 3., spectral descriptors showed difficulty separating W vs. N1, but improves in deeper stages. Delta power ratio and median frequency separate all stages.

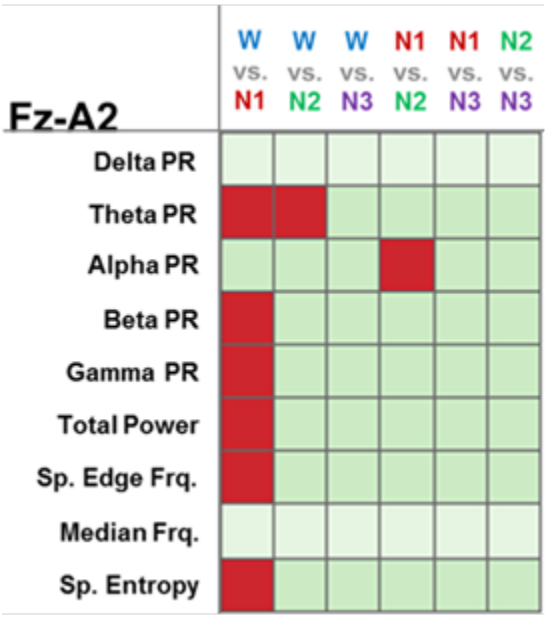

Figure 3. The outcomes of Student's t-test in comparisons between sleep stages for spectral descriptors in 5 Hz and FzA2. (Red, Significantly Different ($p<0.05$)).

Shown in Figure 4., effects of stimulation on EEG spectral descriptors were analyzed via pair wise comparison of stimulation rates: (5Hz, Sil), (30Hz, Sil), and (5Hz, 30Hz). Majority of significant (green) separation observed, occurred in stage N1 and in particular 30 Hz vs. silence. In stage N3 no significant difference (gray) was observed. The effects of stimulation are small in comparison to sleep. For example, compared to silence, the alpha power ratio significantly increments under stimulation; however, this change is very small (~ 12%) compared to sleep (~ 60%).

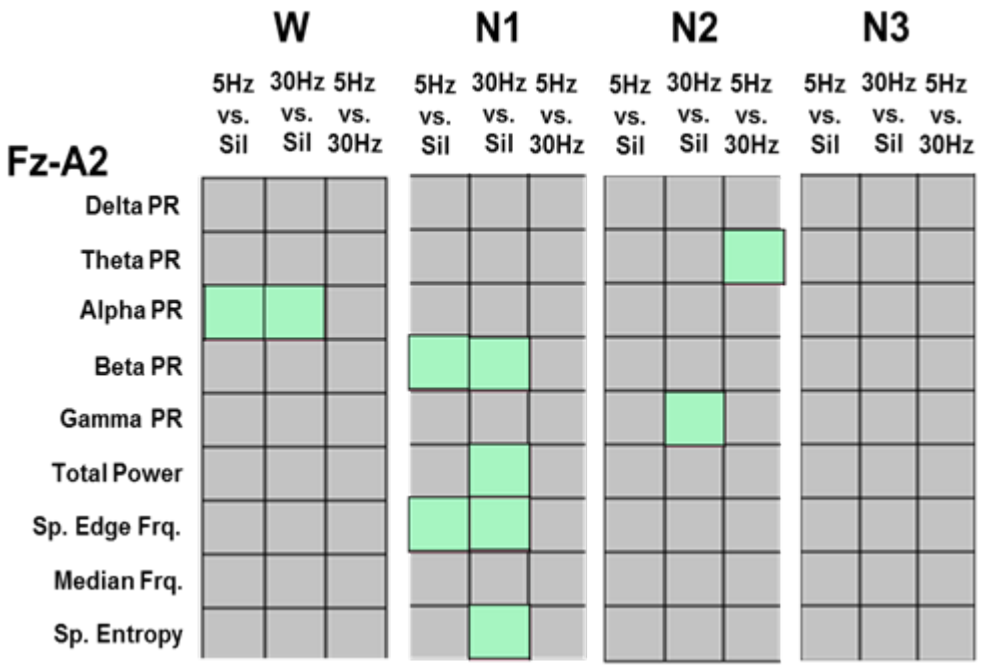

Figure 4. The outcomes of Student's t-test in comparisons between stimulation rates for spectral descriptors in FzA2. (Green, Significantly Different ($p<0.05$)).

5 Hz transient response: The population average for 5 Hz transient responses were analyzed. The observed changes were quantified via component magnitude and the latency measurement. Shown in Figure 5., from stage W to N3, the responses gradually slowed as indicated by increase in magnitude. From stage W to N3 the responses showed the build-up of a low frequency component between 10 to 100 msec., identify as Pα. It occurs in both Pa and Pb latency range, about 44 msec..

In stage W, Pa and Pb components are clearly distinguishable by stage N3 only Pα is. In stage W, Pb component is observed. From stage W to N1, Pb is attenuated and by stages N2 and N3 abolished. For stage N3, N1 component shows a greater negativity than other stages. The Pa-Na magnitude showed no significant difference in sleep. Na latency showed no significant difference in sleep. Pa latency gradually increases with a significant difference between stage W vs. N3 and W vs. N2 and N1 vs. N3. Pα-N1 magnitude gradually increases and latency show small change from stage W vs. N3.

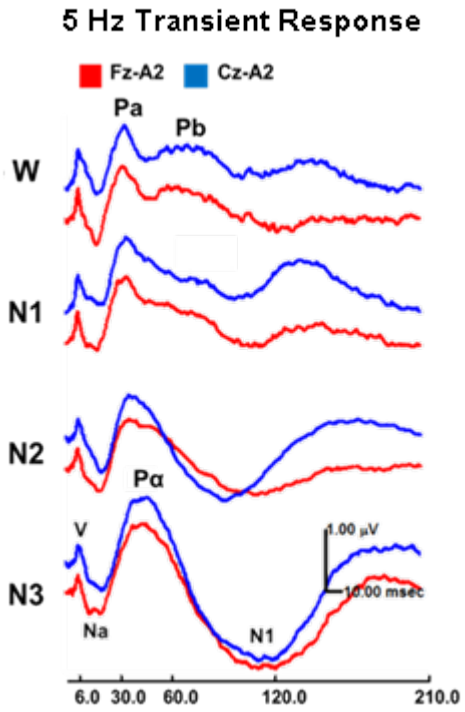

Figure 5. The 5 Hz transient response mean for all subjects for each channel. Shown for each sleep stage is the mean transient response for all subjects for Fz-A2 (red) and Cz-A2 (blue).

30 Hz transient response: The population average for 30 Hz transient responses was analyzed. Pa-Na magnitude showed significant attenuation between W vs. both N2 & N3, N1 vs. both N2 & N3. Na latency showed significant change for all except stage N2 vs. N3. The waveform of N3 response showed greater changes.

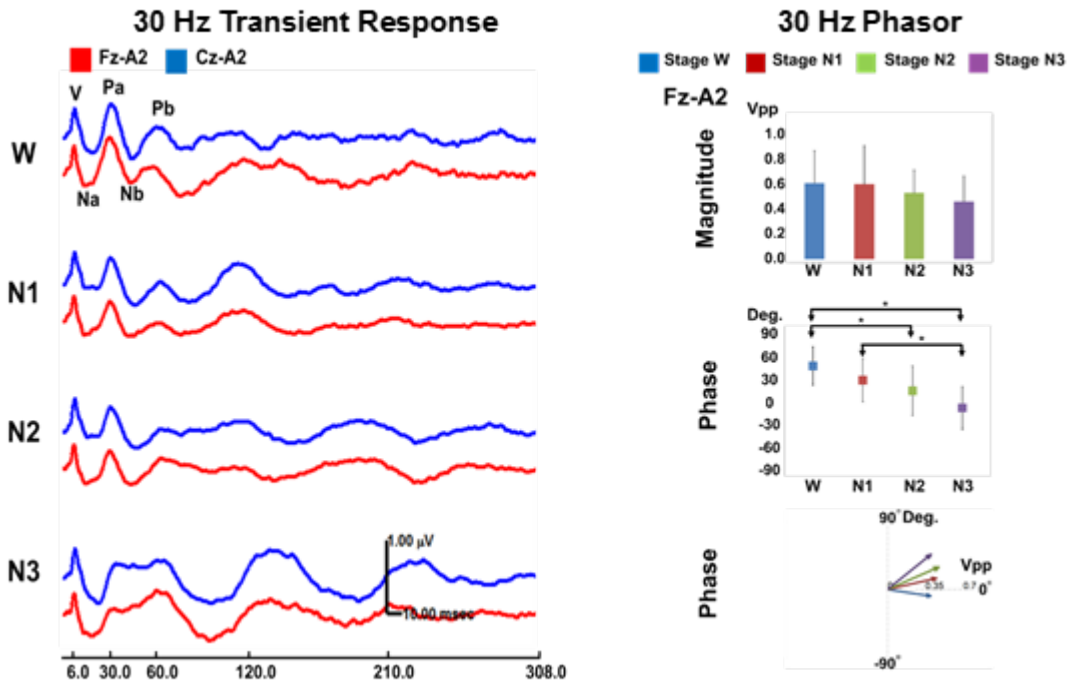

Figure 6. Population average of 30 Hz transient response and phasor. For 30 Hz TR blue denotes CzA2 and red FzA2. For the phasors blue, red, green, and purple denote W, N1, N2, and N3, respectively. (Phasor: ± St.Dev., *, Significantly Different ($p<0.05$)).

30 Hz steady-state response: Shown in Figure 6. column 2 are the phasor magnitude and phase angle of the 30 Hz steady-state responses. The magnitude showed no significant difference between the sleep combinations. However, the phase angle of the phasor showed significant difference for W vs. N3, W vs. N2, and N1 vs. N3.

Discussion - Anesthesia:

Bispectral index: Avidan, et al. (2011) showed BIS-guided administration fails to prevent awareness in anesthesia. Our study shows that, compared to other spectral descriptors, the bispectral index preformed lowest in power of separation between subjects having different anesthetic levels.

Total Power: Total power shows a low separation power. Studies show conflicting findings. Under anesthesia Plourde and Picton (1990) found it increases and Drummond et al. (1991) and Bührer et al. (1987) found it decreases.

Power Ratio: Alpha and delta power ratio shows a high separation power while theta, beta, and gamma power ratio a low. It was observed for all subjects, except for P26, that under anesthesia, the increase in delta was matched by the decrease in alpha power ratio.

These observations are comparable to similar studies (see Schmidt, Bischoff, Standl, Lankenau, Hilbert, & am Esch, 2004 and Kiyama & Takeda, 1997).

Median Frequency: Median frequency shows a high separation power. Its observed changes are in agreement to those of delta and alpha power ratios that is, the decrease in median frequency was matched by the decrease in delta and increase in alpha. These findings are comparable to median frequency studies in anesthesia (see Plourde & Picton, 1990; Drummond, Brann, Perkins, & Wolfe, 1991; Kiyama & Takeda, 1997; and Schmidt et al. 2004).

Spectral edge frequency: Spectral edge frequency shows a lower separation power compared to median frequency and did not separate the P23 and P26 to opposite ends of discrimination axis. The observed corroborate similar studies (see Plourde & Picton, 1990; Gökahmetoglu, Tercan, Bicer, Aksu, & Boyaci, 2013; and Arndt, Hofmockel, & Benad, 1994; Kiyama & Takeda, 1997, and Gurman, Fajer, Porat, Schily, & Pearlman, 1994).

Spectral entropy: Spectral entropy shows a low separation power, and it did not separate P23 and P26 to opposite ends of the discrimination axis. Using Bein's (2006) study as a rubric P23 would be classified as deep anesthesia and the rest as not adequate anesthesia.

Correlation of delta to alpha power ratio: The correlation coefficient between delta and alpha power ratio has not been previously used in anesthesia. The correlation coefficient between delta and alpha decreases from P23 ($r_{delta,alpha}$ = -0.83) to P26 ($r_{delta,alpha}$ = -0.60). This decrease in deep to light anesthetic level may be associated to a decoupling of the systems driving the delta and alpha power ratio.

Moving average 5 Hz transient response: 5 Hz transient responses are extensively altered by the effects of anesthesia. The grand mean shows the responses are attenuated from P26 to P23. 5 Hz transient response separates P23 and P26 to opposite ends of the discrimination axis. P26 is widely disperse from the remaining subjects; it may indicate that 5 Hz transient response preforms best for detecting broad difference in anesthetic levels. Filtering via conventional settings lowers separation ability. The conventional filter settings are from Thorton et al. (1985) (25-2500 Hz). Conventional filter settings have high-pass cut-off frequencies greater than 10 Hz (see Plourde & Picton, 1990; Tatsumi, Hirai, Furuya, & Okuda, 1995; and Thorton et al. 1985).

Moving Average 20, 30 and 40 Hz transient response - Beta entrainment: Entrainment of beta rhythm oscillations was observed in 20, 30, and 40 Hz de-convolved transient responses. It preforms more accurate in separation between low and deep anesthesia levels. 20 Hz entrainment may be associated to lighter anesthesia levels. Its entrainment was robust for P26 and attenuated for the rest.

The entrainment may be elicited sevoflurane via GABA-A receptors (Jenkins, Greenblatt, Faulkner, Bertaccini, Light, Lin, ... & Harrison, 2001; Nishikawa, Jenkins, Paraskevakis,

& Harrison, 2002, Jenkins, Andreasen, Trudell, & Harrison, 2002; Bertaccini & Trudell, 2001; Mascia, Trudell, & Harris, 2000).
If entrainment is independent of sequence jitter then increasing jitter decreases noise in lower frequencies, such as beta, thereby increasing separation.

Discussion - Sleep*:*
Spectral descriptors: Delta power ratio and median frequency separated all sleep stages; the rest did not separate W vs. N1, except alpha power ratio. Alpha power ratio did not separate N1 vs. N2 and theta power ratio did not separate W vs N2.

Effects of Stimulation on Spectral Descriptors: Spectral descriptors afforded the opportunity to verify if the stimulation produces EEG entrainment at different sleep stages. The results in Figure 4. (green/gray blocks) summarize the differential effect as a function of stage and stimulation rate. The effects are prominent in wake and N1 while very negligible in stages N2 and N3. EEG spontaneous activity appears to become more independent of stimulus at deeper stages.

5 Hz transient response: The transient components change with respects to sleep stages. A notable build-up of a low frequency component; identified as Pα, occurs between 10 to 100 in the latency range of both Pa and Pb. Clearly distinguishable in W, by N3 the Pa and Pb components are supersede by Pα. Pb was discernable in W, attenuated by N1, and abolished by N2 and N3. These finding are comparable to Erwin et al..

Pa-Na magnitude remained stable and did not show significant difference between the sleep stages. These findings are comparable to Millan (2006) and Erwin et al.. Millan filtered the MLRs. He found Pa-Na magnitude remain stable.

Pa latency, while slight, shows significant changes for W vs. N2, N1 vs. N3, and W vs. N3. Similar findings were observed by Deiber et al. and Erwin et al.. The latency for V, Na, Pα, and N1 were not significantly different.

The N1 component showed a progressive strengthening in negativity from W to N3. Pα-N1 magnitude increases from W to N3 by about 260%. Among previous studies only Erwin et al. observed similar findings. He elicited MLR at a lower stimulation rate (1 Hz), which leads to a pronounced N1 negativity in awake responses.

His figure shows the N1 magnitude with a larger negativity for stages N2 and N3, however the increase is smaller (around 33%) and not as pronounced as in our results (around 260%). This smaller increased observed by Erwin et al. can be explained by his high-pass cut-off filter frequency 10 Hz that attenuates the low frequencies.

30 Hz transient response: The 30 Hz transient response waveform was altered by effects of sleep. Pa-Na magnitude shows significant decrease for all combinations of sleep stages except W vs. N1, Pb-Nb did not. No significant difference was observed for component latencies, except for Na. Na significantly increases from N1 to N3 and decreases from W to N1, but no significance from N2 to N3.

30 Hz steady-state response: 30 Hz phasor magnitude showed no significant difference for all sleep combinations. Previous studies involving steady-states responses in sleep tend to only focus on 40 Hz responses. Thus, a comparison between 40 Hz (other studies) and 30 Hz (this study) steady-state responses in sleep entails caution. The magnitude of 40 Hz steady-state responses decrease from awake to NREM by a) half (Galambos Makeig, & Talmachoff, 1981) or b) one third (Brown & Shallop, 1982) and (Osterhammel & Shallop, 1985).

30 Hz phase angle showed a significant decrease in angle from W to N3 for all sleep combinations. Jerger et al. (1986) studied the 40 Hz ASSR for waking, Stage N1, and Stage N2 sleep stages and found that, for the 40 Hz frequency component, the phase coherency remains unaffected by sleep. 30 Hz phase angle was more indicative of change in sleep than was the magnitude. The angles did not resolve N2 vs. N3 or W vs. N1. The steady-state phasor may prove promising for uses in identifying the onset of sleep (Khuwaja, Haghighi, & Hatzinakos, 2015).

Summary of new contributions of anesthesia study: To summarize the most notable findings about anesthesia from this body of work were that for electroencephalographic changes during altered levels of consciousness: a) Delta/alpha power ratio correlation coefficient changes with changes in anesthetic level, b) BIS does not appear to be an appropriate feature for risk of unintentional awareness. To summarize the most notable new findings about anesthesia from this body of work were that for evoked potentials changes during altered levels of consciousness: a) 5 Hz transient responses recorded with broader filter bandwidths such 1 to 1500 Hz are sensitive to change in awareness state, b) High-rate transient beta **entrainment** may separate well subjects near clinical reaction from subjects in general anesthesia, 20 Hz would preforms better, c) High-rate (30 and 40 Hz) ASSR does not discriminate well, but lower rate (20 Hz) seems to separate well general anesthesia from clinical reaction.

Summary of new contributions of sleep study: To summarize the most notable new findings about sleep from this body of work were that for electroencephalographic changes during sleep: a) Fz-A2 shows a better discrimination power to classify sleep stages, b) Delta Power Ratio and median frequency have the best discrimination power – W vs. N1 is more difficult to resolve, and c) Auditory stimulation significantly change spectral descriptors but the changes are very small compared to the changes due to sleep stages. To summarize the most notable new findings about sleep from this body of work were that for evoked potentials changes during sleep: a) Fz-A2 shows a better discrimination power to separate sleep stages, b) 5 Hz responses are very sensitive to sleep stages, like anesthesia, preserving the low frequencies is critical to observing theses effects. c) 30 Hz transient responses show entrainment but it may be reduced due to the high-pass filter required by deconvolution. Only in Stage N3 can 30 Hz response be resolved from the remaining stages and c) ASSR phases show sensitivity to stage - can significantly resolve light sleep versus deep sleep.

REFERENCES

Arndt, V. M., Hofmockel, R., & Benad, G. (1994). EEG changes during propofol-alfentanil-nitrous oxide anesthesia. Anaesthesiologie und Reanimation, 20(5), 126-133.

Avidan, M. S., Jacobsohn, E., Glick, D., Burnside, B. A., Zhang, L., Villafranca, A., ... & Evers, A. S. (2011). Prevention of intraoperative awareness in a high-risk surgical population. New England Journal of Medicine, 365(7), 591-600.

Avidan, M. S., Zhang, L., Burnside, B. A., Finkel, K. J., Searleman, A. C., Selvidge, J. A., ... & Hantler, C. (2008). Anesthesia awareness and the bispectral index. New England Journal of Medicine, 358(11), 1097-1108.

Bein, B. (2006). Entropy. Best Practice & Research Clinical Anaesthesiology, 20(1), 101-109.

Bertaccini, E., & Trudell, J. R. (2001). Molecular modeling of ligand-gated ion channels: Progress and challenges. International Review of Neurobiology, 48, 141-166.

Brown, D., & Shallop, J. K. (1982). A clinically useful 500 Hz evoked response. Nicolet potentials, 1(5), 9-12.

Bührer, M., Maitre, P. O., Ebling, W. F., & Stanski, D. R. (1987). Pharmacological quantitation of midazolam's CNS drug effect in hypnotic doses. The Journal of the American Society of Anesthesiologists, 67(3), A658-A658.

Deiber, M. P., Ibanez, V., Bastuji, H., Fischer, C., & Mauguiere, F. (1989). Changes of middle latency auditory evoked potentials during natural sleep in humans. Neurology, 39(6), 806-806.

Drummond, J. C., Brann, C. A., Perkins, D. E., & Wolfe, D. E. (1991). A comparison of median frequency, spectral edge frequency, a frequency band power ratio, total power, and dominance shift in the determination of depth of anesthesia. Acta Anaesthesiologica Scandinavica, 35(8), 693-699.

Erwin, R., & Buchwald, J. S. (1986). Midlatency auditory evoked responses: Differential effects of sleep in the human. Electroencephalography and Clinical Neurophysiology-Evoked Potentials Section, 65(5), 383-392.

Galambos, R., Makeig, S., & Talmachoff, P. J. (1981). A 40-Hz auditory potential recorded from the human scalp. Proceedings of the National Academy of Sciences, 78(4), 2643-2647.

Gökahmetoglu, G., Tercan, E., Bicer, C., Aksu, R., & Boyaci, A. (2013). Comparison of the depth of anesthesia in sevoflurane and halothane anesthesia with bispectral index and 95% spectral edge frequency. Dicle Medical Journal, 40 (3), 350-356.

Gurman, G. M., Fajer, S., Porat, A., Schily, M., & Pearlman, A. (1994). Use of EEG spectral edge as index of equipotency in a comparison of propofol and isoflurane for maintenance of general anaesthesia. European Journal of Anaesthesiology, 11(6), 443-448.

Jenkins, A., Andreasen, A., Trudell, J. R., & Harrison, N. L. (2002). Tryptophan scanning mutagenesis in TM4 of the GABA-A receptor α1 subunit: implications for modulation by inhaled anesthetics and ion channel structure. Neuropharmacology, 43(4), 669-678.

Jerger, J., Chmiel, R., Frost Jr, J. D., & Coker, N. (1986). Effect of sleep on the auditory steady state evoked potential. Ear and Hearing, 7(4), 240-245.

Khuwaja, G. A., Haghighi, S. J., & Hatzinakos, D. (2015). 40-Hz ASSR fusion classification system for observing sleep patterns. EURASIP Journal on Bioinformatics and Systems Biology, 2015(1), 2.

Kiyama, S., & Takeda, J. (1997). Effect of extradural analgesia on the paradoxical arousal response of the electroencephalogram. British Journal of Anaesthesia, 79(6), 750-753.

Mascia, M. P., Trudell, J. R., & Harris, R. A. (2000). Specific binding sites for alcohols and anesthetics on ligand-gated ion channels. Proceedings of the National Academy of Sciences, 97(16), 9305-9310.

Millan, J. (2006). Analysis of auditory middle latency responses at low and high stimulus rates during sleep (Doctorial Dissertation). Retrieved from ProQuest

Nishikawa, K., Jenkins, A., Paraskevakis, I., & Harrison, N. L. (2002). Volatile anesthetic actions on the GABA A receptors: contrasting effects of α1 (S270) and β2 (N265) point mutations. Neuropharmacology, 42(3), 337-345.

Osterhammel, P. A., Shallop, J. K., & Terkildsen, K. (1985). The effect of sleep on the auditory brainstem response (ABR) and the middle latency response (MLR). Scandinavian Audiology, 14(1), 47-50.

Plourde, G., & Picton, T. W. (1990). Human auditory steady-state response during general anesthesia. Anesthesia & Analgesia, 71(5), 460-468.

Schmidt, G. N., Bischoff, P., Standl, T., Lankenau, G., Hilbert, M., & am Esch, J. S. (2004). Comparative evaluation of Narcotrend™, Bispectral Index™, and classical electroencephalographic variables during induction, maintenance, and emergence of a propofol/remifentanil anesthesia. Anesthesia & Analgesia, 98(5), 1346-1353.

Tatsumi, K., Hirai, K., Furuya, H., & Okuda, T. (1995). Effects of sevoflurane on the middle latency auditory evoked response and the electroencephalographic power spectrum. Anesthesia & Analgesia, 80(5), 940-943.

Thornton, C., Heneghan, C. P. H., Navaratnarajah, M., Bateman, P. E., & Jones, J. G. (1985). Effect of etomidate on the auditory evoked response in man. British Journal of Anaesthesia, 57(6), 554-561.